University of Cape Town

Faculty of Engineering and the Built Environment

Studies on Strength and Stability of Toroidal Shell Forms for Containment Applications

Nosakhare Enoma

Supervisor

Professor Alphose Zingoni

Thesis Presented for the Degree of
DOCTOR OF PHILOSOPHY
in the Department of Civil Engineering
UNIVERSITY OF CAPE TOWN

August 2018

Declaration

This thesis is submitted for the degree of Doctor of Philosophy in the Faculty of Engineering & the Built Environment at the University of Cape Town. I hereby declare that the research project reported herein is my own unaided work, unless otherwise stated. The study was carried out within the Structural Engineering and Mechanics Research Group, University of Cape Town between July 2014 and August 2018. No part of this thesis has been submitted in support of an application for a degree in this University or any other educational establishment.

Signed by candidate

Nosakhare Enoma

27 August 2018

This thesis is dedicated to my late parents

Abstract

Shells find applications in many engineering disciplines (Zingoni 1997), with containment shells of revolution being among the most important (Zingoni 2001, 2015). Searching for the most efficient geometrical forms remains one of the most important goals of shell research. Associated with that is the need to develop appropriate analytical tools for novel shell forms. Complete toroidal shells are not widely used shells of revolution owing to their geometries and associated complexities in the theory of the shells. They can offer certain structural and functional advantages over conventional shells and are mainly used for fluid containment. Toroids have also been proposed for nuclear fusion reactors, rocket fuel tanks, medical hyperbaric treatment units and applications in aerospace and underwater fields. Any desired cross-sectional forms of the shells can be developed theoretically, suggesting the possibility of adopting toroidal shells in many engineering applications if the behaviour of the shells can be understood and quantified. The design analysis of thin-walled structures is mostly based on strength and stiffness considerations. Based on linear elastic theory, Zingoni, Enoma & Govender (2015) presented an elegant theoretical solution for the non-shallow bending of an elliptic toroid, while Enoma and Zingoni (2017) have investigated toroidal shells having the same type of multi-shell cross-section as was first proposed by Zingoni (2001) for novel sludge digester shells.

On the basis of classical elastic shell theory and numerical modelling, this thesis attempts to provide a framework upon which complete toroidal shells of any cross-sectional profile can be analysed, and investigates the state of stress and buckling of selected toroidal shell forms including unconventional ones under axisymmetric pressure loading, i.e. when each of the shells is used as a pressure vessel and a storage tank. Following the general strategy developed for shells of revolution by Zingoni (1997) over the past 20 years, reasonably accurate results for shell stresses are derived by combining the membrane solution with an approximate solution of the bending-theory equations for toroidal shells, instead of attempting to solve the exact differential equations, which is extremely difficult. The developed formulations are applied to various cross-sectional types of toroidal vessels under both uniform pressure and hydrostatic pressure loading, and the accuracy of the formulation is verified in each of the cases through numerical examples with finite-element analysis.

For the buckling considerations, governing stability equations of toroidal shells of any cross-section are presented. These are specialised for the problem of a multi-shell toroid under uniform external pressure, and approximately solved to obtain the critical buckling solution for this geometry. The proposed solution approach provides accurate failure loads of pressurised multi-shell toroids when compared with those from a finite-element analysis. Finite element modelling is then used to study the nonlinear effects on the buckling response, post-bifurcation behaviour and geometric imperfection sensitivity of this type of vessel, as well as two other cross-sectional geometries (parabolic-ogival and circular-elliptic). Extensive parametric studies on each of these toroids reveal significant aspects of shell behaviour.

This thesis represents a significant extension of the work of the group of Prof. Zingoni at the University of Cape Town, and provides much-needed information on the design of new forms of toroidal vessels. The simplified theory developed for the determination of stresses and buckling behaviour has facilitated the investigation of the effects of the various geometric parameters, which in turn has led to new insights on the behaviour of the toroidal shell. It has been found that perfect toroidal vessels under external pressure loading can generally have stable post-buckling behaviour and may, therefore, be able to resist further load beyond the elastic bifurcation loads. The imperfection sensitivity of each of the toroids investigated is seen to vary from shell to shell.

Acknowledgements

Firstly, I would like to thank God, the Almighty, without whom nothing gets done, for His mercies, blessings, and protection throughout this PhD journey.

I am indebted to my PhD supervisor at the University of Cape Town, Prof. Alphose Zingoni, who is an acknowledged authority on shells, for his mentorship on the subject, and constructive criticisms, patience and all-round support during this research work. I would wish to acknowledge with gratitude the financial assistance provided through the Bathe SEMC PhD Scholarship and JW Jagger Centenary Gift Scholarship. This study would have never been possible without the support.

I would like to thank Prof. Jan Błachut of the University of Liverpool, for providing valuable input at the early stages of this research. My thanks also go to Mrs Lydia Zingoni, my PhD supervisor's wife, for her exceptional determination in ensuring my comfort at all times during the study in Cape Town. My gratitude also goes to Prof. Dennis Igbinomwanhia of the University of Benin, Dr Olawale Ifayefunmi of the Technical University of Malaysia Malacca and Dr Yongchang Pu of the University of Newcastle upon Tyne, for their advice at different stages of this research.

I am also grateful to a huge number of people within the University of Cape Town community, for their various aspects of contributing towards the successful completion of this thesis and my enjoyable stay in Cape Town. This includes John Okedi, Enoruwa Obayiuwana, Matongo Kabani, Denis Kalumba, Philemon Arito, Kenny Mudenda, Elly Yelverton, Abdulkadir Ibrahim, Ayesha Dalwai, Isabel Ncube, Sebastian Skatulla, Blessing Ojeme. May God bless you all.

Finally, my deepest gratitude goes to my lovely wife Tina and children Osahon and Ivie, for their sacrifice, patience, understanding and encouragement over the course of this study. I would also like to express my appreciation to Mr Enoghayin Enoma, Mrs Iguodala Rinaldi, Mrs Esohe Nosa, Mr Egberanmwen Enoma, Mrs Adesuwa Aigbe, Mr Osagie Enoma, Mrs Egbe Egharevba, Mrs Ikpomwonsa Egharevba, Mr Osazee Enoma, Mr Precious Owa and other members of my family, for their prayers and support throughout the duration of my studies.

Contents

List of figures

List of tables

Nomenclature

A	Mean radius of a toroidal shell
ϕ	Angular coordinate along a meridian
ϕ_c	Angular coordinate measuring the angle from the upward direction of the local axis $y-y$ round the meridian
ϕ_e	Meridional angle at a shell edge
ϕ_o	Meridional angle at the apex of a toroid
ψ	Meridional angle measured from the shell edge
θ	Angular coordinate along a hoop circle
z	Distance from the middle surface of the shell
s	Cumulative distance travelled clockwise to any point on the surface of the toroid from the apex round the meridional profile
P	A point on the toroidal surface
$Y-Y$	Global axis of revolution
$X-X$	Equatorial line
$y-y$	Centre line (axis) of local cross-section
r_1	First principal radius of curvature at a given point
r_2	Second principal radius of curvature at a given point
R	Horizontal coordinate measuring the distance between the global vertical axis of revolution and a given point
x	Horizontal distance coordinate between any point on the toroidal surface and the local axis
t	Thickness of the shell
E	Young's modulus of elasticity of the shell material
υ	Poisson's ratio
D	Flexural rigidity
$N_\phi,\ N_\theta,\ N_{\phi\theta}$	Meridional, hoop and shearing stress resultants
$M_\phi,\ M_\theta,\ M_{\phi\theta}$	Meridional, hoop and twisting memonets per unit length
$Q_\phi,\ Q_\theta$	Transverse shearing stress resultants

$\sigma_\phi,\ \sigma_\theta,\ \tau_{\phi\theta}$	Meridional, hoop and shearing stresses
$\varepsilon_\phi,\ \varepsilon_\theta,\ \gamma_{\phi\theta}$	Meridional, hoop and shearing strains
$p,\ p_{cr}, p_{bif}, p_{col}$	Uniform, critical, bifurcation and collapse pressures
p_{cr}^{imp}	Critical buckling pressures of imperfect shells
Δ	Modulated imperfection amplitude
γ	Weight per unit volume
$H_e,\ M_e$	Horizontal shear force and bending moment - edge redundants
$p_\phi,\ p_\theta,\ p_r$	Load per unit area of the shell middle surface in the meridional, hoop and normal directions
$u,\ v,\ w$	Displacement components in the direction of the tangent to the hoop circle, meridian, and direction of the normal
$V,\ U,\ W$	Meridional, hoop and normal rotation
$\chi_\phi,\ \chi_\theta,\ \chi_{\phi\theta}$	Middle surface curvature changes and twist
δ	The horizontal (or lateral) displacement quantity
λ	Slenderness parameter
$m,\ n$	Longitudinal and circumferential half waves
$(\ )_0, (\ )_1$	Pre-buckling and incremental terms
Φ	Stress function
λ_r	Toroidal rise ratio

Chapter 1

Introduction

1.1 General introduction

Whenever a load is applied to a structural element, e.g. toroidal shell, a set of internal stresses and strains are induced in the structure. This response is dependent on several features such as the curvature of the shell middle surface and boundary conditions. Failure of the structure will occur when the internal action reaches a certain critical value. Buckling is one of the factors that limits the load carrying capacity of thin-walled shells. Hence, strength and stability behaviour are customarily considered in the design analysis of shells for the purpose of withstanding external loads efficiently and rigidly. This is conducted in the current thesis to provide solution algorithms for toroidal shell forms based on fundamental shell theory, validated numerical modelling and simulations. The proposed solutions facilitate the analysis of conventional and novel toroids, and thereby expand the applicability of shells beyond their traditional remit.

The present chapter starts with a general overview of shells. The discussion is systematically narrowed down to containment shells of revolution and then toroidal shells. The motivation and scope of the research work are discussed before the thesis organisation is outlined at the end of the chapter.

1.2 An overview of shells

A shell is a curved 3-dimensional structural member with one of its dimensions very small compared to the other two. A shell structural element, due to its thinness and curvature, is quite effective in resisting transverse surface loading through the action of internal forces in the tangential plane of the shell's middle surface at any given point, thus minimising the internal shear forces and bending moments. The efficiency of the shell form derives from the presence of membrane stresses as the primary means of resistance to loading. In nature, shells are found

in beautiful creatures like snails, and in eggs. See Figure 1.1 below for some examples of natural shells.

Figure 1.1. Examples of natural shells: egg, snail, tortoise and cockle (from left to right)

The requirement for high strength-to-weight ratio often favours the adoption of shell structures in engineering. Shells find application in elegant bridges, large-span roofs, liquid containment structures, nuclear reactors, piping systems, turbine disks, pressure vessels, bodies of cars & aircraft, missiles, ship hulls, cooling towers, offshore platforms, and many other lightweight structures; examples are given in Figure 1.2.

Figure 1.2. Some man-made shell structures

The behaviour of a shell is usually modelled on the basis of its middle surface, which is the locus of interior points equidistant from the inner and outer surfaces of the shell (Zingoni, 1997). The curvature at any given point on a shell plays a very important role in its behaviour. If the curvature is changed, the shell can have a different load carrying capacity even though the material and thickness remain the same (Błachut & Jaiswal, 1999; Redekop, Xu & Zhang, 1999; Ventsel & Krauthammer, 2001; Chapelle & Bathe, 2011). The thickness of the shell and the boundary and loading conditions also play crucial roles in its behaviour. Structural materials are generally more effective when resisting loads in the extensional mode rather than the flexural mode (Zingoni, 1997). The type of shell surface (synclastic, anticlastic, or developable, see Section 1.2.1) affects the relative proportions of the extensional and flexural effects at a point on the shell's middle surface.

Because of the quest for a high strength-to-weight ratio, shell structures are usually constructed as thin as possible. There is no clear cut-off point between thin and thick shells. However, it is generally accepted that a shell is thin if

$$\frac{r_{\min}}{t} > 20 \qquad (1.1)$$

where t is the thickness of the shell and $r_{\min}$ is the smallest radius of curvature of the middle surface of the shell (Ugural, 1981). Other criteria have been discussed by Zingoni (1997). This thesis is concerned primarily with the analysis of toroidal vessels in the category of 'thin' shells.

Buckling is often the controlling failure mode due to the thinness of the shell (Teng, 1996). Buckling in shells often occurs at very low-stress levels; hence the phenomena are often elastic (Teng & Rotter, 2005). To avoid the possibility of buckling, a shell should be designed in such a way that a dominant part of the structure is in tension. The subject of shell buckling is vast and complex owing to some specific difficulties associated with determining correctly the critical values of loads applied to thin shells. These difficulties are directly linked with a complicated mathematical description of the deformed state of shells and with a diversity of situations at which a shell can buckle (Foroughi et al., 2014).

Structural analysis of loaded shells could be done by using the general equations of the three-dimensional theory of elasticity. However, these equations are quite complicated and in only a

few idealised cases can a solution be achieved (Zingoni, 1997). Therefore the three-dimensional behaviour is approximated by making use of the two-dimensional theory of elasticity and other assumptions to form the classical shell theory (Timoshenko & Woinowsky-Krieger, 1959; Baker et al., 1968; Jasion & Magnucki, 2012). In the linear version of the theory of thin shells, the following Love-Kirchhoff assumptions are made (Zingoni, 1997):

(a) the shell thickness is negligibly small in comparison with the least radius of curvature of the shell middle surface;
(b) strains and displacements that arise within the shell are small;
(c) straight lines that are normal to the middle surface before deformation remain straight and normal to the middle surface during deformation, and experience no change in length; and
(d) the direct stress acting in the direction normal to the shell middle surface is negligible.

Most common shell theories are based on linear assumptions which are quite appropriate for predicting stresses and deformations in shells within the elastic range. The nonlinear theory of elasticity forms the basis for the large-deflection and stability theories of shells. Large-deflection theories are required for investigating buckling and collapse behaviour of shells. The nonlinear shell equations are considerably more difficult to solve even for simple shell profiles. For these reasons, most nonlinear investigations are nowadays carried out with the use of numerical methods. Shell structural analysis has been significantly advanced by the development of the finite element method (Argyris, 1960; Clough, 1990; Bathe, 1996; Zienkiewicz, Taylor & Fox, 2014).

1.2.1 Containment shells of revolution

Containment shell structures are widely used throughout the world for enclosing nuclear reactors, for holding water in the form of elevated tanks, for pressure vessel applications and the storage of petroleum products, chemicals and liquefied gases. Figure 1.3 shows: (a) the model of the German reactor building with containment vessel and interior equipment ("ADINA Tech Briefs…", n.d.); and (b) the ground-level view of the underground coal gasification (UCG) oxygen and nitrogen production plant in Alabama, USA ("Universal Industrial Gases…", n.d.).

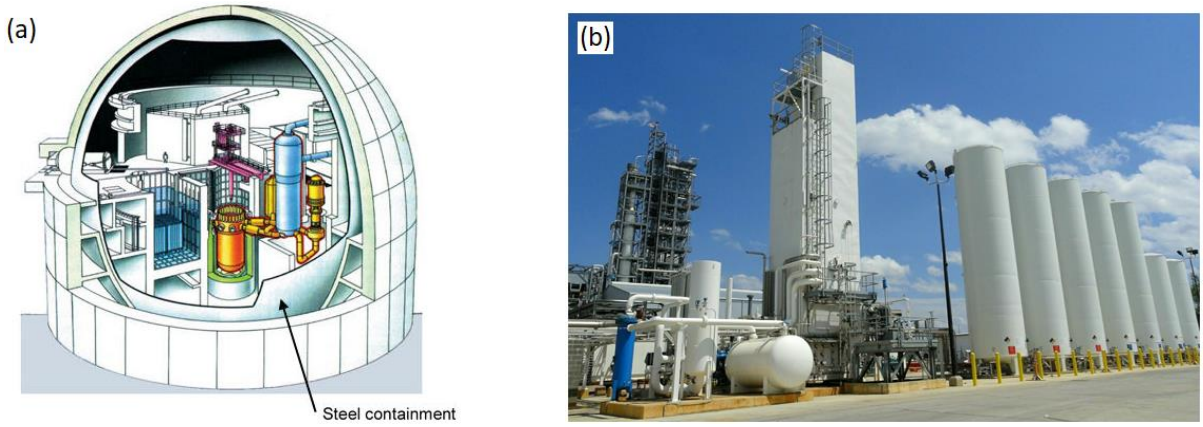

Figure 1.3. Applications of containment shell structures

The commonest class of shell structures for these applications are shells of revolution, where the surface is generated by rotating a plane curve through 360 degrees about an axis of revolution in the plane of the curve. Any given position of the plane curve as it is moved around the axis of revolution constitutes a meridian of the generated surface of revolution. The loading in shells of revolution resulting from the contained fluid is often symmetrical about the axis of revolution.

1.2.1.1 Geometrical considerations of shells of revolution

Following the convention of Zingoni (1997, 2018), it is convenient to regard the axis of revolution of the shell middle surface as vertical, so that the parallel 'circles of latitude' of the shell, which are intersections of the shell middle surface with planes perpendicular to its axis of revolution, lie in horizontal planes. The meridians are generally not parallel, and they lie in vertical planes containing the meridian in question and the vertical axis of revolution of the shell. The planes are inherently referred to as meridional planes. The direction of a tangent to a meridian at a given point on the shell middle surface is called the meridional direction. Hoop circles are the circles of latitude, and the direction of a tangent to a hoop circle is referred to as the hoop direction. Meridians and hoop circles form orthogonal nets of curves on the middle surface of a shell.

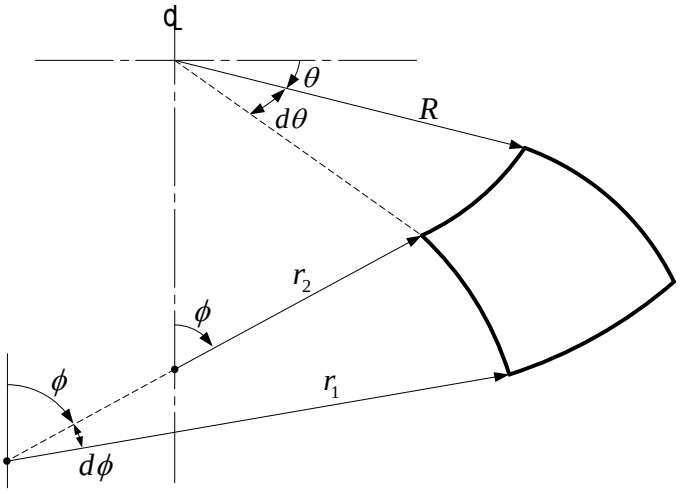

Figure 1.4. The geometry of an elemental shell of revolution

Consider an elemental shell bounded by two adjacent circles of latitude and two adjacent meridians, see Figure 1.4 below. Any position on the shell middle surface can be described by two angular coordinates. These are: the meridional angle ϕ (the angle measured from the axis of revolution of the shell to the normal to the shell middle surface at the point in question); and θ (the angle measured in the horizontal plane of a circle of latitude, defining the position of a given meridional plane relative to some reference meridional plane). The parameter R (the radius of the circle of latitude) whose position is defined by the coordinate ϕ is given by $R = r_2 \sin\phi$.

Also, in Figure 1.4, the parameter r_1 (the maximum radius of curvature), is the principal radius of curvature of the shell middle surface at a given point as seen in the meridional plane. The minimum radius of curvature r_2 is the second principal radius of curvature of the shell middle surface, given by the distance between the point in question and the intercept of the normal to the shell middle surface at that point and the axis of revolution of the shell. The product of the two principal curvatures (the maximum and minimum) at a given point of a curved surface is referred to as the *Gaussian* curvature. This parameter, as earlier mentioned, plays a very important role in the behaviour of a shell.

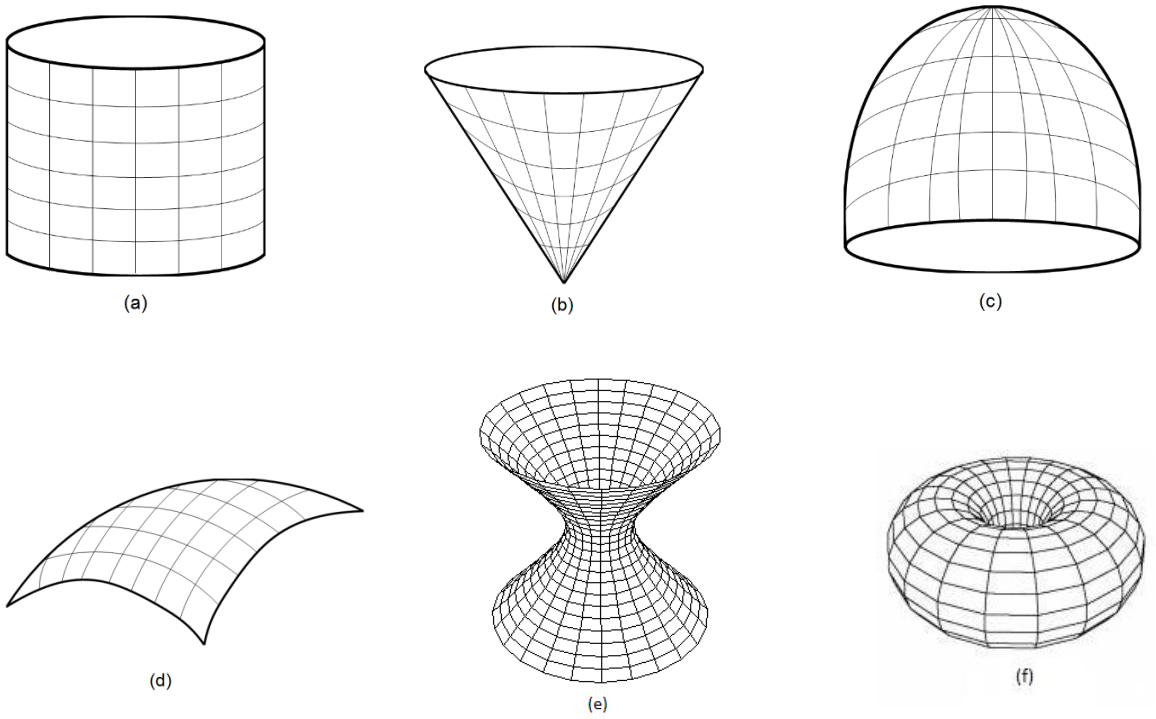

Figure 1.5. Surfaces of shells of revolution

Geometrical classification of containment shells of revolution can be done based on the Gaussian curvature properties of surfaces, see Figure 1.5. Developable surfaces are characterised by zero Gaussian curvature; they can be flattened into a plane surface, either directly or after making a single straight-line cut in the surface. Circular cylinder and cone are examples of developable surfaces (Figure 1.5(a) and (b)). A synclastic surface has a positive Gaussian curvature, the centres of maximum and minimum curvature at a given point lie on the same side of the surface. Paraboloid of revolution and elliptic paraboloid are examples of synclastic surfaces (Figure 1.5(c) and (d)). Anticlastic surfaces possess negative Gaussian curvature, the centres of maximum and minimum curvatures at any given point on the surface lying on opposite sides of the surface. Hyperboloid of revolution is an example of an anticlastic surface (Figure 1.5(e)). A torus (Figure 1.5(f)), is a combination of an anticlastic and a synclastic surface.

1.2.1.2 Classifications of containment shells of revolution

Circular cylindrical, circular conical, toroidal, spherical and ellipsoidal shells are examples of simple geometrical profiles for containment shells of revolution (Figure 1.6).

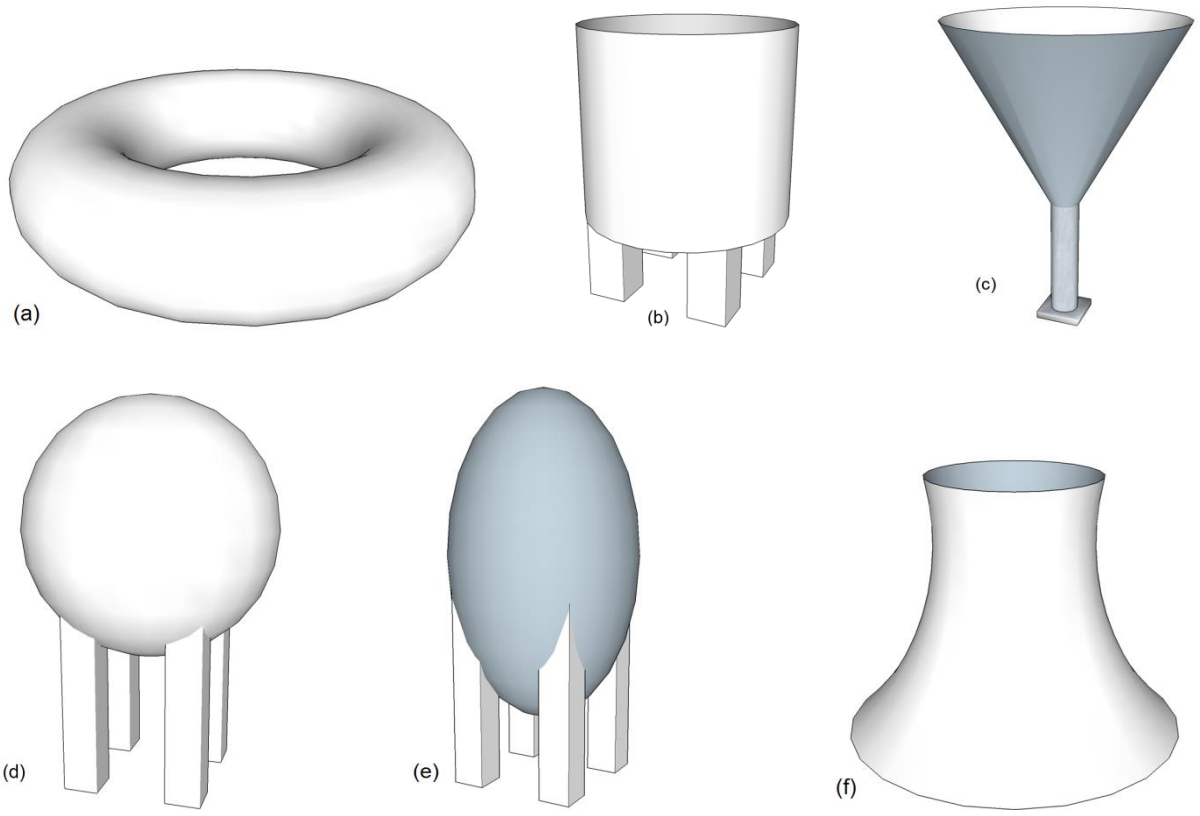

Figure 1.6. Forms of containment shells of revolution: (a) circular toroid; (b) cylindrical; (c) conical; (d) spherical; (e) elliptical, and (f) hyperbolic

Combinations of some of these basic mathematical profiles to form compound shells have been proposed (Zingoni, 2002, 2004; Zingoni, Mokhothu & Enoma, 2015). Jasion & Magnucki (2012) showed that deviations from the conventional cylindrical profile for horizontal liquid-containment vessels could offer enhanced structural efficiencies.

1.3 Toroidal shells

A toroidal shell is a particular type of shell of revolution with a closed cross-sectional profile that does not intersect the axis of revolution. That is, a toroid is generated by the rotation of an arbitrarily closed profile through 360^o about an axis lying outside the profile. If the rotation is incomplete, it is normally referred to as a segmented toroidal shell (typically used in piping systems, among others). Complete toroidal shells, e.g. circular toroids (as earlier shown), belong to the class of doubly curved shells of revolution with a distinctive combination of positive and negative Gaussian curvatures (the outer and inner regions).

The governing equilibrium equations of toroidal shells are more complicated than those of the other common shells of revolution, e.g. cylindrical shells. This is because of the presence of the meeting points of the outer and inner regions in toroidal geometries. For circular and elliptical toroidal shells for examples, the meeting points are at the upper-most and lower-most circles of latitudes of the shells, where the curvatures in one of the principal planes (the minimum radius of curvature r_2) vanish. Hence, it is very difficult to obtain closed-form mathematical solutions that are valid throughout the entire meridian of the cross-section of a toroidal shell of revolution, even for the simplest shapes of cross-sections (e.g. circular) and simplest loading conditions (e.g. uniform pressure).

This difficulty is reflected in the number of investigations that have been carried out on toroidal shells to understand their complex behaviour including buckling, and to establish appropriate design criteria for the shells; there has not been as much progress as for other common shell structures. Most of the studies on toroidal shells have been centred mainly on circular toroids, and to a lesser extent, on elliptical toroids.

1.3.1 Forms of toroidal shells

Toroidal shells are usually classified on the basis of their cross-sectional profiles. They can take almost unlimited cross-sectional forms depending on so many factors like available space, durability, functionality, manufacturability, maintainability and aesthetic concerns. Circular toroidal shell is the most common form of toroidal shells. Figure 1.7 shows some samples of toroidal cross-sections. The distance between the global vertical axis of revolution and the local vertical axis denoted as A in the figures is sometimes referred to as the toroidal mean radius.

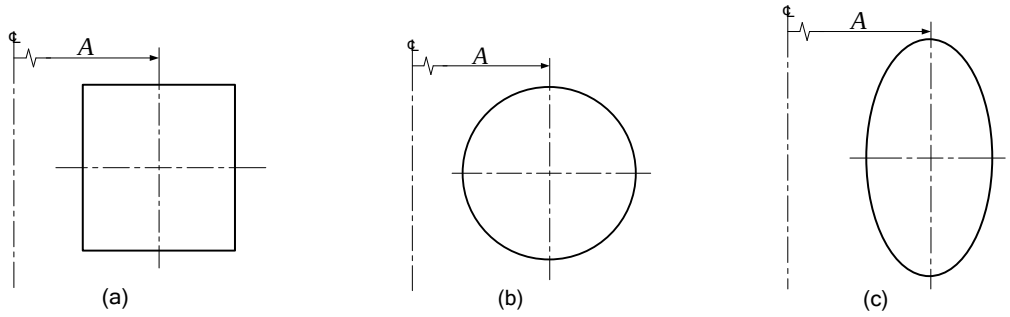

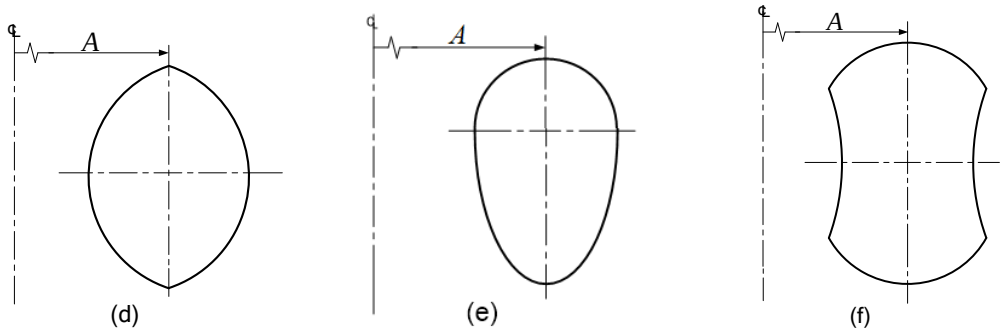

Figure 1.7. Half cross-sectional profiles of some toroidal shell forms: (a) square, (b) circular, (c) elliptical, (d) parabolic-ogival, (e) circular-elliptic compound, and (f) circular-segmented

Figure 1.8. Some applications of toroidal shells

1.3.2 Typical applications of toroidal shells

Complete toroidal shells are mainly used for liquid or gas containment. A picture of the 32m high modern water supply tower with a 3km^3 circular toroidal tank in the form of a donut (torus) of 3m local radius and 14m mean toroidal radius on the Falkland Islands estate in the northern part of Tarnów, Poland ("The tower…", n.d.) is shown in Figure 1.8. To the right of

this, another example of the application of toroidal shell is shown, where a 2.3m diameter toroidal shell is deployed as the floating structure in Brazil's climate monitoring platform on the Prediction and Research Moored Array in the Tropical Atlantic (Campos et al., 2013).

Toroids have also been proposed for nuclear fusion reactors, rocket fuel tanks, medical hyperbaric treatment units and applications in aerospace and underwater fields. Nevertheless, they are not widely used shell structures compared to cylindrical, spherical or conical shells of revolution. This is due to their complex geometries and associated difficulty in manufacturing. It is thus not surprising that there have not been many investigations into the behaviour of this class of shells, and even for the commonest toroids (i.e. circular toroids), designers will find little guidance.

1.3.3 Essential loading on toroidal tanks and vessels

The essential loading on toroidal shells used as liquid or gas vessels is usually symmetrical about the vertical axis of revolution of the shells. When used as toroidal tanks for storing liquids, they are mostly subjected to hydrostatic pressure loading due to the contained liquid. This pressure, which of course varies across the depth of the liquid, acts in the normal direction to the shell-walls. In the case of toroidal pressure (or vacuum) vessels, the essential loading is uniform pressure on the external or internal walls of the toroids. This loading typically acts in the normal direction to the toroidal walls.

It is desirable to design a shell to respond in tension to external loading. If this is not possible and the loading causes compressive stresses within the shell, the shell may deform beyond an allowable limit. It is therefore important to be able to estimate the state of stress and stability behaviour of a loaded toroidal shell.

1.4 Motivation for choice of toroidal form

Deviations from the conventional cylindrical profile for containment vessels may offer enhanced structural efficiencies, and certain functional advantages can be derived from the application of toroidal shells. Furthermore, it is almost possible to employ any cross-sectional profile for toroidal shells. However, information on the structural performance of these shell forms is rare, and even for the commonest toroids (i.e. circular toroids), designers will find little guidance, because the governing equations for toroidal shells are found to be very

cumbersome. Depending on the type of cross-section chosen for a toroid, the stress distribution and stability behaviour can differ quite markedly from one toroidal form to another (Zingoni, Mokhothu & Enoma, 2015). Static and dynamic stability studies of toroidal shells by Błachut (2004) showed that a change of cross-section from circular to elliptical could increase the buckling pressure of a toroidal vessel.

This has spawned interest in the author to explore the double curvature properties and holistically study the strength and buckling response of toroidal shell forms under axisymmetric loading with a fundamental technique.

1.5 The scope of the research work

Despite practical relevance for a wide range of engineering applications of toroidal shells and the possibility of deploying the required cross-sectional profiles, toroidal shell forms are not widely used, and there are not many investigations that have been reported in the open literature on their structural behaviour mainly due to the complexities in the theory of the shells. In lieu of these, the scope of the current research includes the following:

- Examination of the key structural features of elastic toroidal shells of various cross-sections under axisymmetric pressure loadings.
- Development of a platform upon which different cross-sections of toroidal shells of revolution for fluid containment can be analysed, and thereby increase the applicability of the shell type.
- Provision of analytical models for the complete determination of the state of stress and deformations within axisymmetrically loaded toroidal shells, so that the parameters and properties that dictate enhanced structural efficiencies of the shells for a given service condition can be identified.
- Formulation of a stability model for general toroidal shells of revolution; and the presentation of buckling solution for the determination of critical failure loads and mode shapes.
- Computation of buckling characteristics of novel toroidal shell forms under uniform external pressure (see Figure 1.9).
- Examination of the influence of initial geometric imperfections on the buckling behaviour of toroidal shells under applied loads.

- Provision of much-needed knowledge that can help stakeholders within the field of containment shells of revolution to adequately address the problems of buckling and develop new forms of toroidal shells.

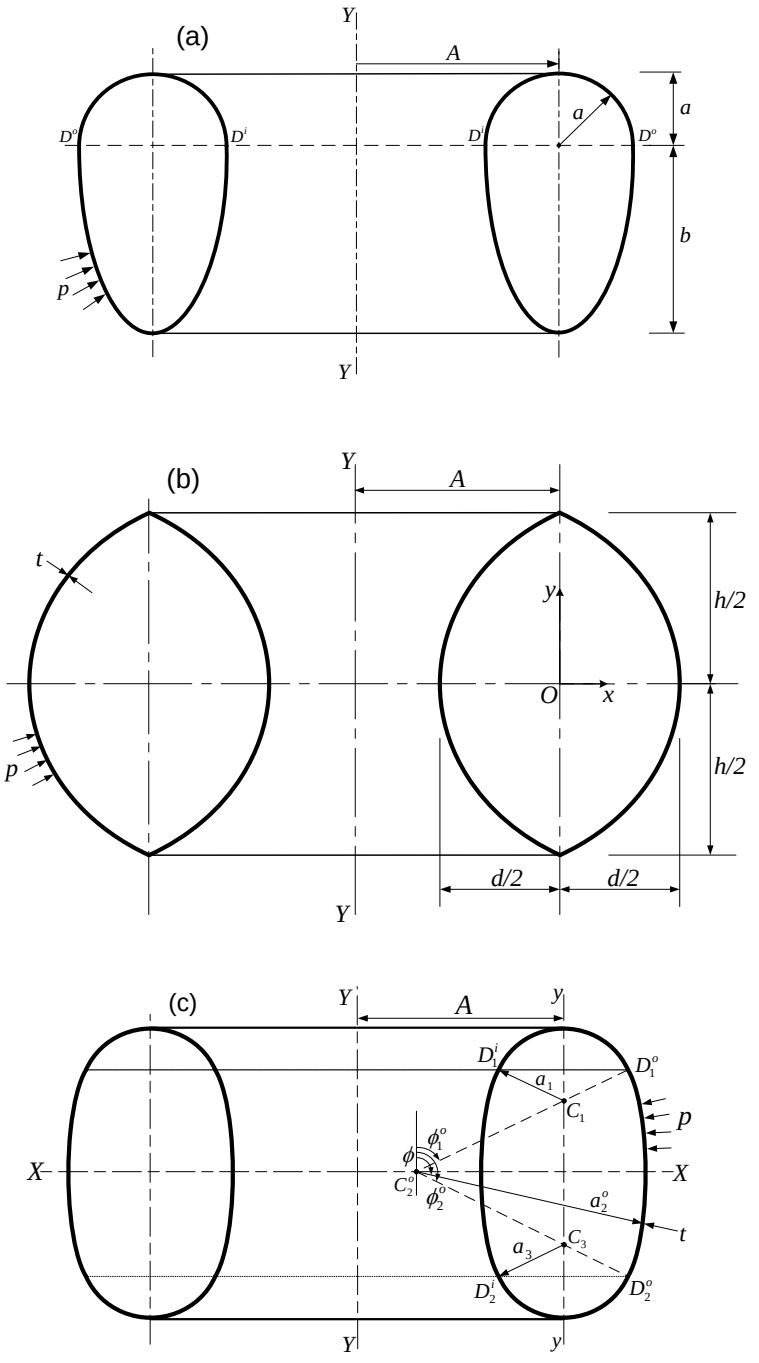

Figure 1.9. Cross-sectional views of toroidal shell with: (a) circular-elliptic compound, (b) parabolic-ogival and (c) multi-segmented circular cross sections

1.6 Limitations of study

This study was limited to:

i. Analytical investigations based on elastic response and resistance to buckling criteria using classical shell theory;
ii. Numerical analyses with ABAQUS and ADINA finite element software packages provided by the Structural Engineering and Mechanics Research Group, University of Cape Town; and
iii. No physical test was carried out in the laboratory environments.

1.7 Outline of thesis

This thesis is presented in eight chapters. The current chapter contains a brief background to the study and provides the scope of the research. An overview of each of the remaining chapters is as follows:

Chapter 2 reviews the literature of previous research into the structural behaviour of loaded toroidal shell forms. It discusses the approaches employed in the investigations and identifies key research findings and gaps in the open literature. The chapter also highlights the significance of the research and the methodology employed.

Chapter 3 provides the governing equations of elastic toroidal shells of revolution that incorporate the two regions - the outer region (extrados) and inner region (intrados) - of the shells, on the basis of linear elastic shell theory.

Chapter 4 introduces a general solution approach for the determination of the membrane state of stress and deformations within a loaded toroidal shell after simplifying and solving the governing equations of chapter 3 by employing the classical approximations of membrane theory of shells. The approach is used to provide membrane solutions for various toroidal shells under axisymmetric loading conditions.

Chapter 5 provides an approximate bending-disturbance solution for toroidal zones where the membrane results of chapter 4 fail. When this is superimposed with the membrane solution (adopted as an approximate integral of the bending-theory equations), the complete stress state

of a toroidal shell is defined. The closed-form stress results permit the parametric studies on the selected toroids.

Chapters 6 and 7 focus on the buckling behaviour of toroidal shells. Chapter 6 presents the stability equations for general toroidal shells of revolution and provides a critical buckling solution for multi-shell toroidal vessels; while Chapter 7 covers the numerical calculations into the buckling response of novel toroidal shells and a study on the influence of initial geometric imperfection sensitivity of the buckling strength of each of the toroidal vessels.

Chapter 8 concludes the thesis by providing a summary of the important findings of the research and suggestions for future studies.

Chapter 2

Literature review

2.1 Introduction

Generally, in comparison with other common shell forms, toroidal shells have not been widely researched. They are barely mentioned in books on shell theory and analysis. Books that give consideration to toroidal shells include the well-known texts of Flügge (1973) and Zingoni (1997, 2018). In a relatively recent review of the strength and stability behaviour of liquid-containment shell structures, Zingoni (2015) also discusses toroidal vessels, among many other shell geometries. The review presented in this chapter mainly covers the studies that have been carried out on static, stability and dynamic behaviour of complete toroidal shells of revolution.

2.2 Static analysis of toroidal shells

Static analysis of shells often embraces two distinct theories that are commonly applied depending on the scope of investigation (Flügge, 1973; Zingoni, 1997, 2018). The first of these, the membrane theory, usually applies to a rather larger part of the entire shell. A membrane is identified as a body of the same shape as the shell which may achieve force equilibrium through the action of in-plane forces alone, but incapable of conveying moments or shear forces. The second, the bending theory, includes the bending effects. This permits the treatment of load or structural discontinuities in the stress distribution taking place in a limited region (Gibson, 1965; Ugural, 1981; Zingoni, 1997; Ventsel & Krauthammer, 2001). The bending theory generally comprises a membrane solution, corrected in those areas in which discontinuity effects are pronounced. The goal is not the improvement of the membrane solution, but rather the analysis of stresses and strains owing to the edge forces or concentrated loadings, which cannot be accomplished by membrane theory only.

For axisymmetrically loaded shells of revolution, the membrane stress resultants: N_ϕ (in the meridional direction) and N_θ (in the hoop direction) are given by the well-known general expressions (Flügge, 1973; Zingoni, 1997)

$$N_\phi = \frac{1}{r_2 \sin^2 \phi}\left[\int r_1 r_2 \left(p_r \cos\phi - p_\phi \sin\phi\right)\sin\phi d\phi + k\right] \tag{2.1a}$$

$$N_\theta = r_2\left(p_r - \frac{N_\phi}{r_1}\right) \tag{2.1a}$$

where r_1 and r_2 are principal radii of curvature of the shell middle surface at the point in question, k is the constant of integration to be determined from an appropriate boundary condition, p_r and p_ϕ are loading components (forces per unit area of the shell surface) normal to the shell middle surface and tangential to the shell meridian respectively. These expressions are based on equilibrium considerations only.

2.2.1 Circular toroids

For a pressurised toroidal shell of revolution with constant thickness (Figure 2.1), $p_r = p$ and $p_\phi = 0$, equations (2.1) give the closed-form membrane solutions:

$$N_\phi^m = \frac{pa}{2}\left\{\frac{2A + a\sin\phi}{A + a\sin\phi}\right\} \tag{2.2a}$$

$$N_\theta^m = \frac{pa}{2} \tag{2.2b}$$

where N_ϕ^m and N_θ^m are the membrane stress resultants in the meridional and hoop directions, respectively, p denotes the uniform pressure applied, and other terms are as defined in Figure 2.1. The principal radii of curvature of the shell are given as

$r_1 = a$, and $r_2 = \dfrac{A + a\sin\phi}{\sin\phi}$.

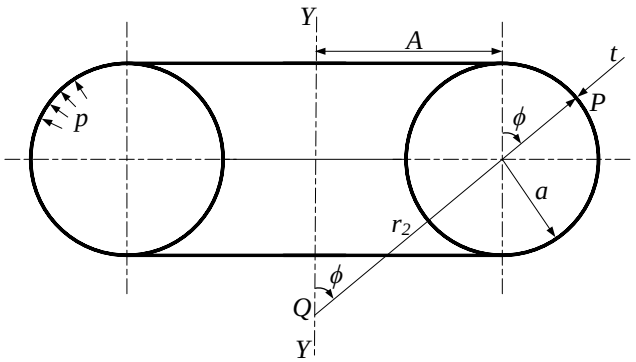

Figure 2.1. Sketch of a pressurised circular toroid

Flügge (1960) indicated that the above membrane solution (equations (2.1)) for pressurized toroidal shells with circular cross-section was first presented by Dean in 1939. He noted that the displacements at the turning points $(\phi = 0,\ \ \pi)$ are discontinuous in the membrane theory and there exists always bending moments which should be taken care of. The localised bending occur around lowermost and uppermost circles of latitude (where the positive and negative Gaussian surfaces of the shell meet), owing to the vanishing of the curvature $1/r_2$ there, as r_2 jumps from $+\infty$ (just within the outer surface) to $-\infty$ (just within the inner surface).

Apart from the membrane solution for circular toroidal shells, approximate bending solutions have also been considered (Zhang, 1949; Clark, 1950; Novozhilov, 1951; Jordan, 1962; Sander & Liepins, 1963; Ming-de, 1985; Sun, 2010a). In the bid to account for the problem of singularities in the linear membrane theory of circular toroids, Zhang (1949) transformed the thin shell equations of Reissner-Meissner into the following Bassel's equation:

$$\frac{d^2w}{dz^2}+\frac{1}{z}\frac{dw}{dz}+\left(1-\frac{1}{9z^2}\right)w=0 \tag{2.3}$$

He obtained the following asymptotic solution for the state of stress of toroidal shells under uniform pressure:

$$w=_{\pm\phi} C_1 J_{1/3}\left(\pm\sqrt{\pm ir_2}\right)+_{\pm\phi} C_1 H^{(1)}_{1/3}\left(\pm\sqrt{\pm ir_2}\right) \tag{2.4}$$

This solution is found not to converge for large opening ratios A/a. Various approaches have been applied by Steele (1965); Clark (1950); Jordan (1962); Sander & Liepins (1963); Novozhilov (1951) and others, in an attempt to obtain an exact solution that is valid for the

complete range $0 \le \phi \le 2\pi$ and all opening ratio A/a. This solution has proved to be very difficult. Most studies were centred on the elastic bending theory of toroidal shell since it was believed that the removal of the inconsistencies in the linear membrane theory of toroidal shells should be possible by the application of linear bending theory (Jordan, 1962). The power series and asymptotic approaches were mainly used to solve the complex variable equation of circular toroidal shells under uniform pressure. The convergence of the series-solution is seen to be good only for large opening ratio A/a, while the convergence of the asymptotic-solution is good only for small opening ratios A/a.

So, for many years, two separate solutions for toroidal shell under axisymmetric loading existed, by the application of linear bending theory: one for small values of A/a and one for large values of A/a. However, in 1986, Zhenhui et al. presented an approximated-asymptotic solution of the complex variable equation of toroidal shells under axial symmetric loading for all values of A/a. They adopted the following complex differential equation of toroidal shell under axisymmetric loading:

$$x_{10}'' + x_{10}\left(i\mu q_1 + q_2\right) = \tau_{10} \tag{2.5}$$

where; $x_{10} = \left(\frac{Q_\phi Ra}{R''} - \frac{Q_0 A^2 a'}{RR''} - i\frac{Et^2}{\sqrt{12\left(1-\nu^2\right)}}V \right)\sqrt{R}$

$$\mu = \sqrt{12\left(1-\nu^2\right)}\frac{a^2}{At}$$

$$q_1 = \frac{\sin\phi}{1+\frac{a}{A}\sin\phi}, \qquad q_2 = -\frac{3}{4}\left(\frac{a}{A}\right)^2\left(\frac{\cos\phi}{1+1+\frac{a}{A}\sin\phi}\right)^2$$

$$\tau_{10} = -\left(3+\nu\right)\rho\varpi^2 ta^3\frac{A}{a}\sqrt{A}\left(1+\frac{a}{A}\sin\phi\right)^{3/2}\cos\phi + \left(\frac{pa^3}{2A} + i\mu Q_0 A\right)\sqrt{A}\left(\frac{\cos\phi}{\left(1+\frac{a}{A}\sin\phi\right)^{3/2}}\right)$$

Q_ϕ is the shear force, Q_0 is the magnitude of Q_ϕ at $\phi = 0$, V is the angular rotation, p is the uniform pressure, ϖ is the angular speed, ρ is the density, υ is the Poisson's ratio, t is the thickness of the shell and all other terms represent their usual meaning. Zhenhui et al. 1986 transformed the above equation into the form:

$$\frac{d^2 W_z}{d\xi^2} + W_z\left(i\mu\xi_z + F_2\right) = \left(\frac{\xi_z}{q_1}\right)^{3/4} \tau_{10} \tag{2.6}$$

where; $\xi_z = \left(\frac{3}{2}\int_0^\phi \sqrt{q_1}\, d\phi\right)^{2/3}$, $x_{10} = \frac{1}{\xi^{,1/2}} W_z$, $F_2 = \frac{5q_1^{,2} - 4q_1 q_1^{,,}}{16 q_1^3}\xi_z - \frac{5}{16\xi^2}\frac{q_2}{q_1}\xi_z$.

When the opening ratio A/a is small, the homogeneous solution of the equation is:

$$W_z = c_1 h_1\left(z_1\right) + c_2 h_2\left(z_1\right) + \mathrm{O}\left(\mu_z^{-1/2}\right) \tag{2.7}$$

where; $z_1 = -i\mu_z^{1/3}\xi_z$, $h_1(z_1)$and $h_2(z_1)$ are Airy functions, $\mathrm{O}\left(\mu_z^{-1/2}\right)$ is the error of the function, and c_1 and c_2 are complex constants which can be found from four boundary conditions. It is seen that as A/a increases, the error also increases. In order to expand the range of applicability of the solution above, Zhenhui et al. let $F_2 = b\xi_z + d + F_2^*$, where F_2^* is the residual error, and b and d are parametric constants to be determined by linear approximation of F_2. They obtained the following homogeneous solution for the transformed equation:

$$W_z\left(z\right) = c_1 h_1\left(z\right) + c_2 h_2\left(z\right) \tag{2.8}$$

where $z = (i\mu_z + b)^{1/3}\xi_z + (i\mu_z + b)^{-2/3} d$. When A/a is small, the influence due to the correction of b and d, the condition that the modulus of $(i\mu_z\xi_z + b\xi_z + d)$ should be much bigger than F_2^* is satisfied. Hence, the adaptability of the solution is expected for all values of A/a.

Similarly, Ruojing (1999) presented higher approximations to the homogeneous solutions for circular toroids. He expressed all the asymptotic expansions for axisymmetric loaded toroidal shells in terms of generalised Airy functions, instead of Bessel or Airy function for the homogeneous and Lommel function for the particular solutions, respectively.

In a different approach, Ming-de (1985) obtained an explicit and closed-form solution for slender $(A/a \to A)$ toroidal shells. He applied the method of integral transform to the Novozhilov's fundamental equations of toroidal shells. From a displacement form governing equations, Sun (2010a) also presented a closed-form solution for a slender toroidal shell under axisymmetric loading. Slender toroids are not very often used in practice. Based on the theory of thin shells (Novozhilov, 1970), Sun obtained the following simplified expressions for slender toroidal shells:

$$N_\phi \approx \frac{Et}{a\left(1-\nu^2\right)}\left(\frac{dv}{d\phi}+w\right), \qquad N_\phi \approx \frac{\nu Et}{a\left(1-\nu^2\right)}\left(\frac{dv}{d\phi}+w\right) \tag{2.9}$$

where $v = C_1\cos\phi + C_2\sin\phi + \int p\left(\xi_s\right)\sin\left(\phi-\xi_s\right)d\xi_s$,

$$w = \frac{a^2\left(1-\nu^2\right)}{Et}\left(C_3 - \int q_1\left(\xi_s\right)d\xi_s\right) + C_1\sin\phi - C_2\cos\phi - \int p\left(\xi_s\right)\cos\left(\phi-\xi_s\right)d\xi_s,$$

$$p\left(\phi\right) = -\frac{q_1 a^2\left(1-\nu^2\right)}{Et} + 2C_3\left(\frac{a}{t}\right)^2\frac{a^2\left(1-\nu^2\right)}{Et}\phi^3 - C_4 - C_5\phi - C_5\phi^2$$

$$-\frac{a^4}{D}\int\left(\phi-\xi_s\right)^2 q_n\left(\xi_s\right)d\xi_s - 12\left(\frac{a}{t}\right)^2\int\left(\phi-\xi_s\right)^3 q_1\left(\xi\right)d\xi_s$$

In equation 2.9, v and w are displacement components, $D = Et^3/12(1-\upsilon^2)$ is the bending stiffness, and $C_i (i = 1,...,6)$ are integration constants to be determined from suitable boundary conditions. Sun applied this solution to find the expansion of a typical thermal compensation device, in which the toroidal shell is used as the expansion mechanism. A similar problem had been independently investigated by Chien (1979) and Dahl (1953), using the complex form equations. They only used the particular solution without deriving the homogeneous solution. Also using the displacement-based toroidal theory, Zhu & Redekop (1995) presented an analytical solution to the problem of a circular toroid subjected to four equally spaced band loads.

Apart from the linear theory, the nonlinear theory has also been used to study circular toroidal shells and to account for the singularities in the linear membrane theory (Reissner, 1963;

Sander & Liepins, 1963; Colbourne & Flügge, 1967; Rossettos & Sanders, 1965). It has been shown generally, that the stresses given by the linear theory are in the limit as ψ_l tends to zero, and for finite ψ_l the stress must be modified by the addition of correction terms. ψ_l is a small dimensionless parameter, defined by the relation $\psi_l = pa/Et$, where E is the Young's modulus, a is the radius of the circular cross-section, p is the internal pressure, and t is the shell thickness.

Sander & Liepins (1963) included the parameter ψ_l in formulating the following nonlinear differential equations of the pressurised circular toroid in equilibrium:

$$\left[RN_\phi\left(\sin\phi+\psi_l\kappa_l\cos\phi\right)\right]' = R\left(\cos\phi+\psi_l\kappa_l\sin\phi\right) \tag{2.10a}$$

$$\left[RN_\phi\left(\cos\phi-\psi_l\kappa_l\sin\phi\right)\right]' - N_\theta = -R\left(\sin\phi+\psi_l\kappa_l\cos\phi\right) \tag{2.10b}$$

where primes denote differentiation with respect to ϕ, and the variables have been made dimensionless or scaled according to the following scheme, bars over quantities indicate the physical or dimensional quantities: $\overline{R} = aR$, $\overline{\kappa} = \psi_l\kappa_l$, $\overline{N}_\phi = paN_\phi$, $\overline{N}_\theta = paN_\theta$, and $\psi_l = pa/Et$. The membrane equations are obtained by setting κ_l equal to zero. The above nonlinear equations are valid for sufficiently thin shell in small strains and rotations. With certain assumptions and simplifications, Sander & Liepins reduced the problem to a solution of differential equations. They exploited methods of asymptotic integration of differential equations based on the assumption that ψ_l is a small parameter, to approximately solve these equations. The stress resultants for a particular geometry was computed and found to compare well with those computed by Jordan (1962).

Reissner (1963) has considered a circular toroidal shell will bending stiffness, and gives conditions under which the nonlinear membrane theory is appropriate. In the particular case when the bending stiffness is zero, his solution reduces to the first-order inner solution of Colbourne & Flügge (1967). Colbourne & Flügge showed that the problem of singularities in the linear membrane theory of pressurised toroidal shells is a singular perturbation one. Based on the consideration of equilibrium of a shell element in its displaced form, they derived non-

linear equations containing the small dimensionless parameter ψ_l. These equations are solved to obtain the inner solutions (valid in the region of the singularity), and the matched asymptotic expansion is used to obtain the outer solutions (valid for the other region).

The above nonlinear membrane theory is only valid for sufficiently thin shell in small strains and rotations. Toroidal pressure vessels sometimes need to have relatively thick walls, for which thin-shell theories are not adequate. The effect of transverse shear deformation becomes important as the shell thickness increases. Modifications to Love's classical shell theory have been made by the inclusion of transverse shear deformation effects (De Silva, 1964; Kutsenko, 1967). Using the linear three-dimensional elasticity theory, Kutsenko (1967) investigated the state of stress and strain of a thick-walled toroidal shell under internal uniform pressure loading. A constant thickness circular toroid under small displacements was considered and represented as a Fourier series of an infinite system. The numerical computations indicated that convergence of the solution is improved both with decreasing A/a and with increasing thickness of the toroidal shell.

Murthy & Kiusalaas (1966) studied a different aspect and showed theoretically that very small changes in the meridian profile of circular toroids could mean the difference between the validity and invalidity of the linear membrane solution. They analytically presented a bending-free meridian of a toroidal shell with a constant thickness and stated that with the linear membrane theory, appropriate values of stresses and displacements could be obtained for the bending-free toroidal shell under uniform pressure without resorting to non-linear or bending theories. Because of the manufacturing difficulties associated with the proposed meridian profile, Murthy & Kiusalaas work was not taken further.

Using the Ogden's three-term strain energy function, Li & Steigmann (1995) investigated the axisymmetric deformation of a pressurised isotropic, rubber-like solid toroid. They formulated the equations that describe axisymmetric equilibrium deformations of the pressurised elastic membrane incorporating the associated wrinkling. These equations are solved using a fourth-order Runge Kutta scheme.

2.2.2 Elliptical toroids

The behaviour of elliptic toroidal shells has also been studied (De Silva, 1964; Sutcliffe, 1971; Zingoni, 1997, 2018; Chernyshenko & Maksimyuk, 2000). The sketch in Figure 2.2 shows the

geometrical parameters of the shell. The closed-form membrane solution of an elliptical toroidal shell subjected to a uniform pressure has been presented by Zingoni (1997, 2018):

$$N_\phi = \frac{pa^2}{\left(a^2\sin^2\phi + b^2\cos^2\phi\right)^{1/2}}\left[\frac{A\left(a^2\sin^2\phi + b^2\cos^2\phi\right)^{1/2} + \dfrac{a^2}{2}\sin\phi}{A\left(a^2\sin^2\phi + b^2\cos^2\phi\right)^{1/2} + a^2\sin\phi}\right] \tag{2.11a}$$

$$N_\theta = \frac{pa^2}{b^2}\left[A\left(\frac{b^2-a^2}{a}\right)\sin\phi + \frac{b^2 - \dfrac{1}{2}\left(a^2\sin^2\phi + b^2\cos^2\phi\right)}{\left(a^2\sin^2\phi + b^2\cos^2\phi\right)^{1/2}}\right] \tag{2.11b}$$

As in the case of pressurised circular toroidal shells, the membrane result of elliptical toroids does not fully predict the stress state around the uppermost and lowermost circles of latitude of the shell, where the positive and negative Gaussian curvature meet. De Silva (1964) had shown that the failure rate of the membrane theory increases as the wall thickness of the shell increases since the effect of transverse shear deformation will become important. He used the asymptotic solution approach to solve the Naghdi's governing equations, in an attempt to quantify the deformation in loaded elliptic toroidal shells. For $b = a$, the solution was found to coincide with that of Clark (1950) for a circular toroidal shell.

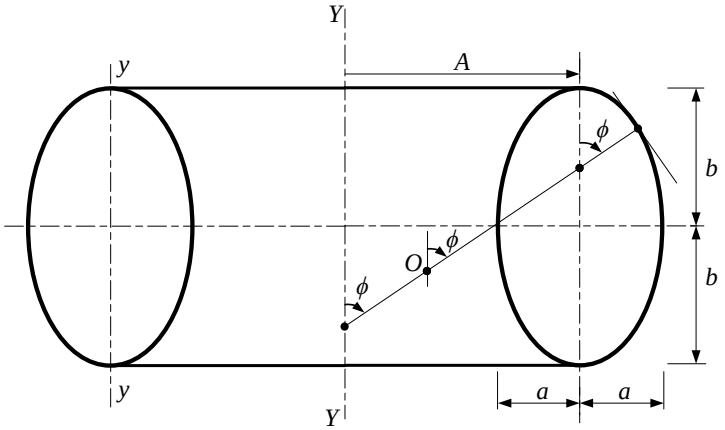

Figure 2.2. Sketch of a pressurised elliptic toroid

Using the Runge-Kutta procedure, Sutcliffe (1971) numerically solved the six first-order differential equations of elliptical toroids obtained from the equations of Timoshenko & Woinowsky-Krieger (1987). The shells are assumed to be subjected to uniform internal

pressure. Sutcliffe found out that, in comparison to the circular toroids, the bending stresses in elliptical toroids are higher. Numerical calculations have also been presented for elliptical toroids made of a nonlinear elastic material (Chernyshenko & Maksimyuk, 2000).

For the bending-related stresses and deformed shape in the vicinity of the equatorial regions of axisymmetrically loaded elliptic toroids, Zingoni, Enoma & Govender (2015) provided simplified closed-form results for the shell type. The fourth-order governing differential equations of the shell are presented and solved on the basis of the Geckeler approximation (Zingoni, 1997). A generalized form of the solution approach for toroidal shells with an arbitrary cross-sectional profile will be developed in Chapter 5 of this thesis.

2.2.3 Ovaloid toroidal tanks

Non-linear structural analyses of ovaloid cross-sectional toroidal tanks of the type used for containing liquid petroleum gas in motor vehicles and a flying platform have been conducted independently by Velickovic (2007) and Cristian & Marcel (2010) respectively with the use of the finite element method. Their analyses did not cover the presence of nozzle in the toroidal tanks. Zhan & Redekop (2009) used the ADINA FE tool to obtain a three-dimensional finite element solution for the linear analysis of a pressurised ovaloid toroidal tank with a circular nozzle, see Figure 2.3.

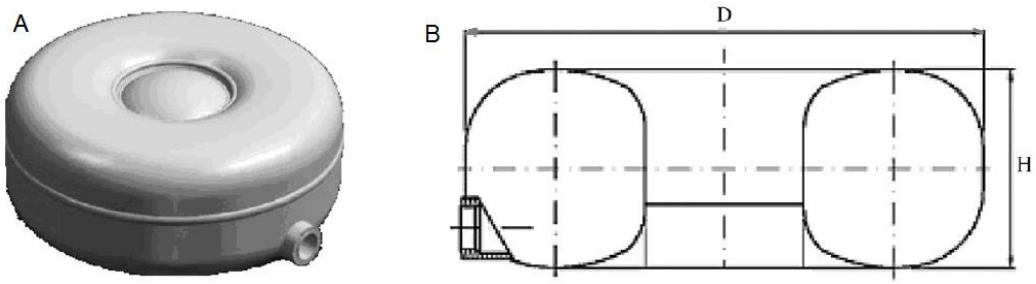

Figure 2.3. Ovaloid toroidal tank with a nozzle at the extrados: (A) view of the fabricated tank; and (B) cross-sectional view showing outside diameter D, total height H. (Zhan & Redekop, 2009)

Zhan & Redekop performed a parametric study of the effect of nozzle location and geometric parameters on the stress concentration and behaviour of the ovaloid toroidal tank. The results showed that the stress concentration factor values vary greatly with nozzle size and thickness, but slightly with the nozzle length; and that the values of stress concentration factor are lower

when the nozzle is placed at the extrados rather than the intrados. They also analysed an ovaloid toroidal tank impacted at the extrados by a flat-nosed projectile. The obtained displacement results using the finite element method were similar to those of equivalent circular toroidal or cylindrical shells.

2.3 Buckling of toroidal shells

Compressive stresses are often experienced in particular areas of a loaded toroidal shell. The effect of a given basic load and/or an imposition of an external force on a toroidal shell in equilibrium results in some deformation, which may or may not vanish upon removal of the loads. In the first case, the equilibrium is stable, while it is unstable in the second. At sufficiently low values of the basic load the equilibrium will be stable, but when the basic load is increased above a critical value, the equilibrium becomes unstable, any insignificant load giving rise to large, permanent deformations. Buckling - a change in configuration is said to occur, and it may lead to the failure of the shell (Bickell & Ruiz, 1967; Flügge, 1973; Calladine, 2007).

Typically, a shell under gradually increasing compressive stresses would deform as shown in Figure 2.4 (Flügge, 1973). The ordinate is a dimensionless representation of the load *P* and the quantity ε in the abscissa is the overall compressive strain of the shell. The perfect shell curve OABD consists of the stable equilibrium branches OA and BD, and the unstable equilibrium branch AB. At the bifurcation point A (upper critical load) there is no equilibrium available except on the right branch BD of the curve, and the diagram point must jump in the direction of the horizontal arrows to a new, buckled and stable configuration of equilibrium at point C on branch BD. This sudden transition from the initial configuration of equilibrium to the buckled configuration of equilibrium is termed as snap-through buckling (Flügge, 1973; Ventsel & Krauthammer, 2001; Singer, Arbocz & Weller, 2002). This why unlike columns and plates, shells usually have a very unstable post-buckling behaviour that strongly influences their buckling characteristics. The behaviour of a real shell with geometric and other imperfections is represented by the dashed curve.

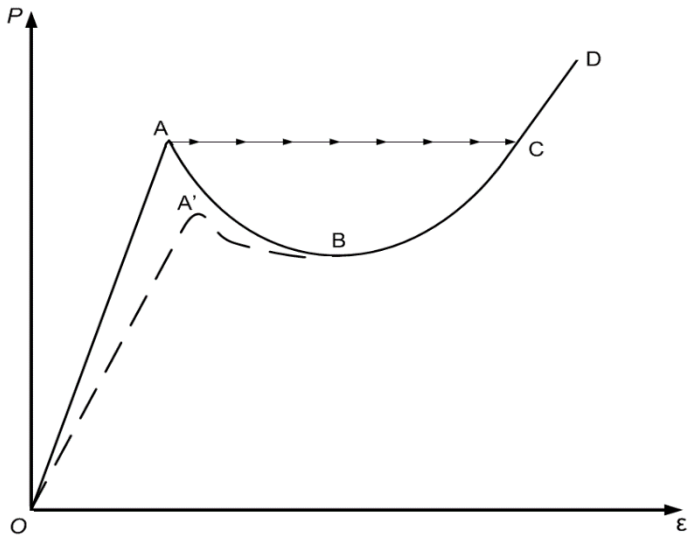

Figure 2.4. Load-deformation curve for a perfect and imperfect shell structure.

In Figure 2.4, the load at point B (lower critical load) on the curve is the largest load up to which the initial configuration of equilibrium of the shell remains stable with respect to both infinitesimal and finite disturbances (Ventsel & Krauthammer, 2001). The exact and analytical solution of the lower critical load is usually obtained by numerical methods because of the complexities involved in solving the geometrically nonlinear equations of the state of the shell, while that of the upper critical load can be obtained using the linear stability differential equations. The critical buckling load of the real shell (point A') is between the upper and lower critical loads of the perfect shell. Its value is greatly influenced by the degree of imperfections and irregularities in the shell which are again very difficult to measure.

Buckling is particularly important in shell structures because it often occurs without any obvious warning and can have catastrophic effects. It is usually the decisive criterion in the design of shell structures such as containment vessels and storage tanks operating under vacuum or, in general, under external pressure. In thick-walled vessels, the critical pressure for the elastic buckling often exceeds the value required to initiate yielding and plastic instability then becomes the design criterion. The classical theory of buckling of thin shells is essentially based on Love's linear differential equations, which were derived assuming that the deflections of the shell were small (Bickell & Ruiz, 1967). For this reason, one would expect that the theory will not be applicable to the study of the post-buckling behaviour of the shell, due to the large deflections that occur.

2.3.1 Buckling of circular toroids

The most common loading that may cause buckling of circular toroidal shells is external pressure, which has indeed been the subject of many theoretical and a few experimental studies. According to the account of Sobel & Flügge (1967), Machnig in the early sixties was the first to investigate the bifurcation buckling of circular toroidal shells under uniform external pressure and predicted that axially symmetric buckling modes give a smaller critical pressure when compared to the asymmetric buckling mode. Machnig used a perturbation technique to solve a system of partial differential equations governing the asymmetric buckling mode. A year later, Koiter (1964) indicated that asymmetric buckling modes may well result in smaller buckling pressures for some values of the shell's geometric parameters and that Machnig's power series expansion must break down for toroidal shells with small opening values of A/a (Van der Heijden, 2009). In 1965, some numerical results obtained by Jordan (1965) were considerably lower than those obtained by Machnig. Jordan performed an asymptotic analysis of an axially symmetric collapse of a pressurised toroidal shell and applied axial loads at the equators. Buckling was assumed to occur at that value of the external pressure for which the stiffness of the toroidal shell vanishes.

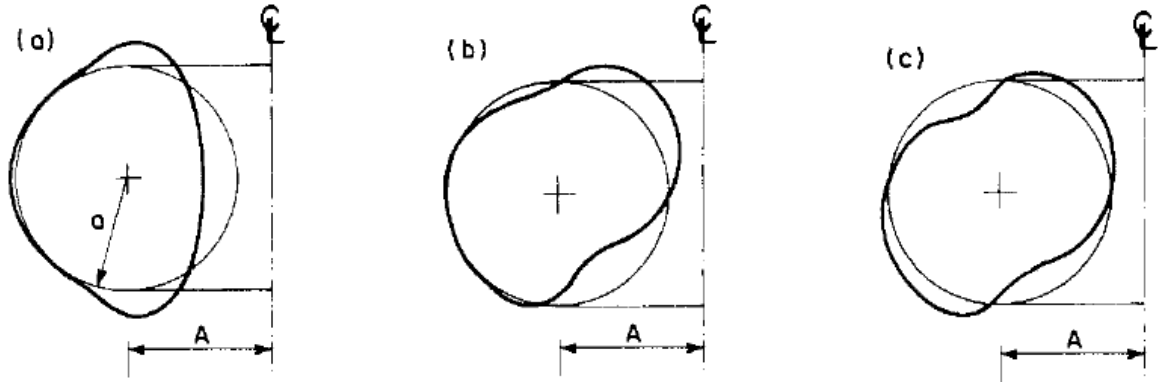

Figure 2.5. Toroidal shell buckling mode shapes predicted by Sobel & Flügge (1967): (a) asymmetric mode A with $n=2$, (symmetric about equatorial line); (b) asymmetric mode B with $n=2$, (antisymmetric about equatorial line); and (c) axisymmetric mode B with $n=0$, (antisymmetric about equatorial line), where n is the number of circumferential lobes or waves into which the shell buckles or collapses

Sobel & Flügge (1967) carried out a complete analysis and introduced an analytical solution using the series expansions for the displacement components to solve the stability equations

for toroidal shells under external pressure. They also conducted experiments at the Lockheed Missiles & Space Company with three slender $(A/a = 8.0)$ steel toroidal shells with a circular cross-section, and compared results with the theoretical predictions of buckling pressures and found the agreement to be within 10%. It was showed that toroidal shell could buckle in two modes: (i) symmetric about the equatorial line, called mode A, and (ii) antisymmetric about the equatorial line, mode B (see Figure 2.5). They can be either axisymmetric or asymmetric, and the critical pressures corresponding to each of the modes are always close. For the axisymmetric buckling mode, mode B yields lower buckling pressure than mode A, whereas for asymmetric buckling modes, mode B usually results in slightly lower pressures (Singer, Arbocz & Weller, 2002).

The axisymmetric form of stability loss by a circular toroid under uniform external pressure on the basis of linear formulation has been considered by Kosheleva (1967). She solved the ensuing displacements terms in the differential equations of the perturbed state of the shell with the well-established Bubnov-Galerkin method, and obtained the critical pressure parameters of the toroid. Hutchinson (1967) investigated the initial post-buckling behaviour and associated imperfection-sensitivity of toroidal shell segments (the outer and inner surfaces over which the Gaussian curvatures are positive and negative respectively were considered separately, see Figure 2.6). The segments were subjected to several loading conditions, and the study was based on the framework of Koiter's general theory of initial post-buckling behaviour (Van der Heijden, 2009).

Figure 2.6. Toroidal segments: (A) outer (synclastic); and (B) inner (anticlastic) surfaces

Because it was not certain whether the good correlation obtained between the test and theory for slender toroids in (Sobel & Flügge, 1967) could also be maintained for relatively non-slender toroids, experiments were conducted on non-slender $(A/a = 2.0)$ toroidal shells by Almroth, Sobel & Hunter (1969). They manufactured the toroidal shell specimens by casting an epoxy resin in two halves, which were glued together by an adhesive resulting to a very high

modulus but also brittle material. External pressure was being applied by partial evacuation of the air in the specimens. Because of the brittleness of the specimens, they shattered at buckling, and one could not observe their pre-buckling and post-buckling behaviours. However, when a very ductile epoxy material was used, it was observed that the experimental buckling pressures were within a few percents of the theoretical predictions. As shown theoretically, axisymmetric buckling mode was first seen before the non-symmetrical buckling mode appeared as the load was increased, see Figure 2.7.

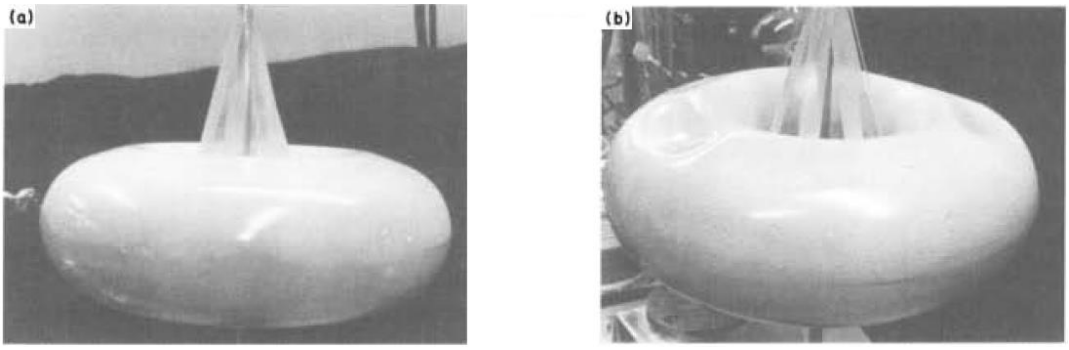

Figure 2.7. Buckling patterns of the toroidal shell under external pressure: (a) axisymmetric; and (b) nonsymmetric (Almroth, Sobel & Hunter, 1969)

As part of a study on the behaviour of a toroidal shell as an underwater structure in the late sixties, a meticulous report was presented by Fishlowitz (1970) on the experimental investigation of elastic buckling behaviour of toroidal shells. A plastic formed by the mixture of equal parts by weight of Veramid 140 polyamide resin and Epon 828 resin was used as the specimen because of its high ratio of the limit of proportionality to Young's modulus. The specimens were instrumented by dozens of strain gages, each on their outer surface and loaded accordingly. The arrangement allowed visual and photographic observation during the test, which facilitated determination of the buckling mode shapes. The measured strains at collapse were elastic in all the models, indicating that they failed by elastic instability. The Southwell method was used to calculate the collapse pressure from the experimental strain data.

Similarly, three series of experiments on pressurised toroidal shells were conducted by Fedosov (1969); Fedosov (1971); Fedosov (1977) in the U.S.S.R. Some of the toroidal specimens were fabricated from aluminium alloy steel and some from stainless steel with variable thickness. The specimens were tested under uniform hydrostatic loading and some under air loading; and in a special reinforced chamber, supported elastically at the outer equatorial circumference of

the torus and in the later tests at both inner and outer equators. In-line with (Jordan, 1965), Fedosov (1977) pointed out that the final deflected shape of a toroid is influenced by an axial force resulting from the weight of the shell and its manner of support. Some of the shells buckled in an axisymmetric mode and some in an asymmetric one. In all the tests the wave formation was most pronounced in the neighbourhood of the poles with buckling occurring in an abrupt snap-through, see Figure 2.7.

Jordan (1973) used the asymptotic formula reported in Jordan (1965):

$$p_{cr} = 0.1738E\left[\frac{t^7}{a^5A^2\left(1-v^2\right)^2}\right]^{1/3} \tag{2.12}$$

where p_{cr} is the buckling pressure and other terms represent their usual meaning, to predict buckling in an axially symmetric and equatorially antisymmetric mode, with associated critical pressure values. The buckling pressures predicted by the formula were found to agree favourably with toroidal shell collapse pressures obtained experimentally in (Fishlowitz, 1970) but appeared to be on the conservative side for small opening ratio A/a. Based on the Sanders shell theory, Wang & Zhang (1991) formulated equations of the axisymmetric deformation of toroidal shells subjected to external hydrostatic pressure and embedded these, using FORTRAN, into a computer program for calculating the critical buckling parameters of circular toroids. They also investigated the post-buckling behaviour of toroidal shells. The results agreed with the experimental results obtained in (Fishlowitz, 1970). Considering nanotorus as a continuum model, Sun (2010b) formulated and presented an algorithm of obtaining the closed-form solution for the instability problem of a slender $(A/a \to A)$ toroidal shell (nanotorus) embedded in an elastic medium. This study is based on the displacement form of the governing equations for toroidal shells.

2.3.2 Buckling of elliptical toroids

A toroidal shell with elliptical cross-section under loading condition behaves differently when compared to a corresponding circular toroidal shell. Galletly & Blachut (1995) used BOSOR 5 to calculate the buckling pressure of circular toroidal shells and compared results with available experimental data to ascertain the accuracy of the computer program. They used the program to investigate both buckling pressures and modes for various geometries of externally

pressurised complete elliptical toroidal shells. It was concluded that depending on the aspect ratio b/a, see Figure 2.2, the buckling pressures of the elliptical toroids can be larger or smaller than those of the corresponding circular toroids, and that this has to be verified experimentally.

During the late nineties, In the absence of toroidal shell buckling experimental data for verification, Galletly (1998) employed BOSOR and INCA shell buckling programs to predict that perfect toroidal shells of elliptical cross-section would buckle when subjected to internal pressure, and presented the buckling pressures of various elliptical toroids for a wide range of geometrical parameters. This was extended by Combescure& Galletly (1999) to cover the effect of non-axisymmetric initial geometric imperfections in toroidal shells and concluded that the imperfections have minimal effect on the buckling pressures of elliptical toroids. Similarly, numerical analysis was carried out on toroidal shells with circular and elliptical cross-sections under external step pressure by Błachut & Jaiswal (1999). They showed that both toroidal shells with circular and elliptical cross-sections failed by indirect snapping and that the corresponding dynamic pressures are marginally larger than static bifurcation loads. Blachut & Jaiswal (2000) also presented new results from a numerically conducted parametric survey on the elastic and elastic-plastic buckling of perfect and imperfect toroidal shells with circular and elliptical cross-sections under external pressures for different geometries and material properties.

2.3.3 Buckling of ovaloid toroids

Using the finite element method, Zhan & Redekop (2008) investigated the buckling behaviour of a toroidal shell with an ovaloid cross-section, see Figure 2.3. They found from a parametric study that the wall thickness of a perfect ovaloid toroidal tank has a higher influence on the buckling pressure than the boundary conditions, and that plastic collapse would occur at a much lower pressure than buckling.

2.3.4 Buckling of stiffened toroids

Linearized buckling study of perfect circular toroidal shells with various meridional ring stiffeners and supports on equatorial lines has been carried out using the FEM by Wang et al. (2006). New results of critical buckling pressures were computed for shells with varying ring (stiffener) properties, a variable number of stiffeners, and for different conditions of equatorial line support. The shells were assumed to be loaded with uniform external pressure. The results

show that the shells produce higher buckling pressure when they are stiffened and that the use of inner and outer equatorial line supports has a significant effect on the buckling pressure. It was also showed that a favourable distribution of the reinforcement weight could be determined from a finite element analysis.

2.3.4.1 Buckling of orthotropic toroids

Continuous fibres can be oriented to match the direction and magnitude of stresses in a laminated light-weight structure, leading to optimal structural performance (Zu, Koussios & Beukers, 2010). These have contributed to its extensive utilisation in the construction of high-pressure composite toroidal vessels. Buckling analysis of composite toroidal shells has mostly been investigated numerically. Panagiotopoulos (1985) presented a finite element procedure for determining the stability behaviour of the toroidal shell under external hydrostatic pressure. This is based on the rotationally symmetric, doubly-curved finite element developed by Navaratna et al. (1968) and the assumption that the pre-buckling state can be adequately described by first-order terms. He concluded that that buckling parameters could be obtained for toroidal shells of laminated construction and with geometrical complexities such as windows, hatches and non-uniform shell thickness with the finite element procedure.

In contribution towards the design of a more efficient underwater pressure hull, Błachut (2004) numerically investigated and presented results of (i) the effect of boundary conditions on the load carrying capacity, (ii) the effect of constant versus variable wall thickness, (iii) the effect of lamination stacking versus geometrical parameters on the bifurcation buckling and first ply failure of externally pressurized carbon fibre reinforced plastic (CFRP) toroids, and (iv) the effect of moving from circular to elliptical cross-sections.

Redekop (2005) derived the general equations which enable the prediction of the buckling characteristics of orthotropic toroids under normal pressure based on the linearised Sanders–Budiansky buckling theory. He obtained numerical results using the differential quadrature method for complete isotropic circular toroids; and carried out a parametric study for both completely free shells and shells with circumferential line restraints. He established that the addition of restraints to orthotropic toroids does not always lead to an increase in the buckling pressure. Khazaeinejad et al. (2010) also numerically obtained new results of buckling

pressures and modes for various geometry and material constituents of functionally graded (composite) toroidal shells of circular cross-section under external uniform pressure.

2.4 Vibration of toroidal shells

Vibration motions which are time-dependent are set up in a shell whenever it is disturbed from a position of stable equilibrium. If these motions occur in the absence of external loads, they are called free vibration; but are referred to as forced vibration if the motions are set up by time-dependent external loads. Because the toroidal shell is made up of an infinite number of mass particles, when it is set into motion it possesses an infinite number of degrees of freedom. Its response is analysed into an infinite number of periodic motions which are referred to as its normal modes of free vibration. Each of these normal modes has an associated natural frequency of free vibration (Kraus, 1967; Calladine, 2007; Zingoni, 2015b). As shown by Zingoni (2015b), symmetry (including axisymmetric of shells of revolution) bestows certain peculiarities in vibration behaviours (e.g. coincident modes), which are best studied using the mathematics of group theory.

It is important to understand the free-vibration characteristics and to ascertain the natural frequencies of toroidal shells in order to avoid the destructive effect of resonance with nearby rotating or oscillating equipment. Majority of toroidal shells vibration studies have been geared toward the free-vibration analysis of toroidal shells with the solution of a homogeneous system of partial differential equations with homogeneous boundary conditions.

2.4.1 Unstiffened toroids

Liepins (1965) studied the free vibration of a pre-stressed toroidal shell using the finite difference method. Gavelya & Kononenko (1974) used the Green matrices to present an algorithm for the calculation of natural frequencies and mode shapes of circular toroidal shells. They also noted that, independently of the method of initial perturbation (using the positive, zero or negative Gaussian curvature), the extremal values of the membrane stresses and moments in the toroidal shell are reached close to the line where the sign of the Gaussian curvature changes.

Based on Love's first approximate theory that was written as a coupled set of first order differential equations, Yamada et al. (1989) analysed the free vibration of a toroidal shell with

an elliptical cross-section, in which the transfer matrix approach (Goldberg, Bogdanoff & Marcus, 1960) is used. They obtained the frequency equations in terms of the elements of the matrix, and numerically calculated the natural frequencies and mode shapes for the toroidal shell with an elliptic cross-section. Kosawada et al. (1985) presented a dynamic analysis of a free vibrating toroidal shell with a circular cross-section. The vibration equations were derived by imposing the stationary conditions of the Lagrangian energetic functions. These equations were solved using a power series expansion procedure. The method was expanded for thicker shells (Kosawada, Suzuki & Takahashi, 1986). In the late eighties, Pomares & Durlofsky (1988) used the finite element method to study the dynamic characteristics of a stainless steel toroidal shell which serves as a protective device of a nuclear fuel container during transportation. The continued incremental loading applied in the analyses using the LIBRA code, corresponded to an impact of an infinite rigid plane oriented normal to the drop direction vector. The results compared well with those in literature.

Based on the theory of elasticity, Jiang & Redekop (2002) adopted the governing equations of McGill & Lenzen (1967) to investigate and formulate the problem of polar axisymmetric vibrations of circular toroids. They used the differential quadrature method to obtain the natural polar axisymmetric frequencies of isotropic toroidal shells with arbitrary uniform thickness. The vibration of a solid axisymmetric toroidal shell was studied by Zhou et al. (2002) using the energy method. They presented an analysis that is based upon solving the equations of three-dimensional elasticity in toroidal coordinates. Vibration analysis of an inflated torus was presented by Jha et al. (2002) whereby the Galerkin method was used to obtain a solution. Wang& Redekop (2005) derived the general equations which enable the prediction of the vibration characteristics of orthotropic toroidal shells based on the Sanders-Budiansky shell theory; and obtained numerical results of natural frequencies and mode shapes for a circular toroid using the differential quadrature method. Xu & Redekop (2006) carried out a similar analysis on an orthotropic thin toroidal shell of elliptical cross-section.

Using the finite element method, Zhan & Redekop (2008) found from a parametric study that the natural frequencies are strongly dependent on the size and thickness of an ovaloid toroidal tank; and that in comparison with the material properties, the type of support has a more significant effect on the natural frequencies of an ovaloid toroid. The free vibration of thick-walled toroidal shells was studied using a finite element analysis based on the dyadic methods of elasticity by Buchanan & Liu (2005). With certain assumptions, they formulated three-

dimensional equations of elasticity in toroidal coordinates and a corresponding finite element model. The numerical results for natural frequencies and mode shapes obtained were compared with existing solutions. A study on vibration has been carried out for moderately thick circular toroidal shells by Wang & Redekop (2011) considering shear deformation effect. They adopted a shear deformation theory and used the differential quadrature method to obtain the natural frequencies with mode shapes.

Tizzi (2015) numerically investigated the dynamic behaviour of composite toroidal shells with non-uniform thickness, based on modified thin shell theory with transverse shear terms. He developed the expressions for the eigenvalue problem with the use of double trigonometric series expansions and obtained the natural frequencies and mode shapes of the toroid with an appropriate algorithm.

2.4.2 Stiffened toroids

Using the matrix method, Balderes & Armenakas (1973) studied the free vibration of ring-stiffened toroidal shells by applying the Love–Reissner shell theory. The shell parameters were expanded in Fourier series in the meridian direction, and the governing equations were numerically integrated in the circumferential direction with the Runge–Kutta method.

Wang et al. (2006) carried out a parametric study on the free vibration of circular toroidal shells under uniform pressure for various meridional ring stiffeners and supported on equatorial lines using the FEM. They obtained results for shells with a variable number of stiffeners and concluded that the fundamental frequency increases when a shell is stiffened, and the frequency increases with an increase in the number of stiffeners. The frequencies are greatly increased in the presence of ‘rigid’ stiffeners, or equatorial lines of support. They noted that the second circumferential harmonic dominates the motion of the stiffened shells.

2.5 Minimum weight design of toroidal shells

Aside from the full account of the stress field, the reduction of toroidal shell mass also plays a significant role in the design of toroidal shells for liquid or gas containment. An optimal weight design relies on the most efficient distribution of shell thickness and stresses around the cross-section of a toroid, in order to maximise the structural performance. A circular toroidal shell with constant thickness and loaded internally with uniform pressure will theoretically fail at

the innermost circle of latitude (i.e. at the location $\phi = 3\pi/2$, see Figure 2.1), while the strength of the other parts is yet to be completely utilised. This mode of failure has been demonstrated below with a simple FE analysis.

Linear finite-element analyses of circular toroids made of $0.05m$ thick mild steel with $200GPa$ Young's modulus and 0.3 Poisson's ratio were performed for various toroidal opening ratios A/a using Abaqus. A $1Pa$ internal pressure loading was assumed, and no boundary condition was required due to the axisymmetric nature of the loading and geometry. Three-node quadratic axisymmetric shell elements (SAX2) with a suitable mesh size were used for the models.

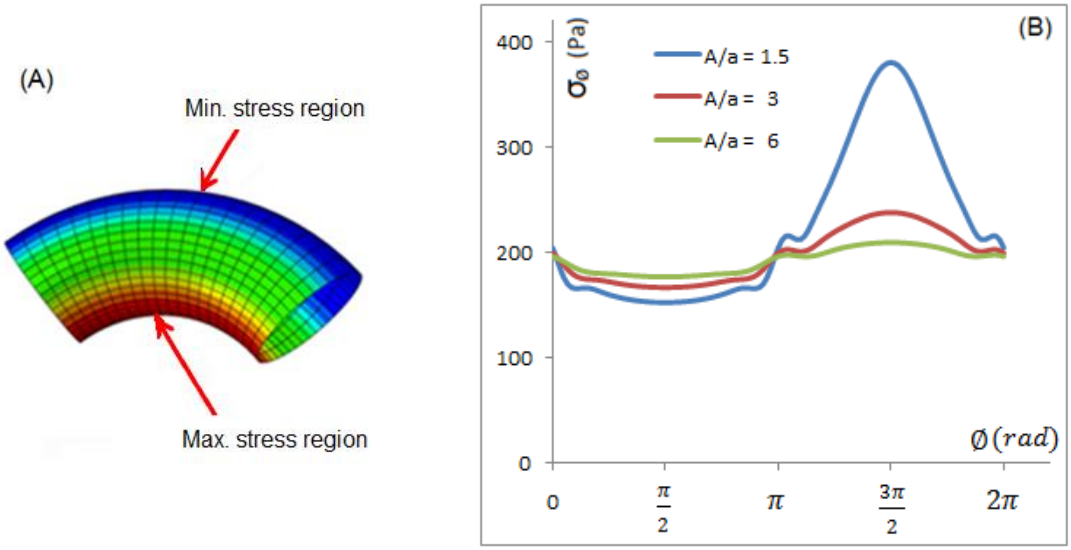

Figure 2.8. (A) Simple FE model of the circular toroid, (B) distribution of meridional stress along the meridian of pressurised circular toroids for various opening ratios A/a, $a/t = 191$.

The results are shown in Figure 2.8. On the plot of the meridional stresses, σ_ϕ versus ϕ, it can be seen that the maximum meridional stresses are experienced in the region of the inner circle of latitude (i.e. at location $\phi = 3\pi/2$). Similar analyses were carried out on toroidal shells with an elliptic cross-section for various ratios $A/(a+b)$, see Figure 2.2. In line with (Sutcliffe, 1971), it is noticed that the stress distribution and behaviour of elliptical toroids are totally different from that of circular toroids. Higher bending disturbances are experienced at $\phi = 0$ and π but the meridional stresses at $\phi = \pi/2$ and $3\pi/2$ are almost the same for all cases of the elliptical toroids, see Figure 2.9.

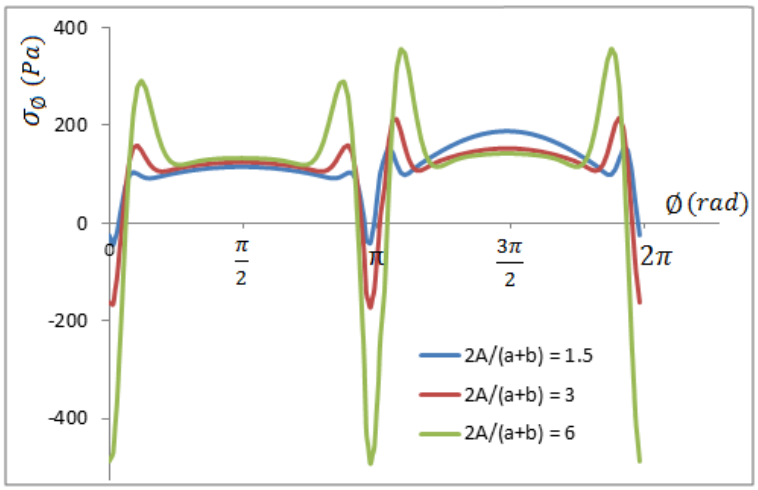

Figure 2.9. Distribution of meridional stress along the meridian of pressurised $b/a = 2.0$ elliptic toroids for various ratios $A/(a+b)$

The tendency for a pressurised circular toroid to fail around the innermost equatorial plane increases as the opening ratio A/a reduces. This mode of failure has been verified experimentally by Vu & Blachut (2009), see Figure 2.10. Wall thickness variation around the circular cross-section is therefore required to provide uniform stress distribution and reduce the toroid weight. A considerable number of researches have been devoted to the design and manufacturing of circular toroidal tanks, with optimal distribution of shell thickness and stresses around the cross-section. Most of these studies have been on orthotropic composite materials; interested reader may see the references in Zu, Koussios & Beukers (2010).

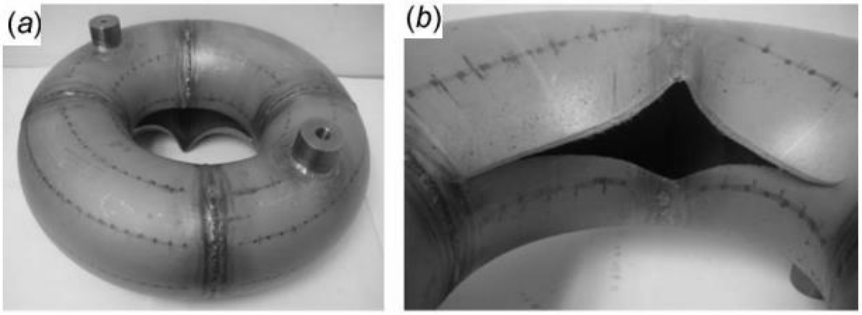

Figure 2.10. (a) Burst shape, and (b) burst position of a toroid assembled from four butt-welded 90 deg elbows (Vu & Błachut, 2009).

In 1965, Steele and later in 1967, Colbourne & Flügge investigated the stresses in thin toroidal shells under internal pressure and found that the maximum stress occurs in the centre of the concave part of the toroid. Steele (1965) studied the volumetric and mass efficiencies of

toroidal pressure vessels with different types of the cross-section. The Tresca yield condition was used as the criterion for finding the minimum weight and the best ratio of contained volume to weight of internally pressurised toroids. He found out that deviations from circular cross-sections caused large decreases in structural performance and concluded that for practical purposes, circular cross-sections produced the lowest mass for constant and variable wall thicknesses. Bogomol'nyl & Zhidyaev (1992) presented the formula for estimating the required variable thickness to reduce the total mass and retain the strength of a circular toroid:

$$t_{(\phi)} = \frac{pa}{2\sigma_{\phi(\max)}}\left(\frac{2A + a\sin\phi}{A + a\sin\phi}\right) \tag{2.13}$$

where $t_{(\phi)}$ is the variable wall thickness, A, a, and ϕ are toroidal parameters as shown in Figure 2.1, and for all values of ϕ, $\sigma_{\phi(\max)} = pa(2A+a)/2t(A+a)$ = constant. This formula is based on the condition for equal meridional stresses in the toroid. They pointed out that the relative decrease in mass together with other factors is mainly a function of one parameter, the toroid mean radius A, and that it is difficult to manufacture a toroid with a wall thickness varying according to the presented formula. A similar approach was adopted by Vu (2013) to fine the optimal shape of circular toroidal shells. His work was based on the distribution of wall thickness along the circular meridian so that Mises stress is constant across the entire cross-section of the circular toroids. In this way, the entire shell under internal pressure will theoretically reach plasticity at the same time, and therefore the toroidal shell weight will be reduced.

Based on the simultaneous use of the first yield pressure, plastic pressure, plastic instability pressure and the contained volume as constraints, Vu (2010) carried out an extensive investigation of minimum weight design for toroidal shell by utilising the Differential Evolution and Particle Swarm Optimization methods. The optimal cross-section is formed from four halves of quadratic curves and the material saving gained from the optimal cross-section can go up to 72% depending on the available manufacturing capabilities. He discovered that elliptical profiles resulted in most material saving, but circular cross-sections with thickness variation were the best balance between material saving and manufacturability; and that the material saving with loading constraint of the fully elastic state is significantly larger than that of elasto-plastic state.

2.6 Summary of literature review

- Studies into the behaviour of toroidal shells of revolution are very few. The structural analyses of shells have been carried out using experimental, analytical and numerical methods. Owing to the high cost often associated with testing, since the early seventies, most of the studies have been based on analytical and numerical methods. Because of the toroidal geometry and the difficulties in obtaining an exact analytical solution and the inherent complications in the analytical formulations of toroidal shell problems, most studies are nowadays completed with the use of numerical methods. This trend has also been reflected in the studies that have been carried out on the vibration of toroidal shells.
- Like the experimental methods, analytical approaches for analysing toroidal shells seem to be going into extinction. More complex numerical simulations are becoming possible, but their impacts on engineering practice are yet very small. Empirical 'knock-down' factors are still primarily relied on in the design of shell structures (Singer, Arbocz & Weller, 2002). A general calculation-based strength prediction method is needed for designers. Analytical solutions are very valuable as they provide more insight into the variation of stresses and strains with the basic shape and property changes, and deeper understanding of the physical behaviour under an applied loading (Zingoni, 1997, 2018). They can also provide the basis for incisively evaluating the results of numerical methods through quantitative comparisons and order-of-magnitude bounds.
- In theory, it is possible to construct a toroidal shell with almost any kind of mathematical closed-profile as the cross-section. Depending on the type of cross-section chosen for the toroid, the stress distribution and stability behaviour can differ quite markedly from one toroidal form to another (Zingoni, Mokhothu & Enoma, 2015). Generally, applications and analysis of toroidal shells of revolution have been mainly centred on toroidal shells with a circular cross-section. There are increasing requirements for the use of toroidal shells with other cross-sectional profile for fluid containment (Redekop, 2005). Hence, the investigation of the behaviour of other toroidal shell forms is needed.
- The most common loading that may cause buckling of circular toroidal shells is external pressure, which has indeed been the subject of many studies on toroidal shells, while

plastic collapse is usually the case for internally pressurised circular toroidal shells. It is not clear if there has been any study on the behaviour of toroidal shells of revolution in consideration of the hydrostatical effects of the internally contained liquid.

- Circular cross-sections with wall thickness variations seem to be the best trade-off between light weighting and manufacturability compared to the elliptical or slight change in the circular cross-sectional profile of toroidal shell of revolution.

2.7 Statement of Research

The main objective of this study is to propose simplified models that could help stakeholders within the field of containment shells of revolution to adequately analyse the response of loaded elastic toroidal shells of any cross-section, with the aim of increasing the applicability of the toroidal shell form. The thesis also sought to generate new knowledge and provide the following sub-objectives that would facilitate the design and development of new toroidal shell forms that are fit for purpose, through the investigation of toroids using classical shell theory in conjunction with an appropriate solution and numerical modelling approaches:

- To develop closed-form solutions for the complete determination of the state of stress and deformation within toroidal vessels of interest;
- To develop simple rules for predicting the buckling characteristics of toroidal vessels under relevant loading conditions;
- Specifically, to investigate and understand the key structural features of each of the following toroidal shell forms under uniform and hydrostatic pressure:
    i. Circular toroids
    ii. Elliptic toroids
    iii. Circular-elliptic toroids
    iv. Parabolic ogival toroids
    v. Multi-shell toroids

2.8 Justification of the research

Toroidal shells offer immense potential application to industries, but unfortunately, information on the structural behaviour of these shell forms is rare, and even for the commonest toroids (i.e. circular toroids), designers will find little guidance. Furthermore, apart from the

structural efficiency and certain functional advantages that can be derived from the application of the shell form, a toroidal shell can be constructed to take any required cross-sectional profile in view of available space. Therefore, there is a need for a justifiably simple means of analysing and designing any toroidal shell form since the structural behaviour of toroids can differ quite markedly from one toroidal form to another. Analytical solution approaches are highly favoured in the design analysis of shell structures, but the theory-equations of toroidal shell geometries are found to be extremely complicated and very difficult to solve. This has contributed to the few investigations that have been reported on the shell type compared to other common shells of revolution and has hindered the design and development of the shell form for wider adoption in engineering applications. The present study aims to bridge this gap by generating a better understanding of the structural behaviour of toroidal vessels, as well as providing some guidance on design.

2.9 Research questions

As part of the effort towards providing usable information for analysts and designers, the following are some of the research questions that this thesis will seek to answer:

- Can the simplified mathematical approach developed for shells of revolution by Zingoni (1997) be extended to the problem of toroidal shells of arbitrary geometry?
- Based on Geckeler's approximations, is it possible to develop an approximate bending solution that can be valid even for the anticlastic surface of the toroidal shell?
- Can closed-form stress and deformation solutions be found for various toroidal shell forms?
- Is it possible to develop simplified buckling formulae for estimating critical buckling load and mode shapes for these toroidal forms?
- What are the key geometrical parameters that affect the strength and buckling response of a toroidal shell under certain loading?
- Can the information generated from this research help in design and analysis, thus increasing the applicability of toroidal shells?

2.10 Methodologies

Two broad aspects of structural analysis will be conducted in this thesis for toroidal shell forms. In the first aspect, which involves the analysis of the state of stress in loaded toroids, linear theory-equations for general toroidal shells on the basis of the theory of thin-shells of revolution (Flügge, 1973), will be presented. These equations are extremely complicated and difficult to solve. However, a simplified mathematical solution approach will be used to approximately solve the equations and determine the stresses in toroidal shells. The general approach will be similar to that adopted in the studies of Zingoni (1991, 1997, 2001a,b, 2002, 2009, 2018) and Zingoni & Pavlović (1991a,b, 1992, 1993a,b), where the membrane solution is used in regions away from discontinuities, and used in combination with a simplified bending theory to account for net stresses around the discontinuities. The difference here is that the formulations will be specialized to the particular geometries of the toroidal types in question, and the particular loading situations of interest for these types of toroidal shells.

For the buckling analysis of toroidal shells, an analytical approach and numerical modelling using finite element (FE) method will be employed. The general governing equations of stability for shells of revolution (Flügge & Sobel, 1965) will be presented and specialised for toroidal shells of any cross-sectional form. The equations will be simplified and approximately solved for a novel multi-shell toroidal vessel under external pressure, using the Galerkin's scheme to obtain an analytical algorithm for the determination of critical buckling pressures of the vessel. Numerical results from the proposed analytical approach will be compared with those from a finite element method solution. The finite element modelling will then be used to study the non-linear effects on buckling response, post-bifurcation behaviour and geometric imperfection sensitivity of the pressurise multi-shell toroid and other new toroidal vessels.

Chapter 3

Governing equations for toroidal shells of revolution

3.1 Introduction

Conventional approaches of analysing shells of revolution have proven not to be completely amenable to toroidal shells (even for the simplest (circular) cross-section) owing mainly to the fact that toroids consist of two regions - the outer region (extrados) and inner region (intrados), and their meeting points - that make them different from the other common shells of revolution. The equations for toroidal shells are found to be cumbersome, and it is generally quite difficult to obtain closed-form mathematical solutions that are valid throughout the entire meridian of the cross-section of the toroidal shells. Hence, the investigation of these shell forms and their adoption in practical applications have been very rare despite the associated intrinsic functional and structural advantages (Galletly & Błachut, 1995; Redekop, 2005; Sun, 2010). In this chapter, a formulation of the governing equations of a toroidal shell of revolution that incorporates the two regions of the shell is presented from the fundamentals of elastic shell theory. This set of equations, which include the equilibrium, kinematic (strain-displacement relations), and constitutive equations, forms the springboard for each of the next three chapters of this thesis. The procedure followed, and the associated assumptions adopted in the development of the equations are not entirely new. Historical developments of the theory of thin shells may be seen in the work of Zingoni (1997, 2018).

In the present chapter, the underlying approximations of the theory of thin elastic shells and some other assumptions adopted here are first given. This is followed by a detailed description of the geometrical parameters of a complete toroidal shell of an arbitrary cross-session before the derivations of partial differential equations of equilibrium and elastic law that relates the stresses and displacements in the toroidal shell. The chapter ends with some concluding remarks.

3.2 Basic assumptions

In the formulation of the governing equations of a toroidal shell, the basic thin-shell assumptions of Love-Kirchhoff as described in Chapter 2, and summarised below are employed:

(a) the shell thickness is negligibly small in comparison with the least radius of curvature of the shell middle surface;
(b) strains and displacements that arise within the shell are small;
(c) straight lines that are normal to the middle surface before deformation remain straight and normal to the middle surface during deformation, and experience no change in length; and
(d) the direct stress acting in the direction normal to the shell middle surface is negligible.

With the application of these approximations, the toroidal shell problem that is ordinarily supposed to be a three-dimensional shell problem is reduced to a two-dimensional problem, so that its middle surface could fully describe the shell element. The shell is assumed to be thin. Hence, in the following derivation, the ratio of the thickness of the shell to the minimum radius of curvature at a reference point on the middle surface of the shell is neglected owing to the assumption that the thickness ratios of toroidal shells under present consideration are less than 1/20 (Novozhilov, 1970). This ratio is, of course, small in comparison with unity, and it has been found that a large number of shells encountered in practical applications are within this thinness range.

Apart from the above Love-Kirchhoff simplifications, it is also assumed that the material of the toroidal shell considered in the development of the governing equations is homogeneous, isotropic and elastic. In addition to this, temperature effects are neglected in the formulations. In what follows in the next section, the geometry of an arbitrary toroidal shell is described.

3.3 Geometrical preliminaries

The relevant geometrical parameters of a toroidal shell of revolution are shown in the diagrams in Figure 3.1. This is consistent with the convention usually adopted in the literature (Flügge, 1973; Zingoni, 1997, 2018). The surface of the shell is generated by rotating an arbitrary closed curve in three-dimensional space through a complete circle about a vertical axis of revolution

$Y-Y$ lying outside the plane curve, at a distance of A from the local vertical axis $y-y$ of the generator curve. A is often called the mean radius of a toroidal shell with a cross-sectional profile that is symmetrical about the local vertical axis. Initial points on the rotated profile move through 360^o and form parallel circles of latitude (or *hoop circles*) in the horizontal plane of the toroidal shell. The generator curve is referred to as the *meridian* of the toroidal surface at any given point during the rotation. Typical of a surface of revolution, the meridians and hoop circles form an orthogonal net (or lines of principal curvature) on the toroidal shell middle surface with each of the meridians appearing at a constant angular coordinate θ along a hoop circle and each of the parallel circles appearing at a constant angular coordinate ϕ along a meridian (refer to Figure 3.1(b)). Accordingly, the position of any point P on the toroidal middle surface is determined by the intersection of a meridian and a hoop circle, where ϕ and θ act as the coordinates. The direction of a tangent to a meridian at a given point on the toroidal shell middle surface is referred to as the meridional direction, while the direction of a tangent to a hoop circle is referred to as the hoop direction.

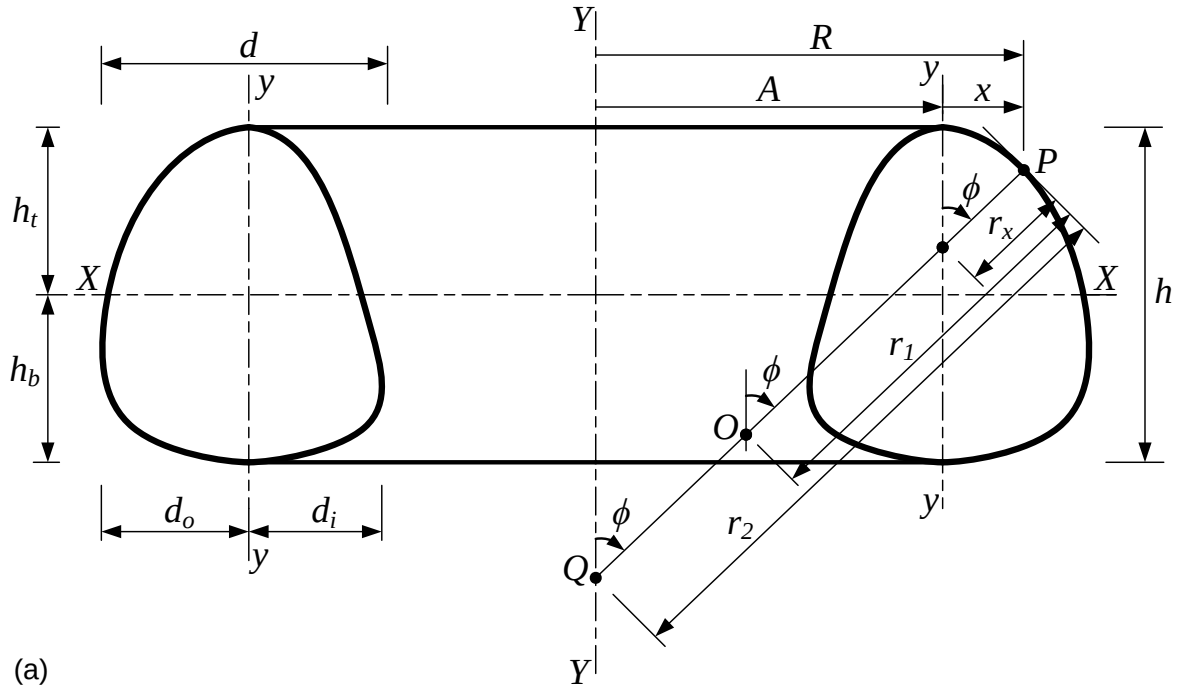

(a)

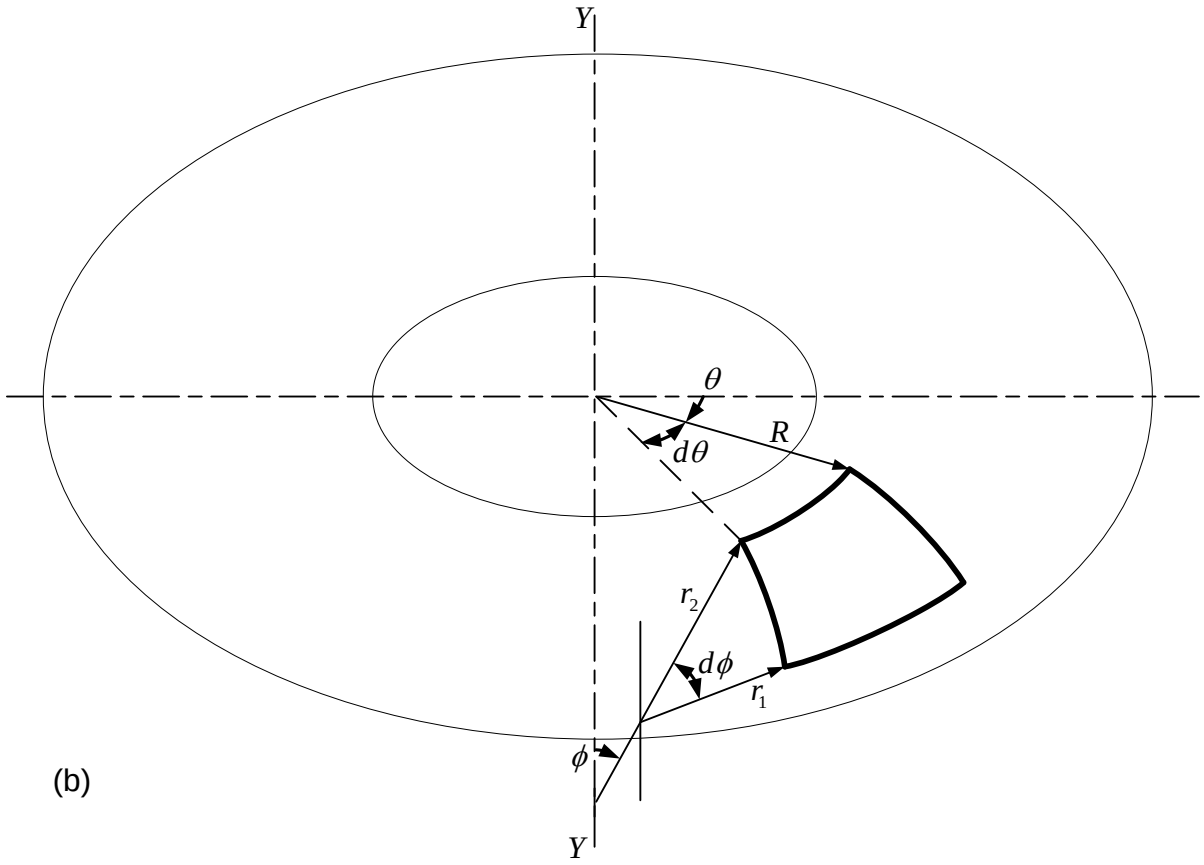

Figure 3.1. The geometry of a toroidal shell with an arbitrary cross section: (a) cross-sectional view; and (b) sketch of an element

For a closed and complete toroidal shell of revolution under investigation in this thesis, it is convenient to measure the angle ϕ from the upward direction of the global axis of revolution $Y-Y$ of the toroid to the normal to the shell middle surface at any point P. With this, two points on the toroidal shell exist for one value of ϕ: one in the outer region (extrados) and the other in the inner region (intrados) of the toroidal vessel. To distinguish between these two points, and by reference to the cross-section on the right of the global axis of revolution $Y-Y$, locations on the right of the local $y-y$ axis will be referred to as the "outer region" of the vessel, while locations to the left of $y-y$ axis will be referred to as the "inner region" of the vessel. In mathematical terms, and typical of the commonest (circular) toroidal surface, the outer region is of positive Gaussian curvatures, while the inner region is of negative Gaussian curvatures, where Gaussian curvature is the product of the two principal curvatures at any given point on the surface (Novozhilov, 1964; Kraus, 1967; Zingoni, 1997; Ventsel & Krauthammer, 2001; Blaauwendraad & Hoefakker, 2014).

At any point P on the toroidal middle surface, there exist one maximum and one minimum radii of curvature, which occur in planes that are perpendicular to each other. These are: r_1, the first principal radius of curvature of the toroidal surface at that point as seen in the meridional plane, (i.e. r_1 is the actual radius of curvature of the local profile at any point P in question); r_2, the second principal radius of curvature of the toroidal shell middle surface, given by the distance of a normal intercept at any reference point on the shell middle surface to the global axis of revolution $Y-Y$ of the toroidal shell, (i.e. r_2 is equal to the distance PQ). Hence, the two principal radii of curvature, r_1 and r_2 may be used to characterise an arbitrary point on the middle surface of a toroidal shell of revolution.

The first principal radius of curvature r_1 which is equal to the distance PO in Figure 3.1(a), must be taken as negative if it appears on the side of the toroidal shell middle surface that is opposite to the global axis of revolution of the toroidal shell. This is usually the case for r_1 in the inner region (intrados) of toroidal shells. For example, r_1 is taken to be negative for any point in the inner region of a toroidal shell with a circular cross-sectional profile, since the Gaussian curvature is negative in this region of the torus. Note also that for a circular toroidal shell, the point O in Figure 3.1(a) coincides with the centre of the circular cross-section of the shell.

It can be seen in Figure 3.1(a) that the second principal radius of curvature r_2 is related to the horizontal coordinate R measuring the distance between the global vertical axis of revolution $Y-Y$ and a given point P on the middle surface of the toroidal shell by

$$r_2 = \frac{R}{\sin\phi} \tag{0.1}$$

The radius R of the horizontal circle of latitude through point P of a complete toroidal surface which is made up of an outer region (extrados) and an inner region (intrados) (a characteristic feature of a complete toroidal shell that makes it different from other common shells of revolution, like the spherical and cylindrical shells), may be defined as

$$R = A + x \tag{0.2}$$

where x denotes the horizontal distance coordinate between any point P on the toroidal surface and the local axis $y-y$ of the cross-sectional profile, is expressed as

$$x = x_o$$

at the outer region of the toroid, and

$$x = -x_i$$

at the inner region of the toroid. Hence, for points at the inner region (intrados), x is taken to be negative. A, which denotes the distance between the vertical axis of revolution $Y-Y$ and the local vertical axis $y-y$, is greater than the horizontal distance coordinate between any point P at the inner region (intrados) of the toroidal shell and the local axis $y-y$ of the cross-section, (that is $A > x_i$). This, of course, is due to the fact that the meridional curve does not touch the global axis of revolution of the toroidal shell that has been considered here.

The total height of the toroidal shell is denoted by $h\ (= h_t + h_b)$, where distance above and below the axis $X-X$ are h_t and h_b, respectively. The total width of the local cross-section along the axis $X-X$ of the toroidal shell is denoted by $d\ (= d_o + d_i)$, where the values of x along the axis $X-X$ are d_o and d_i, respectively, in the outer and inner regions of the toroidal shell. The distance of a normal intercept at any reference point on the shell middle surface to the local axis $y-y$ of the toroidal shell is denoted by r_x.

In Figure 3.1(b), the edges of an indefinitely small toroidal shell element (which is bounded by two adjacent circles of latitude and two adjacent meridians), are of equal arc length $r_1 d\phi$ in the two meridional edges, and of length $Rd\theta$ at the upper horizontal edge. The arc length of the lower horizontal edge of the toroidal element may be written as $(R + dR)d\theta$. However, the area of the toroidal element may be approximated as $r_1 R d\phi d\theta$ on the assumption that the contribution of the term $dRd\theta$ to the arc length of the lower edge is negligibly small when

compared with that of the other terms. Hence, the following simplified expression can be deduced from equation (0.1) and Figure 3.1

$$\frac{dR}{d\phi} = r_1 \cos\phi \tag{0.3}$$

3.4 Differential equations of equilibrium

In this section, the equations representing equilibrium of forces and moments is presented for an arbitrary loaded element of the shell of revolution. The treatment follows conventional steps (Timoshenko & Woinowsky-Krieger, 1959; Flügge, 1973; Zingoni, 1997), unless otherwise indicated. It is customary in shell theory to express internal forces and moments in terms of forces and moments per unit length of the edge of an element of a shell, as in plate theory. Consequently, the shell element in Figure 3.1a has been shown in Figure 3.2 below with the internal actions on the edges and the applied external loading.

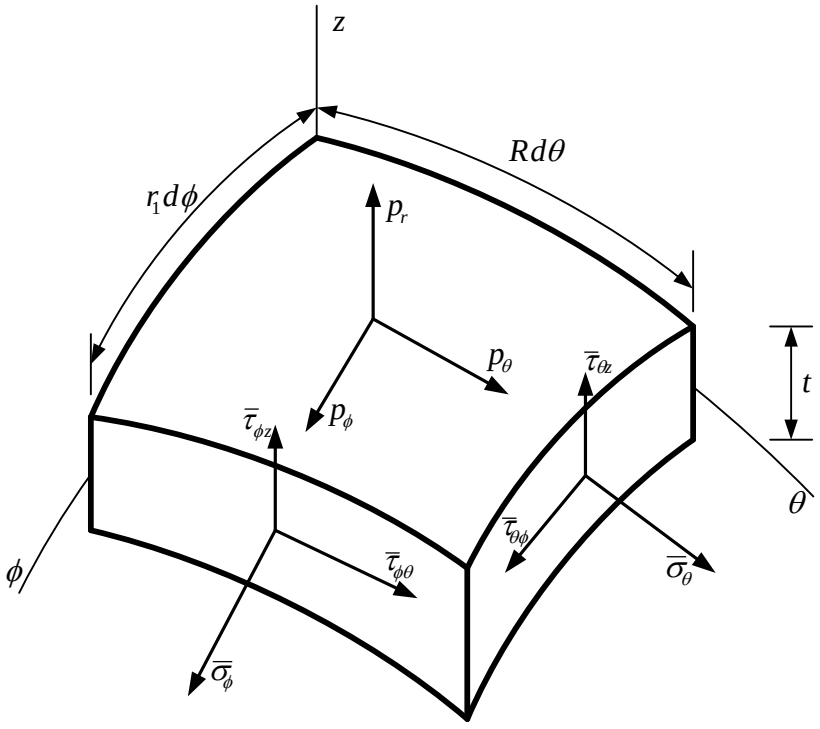

Figure 3.2. Stresses on the shell element

The Internal forces and moments acting on the edges of the element are expressed in terms of forces and moments per unit distance along the shell section of constant ϕ or θ. These are

obtained by the integration of the stress and moment components through the thickness t of the shell (where distances from the middle surface of the shell are measured by the coordinate z). This is depicted in the following approximated expressions (0.4), after the application of the general thin-shell simplifying assumption that the thickness of the shell is negligibly small in comparison with the least radius of curvature of the shell middle surface (that is, z/r_1 and z/r_2 are neglected in comparison with unity (t/r_1 or t/r_2 << 1), and hence $N_{\phi\theta} = N_{\theta\phi}$ and $M_{\phi\theta} = M_{\theta\phi}$, are assumed) (Flügge, 1973; Brush & Almroth, 1975):

$$N_\phi = \int_{-t/2}^{t/2} \bar{\sigma}_\phi dz \tag{0.4a}$$

$$N_\theta = \int_{-t/2}^{t/2} \bar{\sigma}_\theta dz \tag{3.4b}$$

$$N_{\phi\theta} = N_{\theta\phi} = \int_{-t/2}^{t/2} \bar{\tau}_{\phi\theta} dz = \int_{-t/2}^{t/2} \bar{\tau}_{\theta\phi} dz \tag{3.4c}$$

$$Q_\phi = \int_{-t/2}^{t/2} \bar{\tau}_{z\phi} dz \tag{3.4d}$$

$$Q_\theta = \int_{-t/2}^{t/2} \bar{\tau}_{z\theta} dz \tag{3.4e}$$

$$M_\phi = \int_{-t/2}^{t/2} z\bar{\sigma}_\phi dz \tag{3.4f}$$

$$M_\theta = \int_{-t/2}^{t/2} z\bar{\sigma}_\theta dz \tag{3.4g}$$

$$M_{\phi\theta} = M_{\theta\phi} = \int_{-t/2}^{t/2} z\bar{\tau}_{\phi\theta} dz = \int_{-t/2}^{t/2} z\bar{\tau}_{\theta\phi} dz \tag{3.4h}$$

In these equations, $\bar{\sigma}_\phi$, $\bar{\sigma}_\theta$ and $\bar{\tau}_{\phi\theta}$ are the stress components at any point through the thickness of the shell. Their corresponding quantities at $z = 0$ (on the middle surface of the shell) are denoted by σ_ϕ, σ_θ and $\tau_{\phi\theta}$, respectively. The in-plane direct-force per unit length in the meridional direction (which is alternatively called the meridional stress resultant) is denoted by N_ϕ. The in-plane direct-force per unit length in the hoop direction (which is alternatively called the hoop stress resultant) is denoted by N_θ. The in-plane shearing-force stress resultant

is denoted by $N_{\phi\theta}(=N_{\theta\phi})$. The transverse shearing forces per unit length are denoted by Q_ϕ and Q_θ, respectively; and the bending and twisting moments per unit length are denoted by M_ϕ, M_θ and $M_{\phi\theta}(=M_{\theta\phi})$, respectively.

These internal actions are now exposed as edge forces and moments on the elemental shell as shown in Figure 3.3, where, the notation $(\,)^+$ due to the variation of an action across the edge of the element stands for $((\,)+(\,)^\bullet d\phi)$ or $((\,)+(\,)'d\theta)$, in which the notations $(\,)^\bullet$ for the first derivative with respect to ϕ; $(\,)'$ for the first derivative with respect to θ, and the double-headed vector for the directions of the moment couples have been adopted. To simplify the diagrams, the systems of forces and moments are shown in separate sketches, and the shell element is drawn as an element of a surface without thickness.

The internal actions are mobilized when the elemental shell is loaded. As shown, the external loading components include: p_ϕ, the load per unit area of the shell middle surface, in the meridional direction; p_θ, the load per unit area of the shell middle surface, in the hoop direction; and p_r the load per unit area of the shell middle surface, in the direction of the normal to the shell middle surface. The internal and external actions on the shell element are shown in Figure 3.2 and 3.3 in their positive directions.

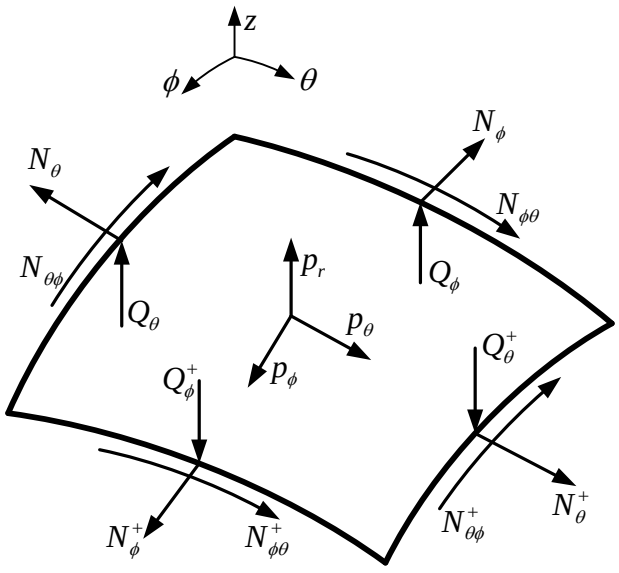

(a)

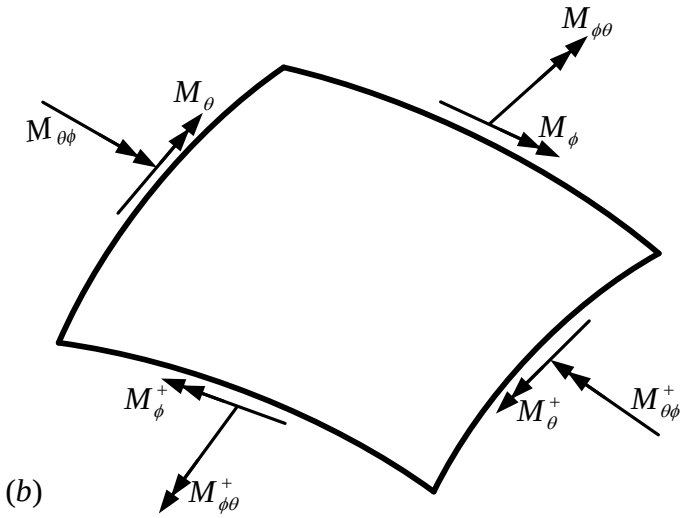

Figure 3.3. Actions on the shell element: (a) force, and (b) moments per unit length

For the element to be in equilibrium, force and moment equilibrium must be achieved. Force equilibrium requires that the sum of internal and external forces acting on the shell element, resolved in the direction of the tangent to a meridian, in the direction of the tangent to a circle of latitude, and in the direction of the normal to the shell middle surface, must in each case be zero. Similarly, moment equilibrium requires that the sum of the moments acting on the shell element, in the meridional plane, and in the horizontal parallel plane, must in both cases be zero. Since the symmetry condition (i.e. $N_{\phi\theta} = N_{\theta\phi}$ and $M_{\phi\theta} = M_{\theta\phi}$) has been adopted, it would suffice to mention here that the moment equilibrium of the elemental shell about a normal to the middle surface will lead to identity and no new information will be obtained. This may be seen by deriving the equation and comparing the result with the expressions that relate the in-plane shearing stress resultants and the actual in-plane shearing stresses (expression (0.4c)). Hence, only the five differential equations that satisfy the approximated equilibrium conditions of an element of the shell of revolution are presented in the following. Furthermore, the usual assumptions of neglecting small terms in comparison with other terms; and replacing sins and cosines of very small angles by the angles themselves and by unity, respectively, (i.e., $\sin\beta \approx \beta$ and $\cos\beta \approx 1$ for very small angle β) are employed.

Summation of forces in the direction of the tangent to a meridian: each of the stress resultants N_{ϕ}, N_{θ} and $N_{\phi\theta}$, transverse shearing force Q_{ϕ} and loading component p_{ϕ} has a resultant force in this direction. The sum of these forces may be simplified to the equilibrium equation

$$\left[RN_\phi + \left\{RN_\phi\right\}^\bullet d\phi\right]d\theta - RN_\phi d\theta + \left(N_{\theta\phi} + N'_{\theta\phi}d\theta\right)r_1 d\phi - r_1 N_{\theta\phi} d\phi$$

$$-r_1 N_\theta \cos\phi d\phi d\theta - RQ_\phi d\theta d\phi + r_1 R p_\phi d\theta d\phi = 0$$

Rearranging and dividing throughout by the common factor $d\phi d\theta$ yields

$$\left(RN_\phi\right)^\bullet + r_1 N'_{\theta\phi} - r_1 N_\theta \cos\phi - RQ_\phi = -r_1 R p_\phi \tag{0.5}$$

Summation of forces in the direction of the tangent to a parallel circle of latitude: each of the stress resultants N_θ and $N_{\theta\phi}$ also contributes a force in this direction, in addition to the in-plane shearing stress resultant $N_{\phi\theta}$, transverse shearing force Q_θ and loading component p_θ. The sum of these forces may be written in the reduced form

$$\left[RN_{\phi\theta} + \left\{RN_{\phi\theta}\right\}^\bullet d\phi\right]d\theta - RN_{\phi\theta} d\theta + \left(N_\theta + N'_\theta d\theta\right)r_1 d\phi - r_1 N_\theta d\phi$$

$$+r_1 N_{\theta\phi} \cos\phi d\phi d\theta - r_1 Q_\theta \sin\phi d\phi d\theta + r_1 R p_\theta d\theta d\phi = 0$$

which can be further simplified to the partial differential equation

$$\left(RN_{\phi\theta}\right)^\bullet + r_1 N'_\theta + r_1 N_{\theta\phi} \cos\phi - r_1 Q_\theta \sin\phi = -r_1 R p_\theta \tag{0.6}$$

Summation of forces in the direction normal to the shell middle surface: the stress resultants N_ϕ and N_θ, including transverse shearing forces Q_ϕ and Q_θ, and the loading component p_ϕ (except the in-plane shears), make contributions in this direction. After the usual simplifications, their sum may be written as

$$RN_\phi d\theta d\phi + r_1 N_\theta \sin\phi d\phi d\theta + \left\{RQ_\phi\right\}^\bullet d\phi d\theta + r_1 Q'_\theta d\phi d\theta - r_1 R p_r d\theta d\phi = 0$$

This has been further simplified to

$$RN_{\phi} + r_1 N_{\theta} \sin\phi + \left(RQ_{\phi}\right)^{\bullet} + r_1 Q'_{\theta} = r_1 R p_r \tag{0.7}$$

Summation of moments on the elemental shell in the meridional plane: each of the moments M_{ϕ}, M_{θ} and $M_{\phi\theta}$ per unit length, and transverse shearing stress resultant Q_{ϕ} per unit length has effects on the moment equilibrium of the element relative to the direction of the tangent to a parallel circle of latitude. The sum of these effects may be simplified as

$$\left[RM_{\phi} + \left\{RM_{\phi}\right\}^{\bullet} d\phi\right] d\theta - RM_{\phi} d\theta + \left(M_{\theta\phi} + M'_{\theta\phi} d\theta\right) r_1 d\phi - r_1 M_{\theta\phi} d\phi$$

$$- r_1 M_{\theta} \cos\phi d\phi d\theta - r_1 R Q_{\phi} d\phi d\theta = 0$$

and reduced to

$$\left(RM_{\phi}\right)^{\bullet} + r_1 M'_{\theta\phi} - r_1 M_{\theta} \cos\phi = r_1 R Q_{\phi} \tag{0.8}$$

Summation of moments on the elemental shell in the horizontal parallel plane: each of the moments per unit length M_{θ}, $M_{\phi\theta}$ and $M_{\theta\phi}$, and transverse shearing force Q_{θ} has a contribution to the moment equilibrium of the element relative to the direction of the tangent to a meridian. The sum of these effects may be written as

$$\left[RM_{\phi\theta} + \left\{RM_{\phi\theta}\right\}^{\bullet} d\phi\right] d\theta - RM_{\phi\theta} d\theta + \left(M_{\theta} + M'_{\theta} d\theta\right) r_1 d\phi - r_1 M_{\theta} d\phi$$

$$+ r_1 M_{\theta\phi} \cos\phi d\phi d\theta - r_1 R Q_{\theta} d\phi d\theta = 0$$

which can be simplified to the partial differential equation

$$\left(RM_{\phi\theta}\right)^{\bullet} + r_1 M'_{\theta} + r_1 M_{\theta\phi} \cos\phi = r_1 R Q_{\theta} \tag{0.9}$$

As earlier mentioned, no additional equilibrium equation can be obtained on account of $N_{\phi\theta} = N_{\theta\phi}$ and $M_{\phi\theta} = M_{\theta\phi}$ assumptions. Therefore, the five partial differential equations (0.5)

– (0.9) that satisfy the condition of equilibrium of an element of the shell of revolution may be recast as:

$$\left(RN_{\phi}\right)^{\bullet} + r_1 N'_{\theta\phi} - r_1 N_{\theta}\cos\phi - RQ_{\phi} = -r_1 R p_{\phi} \tag{0.10a}$$

$$\left(RN_{\phi\theta}\right)^{\bullet} + r_1 N'_{\theta} + r_1 N_{\theta\phi}\cos\phi - r_1 Q_{\theta}\sin\phi = -r_1 R p_{\theta} \tag{0.10b}$$

$$RN_{\phi} + r_1 N_{\theta}\sin\phi + \left(RQ_{\phi}\right)^{\bullet} + r_1 Q'_{\theta} = r_1 R p_r \tag{0.10c}$$

$$\left(RM_{\phi}\right)^{\bullet} + r_1 M'_{\theta\phi} - r_1 M_{\theta}\cos\phi = r_1 R Q_{\phi} \tag{0.10d}$$

$$\left(RM_{\phi\theta}\right)^{\bullet} + r_1 M'_{\theta} + r_1 M_{\theta\phi}\cos\phi = r_1 R Q_{\theta} \tag{0.10e}$$

These are the general equilibrium equations for shells of revolution under arbitrary loading (Flügge, 1973). They can easily be specialized for general toroidal shell forms by the introduction of the toroidal term A, which is related to R by (see Section 3.3):

$$R = A + x$$

When this is substituted into the above equilibrium expressions for shells of revolution, the following equations are obtained for the case of toroidal shells

$$AN_{\phi}^{\bullet} + \left(xN_{\phi}\right)^{\bullet} + r_1 N'_{\phi\theta} - r_1 N_{\theta}\cos\phi - (A+x)Q_{\phi} = -(A+x)r_1 p_{\phi}$$

$$AN_{\phi\theta}^{\bullet} + \left(xN_{\phi\theta}\right)^{\bullet} + r_1 N'_{\theta} + r_1 N_{\phi\theta}\cos\phi - r_1 Q_{\theta}\sin\phi = -(A+x)r_1 p_{\theta}$$

$$(A+x)N_{\phi} + r_1 N_{\theta}\sin\phi + AQ_{\phi}^{\bullet} + \left(xQ_{\phi}\right)^{\bullet} + r_1 Q'_{\theta} = (A+x)r_1 p_r$$

$$AM_{\phi}^{\bullet} + \left(xM_{\phi}\right)^{\bullet} + r_1 M'_{\phi\theta} - r_1 M_{\theta}\cos\phi = (A+x)r_1 Q_{\phi}$$

$$AM_{\phi\theta}^{\bullet} + \left(xM_{\phi\theta}\right)^{\bullet} + r_1 M'_{\theta} + r_1 M_{\phi\theta}\cos\phi = (A+x)r_1 Q_{\theta}$$

This complete set of five equilibrium equations which contain eight unknowns N_ϕ, N_θ, $N_{\phi\theta}$, Q_ϕ, Q_θ, M_ϕ, M_θ and $M_{\phi\theta}$ is, of course, not statically determinate. In the usual way, to proceed toward the determination of these unknown internal actions, additional equations are invoked from the elastic law of a shell of revolution, as we shall see in the next section.

3.5 The elastic law

The relations between the six internal actions (N_ϕ, N_θ, $N_{\phi\theta}$, M_ϕ, M_θ and $M_{\phi\theta}$) and displacements of an arbitrary point on the middle surface of a toroidal shell of revolution are presented here based on Flügge's shell theory (Flügge, 1973; Zingoni, 1997).

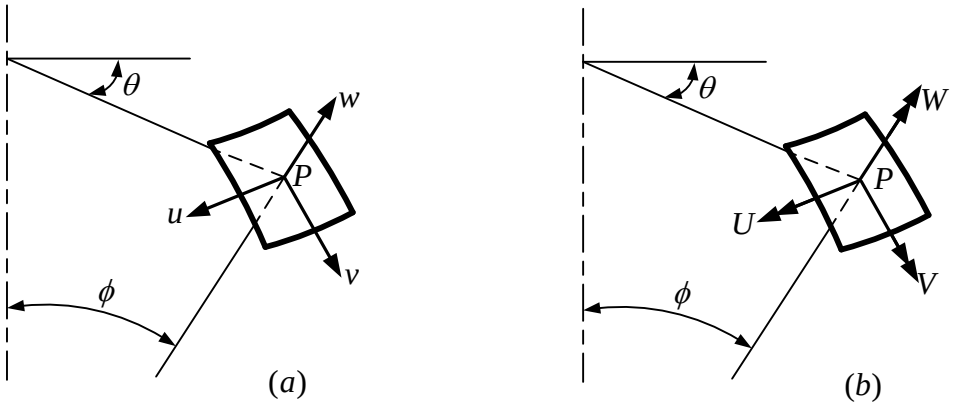

Figure 3.4. Deformation components of a point on the middle surface of the shell: (a) displacements, and (b) rotation components

3.5.1 Deformation components

For a loaded shell of revolution, the basic deformation components of a point in the middle fibre of the shell are the displacement-type components u, v, w and rotation-type components U, V, W as shown in Figure 3.4a and 3.4b, respectively. u denotes the displacement component in the direction of the tangent to the hoop circle, is considered positive in the direction of increasing θ; v denotes the displacement component in the direction of the tangent to the meridian, is considered positive in the direction of increasing ϕ; and w denotes the displacement component in the direction of the normal to the shell middle surface, is considered positive when pointing away from the centre of curvature of the meridian. The rotation component, V denotes the angle of rotation of the normal to the middle surface about the tangent to the hoop circle (the meridional rotation); U denotes the angle of rotation of the

normal to the middle surface about the tangent to the meridian (the hoop rotation); and W is the rotation of the shell around the normal at any point on the middle surface.

Based on the assumption that a straight line normal to the shell middle surface prior to deformation remains straight and normal to the middle surface during and after deformation and retains its original length, the rotation components are expressed in terms of the displacement components of a point on the middle surface of the shell. For the meridional rotation V, only the radial movement w and, of course, the displacement component v contribute to the rotation. To obtain the contribution from v, a point on the middle surface of the shell is assumed to be displaced through a distance of v along the meridian, see Figure 3.5a. As shown, the movement resulted in an anticlockwise rotation of the tangent about the point through an angle $V_1 = d\phi = v / r_1$. The contribution from w is simply obtained by assuming a line element that is unevenly displaced in the direction of the normal to the element, see Figure 3.5b. Owing to the difference dw in the radial displacements of the two ends of the line element, there is a clockwise rotation of the element through an angle $V_2 = d\phi = dw / (r_1 d\phi)$. The sum of these rotations may be simplified to the meridional rotation

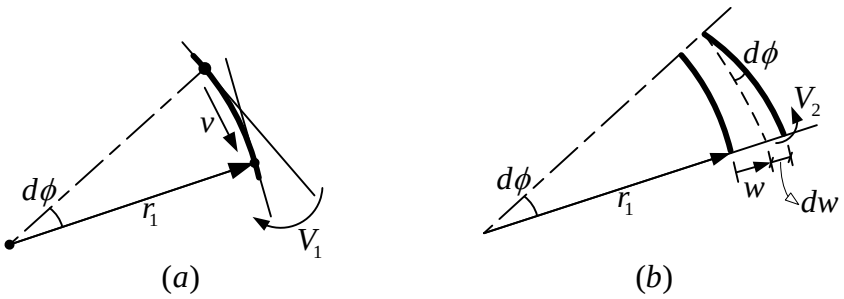

Figure 3.5. Meridional rotation of a point

$$V = \frac{v - w^{\bullet}}{r_1} \tag{0.11}$$

By quite a similar reasoning, the expression for the rotation component U is simply obtained as

$$U = \frac{u\sin\phi - w'}{R} \tag{0.12}$$

Two separate expressions are obtained for the rotation of the shell around the normal at any point on the middle surface $W\,(=W_\theta, W_\phi)$ (Flügge & Sobel, 1965):

$$W_\theta = \frac{v'}{R} \tag{0.13}$$

is the angle of rotation of the tangent to the parallel circle around the normal, while

$$W_\varphi = \frac{u^\bullet}{r_1} - \frac{u\cos\phi}{R} \tag{0.14}$$

is the angle of rotation of the meridian to the parallel circle around the normal. Recall that r_1 is considered negative when the centre of curvature of a point on the meridian is on the side of the shell mid-surface opposite to the global axis of revolution of the toroid. The rotation of the shell around the normal W is very small compared to the other rotations U and V, which are themselves small on the limitations that the strains be small compared to unity. However, as we shall see in Chapter 6, these rotation terms play a role in the formulation of stability equations for toroidal shells of revolution.

On the account that displacements vary through the thickness of a shell, the rotation components may be related to the displacement components u, v and w in the middle fibre of the shell by (Flügge, 1973; Brush & Almroth, 1975):

$$\bar{u} = u + zU \tag{0.15a}$$

$$\bar{v} = v + zV \tag{0.15b}$$

$$\bar{w} = w \tag{0.15c}$$

where $\bar{u}$, $\bar{v}$ and $\bar{w}$ are the corresponding displacement components at any point within the shell at a distance z from the middle surface. In equation (0.15c), also note that, in accordance with the Love-Kirchhoff assumptions, the displacement in the direction of the normal to the middle surface is not a function of z. In what follows, the relationships between the deformation terms and the strains at a point on the shell are given.

3.5.2 Kinematics equations

The expressions for middle surface (or fibre) extensional and shearing strain components: ε_ϕ (the meridional strain); ε_θ (the hoop strain); $\gamma_{\phi\theta}$ (the shear strain), and the middle surface curvature changes and twist: χ_ϕ, χ_θ, $\chi_{\phi\theta}$ of a shell of revolution are presented here on the basis of the simplification of the thin-shell assumptions as before. Starting with the expression for the meridional strain ε_ϕ, an elongated line element of a meridian is adopted as shown in Figure 3.6. The circumferential displacement u does not contribute to the strain in the meridional direction. The initial length of the element is $r_1 d\phi$ before the elongation, which involves two components: $wd\phi$ resulting from the radial displacement w, and dv resulting from the difference in the purely tangential displacements of the two ends. Hence, the total elongation of the line element AB of a meridian is (Zingoni, 1997)

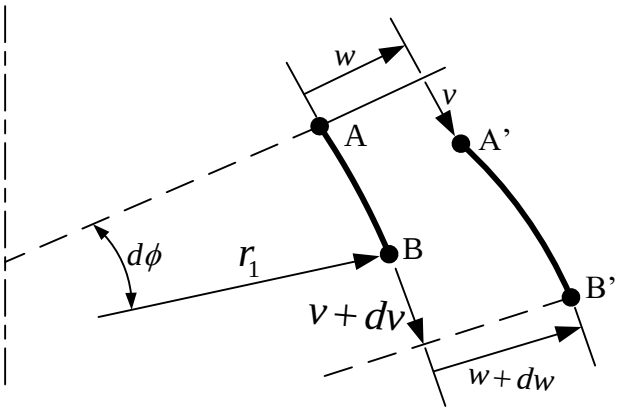

Figure 3.6. Deformation of a line element of in the meridional plane

$$e_\phi = dv + wd\phi$$

Therefore, the strain in the meridional direction may be expressed as

$$\varepsilon_\phi = \frac{1}{r_1}\left(v^{\bullet} + w\right) \tag{0.16a}$$

For the hoop strain ε_θ equation, an elongated line element of a parallel circle is adopted as shown in Figure 3.7. All the displacement components contribute to the strain in the hoop direction. The initial length of the element before the elongation is $Rd\phi$, as viewed on the hoop plane (Figure 3.7(a)). The element elongated by du in the circumferential direction. Hence, the component of hoop strain due to purely tangential displacements of the two ends is

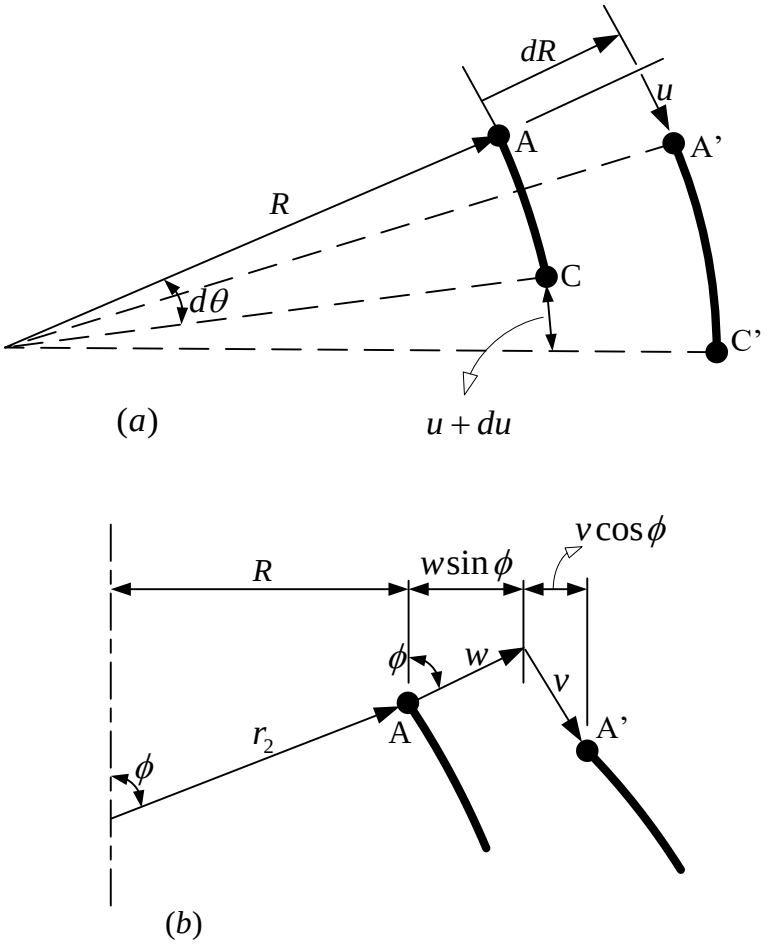

Figure 3.7. Displacement of a line element: (a) hoop plane; (b) meridional plane

$$\varepsilon_{\theta 1} = \frac{1}{R}u'$$

The components of hoop strain due to the displacements v and w can be easily seen when the displacement of end A is viewed on the meridional plane, Figure 3.7(b). The radius R of the circle of latitude at point A increased by $v\cos\phi + w\sin\phi$. Hence, the strain

$$\varepsilon_{\theta 2} = \frac{1}{R}\left(v\cos\phi + w\sin\phi\right)$$

Therefore, the total strain in the hoop direction may be expressed as

$$\varepsilon_{\theta} = \frac{1}{R}\left(u' + v\cos\phi + w\sin\phi\right) \tag{3.16b}$$

For the shear strain $\gamma_{\phi\theta}$ expression, a complete element as shown in Figure 3.8 is adopted. The displacement w in the direction of the normal to the middle surface does not contribute to the shearing that occurs within the element. It can be seen from the figure that the movement of the upper horizontal edge CA to C'A' resulted in the following shearing strain, after neglecting small terms in comparison with other terms and adopting $\sin\beta \approx \beta$ and $\cos\beta \approx 1$ for very small angle β, as usual,

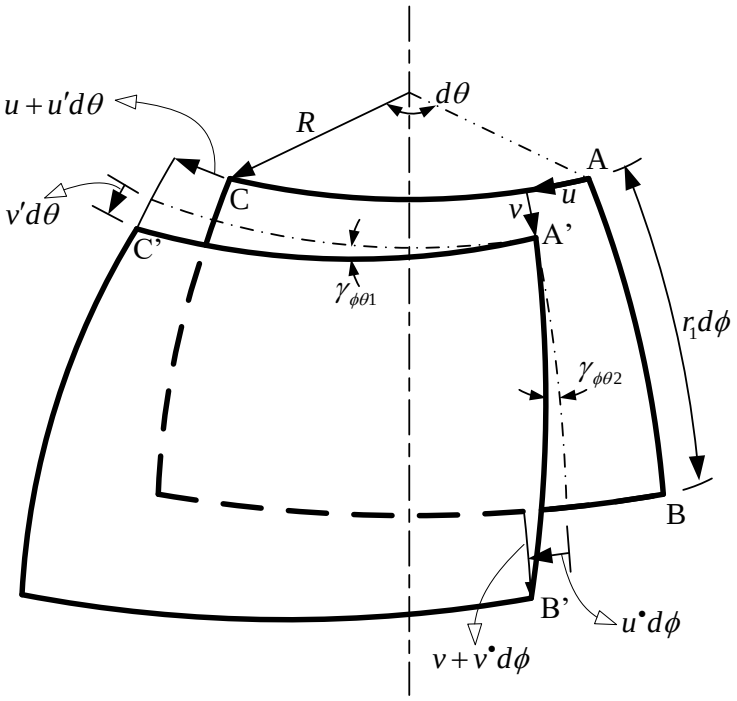

Figure 3.8. Deformation of an element of the shell

$$\gamma_{\phi\theta 1} = \frac{1}{R} v'$$

and the movement of the left meridional edge AB of the element to A'B' resulted in the shearing strain

$$\gamma_{\phi\theta 2} = \frac{1}{r_1} u^{\bullet} - \frac{\cos\phi}{R} u$$

since

$$\frac{dR}{d\phi} = r_1 \cos\phi$$

Therefore, the total shear strain in the element may be expressed as

$$\gamma_{\phi\theta} = \frac{1}{r_1} u^{\bullet} + \frac{1}{R}\left(v' - u\cos\phi\right) \tag{3.16c}$$

In view of expressions (0.15), the extensional and shearing strain components ε_ϕ, ε_θ, and $\gamma_{\phi\theta}$ at points on the shell middle surface may be related to their corresponding quantities at any point through the thickness of the shell by (Flügge, 1973; Brush & Almroth, 1975):

$$\bar{\varepsilon}_\phi = \varepsilon_\phi - z\chi_\phi \tag{0.17a}$$

$$\bar{\varepsilon}_\theta = \varepsilon_\theta - z\chi_\theta \tag{0.17b}$$

$$\bar{\gamma}_{\phi\theta} = \gamma_{\phi\theta} - 2z\chi_{\phi\theta} \tag{0.17c}$$

In which the expressions for the middle surface curvature changes and the twist are

$$\chi_\phi = -\frac{1}{r_1} V^{\bullet} \tag{0.18a}$$

$$\chi_{\phi} = -\frac{1}{r_1}\left(U' + V\cos\phi\right) \tag{0.18b}$$

$$\chi_{\phi\theta} = -\frac{1}{2}\left\{\frac{1}{r_1}U^{\bullet} + \frac{1}{R}\left(V' - U\cos\phi\right)\right\} \tag{0.18c}$$

Remember,

$$V = \frac{v - w^{\bullet}}{r_1}$$

$$U = \frac{u\sin\phi - w'}{R}$$

Note that in the kinematic equations (0.16) and (0.18), all variables are middle fibre quantities (which are related to strain quantities at any point through the thickness of the shell by equation (0.17)), and are functions of ϕ, and θ alone. Next, the relationships between these quantities and the internal actions in a loaded toroidal shell of revolution are given.

3.5.3 Constitutive relations

After applying the thin-shell approximation, the generalised Hooke's law for the stress and strain components in an isotropic medium has the following form

$$\bar{\varepsilon}_{\phi} = \frac{1}{E}\left(\bar{\sigma}_{\phi} - \upsilon\bar{\sigma}_{\theta}\right)$$

$$\bar{\varepsilon}_{\theta} = \frac{1}{E}\left(\bar{\sigma}_{\theta} - \upsilon\bar{\sigma}_{\phi}\right)$$

$$\bar{\gamma}_{\phi\theta} = \frac{2(1+\upsilon)}{E}\bar{\tau}_{\phi\theta}$$

where E is the Young's modulus of elasticity of the shell material and υ is the Poisson's ratio. The expressions can be re-arranged as

$$\bar{\sigma}_{\phi} = \frac{E}{1-\upsilon^2}\left(\bar{\varepsilon}_{\phi} + \upsilon\bar{\varepsilon}_{\theta}\right)$$

$$\bar{\sigma}_\theta = \frac{E}{1-\upsilon^2}\left(\bar{\varepsilon}_\theta + \upsilon\bar{\varepsilon}_\phi\right)$$

$$\bar{\tau}_{\phi\theta} = \frac{E}{2(1+\upsilon)}\bar{\gamma}_{\phi\theta}$$

When these are put in expressions (0.4) in conjunction with equations (0.19), the following constitutive relations are obtained, after integration

$$N_\phi = \frac{Et}{1-\upsilon^2}\left(\varepsilon_\phi + \nu\varepsilon_\theta\right) \tag{0.19a}$$

$$N_\theta = \frac{Et}{1-\upsilon^2}\left(\varepsilon_\theta + \nu\varepsilon_\phi\right) \tag{3.19b}$$

$$N_{\phi\theta} = \frac{Et}{2(1+\upsilon)}\gamma_{\phi\theta} \tag{3.19c}$$

$$M_\phi = \frac{Et^3}{12(1-\upsilon^2)}\left(\chi_\phi + \nu\chi_\theta\right) \tag{3.19d}$$

$$M_\theta = \frac{Et^3}{12(1-\upsilon^2)}\left(\chi_\theta + \nu\chi_\phi\right) \tag{3.19e}$$

$$M_{\phi\theta} = \frac{Et^3}{12(1+\upsilon)}\chi_{\phi\theta} \tag{3.19f}$$

Substitution of the results for strains ε_ϕ, ε_θ, $\gamma_{\phi\theta}$, and the middle surface curvature changes and the twist χ_ϕ, χ_θ, $\chi_{\phi\theta}$ as given by equations (0.16) and (0.18), respectively, the elastic law for a shell of revolution is obtained as

$$N_\phi = \frac{Et}{1-\upsilon^2}\left\{\frac{1}{r_1}\left(v^{\bullet} + w\right) + \frac{\upsilon}{R}\left(u' + v\cos\phi + w\sin\phi\right)\right\} \tag{0.20a}$$

$$N_\theta = \frac{Et}{1-\upsilon^2}\left\{\frac{1}{R}\left(u' + v\cos\phi + w\sin\phi\right) + \frac{\upsilon}{r_1}\left(v^{\bullet} + w\right) + \right\} \tag{3.20b}$$

$$N_{\phi\theta} = \frac{Et}{2(1+\upsilon)}\left\{\frac{u^{\bullet}}{r_1} - \frac{1}{R}\left(u\cos\phi - v'\right)\right\} \tag{3.20c}$$

$$M_{\phi} = D\left[\frac{1}{r_1^{\,2}}\left(w^{\bullet} - v\right)^{\bullet} + \frac{\upsilon}{R^2}\left\{\left(w' - u\sin\phi\right)' + \frac{R\cos\phi}{r_1}\left(w^{\bullet} - v\right)\right\}\right] \tag{3.20d}$$

$$M_{\theta} = D\left[\frac{1}{R^2}\left\{\left(w' - u\sin\phi\right)' + \frac{R\cos\phi}{r_1}\left(w^{\bullet} - v\right)\right\} + \frac{\upsilon}{r_1^{\,2}}\left(w^{\bullet} - v\right)^{\bullet}\right] \tag{3.20e}$$

$$M_{\phi\theta} = D\frac{1-\upsilon}{2}\left[\frac{1}{r_1}\left(\frac{w' - u\sin\phi}{R}\right)^{\bullet} + \frac{1}{R}\left\{\frac{1}{r_1}\left(w^{\bullet} - v\right)' - \frac{\cos\phi}{R}\left(w' - u\sin\phi\right)\right\}\right] \tag{3.20f}$$

So, for the case of toroidal shells, after replacing R with $A+x$, we get

$$N_{\phi} = \frac{Et}{1-\upsilon^2}\left\{\frac{1}{r_1}\left(v^{\bullet} + w\right) + \frac{\upsilon}{A+x}\left(u' + v\cos\phi + w\sin\phi\right)\right\}$$

$$N_{\theta} = \frac{Et}{1-\upsilon^2}\left\{\frac{1}{A+x}\left(u' + v\cos\phi + w\sin\phi\right) + \frac{\upsilon}{r_1}\left(v^{\bullet} + w\right) + \right\}$$

$$N_{\phi\theta} = \frac{Et}{2(1+\upsilon)}\left\{\frac{u^{\bullet}}{r_1} - \frac{1}{A+x}\left(u\cos\phi - v'\right)\right\}$$

$$M_{\phi} = D\left[\frac{1}{r_1^{\,2}}\left(w^{\bullet} - v\right)^{\bullet} + \frac{\upsilon}{(A+x)^2}\left\{\left(w' - u\sin\phi\right)' + \frac{(A+x)\cos\phi}{r_1}\left(w^{\bullet} - v\right)\right\}\right]$$

$$M_{\theta} = D\left[\frac{1}{(A+x)^2}\left\{\left(w' - u\sin\phi\right)' + \frac{(A+x)\cos\phi}{r_1}\left(w^{\bullet} - v\right)\right\} + \frac{\upsilon}{r_1^{\,2}}\left(w^{\bullet} - v\right)^{\bullet}\right]$$

$$M_{\phi\theta} = D\frac{1-\upsilon}{2}\left[\frac{1}{r_1}\left(\frac{w' - u\sin\phi}{A+x}\right)^{\bullet} + \frac{1}{A+x}\left\{\frac{1}{r_1}\left(w^{\bullet} - v\right)' - \frac{\cos\phi}{A+x}\left(w' - u\sin\phi\right)\right\}\right]$$

where D is used to denote the flexural rigidity of the shell, i.e.

$$D = \frac{Et^3}{12\left(1-\upsilon^2\right)} \tag{0.21}$$

In equations (0.20), stress resultants and moment intensities are expressed in terms of the displacement components u, v and w. This is the set of six equations of elastic law required to be added to the five equilibrium equations (0.10) as mentioned in Section 3.3 of this Chapter, for equilibrium analysis of toroidal shells of revolution. Hence, a system of eleven equations in eleven unknown variables (which are only functions of coordinates ϕ, and θ), is obtained.

3.6 Concluding remarks

A formulation for the linear elastic behaviour of toroidal shells of revolution has been presented in this chapter, to facilitate the analysis of complete toroidal shells of various cross-sections. The derived partial differential equations which consist of equilibrium and constitutive relations describe the behaviour of toroids within the framework of Love's simplifying assumptions. From a practical point of view, the formulated equations provide an extremely successful model that permits the ease of investigating loaded toroidal shell forms, and therefore the possibility of enhancing the engineering application of the shell forms.

On the imposition of appropriate boundary conditions and necessary modifications, the developed governing differential equations are employed in the treatments that are presented in the next couple of chapters in this thesis. The membrane hypothesis is adopted to reduce the set of equations in Chapter 4, to first obtain membrane solutions which are already available in the literature, before extending it to new cases. In Chapter 5, the equations in this chapter are simplified, and the approximate bending-disturbance solution is provided to account for the axisymmetric bending that may occur within toroidal shells. The strategy of simplifying the bending theory to make it amenable to closed-form solution has been championed by Zingoni (1991, 1997, 2001a,b, 2002, 2009, 2018) and Zingoni & Pavlović (1991a,b, 1992, 1993a,b), and here we will adopt a similar approach for the toroidal shell form. Finally, in Chapter 6, a nonlinear theory of elastic toroidal shells of revolution under axisymmetric loading is formulated from the derived set of equations in this chapter by relaxing the small deflection assumption of Love-Kirchhoff to obtain equations that incorporate finite deformations which are employed to study the buckling behaviour of the toroidal shells.

Chapter 4

Membrane solution for axisymmetrically loaded toroidal shells

4.1 Introduction

The governing differential equations for toroidal shells of revolution presented in the preceding chapter are specialised here into membrane equations by the application of membrane hypothesis, which assumes that bending and twisting moments within a loaded shell is so small as to be ignored (i.e. the state of stress is essentially 'momentless'). General expressions for the solution of the membrane equations of toroidal shells is then derived for the axisymmetric pressure loading cases considered. These expressions are applied for various toroidal shell forms, and the obtained membrane results are also formulation in non-dimensional form for the conduction of a parametric investigation of each of the vessels. Some of the results presented in this chapter have been previously reported (Enoma et al., 2015; Enoma & Zingoni, 2016a,b, 2017).

In general, and as earlier pointed out in Chapter 2, the exact state of stress and deformation in a shell, within the confines of shell theory can be determined on the basis of the equations of bending theory of shells. These are more general than the membrane theory and take account of extensional, bending, twisting, and shearing effects within the shell material, but are very difficult to solve (Zingoni, 1997). Hence, the membrane-hypothesis solution which, of course, neglects flexural actions is assumed to be, as a rule, a close approximation to the actual state of stress and deformation that occur in the interior of shells of revolution subjected to distributed loadings that are constant (or vary smoothly, continuously and 'not too rapidly') over the surface of the shell, and provided the shell geometry also exhibits the same smoothness properties (Novozhilov, 1970; Zingoni, 1991, 1997).

Both the toroidal shell geometry and loading distribution under present consideration conform to the above requirements so that the membrane solution should be adequate throughout, except in the zones around supports and meeting points of the outer and inner regions of the toroid, and at the joining points of segments in a multi-shells toroid. If required, the bending disturbances that occur around the zones in which the 'momentless' state of stress fails to exist can be estimated with the approximate bending solution, as given in Chapter 5.

In the following, first, a brief outline of membrane hypothesis is presented, before the formulation of a general membrane solution which is used to derive the well-known membrane results for a pressurised circular toroidal shell; and those for hydrostatically loaded circular toroids. The approach is then extended to an elliptic toroid and toroidal shells of other cross-sections: parabolic ogival, semi-elliptic and semi-circular. Multi-shell toroidal vessels under the action of uniform pressure and hydrostatic pressure are also considered. The developed membrane solutions are not only useful in their own right for the determination of the state of stress and deformations within toroidal shells, as we shall see in the next chapter, they can also be adopted as a particular integral to being superimposed with the homogeneous solution of the complete bending-theory equations of toroidal shells. It is shown in Chapter 6 that the membrane solutions are also used to approximate the pre-buckling state in the stability equations.

4.2 Membrane hypothesis and loading preliminaries

The governing equations of membrane state of stress and deformations for a toroidal shell can be obtained from the partial differential equations derived in Chapter 3 by applying the following membrane hypothesis. That is,

$$M_\phi = M_\theta = M_{\phi\theta} = 0$$

and expressions (3.10d) and (3.10e) lead to

$$Q_\phi = Q_\theta = 0$$

The essential loading on the toroidal shells considered in this thesis is assumed to axisymmetric uniform or hydrostatic pressure loading which act in the direction of the normal to the shell middle surface. Hence, in the following treatment under membrane considerations, the external

loading components p_ϕ and p_θ in the meridional and hoop directions are equated to zero in the expressions, and the deformations that occur within the shell are taken to be axisymmetric. Thus, the in-plane shearing-force stress resultant $N_{\phi\theta}$ or $N_{\theta\phi}$ cannot exist under such loading condition, and the equations are expressed as functions of ϕ only.

With these approximations, Figure (3.3) simplifies to

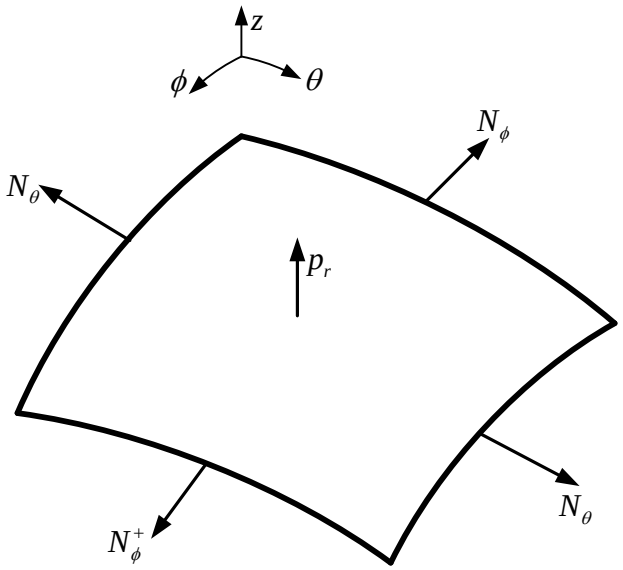

Figure 4.1. A toroidal shell element under membrane actions

Consequently, the equilibrium equations (3.10) reduce to the following two equations

$$\left(RN_\phi^m\right)^\bullet - r_1 N_\theta^m \cos\phi = 0 \tag{4.1a}$$

$$RN_\phi^m + r_1 N_\phi^m \sin\phi = r_1 R p_r \tag{4.1b}$$

which contain two unknown stress resultants N_ϕ^m and N_θ^m, where the superscript m is used to denote 'membrane' effects. Since equations (4.1b) has no derivatives, it can be used to easily remove one of the unknowns from equations (4.1a).

In a similar way, the deformation terms from Section 3.4.1 are now v (in the direction of the tangent to the meridian, considered positive when pointing in the direction of increasing ϕ), w (in the direction of the normal to the shell middle surface, considered positive when pointing

away from the centre of curvature of the meridian), and V^m (the rotation of the tangent to the shell meridian at any point on the shell, considered positive when the tangent rotates clockwise on the side of the shell cross-section to the right of the axis of revolution) only. These are related by equation (3.12)

$$V^m = \frac{v - w^{\bullet}}{r_1} \tag{4.2}$$

and the kinematic equations (3.16a) and (3.16b)

$$\varepsilon_{\phi} = \frac{1}{r_1}\left(v^{\bullet} + w\right) \tag{4.3a}$$

$$\varepsilon_{\theta} = \frac{1}{R}\left(v\cos\phi + w\sin\phi\right) \tag{4.3b}$$

Note that the differential term u' in equation (3.16b) has been dropped in equation (4.1b) since axisymmetrically load shell of revolution is under present considerations.

4.3 Membrane Solution for toroidal shells

4.3.1 Meridional and hoop stress resultants

The system of equations (4.1) for the condition of equilibrium of an axisymmetrically loaded toroidal shell of revolution is seen to be statically determinate, the number of unknowns is equal to the number of equations, so that solutions can be obtained without use of constitutive and kinematic equations. This is a general characteristic of membrane formulation. In solving the equations, and following the solution approach of Zingoni (1997), one may proceed by re-writing equation (4.1b) for the membrane stress resultant in the hoop direction as

$$N_{\theta}^m = \frac{r_2}{r_1}\left(r_1 p_r - N_{\phi}^m\right)$$

This may be written in toroidal terms, as

$$N_{\theta}^m = \frac{A + x}{r_1 \sin\phi}\left(r_1 p_r - N_{\phi}^m\right) \tag{4.4a}$$

since $r_2 = (A+x)/\sin\phi$ for toroidal shells. Elimination of N_θ^m from equation (4.1a) yields

$$\left\{RN_\phi^m\right\}^\bullet - r_2\left(r_1 p_r - N_\phi^m\right) = 0$$

Multiplying throughout by $\sin\phi$ and re-arranging gives

$$\left\{RN_\phi^m\right\}^\bullet \sin\phi + RN_\phi^m \cos\phi = r_1 r_2 p_r \cos\phi \sin\phi$$

which can be further simplified to

$$\left\{RN_\phi^m \sin\phi\right\}^\bullet = r_1 r_2 p_r \cos\phi \sin\phi$$

Integration of both sides and re-arranging gives an expression for the stress resultants N_ϕ^m in the meridional direction of the shell of revolution

$$N_\phi^m = \frac{1}{r_2 \sin^2\phi}\left[\int r_1 r_2 p_r \cos\phi \sin\phi d\phi + k\right]$$

or for a toroidal shell form:

$$N_\phi^m = \frac{1}{(A+x)\sin\phi}\left[\int (A+x) r_1 p_r \cos\phi \sin\phi d\phi + k\right] \qquad (4.4b)$$

where, k is the constant of integration that can be obtained from an appropriate boundary condition, usually by specifying the membrane stress result at a specific location of the shell. When N_ϕ^m is determined, the results can be substituted into expression (4.4a) to obtain the stress resultant N_θ^m in the hoop direction of the toroidal shell of revolution. Since, from equation (3.1),

$$r_2 = \frac{R}{\sin\phi}; \text{ and } R = A + x$$

the solutions (4.4) for the membrane stress resultants in the meridional and hoop directions respectively are seen to be the same as the corresponding solutions obtained by Zingoni (1997,

2018) for general shells of revolution under axisymmetric loading, if the surface loading term in the meridional direction is omitted.

4.3.2 Actual membrane stresses

N_ϕ^m and N_θ^m are the membrane stress resultants in the meridional and hoop directions respectively. These are forces per unit length of the respective edge of a shell element, considered positive when tensile. The actual membrane stresses at a given point in question in the toroidal shell are obtained by simply dividing the membrane stress-resultant values by the thickness of the shell at that point:

$$\sigma_\phi^m = \frac{N_\phi^m}{t}$$

and

$$\sigma_\theta^m = \frac{N_\theta^m}{t}$$

from expression (3.4), where σ_ϕ^m and σ_θ^m are the membrane stresses in the meridional and hoop directions, respectively and t is the shell thickness.

4.3.3 Membrane deformations

The deformations are not only useful for estimating the distortions that occur within a shell under loading conditions but can also play a role in the estimation of edge effects by flexibility method, as we shall see in the next Chapter. The deformation quantities for axisymmetrically loaded shells of revolution have been given in Section 4.2, of interest here are the horizontal displacement quantity δ^m (considered positive when away from the axis of revolution) and the meridional rotation V^m. These quantities may be expressed as in the following, in terms of membrane stress resultants in the meridional and hoop directions.

The horizontal (or lateral) displacement quantity δ^m is the change in radius R of the horizontal circle of latitude through any point on the middle surface of the shell. That is

$$\delta^m = \Delta R = \Delta(A + x)$$

This may be related to hoop stain ε_θ (see expression (4.3b)) by

$$\varepsilon_\theta = \frac{1}{R}\left(v\cos\phi + w\sin\phi\right) = \frac{\delta^m}{R}$$

which can be written in the form, after the elimination of ε_θ using Hooke's law and re-arranging (Zingoni, 2018),

$$\delta^m = \frac{R}{E}\left\{\sigma_\theta - \upsilon\sigma_\phi\right\}$$

This can be expressed in terms of membrane stress resultants as

$$\delta^m = \frac{R}{E}\left\{\sigma_\theta - \upsilon\sigma_\phi\right\}$$

or, for the case of toroidal shell

$$\delta^m = \frac{A+x}{Et}\left\{N_\theta^m - \upsilon N_\phi^m\right\} \tag{4.5}$$

The expression (4.2) for the meridional rotation V^m can also be given in terms of membrane stress resultants N_ϕ^m and N_θ^m in the meridional and hoop directions, respectively. This may be done by first re-writing equations (4.3) as

$$v^\bullet + w = r_1\varepsilon_\phi \tag{4.6a}$$

$$v\cot\phi + w = r_2\varepsilon_\theta \tag{4.6b}$$

Subtraction of equation (4.6) from (4.6a), and multiplying the result throughout by $\cot\phi$, gives

$$v^\bullet\cot\phi - v\cot^2\phi = \left\{r_1\varepsilon_\phi - r_2\varepsilon_\theta\right\}\cot\phi \tag{4.7}$$

Differentiation of equations (4.6b) with respect to ϕ yields

$$v^\bullet\cot\phi - \frac{v}{\sin^2\phi} + w^\bullet = \left\{r_2\varepsilon_\theta\right\}^\bullet \tag{4.8}$$

Subtraction of equation (4.8) from (4.7) yields

$$v - w^{\bullet} = \left\{ r_1 \varepsilon_\phi - r_2 \varepsilon_\theta \right\} \cot\phi - \left\{ r_2 \varepsilon_\theta \right\}^{\bullet}$$

This is used to eliminate $v - w^{\bullet}$ from expression (4.2) to obtain

$$V^m = \frac{1}{r_1} \left[\left\{ r_1 \varepsilon_\phi - r_2 \varepsilon_\theta \right\} \cot\phi - \left\{ r_2 \varepsilon_\theta \right\}^{\bullet} \right]$$

which is expressed as, after using the Hooke's law in terms of membrane stress resultants

$$V^m = \frac{1}{r_1} \left[\frac{\cot\phi}{Et} \left\{ \left(r_1 + \upsilon r_2 \right) N_\phi^m - \left(r_2 + \upsilon r_1 \right) N_\theta^m \right\} - \left\{ \frac{r_2}{Et} \left(N_\theta^m - \upsilon N_\phi^m \right) \right\}^{\bullet} \right]$$

or

$$V^m = \frac{1}{r_1} \left[\frac{\cot\phi}{Et} \left\{ \left(r_1 + \upsilon \frac{A+x}{\sin\phi} \right) N_\phi^m - \left(\frac{A+x}{\sin\phi} + \upsilon r_1 \right) N_\theta^m \right\} - \left\{ \frac{A+x}{Et \sin\phi} \left(N_\theta^m - \upsilon N_\phi^m \right) \right\}^{\bullet} \right] \quad (4.9)$$

since, since $r_2 = \left(A + x \right) / \sin\phi$ for toroidal shells.

4.4 Membrane results for various axisymmetrically loaded toroidal shell forms

The membrane solutions presented in the preceding section are specialised for uniformly pressurised toroidal shells of circular, elliptic, parabolic ogival, semi-elliptic and semi-circular, and multi-segmented cross-sections. The membrane results for each of these toroids under hydrostatic pressure loading which varies linearly across the height of the vessel are also developed.

4.4.1 Circular Toroidal Vessel

4.4.1.1 Circular toroid under uniform internal pressure

Consider an internally pressurised toroidal vessel of circular cross-section, as shown in Figure 4.2, where p and a denote the uniform internal pressure and radius of the circular cross-

section, respectively, and other parameters are as previously defined in Chapter 3. Thus, $r_1 = \pm a$, $p_r = \pm p$, and $x = \pm a\sin\phi$ (where, the upper sign of the double operations applies to the outer region, while the lower sign applies to the inner regions of the toroid. This shall be adopted henceforth, except otherwise stated). When these are put into expression (4.4b) and the integral is evaluated, we obtain after some simplifications, the meridional stress resultant

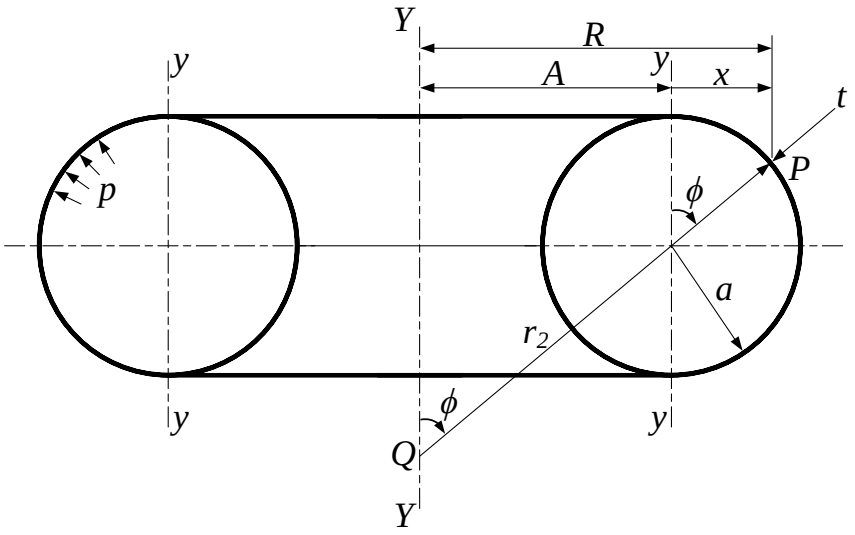

Figure 4.2. Circular toroidal shell under uniform internal pressure

$$N_\phi^m = \frac{1}{(A \pm a\sin\phi)\sin\phi}\left\{ pa\left(A\sin\phi \mp \frac{a}{2}\cos^2\phi \right) + k \right\}$$

where k is obtained from the boundary condition that: at $\phi = 0$ for the outer region (or $\phi = \pi$ for the inner region of the vessel), N_ϕ^m must remain finite. This condition gives

$$k = \pm pa^2/2$$

Therefore,

$$N_\phi^m = \frac{pa}{2}\left\{ \frac{\pm 2A + a\sin\phi}{\pm A + a\sin\phi} \right\} \qquad (4.10a)$$

With N_ϕ^m now known, the membrane stress resultant in the hoop direction follows from expression (4.4a), may be expressed as

$$N_{\theta}^{m} = \frac{pa}{2} \tag{4.10b}$$

This shows that, for a pressurised circular toroid, the membrane stress resultant in the hoop direction is independent on the mean toroidal radius A. Expressions (4.10) are well-known membrane results for pressurised circular toroidal shells (Bickell & Ruiz, 1967; Kraus, 1967; Zingoni, 1997; Vu, 2013; Fowler, Orifici & Wang, 2016). They do not describe the actual state of stress around the top and bottom circles of latitude. Incompatibility of deformations at the meeting points of the synclastic and anticlastic surfaces of the circular toroidal shell suggest that bending occurs in the regions and bending theory has to be used.

The deformation within the pressurised circular toroids may be obtained by the elimination of N_{ϕ}^{m} and N_{θ}^{m} from equations (4.5) and (4.9) using equations (4.10a) and (4.10b), and applying some simplifications. This gives

$$\delta^{m} = \frac{pa}{2Et}\left\{A(1-2\upsilon) \mp a(\upsilon-1)\sin\phi\right\} \tag{4.10c}$$

and

$$V^{m} = \frac{pa}{2Et}\left\{\frac{A\cot\phi}{A \pm a\sin\phi}\right\} \tag{4.10d}$$

If a non-dimensional parameter β_c (which is greater than 1) is defined as the ratio of the toroidal radius to the local cross-sectional radius, and an angular coordinate ϕ_c measuring the angle from the upward direction of the local axis $y-y$ round the circular cross-section of the toroidal shell are introduced into equations (4.10a) and (4.10b). That is

$$\beta_c = \frac{A}{a}$$

$$\phi_c = \phi$$

at the outer region, and

$$\phi_c = \phi + \pi$$

at the inner region. The following non-dimensional membrane stress results are obtained

$$\frac{N_{\phi}^{m}}{pa}=\frac{\beta_c+\frac{1}{2}\sin\phi_c}{\beta_c+\sin\phi_c} \tag{4.11a}$$

and

$$\frac{N_{\theta}^{m}}{pa}=\frac{1}{2} \tag{4.11b}$$

Hence, the non-dimensional hoop stress-resultant result for a pressurised circular toroidal shell is not a function of the introduced non-dimensional parameters ϕ_c and β_c. This is true because β_c is a function of the mean toroidal radius A, which is not a contributor to N_{θ}^{m} as seen in expressions (4.10b). However, the non-dimensional meridional stress-resultant result for the shell is a function of the introduced non-dimensional parameters ϕ_c and β_c; indicating that N_{ϕ}^{m} in the shell is directly proportional to the radius of the circular cross-section a (and, hence mean toroidal radius A).

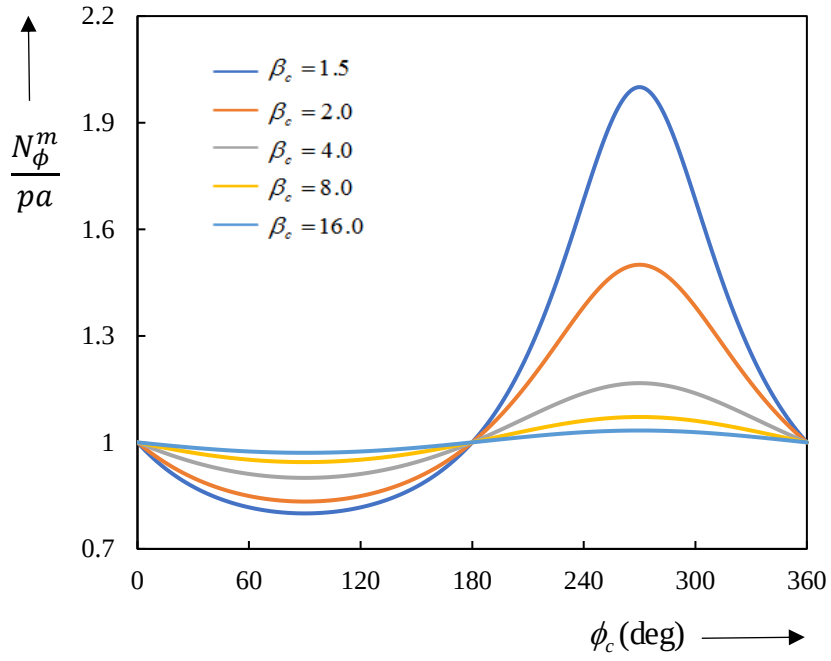

Figure. 4.3. Non-dimensional meridional stress resultant for various β_c of a circular toroid

The non-dimensional stress resultant in the meridional direction has been plotted in Figure 4.3 for various values of β_c as shown. It can be observed that as β_c increase, the non-dimensional stress resultant N_ϕ^m / pa increases in the outer region of the circular toroidal vessel. The reverse is the case in the inner region of the vessel, where N_ϕ^m / pa reduces are β_c increases. The changes in N_ϕ^m / pa at the inner region are more than that at the outer region of the shell as β_c varies. Therefore, if β_c approaches to infinity, the response of the toroid will tend to that of a long cylindrical shell under uniform pressure. The values of meridional stress resultant in the inner region are generally greater than those in the outer region of the internally pressurised circular toroidal vessel. It is also observed that, on the basis of the membrane hypothesis, the stresses in the entire vessel are in tension, suggesting that the vessel will unlikely fail due to buckling (Galletly & Błachut, 1995; Błachut & Jaiswal, 2000). However, if the direction of the pressure is reversed, so that the vessel is compressed, negative membrane results will be obtained throughout the vessel, an indication that buckling will occur in the compressed vessel. Buckling behaviour of this shell type under pressure loading is investigated in Chapter 6 of this thesis.

4.4.1.2 Circular toroidal tank

When the circular toroidal vessel is completely filled with a liquid of weight γ per unit volume, the loading component p_r (per unit area of shell middle surface) due to the internal pressure loading from the contained liquid, acting normal to the shell middle surface becomes

$$p_r = \gamma a\left(\pm 1 - \cos\phi\right)$$

Hence, expression (4.4b) for the membrane stress resultant in the meridional direction may be written as, after eliminating r_1, p_r and x with their appropriate expression as given above, and evaluating the ensuing integral,

$$N_\phi^m = \frac{\gamma a^2}{6\sin\varphi\left(A \pm a\sin\phi\right)}\left\{a\left(\mp 3 + 2\cos\phi\right)\cos^2\phi \mp 3A\left(\phi + (\mp 2 + \cos\phi)\sin\phi\right) + k\right\} \qquad (4.12)$$

The response of this shell type to hydrostatic loading greatly depends on the adopted boundary conditions and support locations within the structure. The boundary conditions leading to the

lowest load carrying capacity for toroidal shells under uniform external pressure have been presented through finite element analyses in (Błachut & Jaiswal, 1998a, 2000). It has been shown analytically that bending disturbances at support regions will be minimal if the support is positioned in such a way that its reactions are tangential to the shell middle surface (Zingoni, 1991, 1997, Zingoni & Pavlović, 1991a,b). However, should an occasion arise when this optimum support location/orientation is not adopted, provision of full geometric constraints should be ensured at the support level of a spherical vessel as these turn out to be a much more efficient arrangement than that in which free movement is allowed to occur (Zingoni & Pavlović, 1991b; Zingoni, 1997). Błachut & Jaiswal (1998b) however showed that critical buckling pressures for the over-restrained configurations of circular toroidal shells under uniform external pressure could be as much as about four times higher than the minimum buckling pressure.

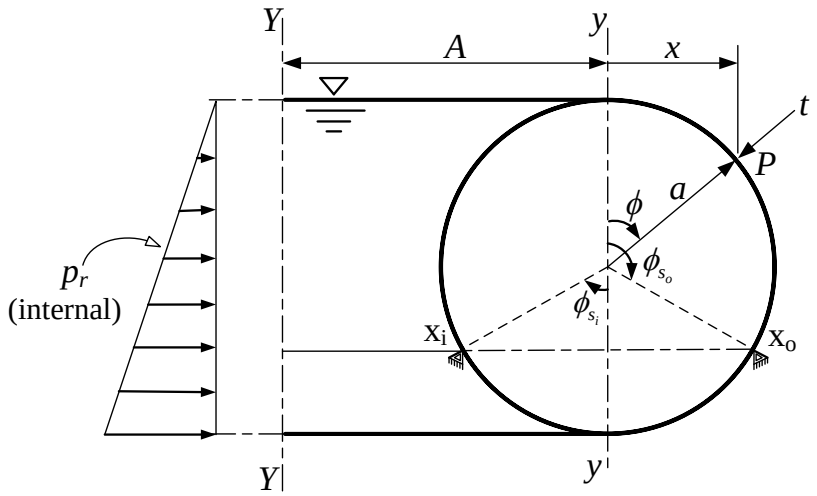

Figure 4.4. Half of a section of the circular toroidal tank

Therefore, if the toroidal vessel under present consideration is supported axisymmetrically at both the inner and outer regions simultaneously (that is, along the two parallel circles ($X_o X_o$ and $X_i X_i$) on the same level at the outer and inner regions of toroidal tank, as shown in Figure 4.4, for example), the tank will be seen to be made up of four regions: the upper-outer (above the support), lower-outer (below the support), upper-inner (above the support), and lower-inner regions (below the support). The support reactions on the toroidal shell are also assumed to be uniformly distributed around supports circumference. The latter assumption is justified since where continuous supports at the inner and outer equators are not used, discrete supports are

positioned close enough to evenly transfer reactions to the vessel so that the support conditions of the vessel are essentially axisymmetric.

4.4.1.2.1 Outer region of the tank

For the upper-outer region of the tank (above the support level), the constant of integration k in expression (4.12) is determined from the boundary condition: at $\phi = 0$, N_ϕ^m must be zero. This condition gives $k = a$, so that

$$N_\phi^m = \frac{\gamma a^2}{6\sin\phi\left(A + a\sin\phi\right)}\left\{a\left(1 + (-3 + 2\cos\phi)\cos^2\phi\right) - 3A\left(\phi + (-2 + \cos\phi)\sin\phi\right)\right\} \quad (4.13a)$$

When this is put into the expression (4.4a), the hoop stress resultant for the upper-outer region of the tank follows as

$$N_\theta^m = \frac{\gamma a}{6\sin^2\phi}\left\{4a(5 + 4\cos\phi)\sin^4\left(\frac{\phi}{2}\right) + 3A(\phi - \cos\phi\sin\phi)\right\} \quad (4.13b)$$

For the lower-outer region of the tank (below the support level), N_ϕ^m must remain finite at the nadir ($\phi = \pi$) of the tank. With this condition, k in expression (4.12) is obtained as $k = 5a + 3A\pi$. Therefore, the membrane stress resultant in the meridional direction may be written as

$$N_\phi^m = \frac{\gamma a^2}{6\sin\phi\left(A + a\sin\phi\right)}\left\{a\left(5 + (-3 + 2\cos\phi)\cos^2\phi\right) + 3A\left(\pi - \phi - (-2 + \cos\phi)\sin\phi\right)\right\} \quad (4.13c)$$

and, using the expression (4.4a), the membrane stress resultant in the hoop direction follows as

$$N_\theta^m = -\frac{\gamma a}{12\sin^2\phi}\left\{a(1 + 6\cos\phi + 3\cos 2\phi - 2\cos 3\phi) + 6A(\pi - \phi + \cos\phi\sin\phi)\right\} \quad (4.13d)$$

4.4.1.2.2 Inner region of the tank

For the upper-inner region of the tank (above the support level), the constant of integration k in expression (4.12) is determined from the boundary condition: at the apex ($\phi = \pi$) of the tank, N_ϕ^m must be zero. This condition gives $k = -(a + 3A\pi)$, so that

$$N_{\phi}^{m} = \frac{\gamma a^{2}}{6\sin\phi\left(A - a\sin\phi\right)}\left\{a\left((1+\cos\phi)^{2}(-1+2\cos\phi)\right)\right. \\ \left. +3A\left(-\pi+\phi+(2+\cos\phi)\sin\phi\right)\right\} \tag{4.13e}$$

and, from expression (4.4a)

$$N_{\theta}^{m} = -\frac{\gamma a}{6\sin^{2}\phi}\left\{4a\left(-5+4\cos\phi\right)\cos^{4}\left(\frac{\phi}{2}\right)+3A\left(\pi-\phi+\cos\phi\sin\phi\right)\right\} \tag{4.13f}$$

For the lower-inner region of the tank (below the support level), N_{ϕ}^{m} must remain finite at $\phi = 0$. With this boundary condition, k in expression (4.12) is obtained as $k = -5a$. Therefore, the membrane stress resultant in the meridional direction may be written as

$$N_{\phi}^{m} = \frac{\gamma a^{2}}{6\sin\phi\left(A - a\sin\phi\right)}\left\{a\left(-5+(3+2\cos\phi)\cos^{2}\phi\right)+3A\left(\phi+(2+\cos\phi)\sin\phi\right)\right\} \tag{4.13g}$$

and the membrane stress resultant in the hoop direction follows as

$$N_{\theta}^{m} = -\frac{\gamma a}{12\sin^{2}\phi}\left\{a\left(1-6\cos\phi+3\cos 2\phi+2\cos 3\phi\right)+3A\left(-2\phi+\sin 2\phi\right)\right\} \tag{4.13h}$$

As a check, for a limiting case of $A = 0$, the inner region of the tank vanishes, and it becomes a spherical tank, the above expressions (4.13) for the membrane stress resultants N_{ϕ}^{m} and N_{θ}^{m} at the upper and lower parts (above and below the support level) of the tank respectively coincide with the well-known results for a spherical tank (Flügge, 1973; Zingoni, 1997; Zingoni, Mokhothu & Enoma, 2015). The results for the lateral displacement δ^{m} and meridional rotation V^{m} of any point within the tank can be obtained from expressions (4.5) and (4.9), respectively, by using the corresponding membrane solution (4.13) for the particular region of interest.

4.4.1.2.3 Actions on ring beams and vertical supports

Since the vertical supports are interposed by ring beams at the outer and inner circles of latitude of the toroidal tank ($\phi = \phi_{s}$), where $\phi_{s} = \phi_{s_o}$ in the outer region of the vessel, and $\phi_{s} = \phi_{s_i}$ in

the inner region of the vessel, the difference in the values of the meridional stress resultants N_{ϕ}^{m} just below and above the supports ($\phi = \phi_s$) level is

$$N_s^m = \frac{\gamma a^2 (4a \pm 3A\pi)}{6 \sin\phi_s \left(a \sin\phi_s \pm A\right)}$$

where, for the sign ($\pm$), the plus sign applies to the outer region, while the minus sign applies to the inner region of the toroid. N_s^m acts tangentially to the shell middle surface, in the direction of increasing ϕ at the outer region and in the direction of decreasing ϕ at the inner region of the tank. Its vertical component causes compressive actions equal to the total weight of the contained liquid (since the weight of the vessel itself is neglected), in the vertical columns at the outer and inner regions of the vessel. The horizontal component of N_s^m for $\phi_s > \pi/2$ at the outer region and $\phi_s < \pi/2$ at the inner region also causes compressive actions in the ring beam at the inner circle of latitude, but the action is tensile in the ring beam at the outer circle of latitude of the toroidal tank. Hence, the vertical columns and horizontal ring beams at the outer and inner regions of the toroid must be designed for their respective actions.

If the support location is at the outermost and innermost circles of latitude ($\phi = \phi_s = \pi/2$) of the tank, so that the support reactions are tangential to the shell middle surface, the bending disturbances at the support regions of the tank will be minimised (Zingoni, 1991, 1997, Zingoni & Pavlović, 1991a,b). The difference in the values of the meridional stress resultants N_{ϕ}^{m} just below and above the supports level acts solely vertical and can be obtained from

$$N_s^m = \frac{\gamma a^2 (4a \pm 3A\pi)}{6(a \pm A)}$$

4.4.1.2.4 Numerical example of a circular toroidal tank supported at the equator

Consider a relatively large circular toroidal vessel made from steel plate of Young modulus $E = 200\times10^9 N/m^2$, Poisson ratio $\upsilon = 0.3$ and constant thickness $t = 0.05m$ throughout. The vessel of toroidal mean radius $A = 30m$ and circular cross-sectional radius $a = 15m$, is assumed to be completely filled with water of unit weight $\gamma = 10\times10^3 N/m^3$. The variations of membrane stresses over the circular profile $(20^o \le \phi \le 160^o)$ of the toroidal vessel are shown

in Figure 4.5; remember $\sigma_\phi^m = N_\phi^m / t$ and $\sigma_\theta^m = N_\theta^m / t$. The values below $\phi = 20^o$ and beyond $\phi = 160^o$ are not presented in the figure, as it is well-known, the membrane solution cannot be used to estimate the state of stress in the vicinity of the top and bottom circles of latitude. This is due to the bending that occurs there, which can be accounted for by the used of the more rigorous bending theory, where necessary.

The σ_ϕ and σ_θ in the outer region of the vessel appreciably rise in tension as one moves from the apex towards the outer support $\phi = 90^o$, where these stresses attain values of 8.94 MPa and 108.19 MPa respectively. The corresponding membrane deformations δ and V are 23.74 mm and -2.03×10^3 respectively. As expected at the support junction between the upper-outer and lower-outer regions, there are discontinuities in the meridional stress and hoop stress in moving across the support junction, where the stress values become 66.06 MPa and -63.19 MPa respectively at the lower-outer region of the vessel, while the deformations δ and V are -18.68 mm and -2.03×10^3 (compressive) respectively. The σ_ϕ continues to rise, but gradually in tension, as one moves from the support location towards the base of the vessel, while the σ_θ changes from being compressive to tensile at $\phi = 128^o$.

Similarly, the σ_ϕ and σ_θ in the inner region of the vessel gradually rise in tension as one moves from the bottom towards the inner support $\phi = 90^o$, where these stresses attain values of 123.19 MPa and 78.19 MPa respectively. The corresponding membrane deformations δ and V are -27.55 mm and 0.23×10^3 respectively. As also expected at the support junction between the upper- inner and lower- inner regions, there are discontinuities in the meridional stress and hoop stress in moving across the support junction, where the stress values become 11.81 MPa and -33.19 MPa (compressive) respectively at the upper-inner region of the vessel, while the deformations δ and V are 3.09 mm and 0.23×10^3 respectively. The σ_ϕ continues to decrease gradually in tension as one moves from the support location towards the apex of the vessel, while the σ_θ continued to be compressive.

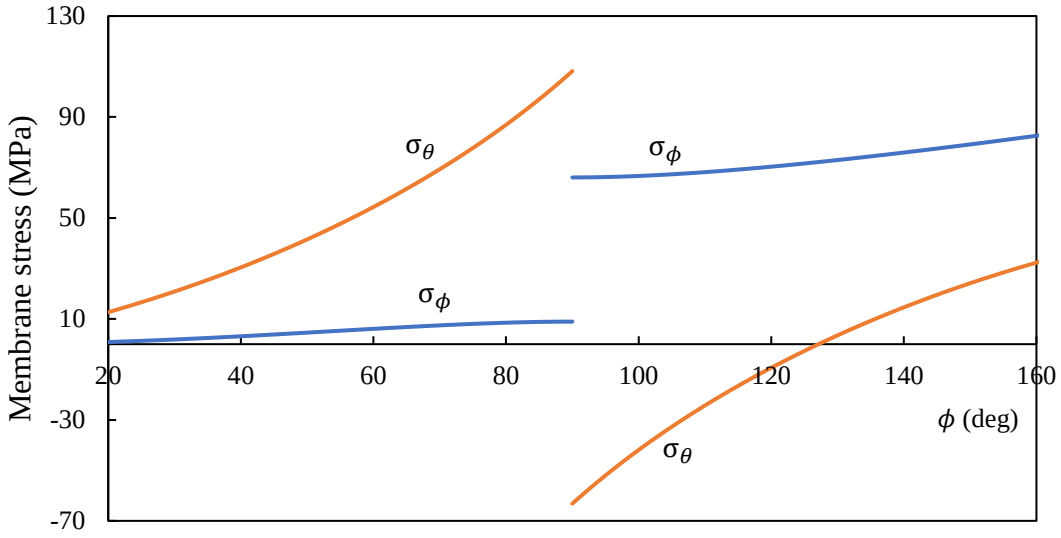

(a) Outer regions

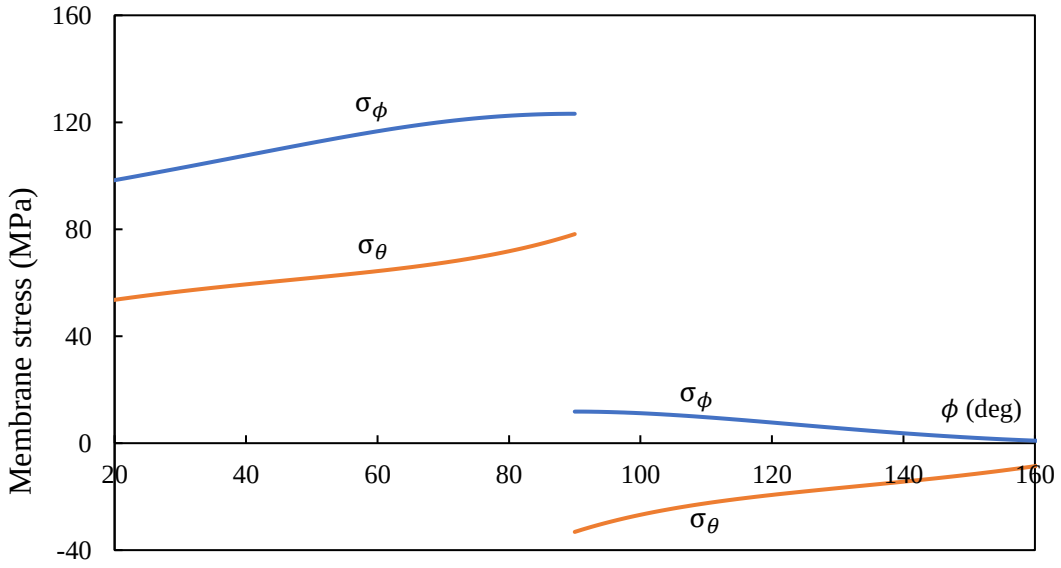

(b) Inner regions

Figure 4.5. Variations of membrane stresses over the circular profile of the toroidal vessel: (a) outer regions, and (b) inner regions

4.4.1.2.5 Non-dimensional membrane results for a circular toroidal tank supported at the nadir

For a specific case of a circular toroidal tank that is supported at the nadir circle of latitude (at $\phi = \pi$ for the outer region or $\phi = 0$ for the inner region) of the toroidal tank, there is of course, no region of the tank below the support. Hence, only the expressions (4.13a), (4.13b), (4.13e)

and (4.13f) for the upper parts of the vessel are sufficient for the membrane solution of the tank. These results may be re-cast in the following non-dimensional form, where the opening ratio β_c of the circular toroid is as earlier defined in Section 4.4.1.1 have been adopted,

$$\frac{N_\phi^m}{\gamma A^2} = \frac{1}{6\beta_c^2 \sin\phi(\beta_c + \sin\phi)} \left\{ \left(1 + (-3 + 2\cos\phi)\cos^2\phi\right) - 3\beta_c\left(\phi + (-2 + \cos\phi)\sin\phi\right)\right\} \quad (4.14a)$$

$$\frac{N_\theta^m}{\gamma A^2} = \frac{1}{6\beta_c^2 \sin^2\phi} \left\{ 4(5 + 4\cos\phi)\sin^4\left(\frac{\phi}{2}\right) + 3\beta_c\left(\phi - \cos\phi\sin\phi\right)\right\} \quad (4.14b)$$

for the outer region, and

$$\frac{N_\phi^m}{\gamma A^2} = \frac{1}{6\beta_c^2 \sin\phi(\beta_c - \sin\phi)} \left\{ \left((1+\cos\phi)^2(-1+2\cos\phi)\right) \right.$$

$$\left. +3\beta_c\left(-\pi + \phi + (2+\cos\phi)\sin\phi\right)\right\} \quad (4.14c)$$

$$\frac{N_\theta^m}{\gamma A^2} = -\frac{1}{6\beta_c^2 \sin^2\phi} \left\{ 4(-5 + 4\cos\phi)\cos^4\left(\frac{\phi}{2}\right) + 3\beta_c\left(\pi - \phi + \cos\phi\sin\phi\right)\right\} \quad (4.14d)$$

for the outer region of the vessel. The concept of non-dimensional membrane stress variations has been employed by Zingoni (2002b) to study liquid-filled parabolic ogival shells of revolution. The non-dimensional membrane stress results show that for circular toroids with the same mean radius to circular cross-sectional radius ratio β_c, membrane stress resultants in the tank are directly proportional to A^2 (or to a^2, since a is proportional to A). That is, doubling the local circular cross-sectional radius a or the global toroidal radius A of the toroid, while maintaining the parameter β_c constant, will quadruple the membrane stress resultants N_ϕ^m and N_θ^m in the shell. This is how the scale of the structure will affect its design.

4.4.1.3 Submerged circular toroidal shells

A submerged circular toroidal shell, which is supported axisymmetrically at both the innermost and outermost equators simultaneously, is depicted in Figure 4.6, where h_o is the distance between the surface of the liquid and the apex of the vessel; h is the overall height of the

vessel, (hence, $H = h + h_o$); and h_ϕ is the vertical distance measured from the apex of the vessel to any point P on the vessel. The other terms are as previously known. From the assumed support locations and definition of ϕ which indicates that two points are located on the middle surface of the toroidal shell for every value of ϕ, the circular toroidal shell is treated as having four regions - the upper-outer ($0 \le \phi \le \pi/2$), lower-outer ($\pi/2 \le \phi \le \pi$), lower-inner ($0 \le \phi \le \pi/2$), and upper-inner ($\pi/2 \le \phi \le \pi$) regions - as shown in Figure 4.7.

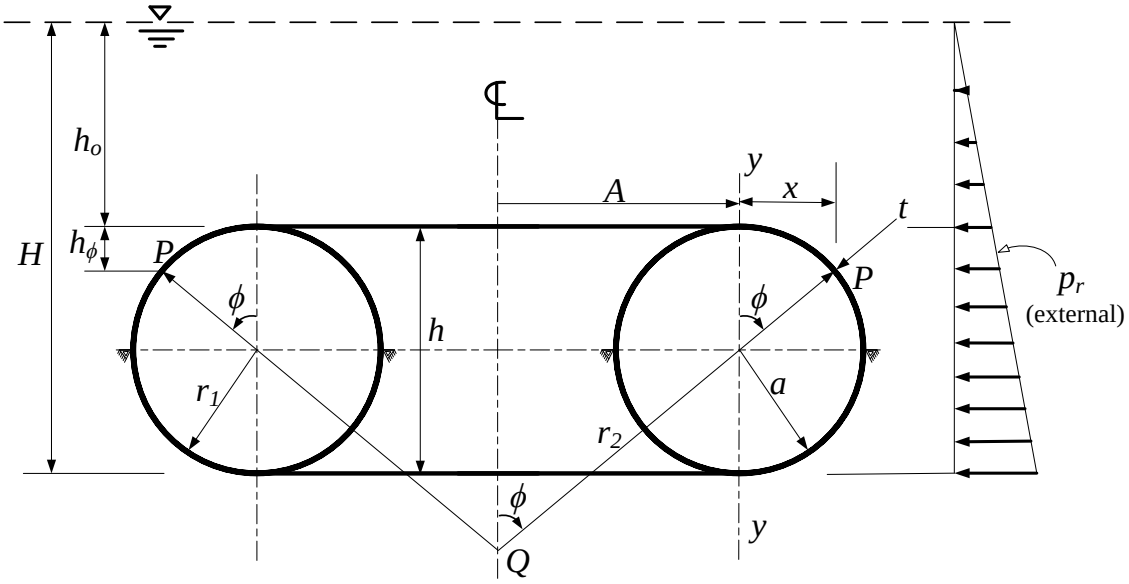

Figure 4.6. Geometry of a submerged circular toroidal shell

The toroidal vessel under consideration is completely submerged in a liquid of weight γ per unit volume. The loading component per unit area of shell middle surface in the direction of the tangent to the shell meridian is zero (i.e. $p_\phi = 0$) since hydrostatic pressure acts purely perpendicular to the shell middle surface. The loading component per unit area of shell middle surface due to the hydrostatic loading from the external liquid, acting normal to the shell middle surface is considered positive if pointing away from the axis of revolution of the shell, while negative if pointing towards the axis of revolution of the shell, may be expressed as:

$$p_r = \pm\gamma\left(h_o + h_\phi\right) \tag{4.15}$$

where,

$$h_\phi = a\left(1 \mp \cos\phi\right)$$

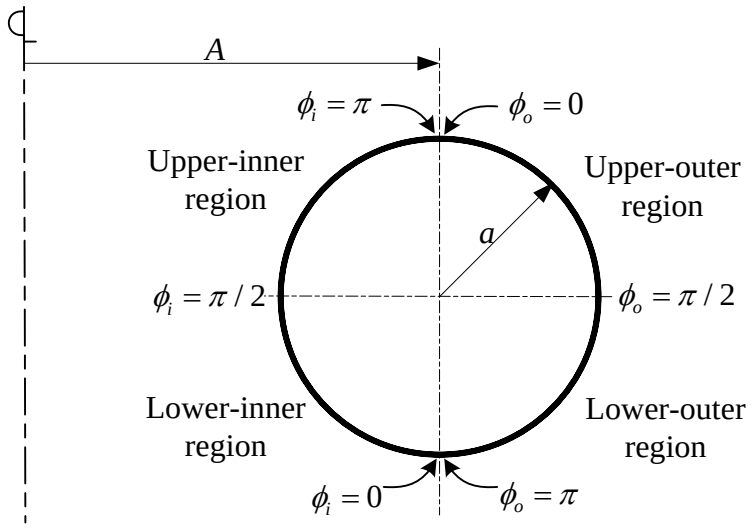

Figure 4.7: Regions of a circular toroidal shell

The maximum pressure $p_{\max}$ acting on the vessel is γH. This acts on the lowermost part of the vessel since hydrostatic pressure increases linearly with depth.

The use of the appropriate expressions to eliminate r_1, x, and p_r for each of the regions of the circular toroidal shell in expression (4.4b), and evaluating the ensuing integral and applying the boundary conditions that: at the apex of the vessel (where, depending on the particular region under consideration, $\phi = 0$ and π for the upper outer region and upper inner region, respectively), N_ϕ^m must remain zero; at the base of the vessel (where, depending on the particular region under consideration, $\phi = 0$ and π for the lower inner region and lower outer region, respectively), N_ϕ^m must be remain finite, gives the following membrane stress resultant N_ϕ^m in the meridional direction, after some basic manipulations:

$$N_\phi^m = -\frac{a\gamma}{6\sin\phi(A + a\sin\phi)}\Big[a^2(\cos\phi - 1)^2(2\cos\phi + 1) - 3aA\{\phi + \sin\phi(\cos\phi - 2)\}$$

$$+ 3h_o \sin\phi(2A + a\sin\phi)\Big] \qquad (4.16a)$$

for the upper-outer region,

$$N_\phi^m = -\frac{a\gamma}{6\sin\phi(A + a\sin\phi)}\Big[a^2(2\cos^3\phi + 3\sin^2\phi + 2) - 3aA\{\phi - \pi + \sin\phi(\cos\phi - 2)\}$$

$$+3h_o \sin\phi(2A + a\sin\phi)\Big] \tag{4.16b}$$

for the lower-outer region,

$$N_\phi^m = -\frac{a\gamma}{6\sin\phi(A - a\sin\phi)}\Big[a^2(2\cos^3\phi - 3\sin^2\phi - 2) + 3aA\{\phi + \sin\phi(\cos\phi + 2)\}$$

$$-3h_o \sin\phi(2A - a\sin\phi)\Big] \tag{4.16c}$$

for the lower-inner region, and

$$N_\phi^m = -\frac{a\gamma}{6\sin\phi(A - a\sin\phi)}\Big[a^2(2\cos^3\phi + 3\cos^2\phi - 1) + 3aA\{\phi - \pi + \sin\phi(\cos\phi + 2)\}$$

$$-3h_o \sin\phi(2A - a\sin\phi)\Big]$$

for the upper-inner region.

The last term (with h_o) in each of the expressions (4.16) is the contribution of the pressure loading from the liquid above the level of the submerged vessel. This contribution is for a particular depth h_o, coincides with the well-known solution (Flügge, 1973; Zingoni, 1997; Ventsel & Krauthammer, 2001) for membrane-stress resultant in meridional direction of uniformly pressurised circular toroidal shells if the pressure term ($-\gamma h_o$) is replaced by p, as obtained in Section 4.4.1.1. If h_o is set to zero in each of the expressions (4.16), the resulting expressions are contributions of the external hydrostatic effects from the top to bottom of the vessel, as presented in Section 4.4.1.2 for internal hydrostatic loading. Hence, the above results can also be applied to a toroidal vessel under combined internal vacuum and external hydrostatic loading from the top to bottom of the vessel. For each of the regions of the vessel, the membrane stress resultants in the hoop direction N_θ, horizontal displacement δ^m and meridional rotation V^m of the submerged vessel may be obtained from expressions (4.4a), (4.5), and (4.9), respectively.

4.4.2 Elliptical toroidal vessel

4.4.2.1 The geometry of the shell

Figure 4.8 shows the parameters of an elliptic toroidal shell that is generated by the rotation of an elliptical plane about a global vertical axis $Y-Y$ through a complete circle. a and b denote the horizontal and vertical semi-axes of the elliptical cross-section, respectively, and other parameters in the figure are as previously defined in Chapter 3. Following the approach used by Zingoni in formulating the problem of the ellipsoid of revolution (Zingoni, 1997), the meridional profile of the local elliptical cross-section may be depicted by the simple equation of an ellipse

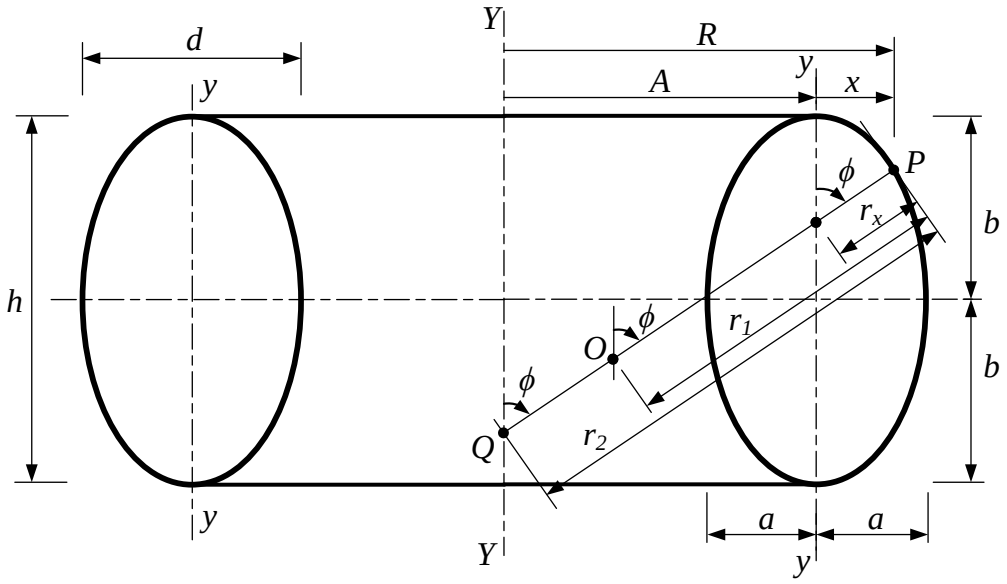

Figure 4.8. An elliptic toroidal shell

$$\frac{x^2}{a^2}+\frac{y^2}{b^2}=1 \tag{4.17}$$

and ϕ may be interpreted as the slope at a point on the meridional profile

$$\phi=\tan^{-1}\left(\frac{dy}{dx}\right) \tag{4.18}$$

The range of ϕ at the outer and inner surfaces of the elliptical toroid follows the description in Figure 4.7 for circular toroids.

Equation (4.17) may be re-written in the form

$$y = \pm \frac{b}{a}\sqrt{a^2 - x^2} \tag{4.19}$$

Differentiation with respect to x gives the slope of the tangent to the meridian at any point

$$\frac{dy}{dx} = \pm \frac{b}{a}\frac{x}{\sqrt{a^2 - x^2}} \tag{4.20}$$

Manipulation of equations (4.18) and (4.20) yields

$$x = \pm \frac{a^2 \sin\phi}{\sqrt{a^2 \sin^2\phi + b^2 \cos^2\phi}} \tag{4.21}$$

where the upper sign of the double operations applies to the outer region, while the lower sign applies to the inner regions of the toroid. Introduction of equation (4.21) into (4.20) gives

$$y = \pm \frac{b^2 |\cos\phi|}{\sqrt{a^2 \sin^2\phi + b^2 \cos^2\phi}} \tag{4.22}$$

Here, the upper sign of the double operations applies for points above the equatorial circle of latitude, while the lower sign applies for points below the equatorial circle of latitude of the elliptical toroid.

The meridional radius of curvature r_1 of the toroidal middle surface at any point may be obtained from the relationship of plane-curve geometry (Zingoni, 1997, 2018):

$$r_1 = \frac{\left\{1 + \left(\frac{dy}{dx}\right)^2\right\}^{3/2}}{\frac{d^2 y}{dx^2}} \tag{4.23}$$

Introduction of equation (4.20), and using equation (4.21) to eliminating x, yields the following expression for the meridional radius of curvature:

$$r_1 = \pm \frac{a^2 b^2}{\left(a^2 \sin^2\phi + b^2 \cos^2\phi\right)^{3/2}} \tag{4.24}$$

4.4.2.2 Under uniform internal pressure

When equations (4.21) and (4.24) are put into expression (4.4b) and the integral is evaluated, by applying similar manipulations and boundary conditions adopted for a pressurised circular toroid in Section 4.4.1.1 (and taking $p_r = \pm p$, the uniform internal pressure, which acts normal to the middle surface of the vessel), the following membrane stress resultants in the meridional and hoop directions of the elliptical toroidal vessel are obtained, respectively,

$$N_{\phi}^{m} = \frac{pa^2}{2x_{el}} \left\{ \frac{2Ax_{el} \pm a^2 \sin\phi}{Ax_{el} \pm a^2 \sin\phi} \right\} \tag{4.25a}$$

and

$$N_{\theta}^{m} = \frac{pa^2}{b^2} \left\{ \frac{2b^2 - x_{el}^2}{2x_{el}} \pm \left(\frac{b^2 - a^2}{a^2} \right) A \sin\phi \right\} \tag{4.25b}$$

where,

$$x_{el} = \sqrt{a^2 \sin^2\phi + b^2 \cos^2\phi} \tag{4.26}$$

This set of membrane results are identical to those derived by (Zingoni, 1997) for a vessel in the form of an elliptic torus. Like in the case of a circular toroid, the membrane solution fails around the upper and lower circles of latitude where the negative and positive Gaussian surfaces of the elliptic torus meet. Using the membrane stress resultants, the deformations that occur within the vessel can be obtained from expressions (4.5) and (4.9) in the usual way. The stress results may be written in a non-dimensional form by introducing parameters: β_{el} (which is greater than 1), defined as the ratio of the main toroidal radius to the horizontal semi-axis of the local elliptical profile; and ξ_{el}, defined as the ratio of vertical semi-axis to the horizontal semi-axis of the local elliptical cross-section of the toroidal shell. That is

$$\frac{N_{\phi}^{m}}{pa} = \frac{1}{2\bar{x}_{el}} \left\{ \frac{2\beta_{el}\bar{x}_{el} + \sin\phi_c}{\beta_{el}\bar{x}_{el} + \sin\phi_c} \right\} \tag{4.27a}$$

and

$$\frac{N_\theta^m}{pa} = \frac{1}{\xi_{el}^2}\left\{\frac{\xi_{el}^2}{\bar{x}_{el}} - \frac{\bar{x}_{el}}{2} + \left(\xi_{el}^2 - 1\right)\beta_{el}\sin\phi_c\right\} \tag{4.27b}$$

where,

$$\bar{x}_{el} = \sqrt{\sin^2\phi_c + \xi_{el}^2\cos^2\phi_c} \tag{4.28}$$

and

$$\beta_{el} = \frac{A}{a} \tag{4.29a}$$

$$\xi_{el} = \frac{b}{a} \tag{4.29b}$$

and ϕ_c is angular coordinate measured clockwise around the entire elliptical cross-section (within the range of $0 \le \phi_c \ge 2\pi$), as earlier illustrated in Section 4.4.1.1.

The non-dimensional membrane stress resultants N_ϕ^m / pa and N_θ^m / pa for an elliptical toroidal shell under internal pressure loading have been plotted in Figure 4.9 – 4.11 for various values of β_{el} (= 1.5, 2.0, 4.0 and 8.0) in each of ξ_{el} (= 1.5, 2.0 and 4.0). In the figure, the subscript el with ξ_{el} has been omitted for simplicity. On a general note, based on the membrane-hypothesis results, the hoop stress increase as ξ_{el} increases from case to case. The meridional stress values within the pressurised vessel are tensile throughout the entire vessel, and the hoop stresses in the outer region of the vessel for all cases considered are also in tension. However, unlike in the case of an internally pressurised circular toroidal shell, the hoop stresses in the inner region of all the vessels considered are in compression, suggesting possible occurrence of local buckling in the region of the vessels (Galletly & Błachut, 1995; Błachut & Jaiswal, 2000).

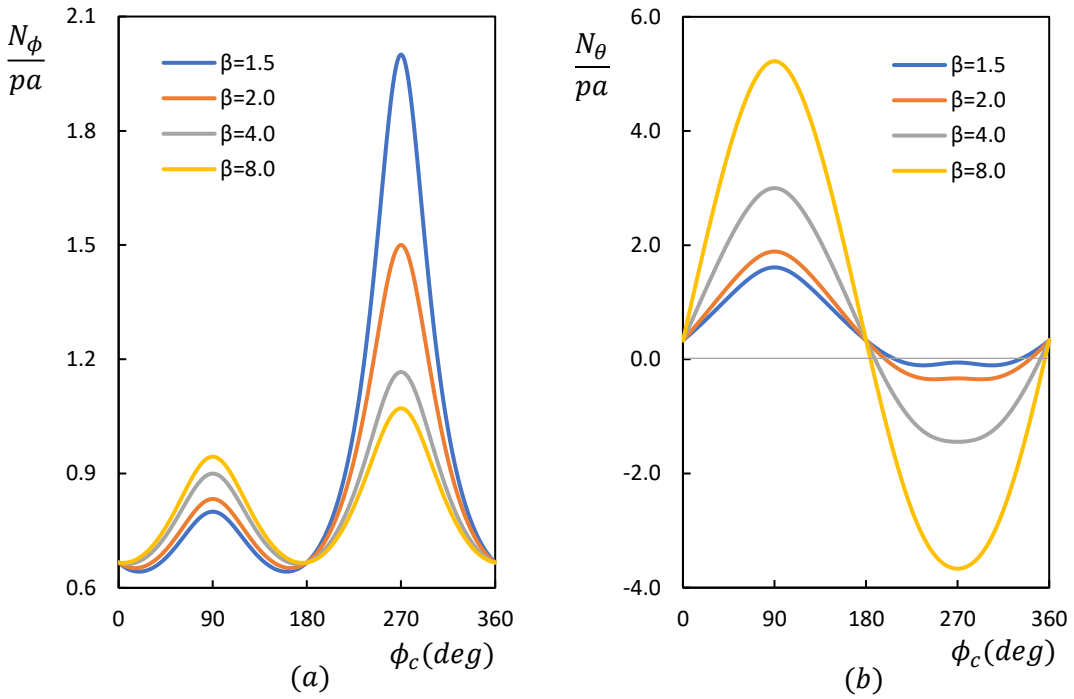

Figure 4.9. Pressurised elliptic toroid: non-dimensional membrane stresses for $\xi_{el} = 1.5$: (a) meridional, and (b) hoop results

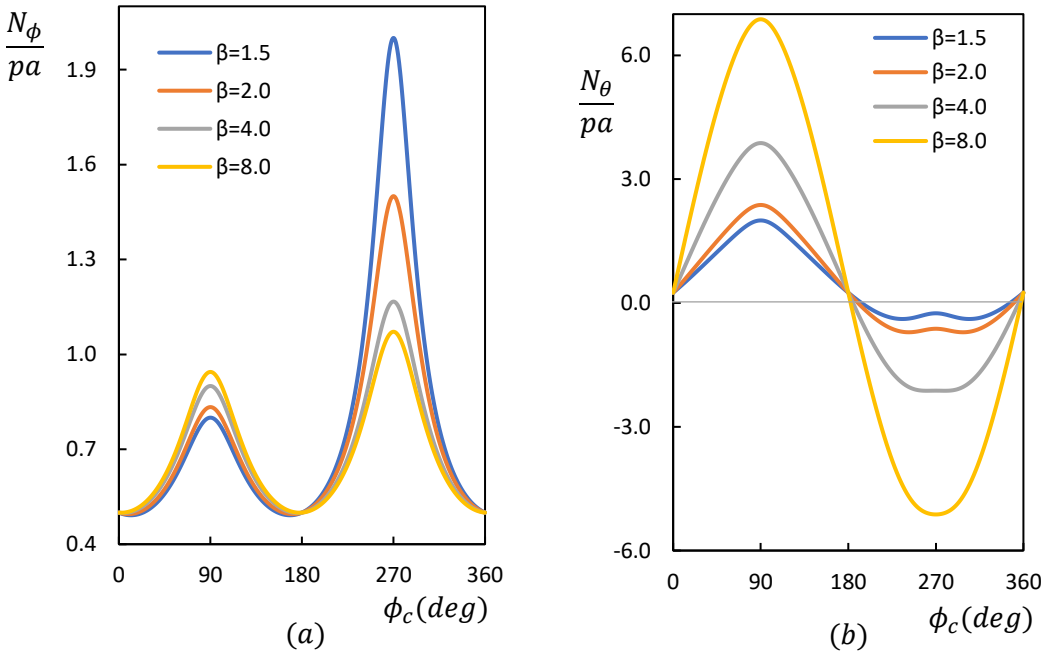

Figure 4.10. Pressurised elliptic toroid: non-dimensional membrane stresses for $\xi_{el} = 2.0$: (a) meridional, and (b) hoop results

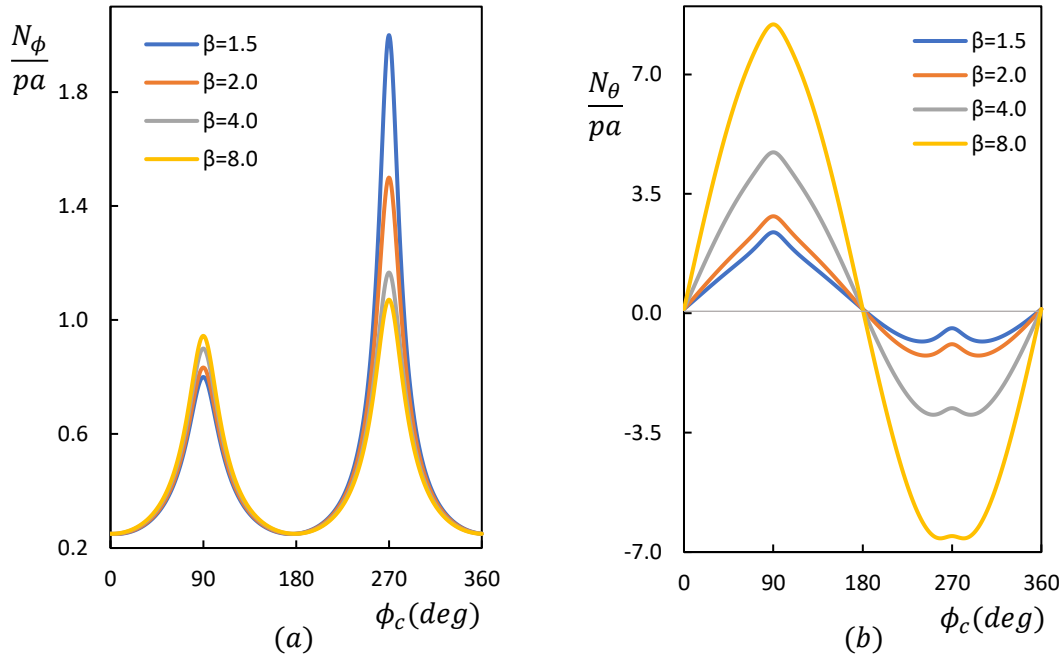

Figure 4.11. Pressurised elliptic toroid: non-dimensional membrane stresses for $\xi_{el} = 4.0$: (a) meridional, and (b) hoop results

4.4.2.3 Elliptic toroidal tank

Consider an elliptic toroidal tank that is completely-filled with a liquid of weight γ per unit volume. The essential load is assumed to be strictly hydrostatic pressure loading, which acts normal to the shell middle surface and is proportional to the depth h_d of liquid along the vertical coordinate y from the apex of the tank. If

$$h_d = b - y$$

then the normal loading component for the completely-filled elliptic toroid can follow from $p_r = \pm\gamma h_d$, which after substituting equation (4.22), may be written in the form

$$p_r = \gamma b\left(\pm 1 - \frac{b\cos\phi}{\sqrt{a^2\sin^2\phi + b^2\cos^2\phi}}\right) \tag{4.30}$$

or, in terms of ϕ_c as

$$p_r = \gamma b\left(1-\frac{b\cos\phi_c}{\sqrt{a^2\sin^2\phi_c+b^2\cos^2\phi_c}}\right)$$

Parameters x and r_1 remain the same as in the case of the pressurised elliptic toroid, and may be rewritten in terms of ϕ_c as

$$x=\frac{a^2\sin\phi_c}{\sqrt{a^2\sin^2\phi_c+b^2\cos^2\phi_c}}$$

$$r_1=\frac{a^2b^2}{\left(a^2\sin^2\phi_c+b^2\cos^2\phi_c\right)^{3/2}}$$

When these, plus equation (4.30) are put into expression (4.4b) for the membrane stress resultant in the meridional direction, the following result is obtained, after the evaluation of the ensuing integral,

$$N_\phi^m=\frac{\gamma a^2 b}{6(A+x)\sin\phi_c}\left[-\frac{3A}{a\sqrt{a^2-b^2}}\left\{\frac{x_{el_2}}{x_{el_1}}\tan^{-1}\left(\frac{b}{x_{el_1}}\tan\left(\frac{\phi_c}{2}\right)\right)+\frac{x_{el_3}}{x_{el_4}}\tan^{-1}\left(\frac{b}{x_{el_4}}\tan\left(\frac{\phi_c}{2}\right)\right)\right\}\right.$$

$$+\frac{\sqrt{2}}{x_{el_5}^{3/2}}\left(4b^3\cos^3\phi_c+3A\left\{\left(3a^2+b^2\right)\sin\phi_c+\left(-a^2+b^2\right)\sin(3\phi_c)\right\}\right)$$

$$\left.+\frac{3b}{x_{el_5}}\left(\frac{2a^2b}{-a^2+b^2}-A\sin\left(2\phi_c\right)\right)+k\right] \qquad (4.31a)$$

where,

$$x_{el_1}=\sqrt{2a^2-b^2-2a\sqrt{a^2-b^2}}$$

$$x_{el_2}=-a^2+b^2+a\sqrt{a^2-b^2}$$

$$x_{el_3}=a^2-b^2+a\sqrt{a^2-b^2}$$

$$x_{el_4}=\sqrt{2a^2-b^2+2a\sqrt{a^2-b^2}}$$

$$x_{el_5} = a^2 + b^2 + \left(-a^2 + b^2\right)\cos\left(2\phi_c\right)$$

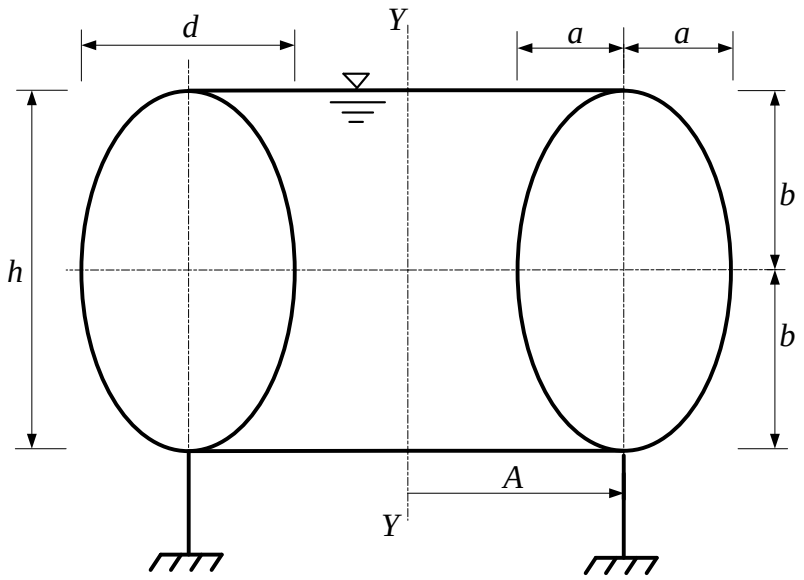

Figure 4.12. Elliptical toroidal tank support at the lowest circle of latitude

If the elliptic toroidal tank is supported axisymmetrically along the nadir parallel circle of latitude $\phi_c = \pi$ (that is, at $\phi = \pi$ for the outer region or $\phi = 0$ for the inner region) of the toroidal tank, then the regions of the tank will be above the support level (see Figure 4.12). For this situation, the constant of integration k in expression (4.31a) may be obtained from the boundary condition: at $\phi_c = 0$, the meridional stress resultant N_ϕ^m must be zero. This gives

$$k = \frac{3a^2}{a^2 - b^2} - 2$$

With N_ϕ^m now known, the hoop stress resultant follows expression (4.4a) as

$$N_\theta^m = \frac{\gamma x_{el}^3}{6b}\left(\frac{a^2}{x_{el}} + \frac{A}{\sin\phi_c}\right)\left[\frac{6b^2}{x_{el}^4}\left(x_{el} - b\cos\phi_c\right) - \frac{x_{el}}{\left(Ax_{el} + a^2\sin\phi\right)\sin\phi}\left[\frac{3a^2}{a^2 - b^2} - 2 - \frac{3A}{a\sqrt{a^2 - b^2}}\right.\right.$$

$$\left.\left.\times\left\{\frac{x_{el_2}}{x_{el_1}}\tan^{-1}\left(\frac{b}{x_{el_1}}\tan\left(\frac{\phi_c}{2}\right)\right) + \frac{x_{el_3}}{x_{el_4}}\tan^{-1}\left(\frac{b}{x_{el_4}}\tan\left(\frac{\phi_c}{2}\right)\right)\right\} + \frac{3b}{x_{el_5}}\left(\frac{2a^2 b}{-a^2 + b^2} - A\sin\left(2\phi_c\right)\right)\right.\right.$$

$$+\frac{\sqrt{2}}{x_{el_5}^{3/2}}\left(4b^3\cos^3\phi_c+3A\left\{\left(3a^2+b^2\right)\sin\phi_c+\left(-a^2+b^2\right)\sin\left(3\phi_c\right)\right\}\right)\Bigg]\Bigg] \qquad (4.31b)$$

Owing to the nature of the closed-form membrane-stress results (expressions (4.4)), it is difficult to see the variation of N_ϕ^m and N_θ^m across the elliptical profile of the hydrostatically loaded toroidal vessel supported at the lowest circle of latitude. Hence, a simple numerical example is conducted with the above solution in the following, to investigate the response of the tank to the fluid loading. The toroidal vessel is assumed to have geometrical parameters: $A=10.0m$, $b=10.0m$ and $a=5.0m$, and be completely filled with water of unit weight $\gamma=10\times10^3 N/m^3$. The variation of the meridional and hoop stress resultants (N_ϕ^m and N_θ^m) against ϕ_c in the outer and inner regions of the elliptic toroidal tank is shown in Figure 4.13.

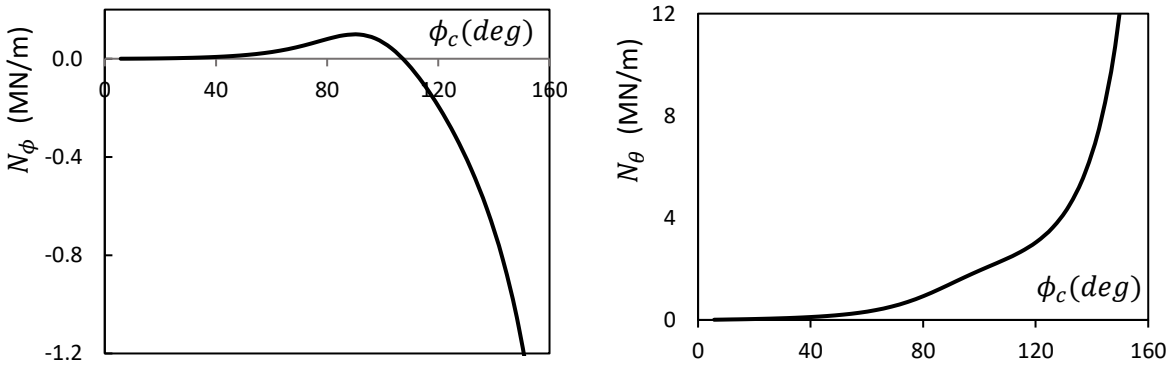

Figure 4.13(a). Variation of membrane stress resultants N_ϕ^m and N_θ^m in the outer region of the elliptic toroidal tank

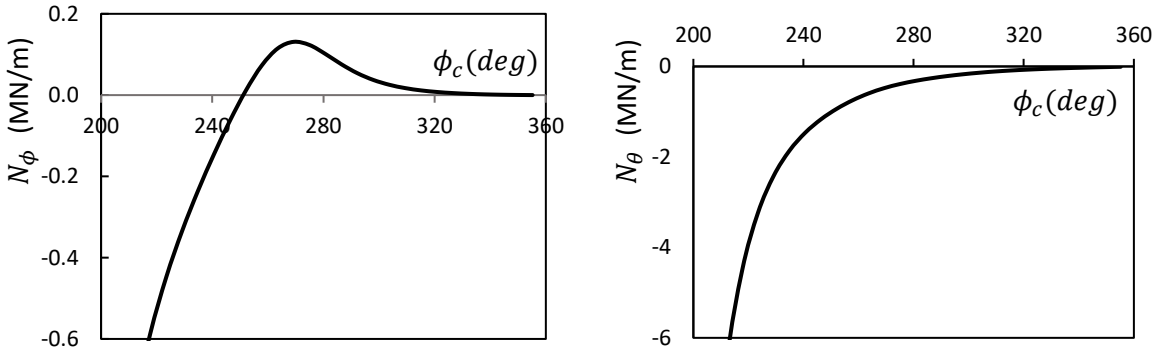

Figure 4.13(b). Variation of membrane stress resultants N_ϕ^m and N_θ^m in the inner region of the elliptic toroidal tank

The trend of the membrane stresses (Figure 4.13(a)) in the outer region of the elliptic toroidal tank is similar to that of the parabolic ogival digester (Zingoni, 2002). A toroidal shell with parabolic ogival cross-section will be studied in the next section. For the present toroidal tank, as expected for a liquid-filled vessel, the meridional stress increases in tension from the apex of the tank in both the outer and inner sides of the toroid. The tensile stress on each of the sides reaches maximum value around the equatorial zones with the inner surface experiencing over 1.3 times the maximum tensile stresses in the outer surface of the vessel. Beyond these points, the tensile stresses begin to reduce until the cross-over lines, (which are approximately $\phi_c = 105^o$ at the outer and $\phi_c = 250^o$ at the inner surfaces). After that, compressive meridional stresses are seen in both sides of the toroid. These become very large in the lower parts of the tank. On the other hand, while the hoop stress resultants in the outer region of the vessel are entirely tensile (with lower values at the upper region and larger values at the lower region of the inner side of the tank), those in the outer region of the vessel are entirely compressive (with lower values at the upper region and larger values at the lower region of the inner side of the tank).

Based on the above, an elliptic toroidal vessel under hydrostatic pressure and supported axisymmetrically at the nadir would buckle at the lower region of the tank, owing to the huge meridional compressive stresses experience there. This problem can be addressed by enhancing the shell thickness around the zones. Also, if the axisymmetric support is positioned on or just above the cross-over lines, the vessel will likely not experience meridional compressive stresses around the lower regions of the tank. Closed-form membrane stress results for elliptic toroidal tanks supported at innermost and outermost circles of latitude have been presented by Govender (2017). For the problem of the huge hoop stresses at the lower regions of the outer surface of the tank (see Figure 4.13(a) above), a controlled prestressing may be required.

4.4.3 Parabolic ogival toroidal vessel

Figure 4.14 shows an unconventional toroidal shell of revolution, which is generated by rotating a 2-pointed parabolic ogival closed section through 360^o about a vertical axis $Y-Y$ that lies at a distance A from the local axis of symmetry (the y-axis) of the parabolic ogival profile. This cross-sectional shape was first proposed by Zingoni (2002b), as a possible profile for egg-shaped digesters. Here, the same shape is adopted as the cross-section of the toroidal vessel. The closed profile is formed by two parabolas that are symmetrical about the horizontal

x-axis and that intersect at a distance of $\pm h/2$ on the y-axis. The overall height of the cross-section is, therefore h, and the width of the cross-section is d. Denoting the origin by O (the intersection of the local x and y axes), and defining an angular coordinate ϕ (the angle measured from the upward direction of the global $Y-Y$ axis of revolution of the toroid to the normal to the shell middle surface at the point P in question), the toroid lies wholly in the intervals:

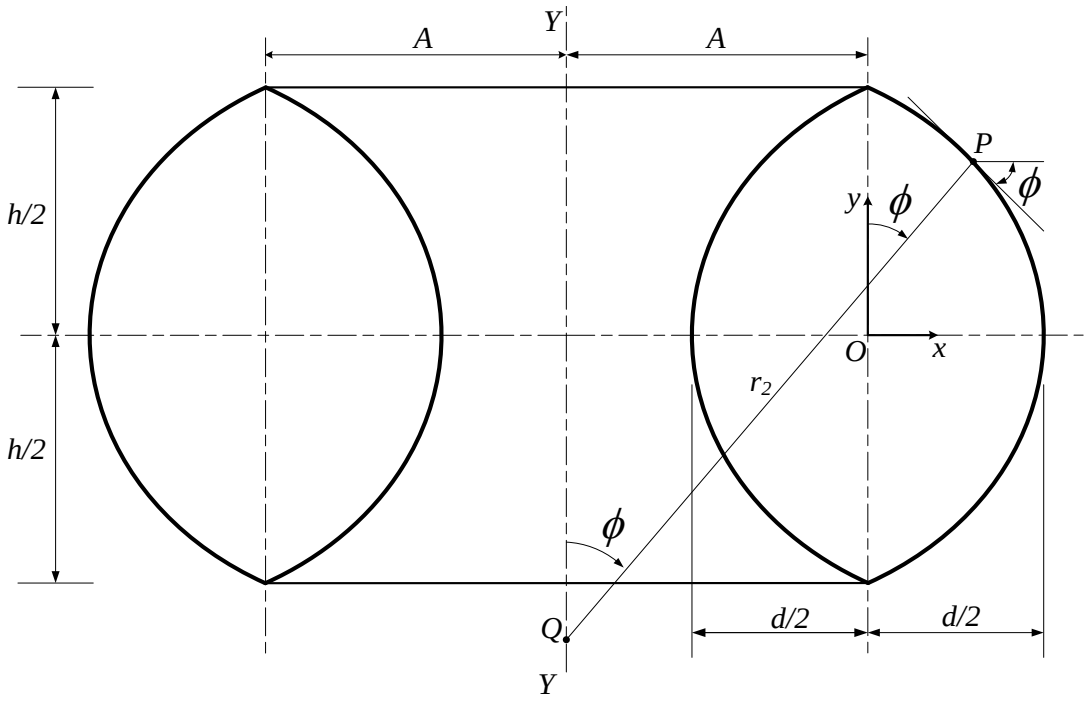

Figure 4.14. An ogival toroidal shell of revolution

$$\phi_o \le \phi \le \bar{\phi}_o$$

for both outer and inner regions, where ϕ_o and $\bar{\phi}_o$ are respectively the angular coordinates at the upper and lower poles of the outer region of the toroid. The reverse is the case for the inner region of the toroid. ϕ_o and $\bar{\phi}_o$ may be obtained easily by starting with the equation of the meridional profile (Zingoni, 2002; Enoma & Zingoni, 2016a)

$$\frac{d}{2} - x = ky^2 \tag{4.32}$$

where the constant k is obtained as

$$k = \frac{2d}{h^2}$$

from the condition: at $x = 0$, $y = \pm h/2$. Consequently, expression (4.32) may be rearranged as

$$y = \pm \frac{h}{\sqrt{2d}} \sqrt{\frac{d}{2} - x} \tag{4.33}$$

Differentiation of this with respect to x, gives the following expression which is equated to the angular coordinate ϕ as

$$\frac{dy}{dx} = \mp \frac{h}{2\sqrt{2d}} \left(\frac{d}{2} - x \right)^{-1/2} = -\tan\phi \tag{4.34}$$

Hence, at the upper and lower poles of the toroid ($x = 0$, $y = \pm h/2$), the angular coordinate ϕ $\left(= \phi_o\right)$ takes the form

$$\phi_o = \pi - \bar{\phi}_o = \tan^{-1}\left(\frac{h}{2d} \right) \tag{4.35}$$

The horizontal distance coordinate between any point on the toroidal surface and the local axis of the cross-sectional profile x, and the first principal radius of curvature r_1 are respectively obtained from expressions (4.34) and (4.23), after some mathematical manipulations, as

$$x = \pm \frac{4d^2 \sin^2\phi - h^2 \cos^2\phi}{8d \sin^2\phi} \tag{4.36a}$$

$$r_1 = \pm \frac{h^2}{4d \sin^3\phi} \tag{4.36b}$$

Remember, the double-sign notation ($\pm$ or $\mp$) refers to the two regions simultaneously, with the upper sign referring to the outer region, and the lower sign referring to the inner region, and that the second principal radius of curvature r_2 is expressed as

$$r_2 = \frac{R}{\sin\phi} = \frac{A+x}{\sin\phi}$$

where, as before, R is the horizontal coordinate measuring the distance between the vertical axis of revolution $Y-Y$ and any point on the middle surface of the toroidal shell.

4.4.3.1 Parabolic ogival toroid under uniform internal pressure

For an ogival toroidal shell under the action of uniformly distributed pressure-loading on the inner surface of the toroid, the internal pressure $p = p_r$ acts solely perpendicular to the shell middle surface. Thus, elimination of r_1 and x from expression (4.4b) with appropriate expressions (4.36), and solving the integral with the boundary conditions that N_ϕ^m vanishes at the poles $\phi = \phi_o, \bar{\phi}_o$ (see equation (4.35)), the following results are obtained for the membrane stress resultants in the meridional direction at the outer and inner regions of the vessel:

$$N_\phi^m = \frac{p\left(4d^2 - h^2\cot^2\phi\right)}{16d\sin\phi}\left\{\frac{4d\left(\pm 4A + d\right) - h^2\cot^2\phi}{4d\left(\pm 2A + d\right) - h^2\cot^2\phi}\right\} \tag{4.37a}$$

When appropriate expressions (4.36) and (4.37) are used to eliminate respectively r_1, x and N_ϕ^m from expression (4.4a), we obtain the following expressions for the membrane stress resultants N_θ^m in the hoop direction, after some simplifications:

$$N_\theta^m = \frac{p\sin\phi}{32dh^2}\left[-h^4\cot^4\phi - 4h^2\cot^2\phi\left\{\mp 2d\left(2A \pm d\right) + \frac{h^2}{\sin^2\phi}\right\}\right.$$

$$\left. -16d\left\{d^2\left(\pm 4A + d\right) \mp \left(2A \pm d\right)\frac{h^2}{\sin^2\phi}\right\}\right] \tag{4.37b}$$

With N_ϕ^m and N_θ^m now known, and using expressions (4.5) and (4.9), the deformation that occurs within the pressurised parabolic ogival toroid may be obtained from:

$$\delta^m = \frac{A+x}{Et}\left\{N_\theta^m - \upsilon N_\phi^m\right\} \tag{4.37c}$$

$$V^m = \frac{1}{r_1}\Bigg[\frac{\cot\phi}{Et}\Bigg\{\left(r_1+\upsilon\frac{A+x}{\sin\phi}\right)N_\phi^m-\left(\frac{A+x}{\sin\phi}+\upsilon r_1\right)N_\theta^m\Bigg\}$$

$$+\frac{p\cos\phi}{128d^2Et\sin^3\phi}\Bigg\{\pm384A^2d^2\pm\frac{2h^2}{\sin^2\phi}\left(4d(\pm2A+d)+h^2\right)\left(-11+4\upsilon\right)$$

$$\mp\left(4d^2+h^2\right)\left(4d(\pm4A+d)+h^2\right)\left(-7+2\upsilon\right)\pm\frac{3h^4}{\sin^4\phi}\left(5-2\upsilon\right)\Bigg\}\Bigg] \qquad (4.37d)$$

Following the strategy first proposed by Zingoni (2002b), but now extended to the present toroidal geometry, the above results for the membrane stress resultants may be written in a non-dimensional form by the introduction of the following non-dimensional terms:

$$\xi = \frac{h}{d} \qquad (4.38a)$$

$$\beta = \frac{A}{d} \qquad (4.38b)$$

In which, ξ is defined as the height-to-width ratio of the cross-sectional profile, β (which is greater than 0.5), is the ratio of the mean toroidal radius to the equatorial width of the cross-sectional profile. When these are employed in expressions (4.37), the following non-dimensional membrane results for the outer and inner regions of the ogival toroidal vessel is obtained after some manipulations:

$$\frac{N_\phi^m}{pA} = \frac{4-\xi^2\cot^2\phi}{16\beta\,\sin\phi}\left\{\frac{4\left(\pm4\beta\,+1\right)-\xi^2\cot^2\phi}{4\left(\pm2\beta\,+1\right)-\xi^2\cot^2\phi}\right\} \qquad (4.39a)$$

and

$$\frac{N_\theta^m}{pA} = -\frac{\sin\phi}{32\beta}\Bigg[\xi^2\cot^4\phi+4\cot^2\phi\left\{\mp2\left(2\beta\pm1\right)+\frac{\xi^2}{\sin^2\phi}\right\}+16\left\{\frac{1\pm4\beta}{\xi^2}\mp\frac{2\beta\pm1}{\sin^2\phi}\right\}\Bigg] \qquad (4.39b)$$

These non-dimensional results show that the stress resultants in pressurised ogival toroidal shells with the same β and ξ ratios are directly proportional to A. To see the response of this shell type to uniform pressure loading, the non-dimensional results are plotted against ϕ in

Figures 4.15 and 4.16 for $\xi = 1.5$ and various value of β as shown. The physical range of ϕ in the inner and outer regions of the $\xi = 1.5$ vessel considered is seen to be approximately $37^o \le \phi \le 143^o$ from equation (4.35), since $\xi = h/d$.

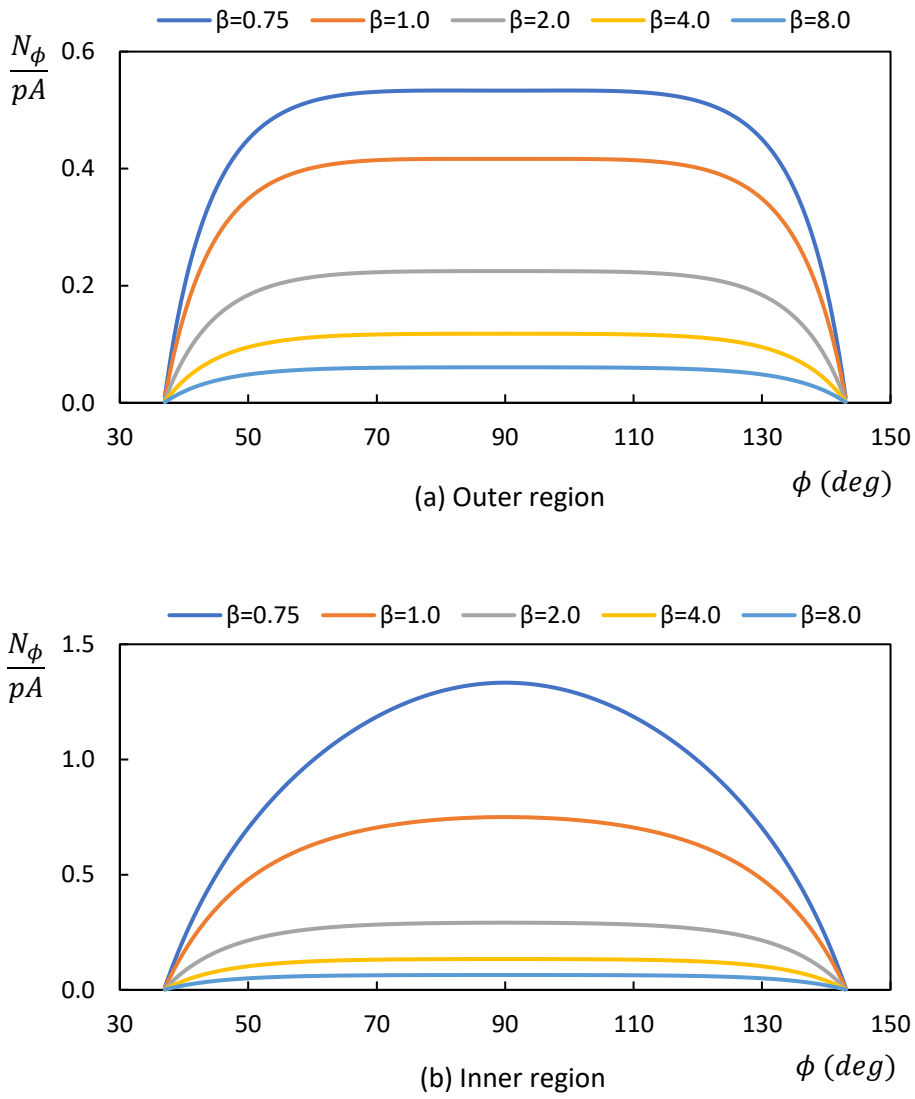

Figure 4.15. Non-dimensional meridional stress resultant against ϕ for $\xi = 1.5$: (a) outer region, (b) inner region of the vessel

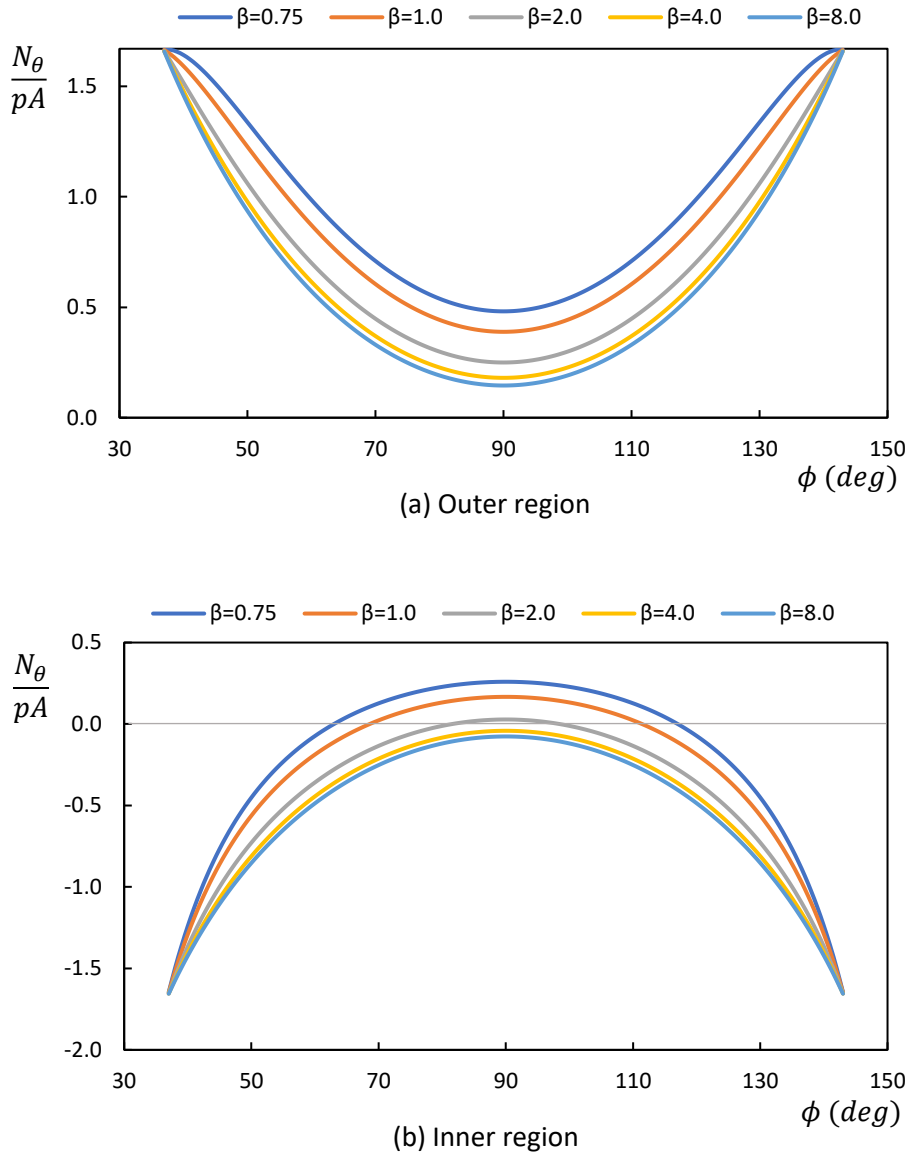

Figure 4.16. Non-dimensional hoop stress resultant against ϕ for $\xi = 1.5$: (a) outer region, (b) inner region of the vessel

For the non-dimensional values of β and $\xi = 1.5$ shown, the membrane stresses in the meridional direction of the internally pressurised vessel are entirely tensile with higher values in the inner region of the vessel. The hoop stresses in the outer region of the vessel are also tensile throughout for all values of β considered. On the other hand, the hoop stresses in the inner regions of the vessel are mostly compressive with greater values at the topmost and lowermost parts of the regions. Total compression is observed for toroids with $\beta > 2$, while the others are seen to have a span of tensile forces around the equator (mid-zones) of the inner region of the toroids. The span of the tensile stress is seen to increase as β reduces. With these

compressive membrane results, one could infer that local buckling might occur in the inner region of the vessel, especially in zones away from the equator. The nature of buckling would depend strongly on the value of the ratio of the mean toroidal radius to the equatorial width of the cross-sectional profile β, if the height-to-width ratio of the cross-sectional profile ξ is constant. The treatment of buckling of the shell type will be given in Chapter 6, while the unavoidable bending disturbances that occur around the meeting zones at the apex and nadir of the vessel are investigated in the next chapter.

4.4.3.2 Liquid-filled parabolic ogival toroidal vessel

The vessel under present consideration has high operational advantages for liquids that produce scum at the top or sediments at the bottom (Zingoni, 2002, 2005). If the ogival toroidal vessel is completely filled with liquids of weight γ per unit volume, the volume capacity V of the vessel is given by

$$V = \frac{4\pi}{3} Ahd$$

The essential loading p_r (per unit area of shell middle surface) due to the pressure loading from the contained liquid, acting normal to the shell internal middle surface is considered positive if pointing away from the global axis of revolution of the toroidal shell may be expressed as:

$$p_r = \gamma\left(\frac{2hd\sin\phi - h^2\cos\phi}{4d\sin\phi}\right) \tag{4.41a}$$

for the outer region of the tank, and

$$p_r = -\gamma\left(\frac{2hd\sin\phi + h^2\cos\phi}{4d\sin\phi}\right) \tag{4.41b}$$

for the inner region of the tank.

The toroidal vessel is assumed to be supported axisymmetrically along its pointed circular edge at the bottom, either directly on a series of closely spaced columns (Figure 4.17), or via an interposing ring beam that serves to transfer the column reactions more uniformly to the shell.

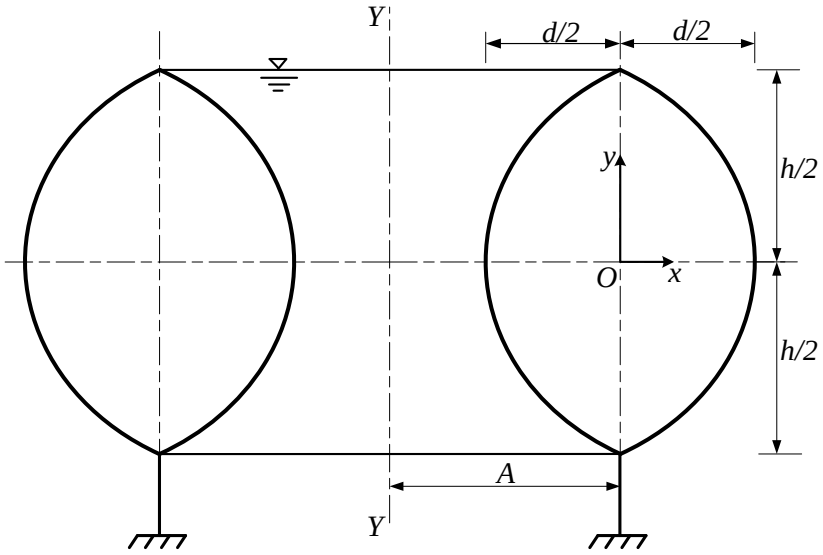

Figure 4.17. Parabolic ogival toroidal supported axisymmetrically at the nadir

4.4.3.2.1 Outer region

Substituting appropriate expressions (4.36), and (4.41) into (4.4b) and evaluating the integral, after some simplifications, yields the meridional stress resultant N_ϕ^m for the outer region of the vessel

$$N_\phi^m = \frac{h^3\gamma\sin\phi}{16d^2\left(4d\left(2A+d\right)\sin^2\phi - h^2\cos^2\phi\right)}\left[-\cot^2\phi\left\{4d^2\left(2A+d\right)-\frac{4}{3}hd\left(2A+d\right)\cot\phi\right.\right.$$

$$\left.\left.-\frac{1}{2}dh^2\cot^2\phi+\frac{1}{5}h^3\cot^3\phi\right\}+k\right] \qquad (4.42)$$

where k is the constant of integration to be determined from a suitable boundary condition. At the apex of the outer region of the toroid $\phi=\phi_o=\tan^{-1}(h/2d)$, N_ϕ^m must be zero. This condition gives

$$k=\frac{d^4}{15h^2}\left(160A+56d\right)$$

so that

$$N_{\phi}^{m}=\frac{h^{3}\gamma\sin\phi}{16d^{2}\left\{4d\left(2A+d\right)\sin^{2}\phi-h^{2}\cos^{2}\phi\right\}}\left[-4d^{2}\left(2A+d\right)\cot^{2}\phi+\frac{4}{3}dh\left(2A+d\right)\cot^{3}\phi\right.$$

$$\left.+\frac{1}{2}h^{2}d\cot^{4}\phi-\frac{1}{5}h^{3}\cot^{5}\phi+\frac{d^{4}}{15h^{2}}\left(160A+56d\right)\right] \qquad (4.43a)$$

Putting this and appropriate expressions (4.36), and (4.41) into (4.4a) for the outer region of the vessel, the following membrane stress resultant N_{θ}^{m} in the hoop direction for the outer region of the vessel is obtained after some simplifications:

$$N_{\theta}^{m}=\frac{h\gamma}{32d^{2}}\left[\frac{h\cot\phi-2d}{\sin\phi}\left\{h^{2}\cot^{2}\phi-4d\left(2A+d\right)\right\}-\sin\phi\left\{\frac{1}{2}h^{2}d\cot^{4}\phi-\frac{1}{5}h^{3}\cot^{5}\phi\right.\right.$$

$$\left.\left.-4d^{2}\left(2A+d\right)\cot^{2}\phi+\frac{4}{3}dh\left(2A+d\right)\cot^{3}\phi+\frac{d^{4}}{15h^{2}}\left(160A+56d\right)\right\}\right] \qquad (4.43b)$$

In the limiting case $A=0$, the above solutions N_{ϕ}^{m} and N_{θ}^{m} for the outer region of the ogival toroidal shell coincide with the respective solutions obtained in (Zingoni, 2002) for a parabolic ogival shell.

4.4.3.2.2 Inner region

Substituting appropriate expressions (4.36), and (4.41) for the inner region of the toroid into expression (4.4b), and using the condition: at $\phi=\overline{\phi}_{o}=\tan^{-1}(-h/2d)$ and $N_{\phi}^{m}=0$ at the apex of the inner region of the toroid to obtain the constant of integration, the meridional stress resultant N_{ϕ}^{m} in the inner region of the vessel is obtained as

$$N_{\phi}^{m}=\frac{h^{3}\gamma\sin\phi}{16d^{2}\left\{4d\left(2A-d\right)\sin^{2}\phi+h^{2}\cos^{2}\phi\right\}}\left[-4d^{2}\left(2A-d\right)\cot^{2}\phi-\frac{4}{3}dh\left(2A-d\right)\cot^{3}\phi\right.$$

$$\left.-\frac{1}{2}dh^{2}\cot^{4}\phi-\frac{1}{5}h^{3}\cot^{5}\phi+\frac{8d^{4}}{15h^{2}}\left(20A-7d\right)\right] \qquad (4.44a)$$

The membrane stress resultant in the hoop direction N_{θ}^{m} for the inner region of the vessel follows from expression (4.4a) as

$$N_\theta^m = \frac{h\gamma}{32d^2}\left[-\frac{h\cot\phi+2d}{\sin\phi}\left\{h^2\cot^2\phi+4d\left(2A-d\right)\right\}+\sin\varphi\left\{-\frac{1}{2}h^2d\cot^4\phi-\frac{1}{5}h^3\cot^5\phi\right.\right.$$

$$\left.\left.-4d^2\left(2A-d\right)\cot^2\phi-\frac{4}{3}dh\left(2A-d\right)\cot^3\phi+\frac{8d^4}{15h^2}\left(20A-7d\right)\right\}\right] \qquad (4.44b)$$

4.4.3.2.3 Parametric results for ogival toroids

(Zingoni, 2002a) has conducted a parametric study for the parabolic ogival sludge digester. A similar approach is followed here. The volume capacity of a parabolic ogival toroidal vessel (expression (4.40)) in a non-dimensional form, in terms ξ and β, is

$$V=\left(\frac{4\pi\beta\xi}{3}\right)d^3=\left(\frac{4\pi\beta}{3\xi^2}\right)h^3=\left(\frac{4\pi\xi}{3\beta^2}\right)A^3 \qquad (4.45)$$

or

$$\frac{V}{d^3}=\frac{4\pi\beta}{3\xi^2}$$

$$\frac{V}{h^3}=\frac{4\pi\beta}{3\xi^2}$$

$$\frac{V}{A^3}=\frac{4\pi\xi}{3\beta^2}$$

The non-dimensional tank capacities V/d^3, V/h^3 and V/A^3 for five benchmark toroids A, B, C, D & E of non-dimensional parameter β (= 1.0, 1.5, 2.0, 2.5, 3.0 respectively) with constant non-dimensional parameter ξ (=2) are presented in Table 1. It may be seen in the table that, for parabolic ogival tanks of the ratio of the mean toroidal radius to the equatorial width of the cross-sectional profiles ξ, as the height-to-width ratio β increases, the non-dimensional volume capacities V/d^3 and V/h^3 increase, while V/A^3 reduces.

Table 4.1. Non-dimensional tank volume for $\xi = 2.0$, $\left(45^o \le \phi \le 135^o\right)$

Toroids	ξ	β	V/d^3	V/h^3	V/A^3
A	2.0	1.0	8.3776	1.0472	8.3776
B	2.0	1.5	12.5664	1.5708	3.7234
C	2.0	2.0	16.7552	2.0944	2.0944
D	2.0	2.5	20.9440	2.6180	1.3404
E	2.0	3.0	25.1327	3.1416	0.9308

When the non-dimensional parameters are also used to eliminate d and h from expressions (4.43) and (4.44), the following non-dimensional forms of the results for the stress resultants are obtained:

$$\frac{N_\phi}{\gamma A^2} = \frac{\xi \sin\phi}{16\beta^2\left\{4(2\beta+1)\sin^2\phi - \xi^2\cos^2\phi\right\}}\left[-4\xi^2(2\beta+1)\cot^2\phi + \frac{4}{3}\xi^3(2\beta+1)\cot^3\phi\right.$$

$$\left. + \frac{1}{2}\xi^4\cot^4\phi - \frac{1}{5}\xi^5\cot^5\phi + \frac{1}{15}(160\beta+56)\right] \qquad (4.46a)$$

$$\frac{N_\theta}{\gamma A^2} = \frac{1}{32\beta^2\xi}\left[\frac{\xi\cot\phi - 2}{\sin\phi}\left\{\xi^4\cot^2\varphi - 4\xi^2(2\beta+1)\right\} - \sin\phi\left\{\frac{4}{3}\xi^3(2\beta+1)\cot^3\phi + \frac{1}{2}\xi^4\cot^4\phi\right.\right.$$

$$\left.\left. -4\xi^2(2\beta+1)\cot^2\phi - \frac{1}{5}\xi^5\cot^5\phi + \frac{1}{15}(160\beta+56)\right\}\right] \qquad (4.46b)$$

for the outer region of the ogival toroid, and

$$\frac{N_\phi}{\gamma A^2} = \frac{\xi \sin\phi}{16\beta^2\left\{4(2\beta-1)\sin^2\phi + \xi^2\cos^2\phi\right\}}\left[-4\xi^2(2\beta-1)\cot^2\phi - \frac{4}{3}\xi^3(2\beta-1)\cot^3\phi\right.$$

$$\left. - \frac{1}{2}\xi^4\cot^4\phi - \frac{1}{5}\xi^5\cot^5\phi + \frac{8}{15}(20\beta-7)\right] \qquad (4.47a)$$

$$\frac{N_\theta}{\gamma A^2} = \frac{1}{32\beta^2\xi}\left[-\frac{\xi\cot\phi + 2}{\sin\phi}\left\{\xi^4\cot^2\phi + 4\xi^2(2\beta-1)\right\} + \sin\phi\left\{-\frac{4}{3}\xi^3(2\beta-1)\cot^3\phi\right.\right.$$

$$\left.\left. -\frac{1}{2}\xi^4\cot^4\phi - 4\xi^2(2\beta-1)\cot^2\phi - \frac{1}{5}\xi^5\cot^5\phi + \frac{8}{15}(20\beta-7)\right\}\right] \qquad (4.47b)$$

for the inner region of the ogival toroid.

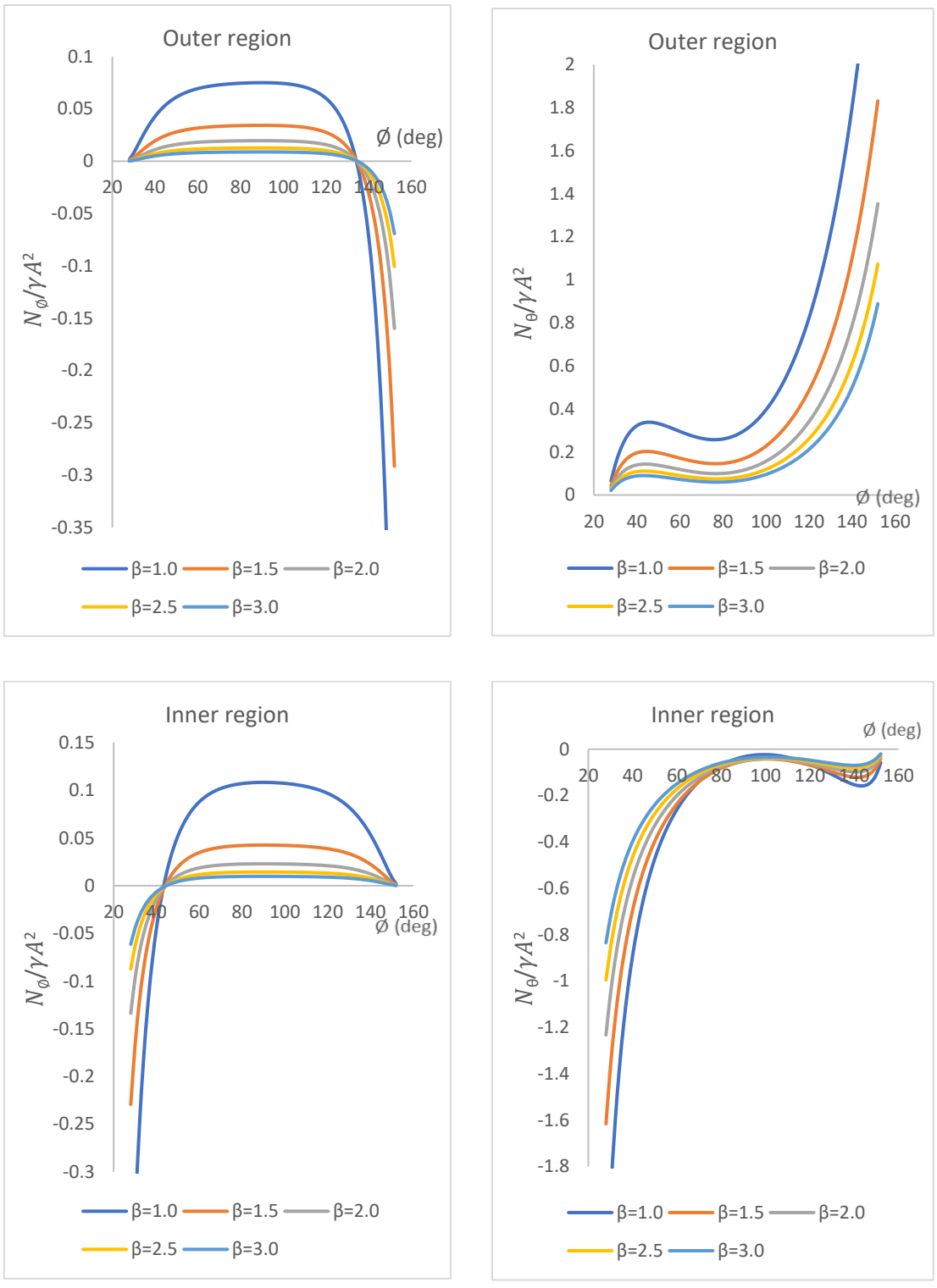

Figure 4.18. Non-dimensional stress variations for the liquid-filled ogival toroidal tank, $\xi = 1.0$

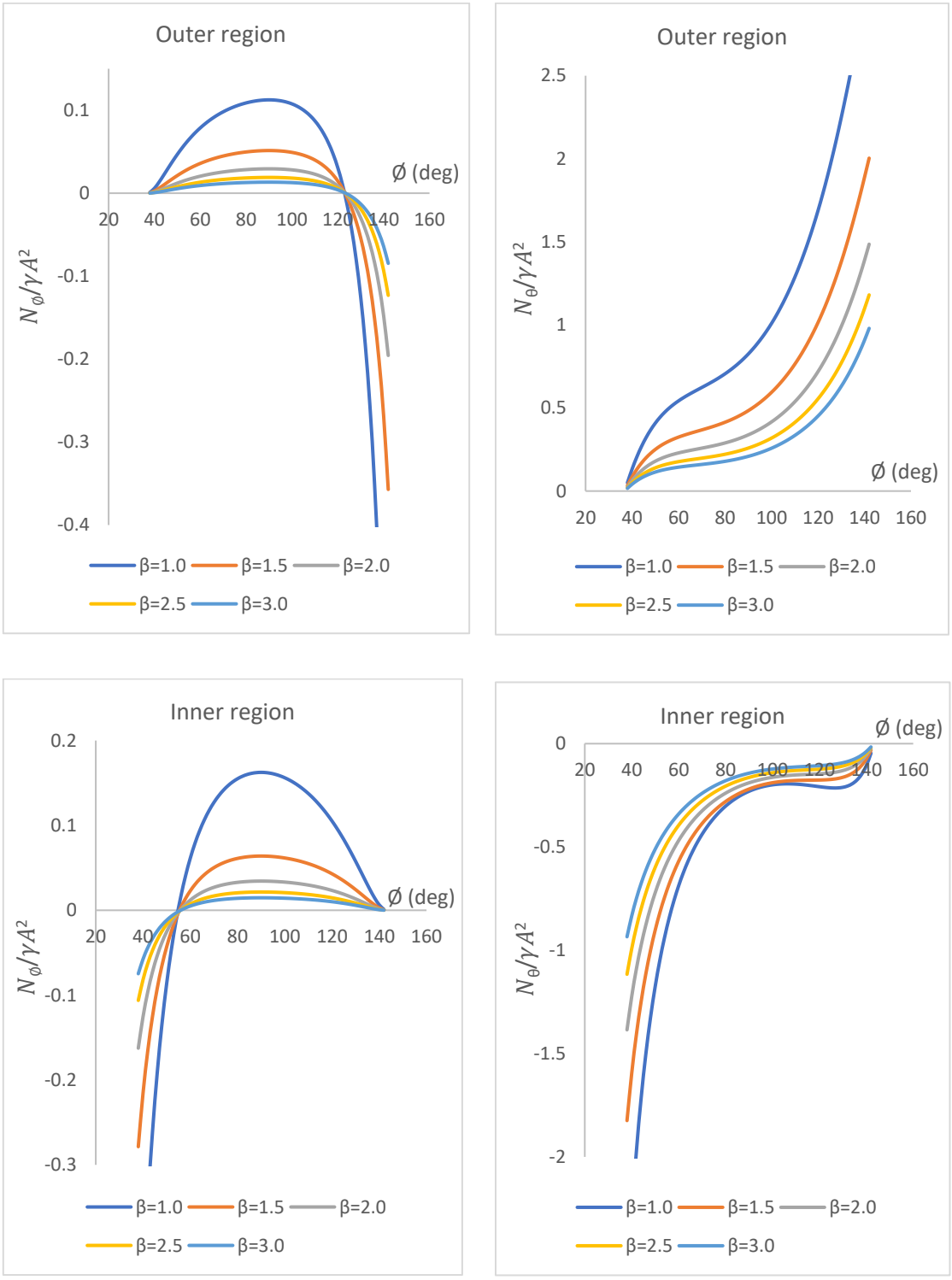

Figure 4.19. Non-dimensional stress variations for the liquid-filled ogival toroidal tank, $\xi = 1.5$

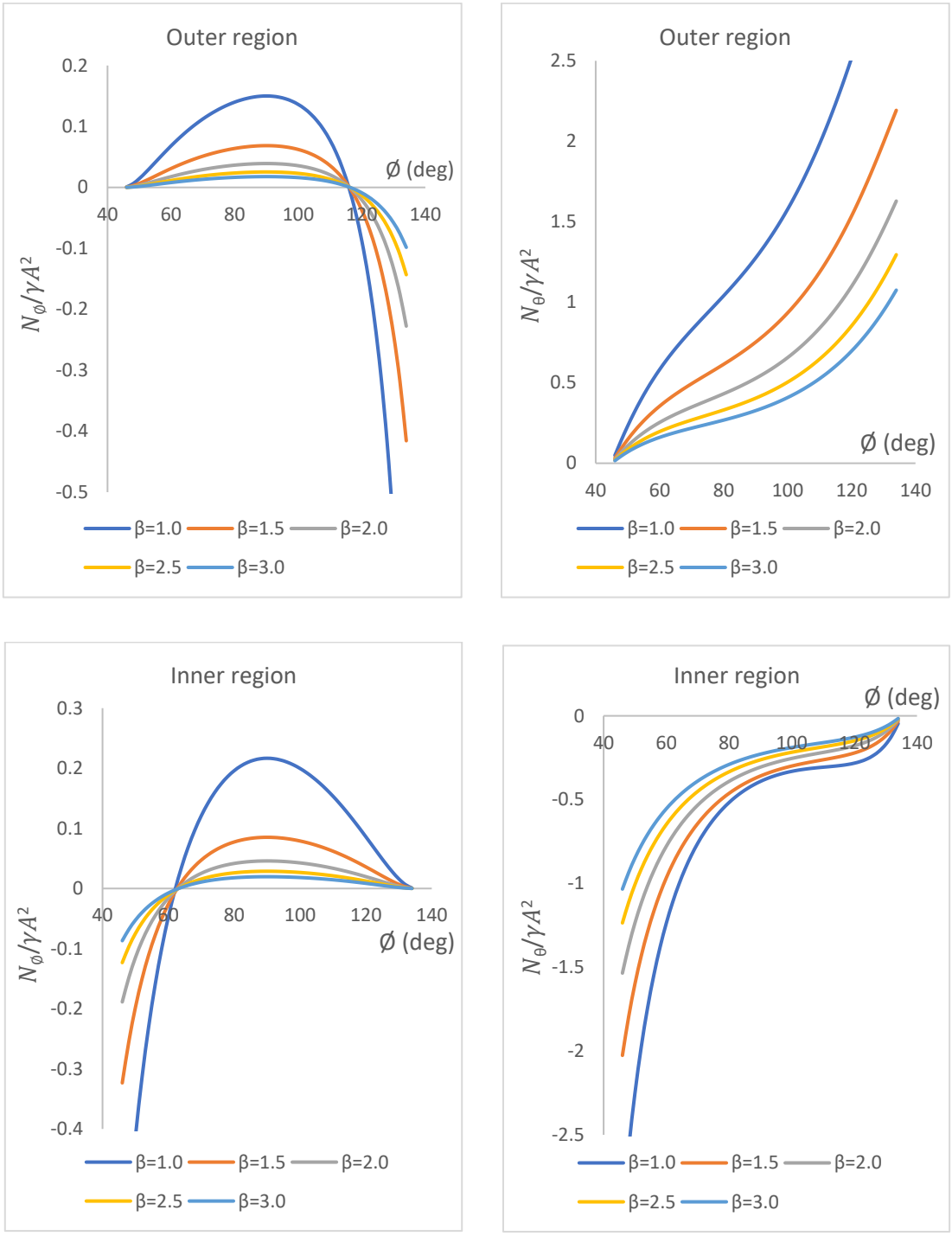

Figure 4.20. Non-dimensional stress variations for the liquid-filled ogival toroidal tank, $\xi = 2.0$

The parametric results, as encapsulated in the expressions (4.46) and (4.47), indicate that doubling the mean radius or height or local width, while maintaining all other parameters constant, will quadruple the stress resultants in the toroidal tank; indicating that structural

efficiency reduces as any of these parameters increases. This also demonstrates how the scale of the structure affects its design.

To explore the effects of change in the dimensions A, h and d on the membrane stress distribution, toroids of non-dimensional parameters β (= 1.0, 1.5, 2.0, 2.5 & 3.0) have been considered. The resulting plots of the non-dimensional stress variations $N_\phi / \gamma A^2$ and $N_\theta / \gamma A^2$ against the meridional angle ϕ in the outer and inner regions of the ogival toroidal shell, for the non-dimensional parameters ξ (=1, 1.5 & 2) are presented in Figures 4.18, 4.19 and 4.20 respectively. The computations are only relevant within the range: $\tan^{-1}(\xi/2) \le \phi \le \pi - \tan^{-1}(\xi/2)$, since the physical domain of the toroidal vessel is defined by this range for both the outer and inner regions (equation (4.35)). This range of ξ is also consistent with that adopted by Zingoni in his study of the parabolic ogival digester (Zingoni, 2002, 2018).

4.4.3.2.4 Discussion of results

It is evident that the plots in Figures 4.18, 4.19, and 4.20 are all similar, with a uniform trend in the crossover points (from tension to compression or vice versa), and a general increase in values of the meridional stress resultants and hoop stress resultants at both the inner and outer regions of the tank as the non-dimensional parameter ξ increases from 1.0, through 1.5, to 2.0 (i.e. as the overall height h of the tank is increased).

Examining the results of the particular case of $\xi = 2.0$ (Figure 4.20) in more detail and noting the definition of the angular coordinate ϕ for the outer and inner regions of the tank, it is seen that, for a given value of β, the stress resultant N_ϕ^m rises from zero at the apex of the tank as expected. The peak values of meridional stress resultants in tension are observed around the equator $\left(\phi = 90^o\right)$ of the outer and inner regions respectively. It is observed that higher peak meridional stress resultant value is experienced around the inner equator compared to the outer equator of the ogival toroidal tank. The cross-over from tension to compression occurs at $\phi = 116^o$ and $\phi = 64^o$ for the outer and inner regions, respectively, for all values of β. These cross-over points occur in the lower parts of the toroid; below this level, the meridional compression on both the inner and outer sides of the vessel rapidly increase. For a thin-walled structure like this one, meridional compression should be avoided. In practice, the position of

the supports can be raised until they are closer to the cross-over level, in order to cut off the excessive meridional compression observed in the lower zones. Correct positioning of the supports, in conjunction with some enhancement of the shell thickness in the lower parts of the vessel, would reduce or even eliminate the likelihood of buckling in the lower parts of the vessel.

For the hoop stress resultant N_θ^m, looking at the outer region of the tank first, it is generally observed that hoop stress resultant N_θ^m rises rapidly in tension from zero at the apex of the tank, and then more gradually between $\phi = 50^o$ and 90^o approximately, beyond which it rises fairly rapidly as on moves toward the bottom of the ogival vessel. It is, therefore, evident that a considerable pre-stressing will be required in the lower parts of the outer region of the tank, to cater for the relatively large hoop tensions noted there. On the inner side of the tank, hoop stress resultant N_θ^m also rises steeply in compression from zero at the apex of the tank, and then gradually between $\phi = 130^o$ and 90^o approximately, before rapidly increasing towards the bottom of the vessel. Note that the hoop stress resultants in the outer region of the tank are entirely tensile while those in the inner region of the tank are entirely compressive, as expected from the hydrostatic loading.

It will suffice to note at this juncture that it is not surprising that the non-dimensional stress variations in the outer regions of liquid-filled parabolic ogival toroidal vessels (Figures 4.18, 4.19, and 4.20) have a similar trend to those of Zingoni (2002b), since the approach here are based on the treatment of parabolic ogival sludge digesters in that paper. A normal parabolic ogival sludge digester is different from a parabolic ogival toroidal vessel in the terms associated with A (or β). In the normal parabolic ogival sludge digester Zingoni (2002b), these terms do not exist. Therefore, when these terms are omitted from the results presented in this subsection for parabolic ogival toroidal vessels, the results for the normal parabolic ogival vessel will be obtained.

4.4.4 Toroidal vessel with a circular-elliptic compound cross-section

Another unorthodox toroidal shell of revolution is considered in this subsection. The meridional cross section of the off-centred toroidal vessel consists of a top semi-circular profile (with local radius a) that is smoothly joined to a bottom semi-elliptical profile (of local semi-

axes a (horizontal) and b (vertical)) at junctions D^o and D^i in the outer and inner regions of the of the toroidal shell, respectively, see Figure 4.21. Hence, the complete toroid comprises a top semi-circular toroidal segment and a bottom semi-elliptical toroidal segment whose ends are tangentially connected to exhibit no slope discontinuity at the junctions in the outer and inner regions of the vessel. This toroidal shell form with its aesthetically pleasing features has been studied here to demonstrate that the present analytical approach could be used for any toroidal cross-sections that are not symmetrical about the equatorial plane. This particular vessel is also shown to have the advantage of relatively low bending disturbance stresses at the meeting junctions of the top and bottom segments of the vessel in Chapter 5.

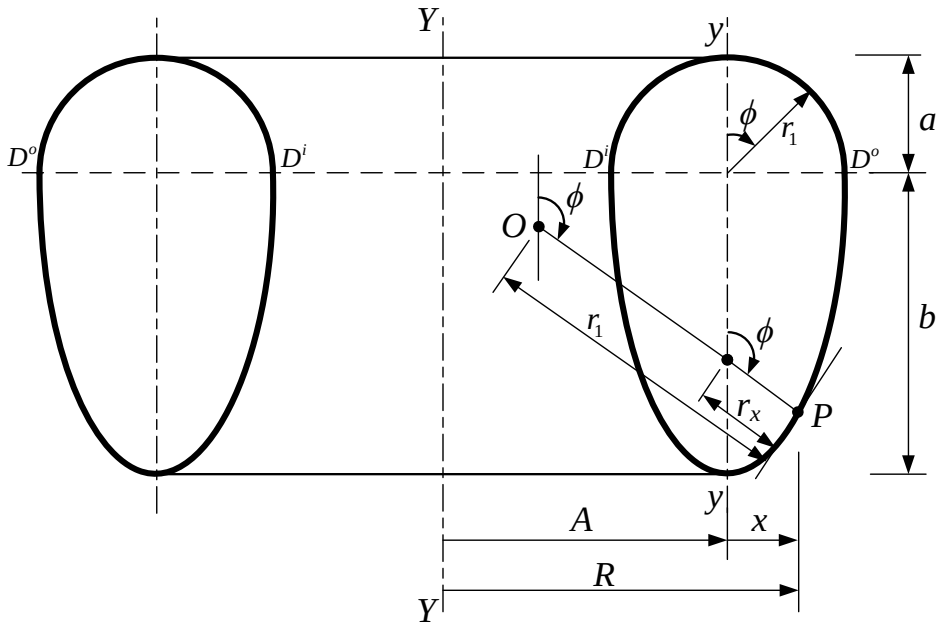

Figure 4.21. Toroid with a circular-elliptic closed profile

The x and r_1 at the top semi-circular segment of the vessel are the same for a complete circular toroid (see Section 4.4.1):

$$x = \pm a \sin\phi$$

$$r_1 = \pm a$$

while expressions for x and r_1 at the bottom semi-elliptic segment of the vessel take the form of expressions (4.21) and (4.24) for an elliptical toroid:

$$x = \pm \frac{a^2 \sin\phi}{\sqrt{a^2 \sin^2\phi + b^2 \cos^2\phi}}$$

$$r_1 = \pm \frac{a^2 b^2}{\left(a^2 \sin^2\phi + b^2 \cos^2\phi\right)^{3/2}}$$

In what follows, the membrane solutions for this toroidal shell under constant pressure loading and hydrostatic pressure loading are derived.

4.4.4.1 Vessel under uniform internal pressure

For the circular-elliptic toroidal assemblies under internal pressure, p, one may adopt the membrane solution of a pressurised circular toroid derived in Section 4.4.1.1, for the semi-circular top region of the present vessel. This has been re-written below, for ease of reference

$$N_\phi^m = pa\left(\frac{\beta_{el} + 0.5\sin\phi_c}{\beta_{el} + \sin\phi_c}\right) \tag{4.48a}$$

and

$$N_\theta^m = \frac{pa}{2} \tag{4.48b}$$

Note that these expressions for the membrane stress resultants within the semi-circular top are in terms of ϕ_c, where, now β_c has been replaced by β_{el}, which is

$$\beta_{el} = \frac{A}{a}$$

Since the edges of the semi-circular top and semi-elliptic bottom/lower region of the vessel meet smoothly at $\phi_c = \pi/2$ in the outer region (and $\phi_c = 3\pi/2$ in the inner region), the membrane solution of a pressurised elliptic toroid in Section 4.4.2.2 must be the same for the bottom part of the present vessel. That is

$$N_{\phi}^{m} = \frac{pa}{2\bar{x}_{el}} \left\{ \frac{2\beta_{el}\bar{x}_{el} + \sin\phi_c}{\beta_{el}\bar{x}_{el} + \sin\phi_c} \right\} \tag{4.49a}$$

and

$$N_{\theta}^{m} = \frac{pa}{\xi_{el}^2} \left\{ \frac{\xi_{el}^2}{\bar{x}_{el}} - \frac{\bar{x}_{el}}{2} + \left(\xi_{el}^2 - 1\right)\beta_{el}\sin\phi_c \right\} \tag{4.49b}$$

where,

$$\bar{x}_{el} = \sqrt{\sin^2\phi_c + \xi_{el}^2\cos^2\phi_c}$$

$$\xi_{el} = \frac{b}{a}$$

The deformations that occur at any point within the semi-elliptic and semi-circular toroidal vessel can be determined from expressions (4.5) and (4.9) by substituting the appropriate membrane solutions (4.48) and (4.49) for the particular region of interest.

4.4.4.2 Toroidal tank with a circular-elliptic cross-section

Consider a toroidal tank with semi-circular and semi-elliptical compound cross-section that is supported axisymmetrically along the lowest circle of latitude. If the tank is completely filled with a liquid weight γ per unit volume, the contained volume of the liquid can be obtained from (see Figure 4.21)

$$V_{vol} = aA\pi^2\left(a + b\right) \tag{4.50}$$

The essential loading on the surface of the shell, is

$$p_r = \gamma a\left(\pm 1 - \cos\phi\right) \tag{4.51a}$$

for the semi-circular segment of the tank, and

$$p_r = \gamma\left(\pm a - \frac{b^2\cos\phi}{\sqrt{a^2\sin^2\phi + b^2\cos^2\phi}}\right) \tag{4.51b}$$

for the semi-elliptical bottom segment of the tank.

4.4.4.2.1 Semi-circular top segment

In the semi-circular top segment of the tank, the stress resultants in the meridional and hoop directions may be obtained from expressions for circular toroidal tanks in Section 4.4.1.2. These are re-written below, with the deformation results obtained after substituting the membrane stress resultants into expressions (4.5) and (4.9) and simplifying:

$$N_\phi^m = \frac{\gamma a^2}{6\sin\phi(A + a\sin\phi)}\left\{a\left(1 + (-3 + 2\cos\phi)\cos^2\phi\right) - 3A\left(\phi + (-2 + \cos\phi)\sin\phi\right)\right\} \tag{4.52a}$$

$$N_\theta^m = \frac{\gamma a}{6\sin^2\phi}\left\{4a(5 + 4\cos\phi)\sin^4\left(\frac{\phi}{2}\right) + 3A(\phi - \cos\phi\sin\phi)\right\} \tag{4.52b}$$

$$\delta^m = \frac{\gamma a}{6Et\sin\phi}\left[\frac{(A + a\sin\phi)}{\sin\phi}\left\{4a\left(5 + 4\cos\phi\right)\sin^4\left(\frac{\phi}{2}\right) + 3A\left(\phi - \cos\phi\sin\phi\right)\right\}\right.$$

$$\left. -a\nu\left[a\left\{1 + \left(-3 + 2\cos\phi\right)\cos^2\phi\right\} - 3A\left\{\phi + \left(-2 + \cos\phi\right)\sin\phi\right\}\right]\right] \tag{4.52c}$$

$$V^m = -\frac{\gamma}{48Et\sin^4\phi\left(A + a\ \sin\phi\right)}\left[48a^3\sin^6\phi + 96a^2A\sin^5\left(\frac{\phi}{2}\right)\left\{25\cos\left(\frac{\phi}{2}\right)\right.\right.$$

$$\left.\left. + 11\cos\left(\frac{3\phi}{2}\right) + 2\cos\left(\frac{5\phi}{2}\right)\right\} + aA^2\left(81 - 32\cos\phi - 56\cos 2\phi + 7\cos 4\phi\right.\right.$$

$$-36\phi\sin 2\phi)+48A^3\left(-\phi\cos\phi+\sin\phi\right)\ \Big] \tag{4.52d}$$

for the upper-outer region of the tank, and

$$N_\phi^m=\frac{\gamma a^2}{6\sin\phi\left(A-a\sin\phi\right)}\Big\{a\Big((1+\cos\phi)^2(-1+2\cos\phi)\Big) +3A\left(-\pi+\phi+(2+\cos\phi)\sin\phi\right)\Big\} \tag{4.52e}$$

$$N_\theta^m=-\frac{\gamma a}{6\sin^2\phi}\left\{4a\left(-5+4\cos\phi\right)\cos^4\left(\frac{\phi}{2}\right)+3A\left(\pi-\phi+\cos\phi\sin\phi\right)\right\} \tag{4.52f}$$

$$\delta^m=\frac{\gamma a}{6Et\sin\phi}\Bigg[-\frac{(A-a\sin\phi)}{\sin\phi}\left\{4a\left(-5+4\cos\phi\right)\cos^4\left(\frac{\phi}{2}\right)+3A\left(\pi+\cos\phi\sin\phi-\phi\right)\right\}$$

$$-a\upsilon\left\{a\left((1+\cos\phi)^2(-1+2\cos\phi)\right)+3A\left(-\pi+\phi+(2+\cos\phi)\sin\phi\right)\right\}\ \Bigg] \tag{4.52g}$$

$$V^m=\frac{\gamma}{48Et\sin^4\phi\left(A-a\sin\phi\right)}\Bigg\{-48a^3\sin^6\phi+96a^2A\cos^5\left(\frac{\phi}{2}\right)\Bigg(25\sin\left(\frac{\phi}{2}\right)$$

$$-11\sin\left(\frac{3\phi}{2}\right)+2\sin\left(\frac{5\phi}{2}\right)\Bigg)-aA^2\left(81+32\cos\phi-56\cos 2\phi+7\cos 4\phi\right.$$

$$\left.+36(\pi-\phi)\sin 2\phi)+48A^3\left((\pi-\phi)\cos\phi+\sin\phi\right)\ \right\} \tag{4.52h}$$

for the upper-inner region of the tank.

4.4.4.2.2 Semi-elliptical bottom segment

For the semi-elliptical region of the toroidal tank, the appropriate expressions for x, r_1 and p_r are substituted into expression (4.4b). When the integral in the ensuing equation is solved and simplified, the following expression for the meridional stress resultant is obtained

$$N_\phi^m = \frac{\gamma a}{6(A+x)\sin\phi}\left[3Ab\left\{\pm\tan^{-1}\left(x_{ce_1}\right)\mp\tan^{-1}\left(x_{ce_2}\right)\right\}+\frac{4\sqrt{2}\left(a^3b^4\cos\phi\right)}{\left(a^2-b^2\right)\left(x_{el_5}\right)^{3/2}}\right.$$
$$+\frac{2\sqrt{2}\left\{a\left(-b^4\cos\phi+3aA\left(a^2-b^2\right)\sin\phi\right)\right\}}{\left(a^2-b^2\right)\sqrt{x_{el_5}}} \qquad (4.53a)$$
$$\left.+\frac{3ab^2\left\{\pm2a^3+A\left(\pm a\mp b\right)\left(a+b\right)\sin2\phi\right\}}{-a^4+b^4+\left(a^2-b^2\right)^2\cos2\phi}+k\right]$$

where,

$$x_{ce_1}=\frac{1}{a}\left\{\left(\sqrt{b^2-a^2}\right)-b\tan\frac{\phi}{2}\right\}$$

$$x_{ce_2}=\frac{1}{a}\left\{\left(\sqrt{b^2-a^2}\right)+b\tan\frac{\phi}{2}\right\}$$

$$x_{el_5}=a^2+b^2+\left(b^2-a^2\right)\cos\left(2\phi\right)$$

The constant k in the above expression may be obtained from the boundary conditions at the meeting edges of the top and bottom segments of the toroidal tank. At $\phi=\pi/2$ in the outer and inner regions of the vessel, N_ϕ^m in the lower semi-elliptical segment and the upper semi-circular segment must be equal at each of the junctions. These conditions yield

$$k=\mp\frac{1}{2}\left[a\left\{a\left(-2+\frac{6b^2}{b^2-a^2}\right)\pm3A\pi\right\}-6Ab\left\{\tan^{-1}\left(\frac{b-\sqrt{b^2-a^2}}{a}\right)+\tan^{-1}\left(\frac{b+\sqrt{b^2-a^2}}{a}\right)\right\}\right]$$

The membrane stress resultant in the hoop direction of the toroidal tank may follow from expression (4.51b), which after eliminating x, r_1 and p_r with their appropriate equations, gives

$$N_\theta^m = \left(\frac{A}{\sin\phi} \pm \frac{a^2}{x_{el}} \right) \left\{ \gamma \left(\pm a - \frac{b^2 \cos\phi}{x_{el}} \right) \mp \frac{(x_{el})^3}{a^2 b^2} N_\phi^m \right\} \tag{4.53b}$$

for the outer and inner regions of the bottom part of the toroidal tank. Recall that

$$x_{el} = \sqrt{a^2 \sin^2\phi + b^2 \cos^2\phi}$$

4.4.4.2.3 Deformations in the semi-elliptical bottom of the vessel

With the membrane stress resultants now known, the lateral displacement and meridional rotation at any point within the semi-circular top (or the semi-elliptical bottom) segment of the toroidal tank can be obtained, respectively, from

$$\delta^m = \frac{A+x}{Et} \left\{ N_\theta^m - \upsilon N_\phi^m \right\} \tag{4.54a}$$

and

$$V^m = \frac{1}{r_1} \left[\frac{\cot\phi}{Et} \left\{ \left(r_1 + \upsilon \frac{A+x}{\sin\phi} \right) N_\phi^m - \left(\frac{A+x}{\sin\phi} + \upsilon r_1 \right) N_\theta^m \right\} - \left\{ \frac{A+x}{Et \sin\phi} \left(N_\theta^m - \upsilon N_\phi^m \right) \right\}^\bullet \right] \tag{4.54b}$$

4.4.5 Multi-segmented toroidal vessel

Figure 4.22 shows a novel multi-shell toroidal vessel with a cross-section first proposed by Zingoni (2001a,b) in exploring new shell forms for egg-shaped sludge digesters. It comprises an upper toroidal segment of local radius a_1 (centre C_1) and a lower toroidal segment of local radius a_3 (centre C_3), the two portions being connected tangentially by two middle toroidal segments - one on the outer face and the other on the inner face of the toroid - with local radii

a_2^o (centre C_2^o) and a_2^i (centre C_2^i), respectively. a_2^i and C_2^i are not shown in the figure. Here, the superscripts o and i are used to denote the outer and inner surfaces, respectively, of the toroid. The junctions D_1^o, D_2^o, D_1^i and D_2^i of the four segments of the vessel exhibit no slope discontinuity, but an abrupt jump in the local radius from one segment to the other. For egg-shaped containment shells of revolution having this profile, Zingoni (2001a,b) found that the discontinuity stresses were relatively small in comparison with the membrane stresses, so we are hoping toroidal vessels with this same cross-section will have the same advantage.

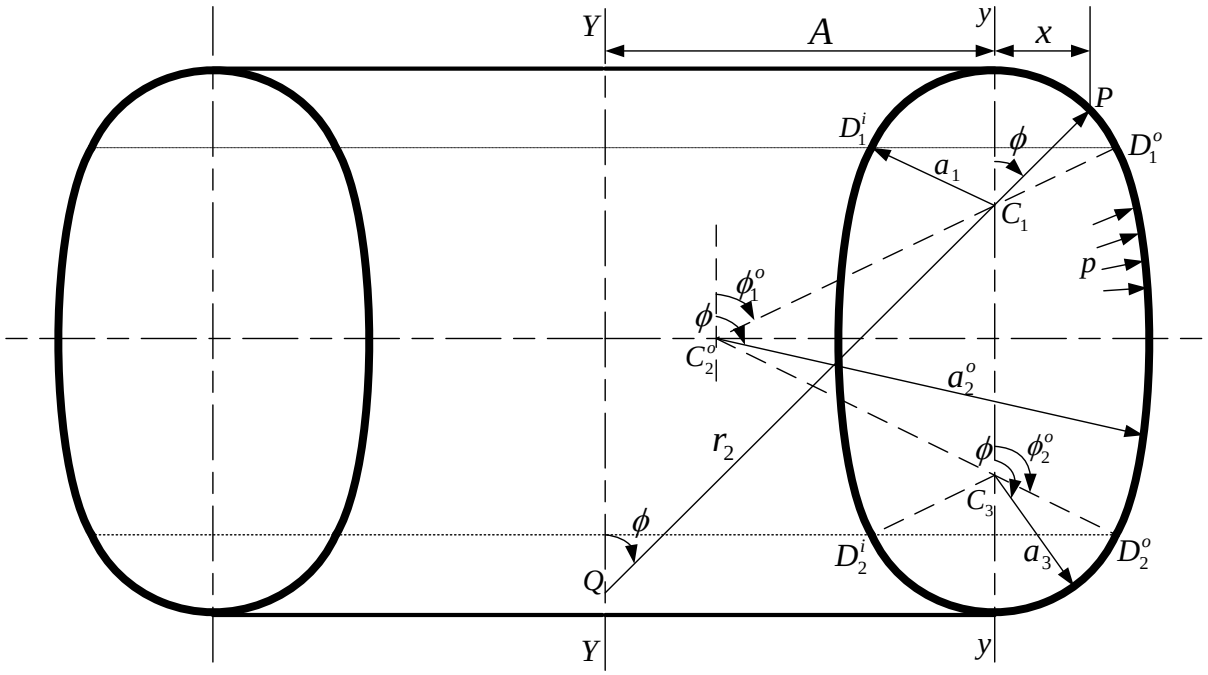

Figure 4.22. Geometric parameters of the pressurised segmented toroid.

Remember A is the mean toroidal radius, x is the horizontal distance coordinate between any point P and the local centreline $y-y$ of the cross-section, and the angular coordinate ϕ is the angle from the upward direction of the global axis of revolution $Y-Y$ of the toroid to the normal to the shell middle surface at any point P. Hence, in the usual way, the locations on the right of the local $y-y$ axis are referred to as the "outer region" of the vessel, while locations to the left of $y-y$ axis are referred to as the "inner region" of the vessel. The values of ϕ at junctions D_1^o, D_2^o, D_1^i and D_2^i are denoted by ϕ_1^o, ϕ_2^o, ϕ_1^i and ϕ_2^i respectively. The principal radii of curvature of a point on the middle surface of the toroidal vessel may be written as

$$r_1 = a \tag{4.55a}$$

$$r_2 = \frac{R}{\sin\phi} = \frac{A+x}{\sin\phi} \tag{4.55b}$$

where, as before, R is the horizontal coordinate measuring the distance between the vertical axis of revolution $Y-Y$ and any point P on the middle surface of the toroidal shell, and a is the radius of the circular segment containing the point P. Note that r_1 for the inner region of the toroid is on the side of the shell mid-surface opposite to the axis of revolution of the toroid, and hence must be taken as negative.

4.4.5.1 Uniformly pressurised multi-shell toroid

For the pressurised vessel, vertical support conditions need not be specified in the following membrane analysis, since the uniform distribution of pressure over the closed toroidal surface gives a zero resultant of forces in the vertical direction (ignoring the self-weight of the shell itself). No lateral supports are required either since the system is laterally self-equilibrating under the axisymmetric loading. The loading component p_r (per unit area of shell middle surface) due to the pressure loading, acting normal to the shell middle surface, is considered positive on the inner wall of the vessel and negative on the outer wall of the vessel. Its magnitude is given by

$$p_r = p \tag{4.56}$$

4.4.5.1.1 The top segment of the pressurised vessel

For the upper regions of the toroidal vessel,

$$x = \pm a_1 \sin\phi \tag{4.57}$$

The membrane stress resultants and deformations within the upper regions of the multi-shell toroid are the same as those obtained in Section 4.4.1.1 for a pressurised circular toroid. These are:

$$N_{\phi}^{m} = \frac{pa_1}{2}\left\{\frac{\pm 2A + a_1 \sin\phi}{\pm A + a_1 \sin\phi}\right\} \tag{4.58a}$$

$$N_{\theta}^{m} = \frac{pa_1}{2} \tag{4.58b}$$

$$\delta^{m} = \frac{pa_1}{2Et}\left\{A(1-2\upsilon) \mp a_1(\upsilon - 1)\sin\phi\right\} \tag{4.58c}$$

$$V^{m} = \frac{pa_1}{2Et}\left\{\frac{A\cot\phi}{A \pm a_1 \sin\phi}\right\} \tag{4.58d}$$

where, now the a is the local radius of the upper toroidal segment.

4.4.5.1.2 Middle segments of the pressurised vessel

For the middle regions of the vessel, the horizontal distance coordinate between any point P and the local centreline $y - y$ of the cross-section is expressed as

$$x = \pm\left(a_2 \sin\phi - q\right) \tag{4.59}$$

where,

$$q = \left(a_2 - a_1\right)\sin\phi_1 \tag{4.60}$$

Using appropriate equations (4.55), (4.56), and (4.59) to eliminate r_1, p_r and x from equation (4.4b) and evaluating the integral, we obtain after some simplifications, the meridional stress resultant

$$N_{\phi}^{m} = \frac{1}{\left(A \mp q \ \pm a_2 \sin\phi\right)\sin\phi}\left\{\mp\frac{pa_2}{2}\left(2(\mp A + q\ )\sin\phi + a_2\cos^2\phi\right) + k\right\} \tag{4.61a}$$

where, as usual, for the double operations, the upper sign applies to the outer region, while the lower sign applies to the inner regions of the toroid, and k is a constant of integration which must be obtained from appropriate boundary conditions. On the account that the vessel junctions exhibit no slope discontinuity, one may obtain k from the condition that N_{ϕ}^{m} in the upper region of the vessel and the respective middle region of the vessel must have the same values at the junction $\phi = \phi_1$ of the two segments at the outer or inner regions of the vessel. These conditions give

$$k = \frac{p}{4}\left\{\pm 2a_1^2\sin^2\phi_1 \ \mp a_2\left(\pm 4A\sin\phi_1 \ + a_2(-3+\cos 2\phi_1\ )\right)\mp 4a_1(\mp A + a_2\sin\phi_1\ )\sin\phi_1\ \right\}$$

Therefore, the membrane stress resultant in the hoop direction follows from expression (4.4b). For the middle region of the vessel, use of the applicable values of r_1, p_r and x leads to the result

$$N_{\theta}^{m} = \frac{1}{2a_2}\left\{pa_2^2\left(2+\cot^2\phi\right)\mp\frac{2k}{\sin^2\phi}\right\} \tag{4.61b}$$

The deformations follow by substituting appropriate expressions (4.55), (4.56), (4.59) and (4.61) for the middle regions of the toroidal vessel into expressions (4.5) and (4.9):

$$\delta^{m} = \frac{1}{4Eta_2\sin^2\phi}\Big[\, p\left\{a_2^2(A\mp q)\left(3-2\upsilon+(2\upsilon-1)\cos 2\phi\right)\right.$$

$$\left.\pm a_2^3\left(3+\nu+(\upsilon-1)\cos 2\phi\right)\sin\phi\right\} \pm 4k\left\{-A\pm q\mp a_2\left(1+\upsilon\right)\sin\phi\right\}\Big] \tag{4.62a}$$

and

$$V^m = \frac{-\left(A \mp q\right)\cot\phi}{8a_2^2 Et\sin^3\phi\left(A \mp q \pm a_2\sin\phi\right)}\Big[\, p\left\{8a_2^2\left(\mp A + q\right)\right.$$

$$\left. + a_2^3\left(-15\sin\phi + \sin 3\phi\right)\right\} + 8k\left\{2(A \mp q) \pm 3a_2\sin\phi\right\}\Big] \tag{4.62b}$$

4.4.5.1.3 The bottom segment of the pressurised vessel

For the lower regions of the toroidal vessel, at the lower junction $\phi = \phi_2$, the value of the meridional stress resultant N_ϕ^m in the middle region of the vessel must match the value of N_ϕ^m in the lower region of the vessel, for both the outer and inner walls of the vessel. This condition of continuity of the meridional stress resultant may be used to evaluate the constant of integration k for the lower region to be evaluated. However, the condition that at the nadir of the vessel, N_ϕ^m vanishes has been employed here to obtain k. Consequently, the membrane stress resultants and deformations derived are respectively the same as those for a circular toroid. These may be recast here in terms of the local radius a_3 of the lower toroidal segment:

$$N_\phi^m = \frac{pa_3}{2}\left\{\frac{\pm 2A + a_3\sin\phi}{\pm A + a_3\sin\phi}\right\} \tag{4.63a}$$

$$N_\theta^m = \frac{pa_3}{2} \tag{4.63b}$$

$$\delta^m = \frac{pa_3}{2Et}\left\{A(1-2\upsilon) \mp a_3\left(\upsilon - 1\right)\sin\phi\right\} \tag{4.63c}$$

$$V^m = \frac{pa_3}{2Et}\left\{\frac{A\cot\phi}{A \pm a_3\sin\phi}\right\} \tag{4.63d}$$

The smoothness of junctions D_1^o, D_2^o, D_1^i and D_2^i of the four segments of the vessel leads to the continuity of membrane stress resultants in the meridional direction from one segment to

the other. However, some degree of mismatch is expected in the values of meridional lateral movements and rotations, and in the membrane stress resultants in the hoop direction, owing to the abrupt jump in the local radius from one segment to the other. This is an indication that some bending will likely occur around the junctions of the four segments of the vessel. In addition to this, it is well known that singularities exist in the membrane solution at $\phi = 0$, π, (the meeting points of positive and negative Gaussian curvatures) of toroids with closed cross-sectional profiles. In the next Chapter, the bending theory of shells of revolution will be invoked to cater for the bending that will occur at the junctions of the vessel.

4.4.5.2 Liquid-filled segmented toroid

4.4.5.2.1 Loading and geometric preliminary

Let us assume the toroidal shell of multi-segmented spherical cross-section is supported circumferentially at the nadir and filled with a liquid of weight γ per unit volume. The essential loading p_r (per unit area of shell middle surface) due to the internal hydrostatic loading from the contained liquid, acting normal to the shell middle surface may be obtained from

$$p_r = \pm \gamma h_d \tag{4.64}$$

where, the depth h_d of a point on the surface of the tank along the vertical coordinate y from the apex is

$$h_1 = a_1 \left(1 \mp \cos\phi\right) \tag{4.65a}$$

for the upper regions,

$$h_2 = h_{D_1} \pm a_2 \left(\cos\phi_1 - \cos\phi\right) \tag{4.65b}$$

for the middle regions,

$$h_3 = h_{D_2} \pm a_3\left(\cos\phi_2 - \cos\phi\right) \tag{4.65c}$$

for the lower regions, and the at the junctions of the vessel

$$h_{D_1} = a_1\left(1 \mp \cos\phi_1\right)$$

$$h_{D_2} = h_{D_1} + a_2\left(\cos\phi_1 - \cos\phi_2\right)$$

From Figure 4.22, and as presented above, the expression for x may be recast here as

$$x_1 = \pm a_1 \sin\phi \tag{4.66a}$$

for the upper regions,

$$x_2 = \pm\left(a_2 \sin\phi - q\right) \tag{4.66b}$$

for the middle regions, and

$$x_3 = \pm a_3 \sin\phi \tag{4.66c}$$

for the lower regions.

4.4.5.2.2 Outer regions of the segmented tank

For the upper-outer region of the tank, using appropriate equations (4.55), (4.64), and (4.66) to eliminate r_1, p_r and x from equation (4.4b), and evaluating the integral, the following meridional stress resultant is obtained, after some simplifications,

$$\left(N_\phi^m\right)_1^o = \frac{\gamma a_1^2}{6\sin\phi\left(A + a_1\sin\phi\right)}\left[a_1\left(-3 + 2\cos\phi\right)\cos^2\phi - 3A\left\{\phi + \left(-2 + \cos\phi\right)\sin\phi\right\} + C_1^o\right]$$

C_1^o may be determined from the condition at the apex of the tank, where $\phi = 0$, $\left(N_\phi^m\right)_1^o$ must be zero. This condition gives $C_1^o = a_1$, so that the stress resultant in the meridional direction becomes

$$\left(N_\phi^m\right)_1^o = \frac{\gamma a_1^2}{6\sin\phi\left(A + a_1\sin\phi\right)}\Big[a_1\left\{1+\left(-3+2\cos\phi\right)\cos^2\phi\right\}$$

$$-3A\left\{\phi+\left(-2+\cos\phi\right)\sin\phi\right\}\Big] \qquad (4.67a)$$

With $\left(N_\phi^m\right)_1^o$ now known, the membrane stress resultant in the hoop direction follows from equation (4.4b) which after eliminating r_1, p_r and x for the upper-outer region of the vessel, may be written as

$$\left(N_\theta^m\right)_1^o = \frac{\gamma a_1}{6\sin^2\phi}\left\{4a_1\left(5+4\cos\phi\right)\sin^4\left(\frac{\phi}{2}\right)+3A\left(\phi-\cos\phi\sin\phi\right)\right\} \qquad (4.67b)$$

These membrane stress results are respectively the same as those derived in Section 4.4.1.2 for a toroidal tank with a circular cross-section. Substitution of appropriate expressions (4.55), (4.64), (4.66) and (4.67) for the upper-outer region of the toroidal tank into expressions (4.5) and (4.9) and simplifying, yield the deformations:

$$\left(\delta^m\right)_1^o = \frac{\gamma a_1}{6Et\sin\phi}\Bigg[\frac{\left(A+a_1\sin\phi\right)}{\sin\phi}\left\{4a_1\left(5+4\cos\phi\right)\sin^4\left(\frac{\phi}{2}\right)+3A\left(\phi-\cos\phi\sin\phi\right)\right\}$$

$$-a_1\nu\Big[a_1\left\{1+\left(-3+2\cos\phi\right)\cos^2\phi\right\}-3A\left\{\phi+\left(-2+\cos\phi\right)\sin\phi\right\}\Big]\Bigg] \qquad (4.68a)$$

$$\left(V^m\right)_1^o = -\frac{\gamma}{48Et\sin^4\phi\left(A+a_1\sin\phi\right)}\Bigg[48a_1^3\sin^6\phi+96a_1^2A\sin^5\left(\frac{\phi}{2}\right)\left\{25\cos\left(\frac{\phi}{2}\right)\right.$$

$$+11\cos\left(\frac{3\phi}{2}\right)+2\cos\left(\frac{5\phi}{2}\right)\Big\}+a_1A^2\left(81-32\cos\phi-56\cos 2\phi+7\cos 4\phi\right.$$

$$\left.-36\phi\sin 2\phi\right)+48A^3\left(-\phi\cos\phi+\sin\phi\right)\Big] \qquad (4.68b)$$

For the middle-outer region of the vessel, substituting appropriate equations (4.55), (4.64), and (4.66) into equation (4.4b), the following meridional stress resultant is obtained

$$\left(N_\phi^m\right)_2^o=\frac{\gamma}{12\left(A-q\ +a_2\sin\phi\right)\sin\phi}\Big[a_2\left\{a_2^2\left(3\cos\phi+\cos 3\phi-3\cos\phi_1\cos 2\phi\right)-3a_2\left\{\left(A-q\right)\right.\right.$$

$$\left.\left.\times\left(2\phi-4\cos\phi_1\sin\phi+\sin 2\phi\right)+h_{D_1}\cos 2\phi\right\}+12h_{D_1}\left(A-q\right)\sin\phi\right\}+C_1^o\Big] \qquad (4.69a)$$

C_1^o is obtained from the condition that N_ϕ^m in the upper-outer region of the vessel and in the middle-outer region of the vessel must have the same values at the junction $\phi=\phi_1$ of the two regions. This condition gives

$$C_1^o=8a_1^3\left(1+2\cos\phi_1\right)\sin^4\left(\frac{\phi_1}{2}\right)-3a_1a_2\sin\phi_1\left\{4h_{D_1}\sin\phi_1+a_2\left(\sin 2\phi_1-2\phi_1\right)\right\}-3Aa_1^2$$

$$\times\left(-4\sin\phi_1+\sin 2\phi_1+2\phi_1\right)-a_2\Big[12Ah_{D_1}\sin\phi_1+3a_2\left\{h_{D_1}\left(-2+\cos 2\phi_1\right)+A\left(\sin 2\phi\right.\right.$$

$$\left.\left.-2\phi_1\right)\right\}+a_2^2\left(\cos 3\phi_1+6\phi_1\sin\phi_1\right)\Big]$$

With $\left(N_\phi^m\right)_2^o$ now known, the membrane stress resultant in the hoop direction follows from equation (4.4b) which after eliminating r_1, p_r and x for the middle-outer region of the tank, may be written as

$$\left(N_\theta^m\right)_2^o=-\frac{\gamma}{12a_2\sin^2\phi}\Big[-a_2^3(-2+\cos 2\phi)\left(4\cos\phi-3\cos\phi_1\right)+3a_2^2\left\{\left(A-q\right)\left(-2\phi\right.\right.$$

$$+\sin 2\phi)+h_{D_1}\left(-2+\cos 2\phi\right)\}+C_1^o\Big] \tag{4.69b}$$

The deformations follow by substituting appropriate expressions (4.55), (4.64), (4.66) and (4.69) for the middle-outer region of the toroidal vessel into expressions (4.5) and (4.9):

$$\left(\delta^m\right)_2^o=\frac{\gamma}{12Et\sin\phi}\Bigg[-\frac{A-q+a_2\sin\phi}{a_2\sin\phi}\{-a_2^3\left(-2+\cos 2\phi\right)\left(4\cos\phi-3\cos\phi_1\right)$$

$$+3a_2^2\left\{\left(A-q\right)\left(-2\phi+\sin 2\phi\right)+h_{D_1}\left(-2+\cos 2\phi\right)\right\}+C_1^o\}$$

$$-\upsilon\Big[a_2^3\left(3\cos\phi+\cos 3\phi-3\cos\phi_1\cos 2\phi\right)-3a_2^2\left\{\left(A-q\right)\left(2\phi-4\cos\phi_1\sin\phi\right.\right.$$

$$\left.\left.+\sin 2\phi\right)+h_{D_1}\cos 2\phi\right\}+12a_2h_{D_1}\left(A-q\right)\sin\phi+C_1^o\Big]\Bigg] \tag{4.70a}$$

and

$$\left(V^m\right)_2^o=\frac{\gamma}{48Eta_2^2\sin^4\phi\left(A-q+a_2\sin\phi\right)}\Big[-48a_2^5\sin^6\phi+6a_2^4\left(A-q\right)\sin\phi\{-14+8\cos 2\phi$$

$$-2\cos 4\phi+\cos\phi_1\left(7\cos\phi-\cos^3\phi+3\cos\phi\sin^2\phi\right)\}+a_2^3(A-q)\{(A-q)(-81$$

$$+56\cos 2\phi-7\cos 4\phi+24\cos\phi_1\cos\phi+36\phi\sin 2\phi)-3h_{D_1}\left(-8\sin 2\phi+\sin 4\phi\right)\}$$

$$+24a_2^2\left(A-q\right)^2\left\{2\left(A-q\right)\left(\phi\cos\phi-\sin\phi\right)+h_{D_1}\cos\phi\right\}-2\left(A-q\right)C_1^o\{4\left(A-q\right)$$

$$\left.\times\cos\phi+3a_2\sin 2\phi\right\}\Big] \tag{4.70b}$$

For the lower-outer region of the tank, substituting appropriate equations (4.55), (4.64), and (4.66) into (4.4b) and evaluating the integral, and using the condition that N_ϕ^m in the middle-outer region of the vessel and in the lower-outer region of the vessel must have the same values

at the junction $\phi = \phi_2$ of the two regions, the following meridional stress resultant are obtained after some simplifications

$$\left(N_{\phi}^{m}\right)_3^o = \frac{\gamma}{12\sin\phi\left(A + a_3\sin\phi\right)}\Big[2a_3^3\cos^2\phi\left(2\cos\phi - 3\cos\phi_2\right) - 3a_3^2\Big\{A\left(2\phi - 4\cos\phi_2\sin\phi\right.$$

$$\left.+\sin 2\phi\right) + 2h_{D_2}\cos^2\phi\Big\} + 12a_3 A h_{D_2}\sin\phi + C_2^o\Big] \qquad (4.71a)$$

where

$$C_2^o = -a_3\Big\{-2a_3^2\cos^3\phi_2 + 12Ah_{D_2}\sin\phi_2 + 3a_3\Big\{-2h_{D_2}\cos^2\phi_2 + A\left(\sin 2\phi_2 - 2\phi_2\right)\Big\}\Big\}$$

$$+\frac{A + a_3\sin\phi_2}{A + a_2\sin\phi_2 + \left(a_1 - a_2\right)\sin\phi_1}\Big[a_2^3\left(3\cos\phi_2 - 3\cos\phi_1\cos 2\phi_2 + \cos 3\phi_2\right)$$

$$-3a_2^2\Big\{h_{D_1}\cos 2\phi_2 + \Big\{A + \left(a_1 - a_2\right)\sin\phi_1\Big\}\left(-4\cos\phi_1\sin\phi_2 + \sin 2\phi_2 + 2\phi_2\right)\Big\}$$

$$+12a_2 h_{D_1}\Big\{A + \left(a_1 - a_2\right)\sin\phi_1\Big\}\sin\phi_2 + C_1^o\Big]$$

The hoop stress resultant follows as

$$\left(N_{\theta}^{m}\right)_3^o = -\frac{\gamma}{12a_3\sin^2\phi}\Big[a_3^3\Big\{6\cos\phi - 2\cos 3\phi + 3\cos\phi_2\left(-3 + \cos 2\phi\right)\Big\} + 3a_3^2\Big\{A\left(-2\phi\right.$$

$$\left.+\sin 2\phi\right) + h_{D_2}\left(-3 + \cos 2\phi\right)\Big\} + C_2^o\Big] \qquad (4.71b)$$

Similarly, the deformations are:

$$\left(\delta^m\right)_3^o = \frac{\gamma}{12Et\sin\phi}\Bigg[-\left(\frac{A}{a_3\sin\phi} + 1\right)\Big[a_3^3\Big\{6\cos\phi - 2\cos 3\phi + 3\cos\phi_2\left(-3 + \cos 2\phi\right)\Big\}$$

$$+3a_3^2\Big\{A\left(-2\phi + \sin 2\phi\right) + h_{D_2}\left(-3 + \cos 2\phi\right)\Big\} + C_2^o\Big] - \upsilon\Big[2a_3^3\cos^2\phi\left(2\cos\phi\right.$$

$$-3\cos\phi_2\big)-3a_3^2\left\{A\big(2\phi-4\cos\phi_2\sin\phi+\sin 2\phi\big)+2h_{D_2}\cos^2\phi\right\}$$

$$+12a_3Ah_{D_2}\sin\phi+C_2^o\Big]\Big] \tag{4.72a}$$

and

$$\left(V^m\right)_3^o=\frac{\gamma}{48Eta_3^2\sin^4\phi\big(A+a_3\sin\phi\big)}\Big[-48a_3^5\sin^6\phi+6a_3^4A\sin\phi\{-14+8\cos 2\phi$$

$$-2\cos 4\phi+\cos\phi_2\big(13\cos\phi-\cos^3\phi+3\cos\phi\sin^2\phi\big)\}+a_3^3A\{A(-81$$

$$+56\cos 2\varphi-7\cos 4\phi+48\cos\phi_2\cos\phi+36\phi\sin 2\phi\big)-3h_{D_2}\big(-14\sin 2\phi$$

$$+\sin 4\phi\big)\}+48a_3^2A^2\left\{A\big(\phi\cos\phi-\sin\phi\big)+h_{D_2}\cos\phi\right\}$$

$$-2AC_2^o\left\{4A\cos\phi+3a_3\sin 2\phi\right\}\Big] \tag{4.72b}$$

4.4.5.2.3 Inner regions of the segmented tank

For the upper-inner region of the tank, using appropriate equations (4.55), (4.64), and (4.66) to eliminate r_1, p_r and x from equation (4.4b), and evaluating the integral, the following meridional stress resultant is obtained, after some simplifications,

$$\left(N_\phi^m\right)_1^i=\frac{\gamma a_1^2}{6\sin\phi\big(A-a_1\sin\phi\big)}\left\{a_1\big(3+2\cos\phi\big)\cos^2\phi+3A\big(\phi+(2+\cos\phi)\sin\phi\big)+C_1^i\right\}$$

where C_1^i is the constant of integration that may be determined from the boundary condition: at $\phi=\pi$, $\left(N_\phi^m\right)_1^i$ must be zero. This condition gives $C_1^i=-\big(a_1+3A\pi\big)$, so that

$$\left(N_\phi^m\right)_1^i=\frac{\gamma a_1^2}{6\sin\phi\big(A-a_1\sin\phi\big)}\left\{a_1\big((1+\cos\phi)^2(-1+2\cos\phi)\big)\right.$$

$$+3A\left(-\pi+\phi+(2+\cos\phi)\sin\phi\right)\Big\} \tag{4.73a}$$

With $\left(N_{\phi}^{m}\right)_1^i$ now known, the membrane stress resultant in the hoop direction follows from equation (4.4b) which after eliminating r_1, p_r and x for the upper-inner region of the vessel, may be written as

$$\left(N_{\theta}^{m}\right)_1^i=-\frac{\gamma a_1}{6\sin^2\phi}\left\{4a_1\left(-5+4\cos\phi\right)\cos^4\left(\frac{\phi}{2}\right)+3A\left(\pi-\phi+\cos\phi\sin\phi\right)\right\} \tag{4.73b}$$

Substitution of the appropriate expressions (4.55), (4.64), (4.66) and (4.73) for the upper-inner region of the toroidal tank into expressions (4.5) and (4.9) and simplifying, yield the deformations:

$$\left(\delta^{m}\right)_1^i=\frac{\gamma a_1}{6Et\sin\phi}\Bigg[-\frac{(A-a_1\sin\phi)}{\sin\phi}\left\{4a_1\left(-5+4\cos\phi\right)\cos^4\left(\frac{\phi}{2}\right)+3A\left(\pi+\cos\phi\sin\phi-\phi\right)\right\}$$

$$-a_1\upsilon\left\{a_1\left((1+\cos\phi)^2(-1+2\cos\phi)\right)+3A\left(-\pi+\phi+(2+\cos\phi)\sin\phi\right)\right\}\Bigg] \tag{4.74a}$$

$$\left(V^{m}\right)_1^i=\frac{\gamma}{48Et\sin^4\phi\left(A-a_1\sin\phi\right)}\Bigg\{-48a_1^3\sin^6\phi+96a_1^2A\cos^5\left(\frac{\phi}{2}\right)\Bigg(25\sin\left(\frac{\phi}{2}\right)$$

$$-11\sin\left(\frac{3\phi}{2}\right)+2\sin\left(\frac{5\phi}{2}\right)\Bigg)-a_1A^2\left(81+32\cos\phi-56\cos2\phi+7\cos4\phi\right.$$

$$\left.+36(\pi-\phi)\sin2\phi\right)+48A^3\left((\pi-\phi)\cos\phi+\sin\phi\right)\Bigg\} \tag{4.74b}$$

For the middle-inner region of the vessel, substituting appropriate equations (4.55), (4.64), and (4.66) into equation (4.4b), the following meridional stress resultant is obtained

$$\left(N_{\phi}^{m}\right)_2^i = \frac{\gamma}{12\left(A+q\ -a_2\sin\phi\right)\sin\phi}\left\{a_2^3\left(3\cos\phi+\cos3\phi-3\cos\phi_1\cos2\phi\right)+3a_2^2\left((A+q)\right.\right.$$

$$\left.\left.\times(2\phi-4\cos\phi_1\sin\phi+\sin2\phi)+h_{D_1}cos2\phi\right)+12a_2h_{D_1}(A+q)\sin\phi+C_1^i\right\} \qquad (4.75a)$$

C_1^i is obtained from the condition that N_{ϕ}^{m} in the upper-inner region of the vessel and in the middle-inner region of the vessel must have the same values at the junction $\phi=\phi_1$ of the two regions. This condition gives

$$C_1^i = 8a_1^3\left(-1+2\cos\phi_1\right)\cos^4\left(\frac{\phi_1}{2}\right)+3a_1a_2\sin\phi_1\left(4h_{D_1}\sin\phi_1-a_2(\sin2\phi_1-2\phi_1)\right)+3Aa_1^2$$

$$\left(-2\pi+4\sin\phi_1+\sin2\phi_1+2\phi_1\right)-a_2\left\{12Ah_{D_1}\sin\phi_1-3a_2\left((-2+\cos2\phi_1)h_{D_1}\right.\right.$$

$$\left.\left.+A(\sin2\phi_1-2\phi_1)\right)+a_2^2\left(\cos3\phi_1+6\phi_1\sin\phi_1\right)\right\}$$

With $\left(N_{\phi}^{m}\right)_2^i$ now known, the membrane stress resultant in the hoop direction follows from expression (4.4b) which after eliminating r_1, p_r and x for the middle-inner region of the tank, may be written as

$$\left(N_{\theta}^{m}\right)_2^i = \frac{\gamma}{12a_2\sin^2\phi}\left[-a_2^3(-2+\cos2\phi)\left(4\cos\phi-3\cos\phi_1\right)-3a_2^2\left\{(A+q)\left(-2\phi\right.\right.\right.$$

$$\left.\left.\left.+\sin2\phi\right)+h_{D_1}\left(-2+\cos2\phi\right)\right\}+C_1^i\right] \qquad (4.75b)$$

The deformations follow by substituting appropriate expressions (4.55), (4.64), (4.66) and (4.75) for the middle-inner region of the toroidal vessel into expressions (4.5) and (4.9):

$$\left(\delta^m\right)_2^o = \frac{\gamma}{12Et\sin\varphi}\left[\frac{A+q-a_2\sin\phi}{a_2\sin\phi}\left\{-a_2^3(-2+\cos2\phi)\left(4\cos\phi-3\cos\phi_1\right)\right.\right.$$

$$\left.\left.-3a_2^2\left\{(A+q)\left(-2\phi+\sin2\phi\right)+h_{D_1}\left(-2+\cos2\phi\right)\right\}+C_1^i\right\}\right.$$

$$-\upsilon\left\{a_2^3\left(3\cos\phi+\cos 3\phi-3\cos\phi_1\cos 2\phi\right)+3a_2^2\left((A+q)(2\phi-4\cos\phi_1\sin\phi\right.\right.$$

$$\left.\left.+\sin 2\phi)+h_{D_1}cos2\phi\right)+12a_2h_{D_1}(A+q)\sin\phi+C_1^i\right\}\Big] \tag{4.76a}$$

and

$$\left(V^m\right)_2^i=\frac{\gamma}{48Eta_2^2\sin^4\phi\left(A+q-a_2\sin\phi\right)}\Big[-48a_2^5\sin^6\phi+6a_2^4(A+q)\sin\phi\{14-8\cos 2\phi$$

$$+2\cos 4\phi+\cos\phi_1\left(-7\cos\phi+\cos^3\phi-3\cos\phi\sin^2\phi\right)\}+a_2^3(A+q)\{(A+q)(-81$$

$$+56\cos 2\phi-7\cos 4\phi+24\cos\phi_1\cos\phi+36\phi\sin 2\phi)-3h_{D_1}\left(-8\sin 2\phi+\sin 4\phi\right)\}$$

$$-24a_2^2(A+q)^2\{2(A+q)(\phi\cos\phi-\sin\phi)+h_{D_1}\cos\phi\}-2(A+q)C_1^i\{4(A+q)$$

$$\times\cos\phi-3a_2\sin 2\phi\}\Big] \tag{4.76b}$$

For the lower-inner region of the tank, substituting appropriate equations (4.55), (4.64), and (4.66) into (4.4b). The ensuing integral is evaluated, and using the condition that N_ϕ^m in the middle-inner region of the vessel and the lower-inner region of the vessel must have the same values at the junction $\phi=\phi_2$ of the two regions (since the support is at the nadir circle of latitude of the vessel), the following meridional stress resultant are obtained after some simplifications

$$\left(N_\phi^m\right)_3^i=\frac{\gamma}{12\sin\phi\left(A-a_3\sin\phi\right)}\left\{2a_3^3\cos^2\phi\left(2\cos\phi-3\cos\phi_2\right)+3a_3^2\left(A(2\phi-4\cos\phi_2\sin\phi\right.\right.$$

$$\left.\left.+\sin 2\phi)+2h_{D_2}\cos^2\phi\right)+12a_3Ah_{D_2}\sin\phi+C_2^i\right\} \tag{4.77a}$$

where

$$C_2^i=-a_3\left\{-2a_3^2\cos^3\phi_2+12Ah_{D_2}\sin\phi_2+a_3\left(-3A\sin 2\phi_2+6h_{D_2}\cos^2\phi_2+6A\phi_2\right)\right\}$$

$$+\frac{A-a_3\sin\phi_2}{A-a_1\sin\phi_2+(a_2-a_1)\sin\phi_1}\left\{a_2^3\left(3\cos\phi_2-3\cos\phi_1\cos2\phi_2+\cos3\phi_2\right)\right.$$

$$+3a_2^2\left(h_{D_1}\cos2\phi_2+(A+(a_2-a_1)\sin\phi_1)(-4\cos\phi_1\sin\phi_2+\sin2\phi_2+2\phi_2)\right)$$

$$\left.+12a_2h_{D_1}\sin\phi_2\left(A+(a_1-a_2)\sin\phi_2\right)+C_1^i\right\}$$

The hoop stress resultant follows from equation (4.4b) as

$$\left(N_\theta^m\right)_3^i=\frac{\gamma}{12a_3\sin^2\phi}\left\{a_3^3\left(6\cos\phi-2\cos3\phi+3\cos\phi_2(-3+\cos2\phi)\right)-3a_3^2\left(A(-2\phi\right.\right.$$

$$\left.\left.+\sin2\phi)+h_{D_2}(-3+\cos2\phi)\right)+C_2^i\right\} \qquad (4.77b)$$

Similarly, the deformations from expressions (4.5) and (4.9) become:

$$\left(\delta^m\right)_3^i=\frac{\gamma}{12Et\sin\phi}\left[\left(\frac{A}{a_3\sin\phi}-1\right)\left\{a_3^3\left(6\cos\phi-2\cos3\phi+3\cos\phi_2(-3+\cos2\phi)\right)\right.\right.$$

$$-3a_3^2\left(A(-2\phi+\sin2\phi)+h_{D_2}(-3+cos2\phi)\right)+C_2^i\Big\}-\upsilon\Big\{2a_3^3\cos^2\phi\left(2\cos\phi\right.$$

$$\left.-3\cos\phi_2\right)+3a_3^2\left(A(2\phi-4\cos\phi_2\sin\phi+\sin2\phi)+2h_{D_2}\cos^2\phi\right)$$

$$\left.\left.+12a_3Ah_{D_2}\sin\phi+C_2^i\right\}\right] \qquad (4.78a)$$

and

$$\left(V^m\right)_3^i=\frac{\gamma}{48Eta_3^2\sin^4\phi\left(-A+a_3\sin\phi\right)}\left[48a_3^5\sin^6\phi+6a_3^4A\sin\phi\{-14+8\cos2\phi\right.$$

$$-2\cos4\phi+\cos\phi_2\left(13\cos\phi-\cos^3\phi+3\cos\phi\sin^2\phi\right)\}+a_3^3A\{A(81$$

$$\left.-56\cos2\phi+7\cos4\phi-48\cos\phi_2\cos\phi-36\phi\sin2\phi\right)+3h_{D_2}\left(-14\sin2\phi\right.$$

$$+\sin 4\phi)\}+48a_3^2A^2\left\{A(\phi\cos\phi-\sin\phi)+h_{D_2}\cos\phi\right\}$$

$$+2AC_2^i\left\{4A\cos\phi-3a_3 sin\,2\phi\right\}\Big] \qquad (4.78b)$$

4.4.5.2.4 Actual membrane stresses in the multi-segmented vessel

In the usual way, the actual membrane stresses at a given point within the segmented toroidal shell are obtained by simply dividing the membrane stress-resultant values by the thickness of the shell at that point:

$$\sigma_\phi^m=\frac{N_\phi^m}{t} \qquad (4.79)$$

$$\sigma_\theta^m=\frac{N_\theta^m}{t} \qquad (4.80)$$

where σ_ϕ^m and σ_θ^m are the membrane stresses in the meridional and hoop directions, respectively. With these final expressions, the formulated results for the membrane stress resultants are also valid for non-uniform shell-thickness variations.

4.4.5.2.5 Numerical example and discussion of results

In his study of multi-segmented egg-shaped digesters of a spherical profile, Zingoni (2001a,b) considered a numerical example with a configuration that was symmetrical about the equatorial plane. Here, a toroidal shell of segmented spherical cross-section with a geometrical configuration that is not symmetrical about the equatorial plane is considered. This example is adopted to show that the formulated results can also be applied to segmented toroids that are not symmetrical about the equatorial (middle) plane. The numerical values for the geometric, material and loading parameters of the toroid are:

Outer region: $\phi_1=80^o;\ \phi_2=120^o;$

Inner region: $\phi_1=100^o;\ \phi_2=60^o;$

$A = 23.57\ mm;\ a_1 = 14.31\ mm;\ a_2 = 14.31\ mm;\ a_3 = 14.31\ mm;$

$t = 0.05\ mm;\ E = 200\ GPa;\ \upsilon = 0.3;$ and $\gamma = 10 \times 10^3\ N/m^3$.

To obtain the membrane results for most of the middle surfaces of the vessel without the interference of support effects, a hypothetical location of the support at the region of the lower circle of latitude, far enough, at least 30^o from the lower edge location of the vessel is assumed (Zingoni, 2001a). As has been shown by Zingoni (1991, 1997); Zingoni & Pavlović, (1991a,b), the best location of the support will be at the equatorial plane (the innermost and outermost circles of latitude), where the support reaction will be tangential to the shell middle surface, hence providing less bending disturbances at that region. Numerical modelling will be required to determine the behaviour of the shell in the support region of the vessel which, as earlier mention, is beyond the scope of the present study. The variations of stresses with angular coordinate ϕ over the full profile of the vessel are shown in Figure 4.23 and 4.24. Note that the values below $\phi = 20^o$ and beyond $\phi = 160^o$ at the outer and inner regions of the vessel are not presented in the figures. This is because the membrane solution cannot be used to estimate the state of stress in the vicinity of the top and bottom circles of latitude without additional bending due to the incompatibility of deformations at the meeting points of the synclastic and anticlastic surfaces of the toroidal shell.

In the upper-outer region of the vessel, Figure 4.23, σ_ϕ^m gradually rise in tension as one moves from the apex towards the upper-outer edge $\phi = 80^o$ attaining a value of 7.66 MPa, while σ_θ^m appreciably rise in tension to a value of 66.98 MPa. The corresponding membrane deformations δ^m and V^m are 12.75 mm and -1.25×10^3 respectively. At the junction $\phi = 80^o$, there are discontinuities in σ_θ^m, δ^m and V^m, but not in σ_ϕ^m in moving across the junction to the middle-outer region, where σ_θ^m, δ^m and V^m become 79.60 MPa, 14.56 mm and -1.39×10^3 respectively at the upper-outer edge of the middle-outer region of the vessel.

In the middle-outer region, the meridional stress σ_ϕ^m continues to rise until it reaches a maximum tensile value of 8.55 MPa at $\phi = 90^o$ (around the equator), then began to decrease beyond that point to zero at approximately $\phi = 111.5^o$, becoming compressive afterwards to

attain a compressive value of -11.55 MPa at the lower-outer edge $\phi = 120^o$. The hoop stress σ_θ^m continues to rise more appreciably from the upper-outer edge to the lower-outer edge, where it attained a value of 255.85 MPa. The corresponding membrane deformations δ^m and V^m are 44.68 mm and -2.09×10^3 respectively. Just as in the upper- outer edge, at the junction $\phi = 120^o$, there are discontinuities in σ_θ^m, δ^m and V^m, but not in σ_ϕ^m in moving across the junction to the lower-outer region, where σ_θ^m, δ^m and V^m become 275.40 MPa, 4.00 mm and -4.89×10^3 respectively at the lower-outer edge of the lower-outer region of the vessel. Both σ_ϕ^m and σ_θ^m thereafter in the lower-outer region of the vessel continue to increase more and rapidly in compression and tension, respectively, with ϕ.

Interestingly, it is seen that the meridional and hoop stress plots in Figure 4.23 for the outer region of the multi-shell toroidal tank exhibit the same trend as those obtained by Zingoni (2001a) for egg-shaped sludge digesters. This is particularly the case since the outer cross-section of the present toroid is the same as that of the egg-shaped sludge digester, as earlier indicated. However, the formulation here involves a toroidal shell with eccentricity A, while that for egg-shaped sludge digester is a normal shell of revolution without A. Therefore, for $A = 0$, the membrane results present here are found to coincide with those for egg-shaped sludge digesters (Zingoni, 2001a).

In the outer regions of the present toroidal vessel, it is noted that the hoop stress σ_θ^m is tensile throughout the vessel with relatively large values at the lower parts. The meridional stress σ_ϕ^m became compressive in the lower parts of the vessel (from $\phi = 111.5^o$) indicating that stiffeners should be added to, or the thickness of the shell t should be increased in these regions to avoid buckling of the vessel, which will be more prevalent in much larger vessels. The values of the horizontal displacement δ^m obtained at the edges of the outer region of the vessel, though generally small, show that all edges move laterally outwards of the axis of revolution of the toroid as expected of the internally contained water.

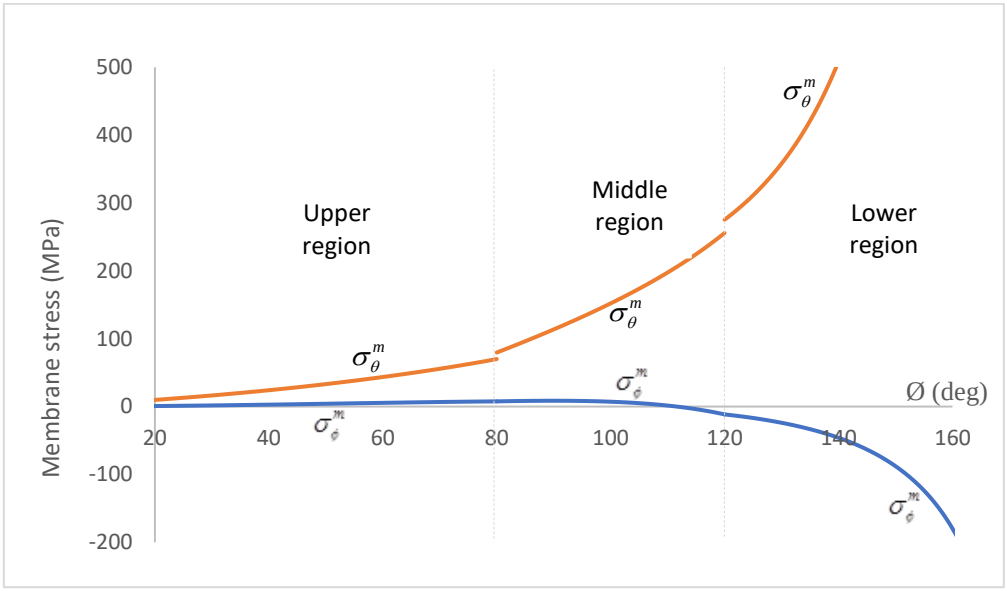

Figure 4.23. Variations of membrane stresses over the outer cross-sectional profile of the toroidal vessel

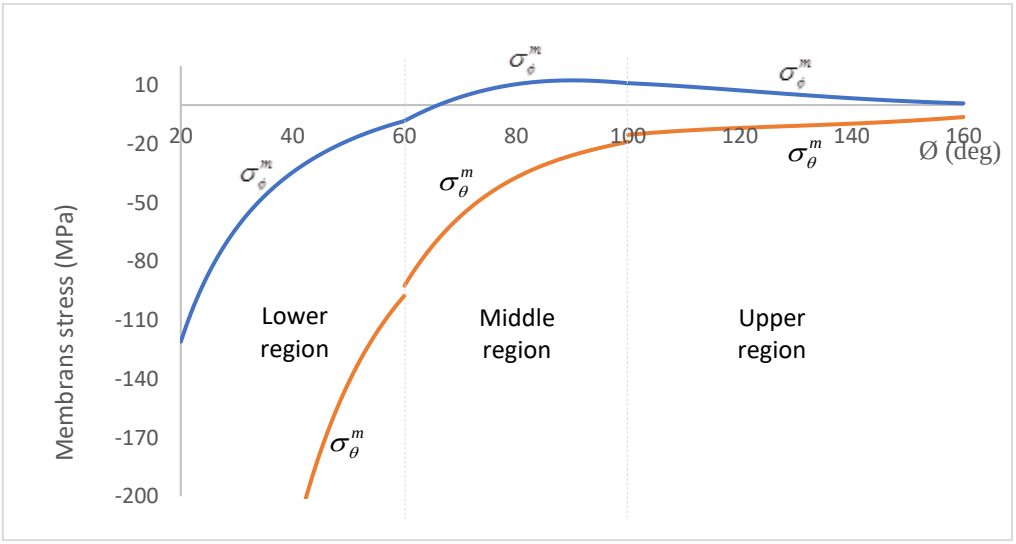

Figure 4.24. Variations of membrane stresses over the inner cross-sectional profile of the toroidal vessel

In the lower-inner region of the vessel, Figure 4.24, both σ_ϕ^m and σ_θ^m significantly decrease in magnitude as one moves from the base towards the lower-inner edge $\phi = 60^o$ to -8.16 MPa and -97.42 MPa (compressive) respectively. The corresponding membrane deformations δ^m and V^m are -6.02 mm and 1.35×10^3 respectively. At the junction $\phi = 60^o$, there are discontinuities in σ_θ^m, δ^m and V^m (but not in σ_ϕ^m) when moving across the junction to the

middle-inner region, where σ_θ^m, δ^m and V^m become -92.35 MPa, -5.70 mm and 0.97×10^3 respectively at the lower-inner edge of the middle-inner region of the vessel.

In the middle-inner region, the meridional stress σ_ϕ^m continues to decrease in magnitude until it reaches zero at approximately $\phi=66^o$, then began to increase in tension beyond that point to a maximum tensile value of 12.63 MPa at $\phi=90^o$ (around the inner equator). It then began to decrease from the maximum tensile value to attain a value of 11.15 MPa at the upper-inner edge $\phi=100^o$. The hoop stress σ_θ^m continues to reduce less appreciably from the lower-inner edge to the upper-inner edge, where it reaches a value of -18.78 MPa. The corresponding membrane deformations δ^m and V^m are -1.05 mm and 3.29×10^5 respectively. Just as in the lower-inner edge, at the junction $\phi=100^o$, there are discontinuities in σ_θ^m, δ^m and V^m (but not in σ_ϕ^m) when moving across the junction to the upper-inner region, where σ_θ^m, δ^m and V^m become -15.24 MPa, -0.88 mm and 2.98×10^5 respectively at the upper inner edge of the upper-inner region of the vessel. Both σ_ϕ^m and σ_θ^m thereafter in the upper-inner region of the vessel continue to decrease but more gradually in tension and compression respectively with ϕ.

The meridional stress σ_ϕ^m is only compressive in the lower parts of the vessel, while the hoop stress σ_θ^m is compressive throughout the inner region of the vessel with relatively large hoop compression at the lower parts, indicating that stiffeners should be added to, or the thickness of the shell t should be increased in these regions to avoid local buckling of the vessel. The values of the horizontal displacement δ^m obtained at the edges of the inner region of the vessel show that all edges move laterally inwards of the axis of revolution of the toroid as expected of the internally contained water.

The maximum tensile value of meridional stress at the inner regions of the vessel is higher than that at the outer regions of the vessel, indicating that the vessel will most likely fail at the inner region. These maximum tensile values occur at the equator ($\phi=90^o$) of the vessel for both the outer and inner regions. It will suffice to note here that bending will occur around the edges of the vessel, due to the discontinuities in the deformations there.

4.5 Concluding remarks

In this chapter, based on membrane theory and on account of axisymmetric loading, the partial differential equations that describe the behaviour of a toroidal shell of revolution which were developed in Chapter 3 have been reduced to expressions for the solution of the membrane state of stress and deformation of the shell. These expressions were used to formulate membrane results for various toroidal shells: circular toroidal shell, elliptic toroid, parabolic ogival toroid, circular-elliptic toroid, and the multi-shell toroidal vessel under uniform pressure loading. Membrane results were also presented for the selected vessels when loaded hydrostatically. The developed approach can be used for toroidal shells of almost any kind of cross-section. The results were validated with those available in the literature (and in some cases with limiting results). It was demonstrated that toroidal shells of the same cross-section respond differently under the action of uniform pressure and linearly varying (hydrostatic) pressure. The membrane results were also presented in non-dimensional form. These were used to conduct parametric investigations that span over the most practical range of the toroidal shells. Some insightful behaviour of each of the shell forms studied were identified, and a set of design recommendations has been proposed for each of the toroidal shells, including the positioning of supports.

Generally, each of the investigated toroidal vessels under uniform internal pressure, experiences the highest membrane stress resultants in the meridional direction N_ϕ^m around inner equatorial zones (where $\phi_i = \pi/2$ or $\phi_s = 3\pi/2$), while, relatively lower values of N_ϕ^m are seen in the equatorial zones (where $\phi_i = \phi_s = \pi/2$). The difference in the meridional stress resultants N_ϕ^m in these zones is related to the mean toroidal radius R, with higher discrepancy observed for smaller R. The high meridional stresses in the inner zones, which span in a wider range for the parabolic ogival toroid compared to those in circular or elliptic toroids, suggests the initiation of local plastic instability in the zones. This can be avoided by systematically changing the cross-sectional profile or varying the thickness of the shell (or both) until the meridional stress across the cross-section of the toroid is the same. A study of this type has been conducted by Vu (2010) for a circular toroidal shell.

Most of the internally pressurised toroids considered are seen to be in tension throughout. Specifically, the circular toroids experience tensile membrane stresses entirely in both the

meridional and hoop directions. An indication that the toroid will likely not buckle when loaded internally with uniform pressure, as already demonstrated by Galletly & Błachut (1995). Each of the other vessels investigated in this chapter are observed to be generally in tension for certain geometrical parameters. For some other parameters, the stresses in the internally pressurised vessels, mostly around the inner regions of the shells, are seen to be in compression. These are usually the hoop stresses and can trigger local buckling in the toroids. The compressive hoop stresses in the zones of the shells can be catered for by the addition of stiffeners or thickening of the shells in the localised zones of the toroids.

For the hydrostatically loaded cases, it was found that the membrane stresses in the vessels supported axisymmetrically at the lowest circle of latitude are largely in compression around the lower parts of the tanks. When the supports are placed just above the cross-over lines (where the meridional stresses change from tension to compression, and vice versa) and/or the thickness of the shells are enhanced in the lower parts of the tanks, the possible local instability that may be triggered by the compressive stresses there will likely be avoided. Special attention will also be required for the larger hoop membrane stresses observed in the outer lower region of that toroidal vessel studied.

The membrane solution presented in this chapter will also be used in the next two chapters of this thesis. In Chapter 5, the membrane solution is employed as the particular solution of the axisymmetric bending equations for estimating the bending disturbances that occur within the toroidal shell where the membrane solution fails. When the bending disturbance solution is superimposed with the membrane solution, the total internal actions in an axisymmetrically loaded toroidal vessel will be determined. The membrane solution will also be adopted to serve as the pre-buckling state in the stability equations in Chapter 6. This, as we shall see, will drastically reduce the complexity of the governing differential equations, so that a reasonably accurate buckling solution can be obtained for predicting the critical buckling behaviour of toroidal shells.

Chapter 5

Approximate bending solution

5.1 Introduction

For axisymmetrically pressurised thin-toroidal shells of revolution under consideration in this thesis, the membrane solution presented in the preceding chapter is practically appropriate for the determination of the stress state in the regions away from the bending disturbance zones of the shells. Therefore, only a few practical problems can be fully analysed with the membrane theory. The practising engineer mainly encounters shell problems with edge-zone effects. These zones are typically around support locations, meeting points of segments, turning points where the surfaces of positive and negative Gaussian curvature meet, and some other axisymmetric lines of distortions for general shells of revolution (Kraus, 1967; Zingoni, 1997). To account for the bending disturbances around these zones (where the membrane solution fails to satisfy the conditions of middle-surface continuity, shell equilibrium and support constraints), the bending-theory differential equations developed in Chapter 3 will be invoked in this chapter. The solution to these exact differential equations is extremely difficult, more so for the present toroidal shell geometries. Therefore, the Geckeler-type approximations (Zingoni, 1997) which are based on the premise that the resultant bending effects decrease in a very rapid manner as one moves away from the source of the disturbance, are adopted here. The ensuing bending effects from the simplified homogeneous bending equations may be superimposed with the membrane solution (which act as an approximate integral of the bending-theory equations) to obtain closed-form stress results for toroidal shells.

In effect, the complete mathematical formulation given in Chapter 3 for toroidal shells of revolution would be approximately solved systematically. The solution as we shall see, consists of the particular-solution part (which includes the solution of all terms involving loading and are approximated by the membrane theory) and the homogeneous-solution part (which includes the solution of the relations that ensure the compatibility of the boundary conditions with the conditions of equilibrium).

This solution approach saves the analyst the laborious task of attempting to solve the complex system given by the governing equations of the shells. In his work on shells dating back to 1990, Zingoni has championed the simplified mathematical approach for the bending of shells of revolution, which he has used to develop numerous closed-form results for cylindrical, spherical and conical shells (Zingoni & Pavlović, 1990, 1991a,b, 1992, 1993a,b, Zingoni, 1997, 2001a,b, 2002a,b, 2004, 2009; Zingoni, Mokhothu & Enoma, 2015). The approach is usually applied for axisymmetrically loaded thin-shells of revolution of zero or positive Gaussian curvature. It was recently extended to the evaluation of bending disturbances that occur around equatorial regions of semi-elliptic toroidal shells (Zingoni, Enoma & Govender, 2015), and to the analysis of segmented toroidal vessels (Enoma & Zingoni, 2016, 2017). An attempt will be made in this chapter to generalise the solution approach for toroidal shell forms.

Here, the general governing equations of toroidal shells of revolution derived in Chapter 3 is first re-casted in axisymmetric loading and deformation form, which is further reduced to a homogeneous problem of two coupled differential equations in Q_ϕ and V^b. The Geckeler's simplifying assumptions are then applied to the equations before a general solution is adopted, which leads to the approximate bending solution after the implementation of appropriate boundary conditions. The accuracy of the Geckeler approximation in estimating bending effects in shells of revolution was formally studied by Zingoni & Pavlović (1990, 1992, 1993c), and Zingoni (1991). This simplification of the bending theory works very well (errors are small) if the shell is sufficiently thin and non-shallow in the region experiencing bending. The approximate solution for the toroidal shell is then superimposed with the membrane solution of Chapter 4 to determine the complete state of stress for axisymmetrically pressurised toroidal shells of revolution. The formulated solution is applied to each of the novel toroidal vessels considered in the preceding chapter and the results obtained are discussed and compared with those from the commercial finite element program (Abaqus).

5.2 Axisymmetric bending-theory equations for toroidal shells

The differential equations of toroidal shells of revolution presented in Chapter 3 are seen to be functions of coordinates ϕ, and θ. These can be specialised for axisymmetric bending-theory equations if the applied loading on the shell and the deformations that occur within the shell are assumed to be axisymmetric so that the equations are functions of ϕ alone and the external

loading component p_θ in the hoop direction is set to zero. In addition to these simplifications, the toroidal shells under investigation are not subjected to torsional loading. Thus, the following also apply:

$$N_{\phi\theta} = 0$$

$$M_{\phi\theta} = 0$$

As a result, the expression 3.10(e) yields

$$Q_\theta = 0$$

On the application of the above axisymmetric loading and deformation conditions, the actions on the toroidal shell element of Figure 3.3 reduce to the ones shown in Figure 5.1, where the systems of forces and moments are now combined in one sketch, and the arc lengths of the edges remain as defined in Section 3.3 of Chapter 3.

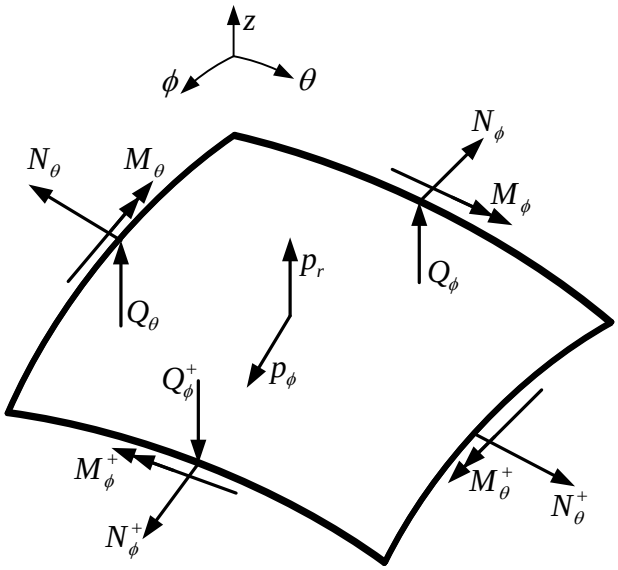

Figure 5.1. Actions on an axisymmetrically loaded toroidal shell element

Accordingly, the partial differential equations (3.10) reduces to the following set of ordinary differential equations of equilibrium of axisymmetrically loaded toroidal shells of revolution

$$\left(RN_\phi\right)^\bullet - r_1 N_\theta \cos\phi - RQ_\phi = -r_1 R p_\phi \tag{5.1a}$$

$$RN_\phi + r_1 N_\theta \sin\phi + \left(RQ_\phi\right)^\bullet = r_1 R p_r \tag{5.1b}$$

$$\left(RM_\phi\right)^\bullet - r_1 M_\theta \cos\phi = r_1 R Q_\phi \tag{5.1c}$$

These contain five unknown variables: N_ϕ, N_θ, Q_ϕ, M_ϕ and M_θ in three equations, and hence, is statically indeterminate. Consequently, unlike in the equilibrium equation of membrane theory, as seen in Chapter 4, the elastic law of a shell of revolution will be required in conjunction with the above equilibrium equations, in an attempt to obtain a solution to the bending-theory equations. If the above axisymmetric deformation conditions are applied to the constitutive relations (3.20), the following will be obtained

$$N_\phi = \frac{Et}{1-\upsilon^2}\left\{\frac{1}{r_1}\left(v^\bullet + w\right) + \frac{\upsilon}{R}\left(v\cos\phi + w\sin\phi\right)\right\} \tag{5.2a}$$

$$N_\theta = \frac{Et}{1-\upsilon^2}\left\{\frac{1}{R}\left(v\cos\phi + w\sin\phi\right) + \frac{\upsilon}{r_1}\left(v^\bullet + w\right)\right\} \tag{5.2b}$$

$$M_\phi = D\left[\frac{1}{r_1^2}\left(w^\bullet - v\right)^\bullet + \frac{\upsilon}{R^2}\left\{\frac{R\cos\phi}{r_1}\left(w^\bullet - v\right)\right\}\right] \tag{5.2c}$$

$$= -D\left[\frac{1}{r_1}V^\bullet + \frac{\upsilon\cos\phi}{R}V\right]$$

$$M_\theta = D\left[\frac{1}{R^2}\left\{\frac{R\cos\phi}{r_1}\left(w^\bullet - v\right)\right\} + \frac{\upsilon}{r_1^2}\left(w^\bullet - v\right)^\bullet\right] \tag{5.2d}$$

$$= -D\left[\frac{\cos\phi}{R}V + \frac{\upsilon}{r_1}V^\bullet\right]$$

since, the kinematic relations (3.16) reduced to

$$\varepsilon_\phi = \frac{1}{r_1}\left(v^\bullet + w\right)$$

$$\varepsilon_\theta = \frac{1}{R}\left(v\cos\phi + w\sin\phi\right)$$

and, the only relevant rotation component in the present axisymmetric consideration is the meridional rotation (equation (3.11)), is

$$V = \frac{v - w^\bullet}{r_1} \tag{5.3a}$$

Equation (4.5) for the lateral displacement in the shell may also be rewritten below for ease of reference as we shall later.

$$\delta^m = \frac{R}{Et}\left\{N_\theta^m - \upsilon N_\phi^m\right\} \tag{5.3b}$$

The sets of equations (5.1) and (5.2) are the complete differential equations governing the axisymmetric bending of toroidal shells of revolution. In these equations, recall that A denotes the global toroidal radius; r_1 denotes the actual radius of curvature of the local profile at any point in question; x denotes the horizontal distance coordinate between any on the toroidal surface and the local axis; E and t denote the Young's modulus of elasticity and the thickness of the shell material, respectively; υ and D denote the Poisson's ratio and the flexural rigidity of the shell, respectively; v and w denote the displacement component in the direction of the tangent to the hoop circle and in the direction of the normal to the shell middle surface, respectively; p_ϕ and p_r denote the external loading components per unit area of the toroidal middle surface in the meridional direction and in the direction of the normal to the shell middle surface, respectively; N_ϕ and N_θ denote the in-plane direct-force per unit length in the meridional and hoop directions, respectively; M_ϕ and M_θ denote the bending moments per

unit length, respectively; and Q_ϕ denotes the transverse shearing force, as shown in Figure 5.1 in their positive directions.

Equations (5.2) may be used to eliminate the five unknown variables N_ϕ, N_θ, Q_ϕ, M_ϕ and M_θ in expressions (5.1), and the ensuing equations may be formulated as a homogeneous problem by the application of

$$p_\phi = 0$$

$$p_r = 0$$

When this is done, the following coupled set of three differential equations for the axisymmetric bending of toroidal shells of revolution, in terms of variables u, w, and Q_ϕ will be obtained:

$$\frac{Et}{1-\upsilon^2}\left[A\left\{\frac{1}{r_1}\left(v^\bullet + w\right)+\frac{\upsilon}{R}\left(v\cos\phi + w\sin\phi\right)\right\}^\bullet + \left(x\left\{\frac{1}{r_1}\left(v^\bullet + w\right)+\frac{\upsilon}{R}\left(v\cos\phi + w\sin\phi\right)\right\}\right)^\bullet\right.$$

$$\left. -r_1\cos\phi\left\{\frac{1}{R}\left(v\cos\phi + w\sin\phi\right)+\frac{\upsilon}{r_1}\left(v^\bullet + w\right)+\right\}\right] - RQ_\phi = 0 \qquad (5.4a)$$

$$\frac{Et}{1-\upsilon^2}\left[R\left\{\frac{1}{r_1}\left(v^\bullet + w\right)+\frac{\upsilon}{R}\left(v\cos\phi + w\sin\phi\right)\right\}\right.$$

$$\left. +r_1\sin\phi\left\{\frac{1}{R}\left(v\cos\phi + w\sin\phi\right)+\frac{\upsilon}{r_1}\left(v^\bullet + w\right)+\right\}\right] + \left(RQ_\phi\right)^\bullet = 0 \qquad (5.4b)$$

$$D\left[\left(R\left\{\frac{1}{r_1^2}\left(w^\bullet - v\right)^\bullet + \upsilon\left(\frac{\cos\phi}{(A+x)r_1}\left(w^\bullet - v\right)\right)\right\}\right)^\bullet\right.$$

$$-r_1\cos\phi\left\{\left(\frac{\cos\phi}{Rr_1}\left(w^{\bullet}-v\right)\right)+\frac{\upsilon}{r_1^{\,2}}\left(w^{\bullet}-v\right)^{\bullet}\right\}\Bigg]-r_1RQ_{\phi}=0 \qquad (5.4c)$$

5.3 Reduced homogeneous equations of axisymmetric bending theory

The seven axisymmetric bending equations (5.1) and (5.2) in respect of seven unknown variables (N_{ϕ}, N_{θ}, Q_{ϕ}, M_{ϕ}, M_{θ}, v and w) have been reduced to the three differential equations (5.4), in terms of u, w, and Q_{ϕ}, which may be solved for a toroidal shell with the application of appropriate boundary conditions. However, a simpler solution approach of the type exquisitely presented in (Zingoni, 1997, 2001a), of reducing the total number of the axisymmetric bending equations (in conjunction with the expression for the meridional rotation derived in Chapter 3) to a set of two ordinary differential equations in variables Q_{ϕ} and V only, and assuming that the surface-loading components are zero (i.e. homogeneous solution) is adopted here for the axisymmetric toroidal shells problem.

Starting with expressions (5.1a) and (5.1b) for a relationship between N_{ϕ} and Q_{ϕ}, the following is obtained by the application of $p_{\phi}=p_{\theta}=0$ and multiplying the first equation by $\sin\phi$ and the second equation by $\cos\phi$, and after some manipulations,

$$N_{\phi}^{b}=-Q_{\phi}\cot\phi \qquad (5.5)$$

Introduction of this into equation (5.1b), and applying some simplifications gives

$$N_{\theta}^{b}=-\frac{r_2}{r_1}\frac{dQ_{\phi}}{d\phi}-\frac{Q_{\phi}}{r_1}\frac{dr_2}{d\phi} \qquad (5.6)$$

Note that the notation $(\,)^{\bullet}$ for the first derivative with respect to ϕ has been replaced by $d(\,)/d\phi$ which will adopt henceforth for ordinary differential equations and A is independent of ϕ. Also, recall that

$$r_2 = \frac{R}{\sin\phi}$$

and the expression the meridional rotation V (equation (4.9)) is

$$V^b = \frac{1}{r_1}\left[\frac{\cot\phi}{Et}\left\{(r_1+\upsilon r_2)N_\phi^b - (r_2+\upsilon r_1)N_\theta^b\right\} - \frac{d}{d\phi}\left\{\frac{r_2}{Et}\left(N_\theta^b - \upsilon N_\phi^b\right)\right\}\right] \tag{5.7}$$

where, now the superscript b indicates bending effects.

When equations (5.2c) and (5.2d) are used to eliminate M_ϕ and M_θ, respectively from equation (5.1c), as obtained in expression (5.4c), and equations (5.5) and (5.6), are used to eliminate N_ϕ^b and N_θ^b, respectively from expression (5.7), the following pair of governing differential equations in Q_ϕ and V^b for axisymmetric bending of shells of revolution are respectively obtained, after some simplifications

$$\left[D\left(\frac{r_2}{r_1}\right)\sin\phi\right]\frac{d^2V^b}{d\phi^2} + \left[D\left(\frac{r_2}{r_1}\right)\cos\phi + \sin\phi\frac{d}{d\phi}D\left(\frac{r_2}{r_1}\right)\right]\frac{dV^b}{d\phi}$$

$$+\left[\upsilon\left(\cos\phi\frac{dD}{d\phi} - D\sin\phi\right) - D\left(\frac{r_1}{r_2}\right)\frac{\cos^2\phi}{\sin\phi}\right]V^b = -r_1r_2(\sin\phi)Q_\phi \tag{5.8a}$$

and,

$$\frac{r_2^{\,2}}{tr_1}\frac{d^2Q_\phi}{d\phi^2} + \left[\frac{r_2^{\,2}}{tr_1}\cot\phi + \frac{r_2}{tr_1}\frac{dr_2}{d\phi} + \frac{d}{d\phi}\left(\frac{r_2^{\,2}}{tr_1}\right)\right]\frac{dQ_\phi}{d\phi}$$

$$+\left[\frac{r_2}{tr_1}\frac{d^2r_2}{d\phi^2} + \left\{\frac{d}{d\phi}\left(\frac{r_2}{tr_1}\right)\right\}\frac{dr_2}{d\phi} + \left\{\left(\frac{r_2+\upsilon r_1}{r_1}\right)\frac{dr_2}{d\phi} - (r_1+\upsilon r_2)\cot\phi\right\}\frac{\cot\phi}{t}\right.$$

$$\left.-\upsilon\left\{(\cot\phi)\frac{d}{d\phi}\left(\frac{r_2}{t}\right) - \left(\frac{r_2}{t}\right)\frac{1}{\sin^2\phi}\right\}\right]Q_\phi = r_1EV^b \tag{5.8b}$$

5.1 Approximate general solution

The Geckeler-type simplifying assumption (Zingoni, 1997) is based on the fact that the rapidly decaying behaviour of edge disturbances indicate that the two dependent variables Q_ϕ and V in the axisymmetric bending equations are small compared to their first derivatives (which are also small compared to the second derivatives of the variables), so that the first-derivative and zero-derivative terms may be neglected due to their smallness. This is applied in this section to reduce the governing equations (5.8) further, and then a general solution to the ensuing fourth-order ordinary differential equation is adopted with the relevant kinematic boundary conditions to approximate the edge-zone bending stresses in the non-shallow regions of the axisymmetrically loaded thin-toroidal shells of constant thickness. This approach has been shown to be reasonably accurate for thin shells of revolution which are non-shallow (Zingoni & Pavlović, 1990; Zingoni, 1997).

5.1.1 Application of Geckeler's simplifications

In accordance with the Geckeler's approximation, as mentioned above, the first-derivative and zero-derivative terms of V^b and Q_ϕ in the left-hand side of expressions (5.8) are dropped, since they are small compared to the second derivative. This leads to

$$Q_\phi \approx -\left[D\left(\frac{1}{r_1^{\,2}}\right)\right]\frac{d^2V^b}{d\phi^2} \tag{5.9a}$$

and,

$$V^b \approx \left[\frac{1}{Et}\left(\frac{r_2^{\,2}}{r_1^{\,2}}\right)\right]\frac{d^2Q_\phi}{d\phi^2} \tag{5.9b}$$

Consistent with the accuracy of the present approach, the following simplified form of expressions (5.5) and (5.5) for the meridional and hoop stress resultants are respectively

$$N_\phi^b = -Q_\phi \cot\phi \tag{5.10a}$$

and

$$N_{\theta}^{b} \approx -\frac{r_2}{r_1}\frac{dQ_{\phi}}{d\phi} \tag{5.10b}$$

where, the term in the zero-derivative of Q_{ϕ} has been neglected in comparison with terms in the first-derivative Q_{ϕ}, and expressions (5.2c) and (5.2d) for the bending moments are respectively reduced to

$$M_{\phi} \approx -D\left(\frac{1}{r_1}\right)\frac{dV^{b}}{d\phi} \tag{5.11a}$$

and

$$M_{\theta} \approx -D\left(\frac{\upsilon}{r_1}\right)\frac{dV^{b}}{d\phi} = \upsilon M_{\phi} \tag{5.11b}$$

where, the terms in the zero-derivative of V^{b} have been neglected in comparison with terms in the first derivative V^{b}.

In a similar way, if expressions (5.10) are substituted into the expression (5.3b) for the lateral displacement of a point within the toroidal shell, and then the term in the zero-derivative of Q_{ϕ} are neglected in comparison with terms in the first-derivative Q_{ϕ}, the following reduced form of expression for the lateral displacement is obtained. Zingoni (1997) however, observed that the approximation $N_{\phi}^{b} << N_{\theta}^{b}$ in the resulting expression (5.12) is not valid in shallow regions (as $\phi \to 0, \pi$) of shells of revolution, where $\cot\phi$ becomes large, so that the contribution from the term in the variable Q_{ϕ} becomes comparable with the term in the first-derivative of Q_{ϕ}. This further emphasises that the present solution approach is applicable mainly for the non-shallow regions of the shell.

$$\delta^b \approx -\frac{r_2^2 \sin\phi}{r_1 Et}\frac{dQ_\phi}{d\phi} = \frac{1}{Et}(r_2 \sin\phi)N_\theta^b \tag{5.12}$$

Returning to the reduced pair of ordinary differential equations of second order for the transverse shearing force Q_ϕ and meridional rotation V^b, it is seen that when expression (5.9b) is substituted into (5.9a) and after some manipulations, one gets a fourth-order differential equation which may be written as

$$\frac{d^4 Q_\phi}{d\phi^4} + 4\lambda Q_\phi \approx 0 \tag{5.13}$$

where the dimensionless term λ is the slenderness parameter, expressed as

$$\lambda^4 = 3(1-\upsilon^2)\frac{r_1^4}{r_2^2 t^2} \tag{5.14}$$

The approach adopted in the rest of this section generally follows that of Zingoni (1997, 2018) as regards basic notation and derivational steps.

5.1.2 General solution of the fourth-order differential equation

The slenderness parameter (λ) which determines the distance from the edge at which the edge effects are effectively diminished, as defined by expression (5.14) above, is a function of ϕ, since r_2 (and r_1 in certain instances) are functions of ϕ. Given that the Poisson's ratio υ and shell thickness t are constant throughout the shell and the application of the approximation that each of r_2 and r_1 is constant within the bending disturbance zone. This is due to the fact that edge effects rapidly decay as one moves away from the edge, λ may, therefore, be assumed to take the value of the constant at a particular edge of the vessel under consideration. Hence, the solution of the fourth-order differential equation (5.13) may take the general form ref:

$$Q_\phi = Ce^{-\lambda\psi}\sin(\lambda\psi + \beta) \tag{5.15}$$

Note that only the solution part that decays with increasing distance from a shell edge is retained in this general solution, where C and β are constants of integration to be determined from suitable boundary conditions, and ψ is the meridional angle measured from the shell edge.

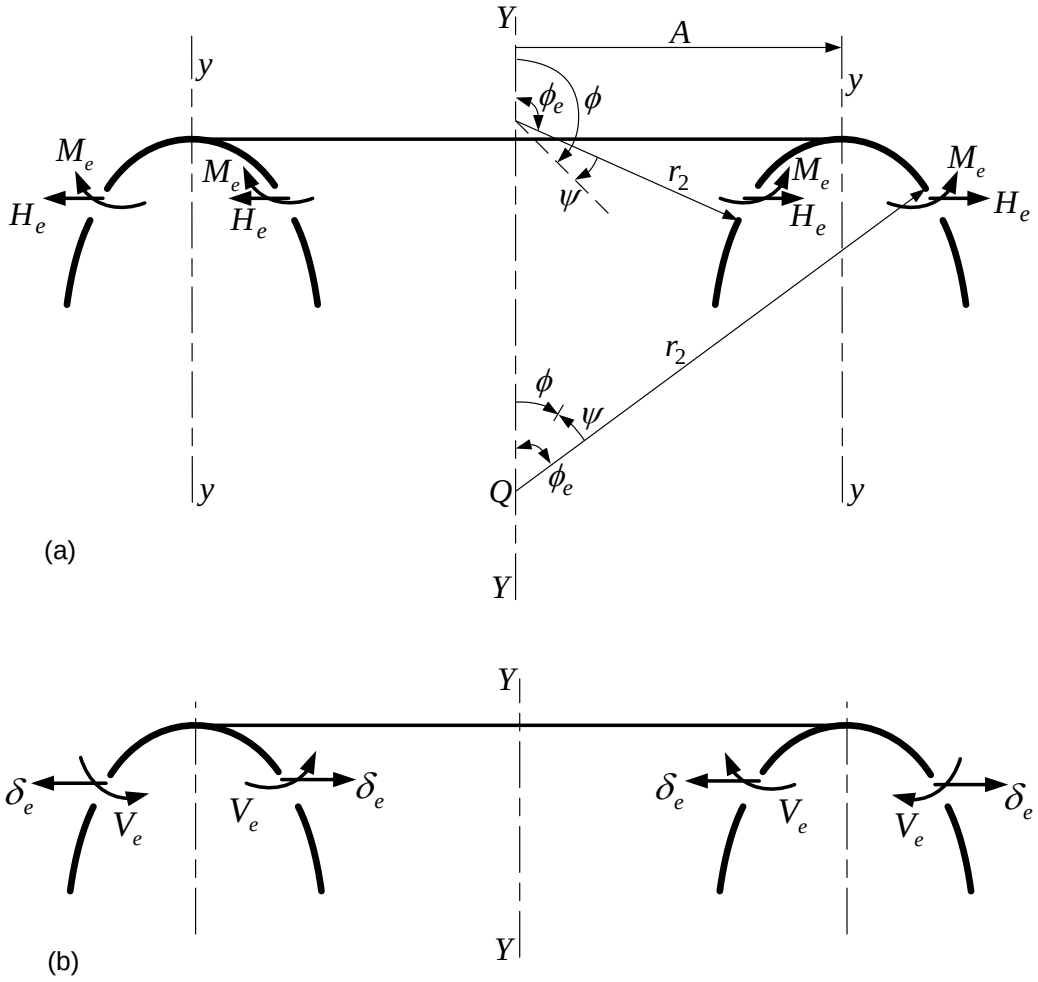

Figure 5.2. Edge parameters in a toroidal shell: (a) edge actions; and (b) edge deformations

If the value of ϕ is decreasing as one moves away from a particular edge, we shall call the shell segment the "first shell" or "second shell" if ϕ is increasing. A similar analogy applies for the edges in the inner regions of the vessel, since angular coordinate ϕ is measured from the upward direction of the global axis of revolution $Y-Y$ of the toroid to the normal to the shell middle surface at any point in question. In Figure 5.2, for example, when considering the bending effects around the edge at the outer region and within the upper segment of the vessel, the upper shell be referred to as the first shell, since ϕ decreases within this segment as one

moves away from the edge, while the adjacent segment/shell in the outer region of the vessel will be referred to as the second shell, since ϕ increases within this segment as one moves away from the edge. On the other hand, when considering the bending effects around the edge at the inner region and within the upper segment of the vessel, the upper shell is referred to as the second shell, since ϕ increases within this segment as one moves away from the edge, while the adjacent segment/shell in the inner region of the vessel will be referred to as the first shell, since ϕ increases within this segment as one moves away from the edge.

Therefore, the angle ψ measured from the shell edge is given by

$$\psi = \pm(\phi_e - \phi) \tag{5.16}$$

so that $d\psi = \mp d\phi$, where, this time, the upper sign of the double operations applies to the first shell, while the lower sign applies to the second shell, and ϕ_e is the value of ϕ at the shell edge.

On the application of the assumed general solution (5.15) into the various expressions (5.9b) - (5.12) for the internal actions and deformations, and taken account of expression (5.16) and its derivatives, the following bending related effects are obtained:

$$N_\phi^b = -\cot(\phi_e \mp \psi) Ce^{-\lambda\psi} \sin(\lambda\psi + \beta) \tag{5.17a}$$

$$N_\theta^b = \pm \frac{r_2}{r_1} \lambda Ce^{-\lambda\psi} \{\cos(\lambda\psi + \beta) - \sin(\lambda\psi + \beta)\} \tag{5.17b}$$

$$M_\phi = \pm \frac{2D\lambda^3}{Etr_1} \left(\frac{r_2^2}{r_1^2}\right) Ce^{-\lambda\psi} \{\cos(\lambda\psi + \beta) + \sin(\lambda\psi + \beta)\} \tag{5.17c}$$

$$M_\theta = \nu M_\phi \tag{5.17d}$$

$$V^b = -\frac{2\lambda^2}{Et} \left(\frac{r_2^2}{r_1^2}\right) Ce^{-\lambda\psi} \{\cos(\lambda\psi + \beta)\} \tag{5.17e}$$

$$\delta^b = \pm \frac{r_2}{Et}\left(\frac{r_2}{r_1}\right)\sin\left(\phi_e \mp \psi\right)\lambda C e^{-\lambda\psi}\left\{\cos(\lambda\psi+\beta)-\sin(\lambda\psi+\beta)\right\} \tag{5.17f}$$

where the upper and lower signs apply for the first and second shells respectively.

5.1.3 Evaluation of constant parameters

The parameters C and β are now evaluated by first applying only an edge bending moment M_e uniformly around the edge $\phi = \phi_c$, so that the boundary conditions

$$\left(M_\phi\right)_{\phi=\phi_e} = M_e$$

$$\left(Q_\phi\right)_{\phi=\phi_e} = 0$$

are satisfied (see Figure 5.2). When these are applied to equations (5.15) and (5.17c), the resulting expressions may be written as

$$\beta = 0 \tag{5.18a}$$

$$C = \pm \frac{Etr_1}{2\lambda^3 D}\left(\frac{r_1^2}{r_2^2}\right)M_e \tag{5.18b}$$

Similarly, only an edge horizontal shear force H_e is then applied uniformly around the edge $\phi = \phi_c$, so that the boundary conditions

$$\left(M_\phi\right)_{\phi=\phi_e} = 0$$

$$\left(Q_\phi\right)_{\phi=\phi_e} = H_e$$

are satisfied (see Figure 5.2). When these are applied to equations (5.15) and (5.17c), the resulting expressions may be written as

$$\beta = -\frac{\pi}{4} \tag{5.19a}$$

$$C = -\sqrt{2}H_e \tag{5.19b}$$

Note that, the values of edge redundants M_e and H_e determine the initial magnitude of the oscillating moment.

5.1.4 Implementation of kinematic boundary conditions at the shell edge

The constants C and β of equations (5.18) and (5.19) are used to obtain the separate edge effects V_e^b and δ_e^b (from equations (5.17e) and (5.17f)) caused by the individual application of the M_e and H_e. Superimposing these separate edge effects, the following net deformations V_e^b and δ_e^b due to the two bending-related edge actions at the edge of the shell, are obtained:

$$V_e^b = \mp\frac{r_1}{\lambda D}M_e + \frac{2\lambda^2}{Et}\left(\frac{r_2^2}{r_1^2}\right)H_e \tag{5.20a}$$

$$\delta_e^b = \frac{r_1^2\sin\phi_e}{2\lambda^2 D}M_e \mp \frac{2\lambda}{Et}\left(\frac{r_2^2}{r_1}\right)(\sin\phi_e)H_e \tag{5.20b}$$

where the upper and lower signs, as stated before, apply for the first and second shells respectively.

These bending-related deformations at the edge of the shell may be considered simultaneously with the contributions from membrane-solution effects. This gives the total edge deformations

$$V_e^T = V_e^b + V_e^m = \mp\frac{r_1}{\lambda D}M_e + \frac{2\lambda^2}{Et}\left(\frac{r_2^2}{r_1^2}\right)H_e + V_e^m \tag{5.21a}$$

$$\delta_e^T = \delta_e^b + \delta_e^m = \frac{r_1^2\sin\phi_e}{2\lambda^2 D}M_e \mp \frac{2\lambda}{Et}\left(\frac{r_2^2}{r_1}\right)(\sin\phi_e)H_e + \delta_e^m \tag{5.21b}$$

In which, V_e^m and δ_e^m are meridional rotation and lateral displacement associated with membrane solution, respectively, that can be obtained for a particular loading case as demonstrated in the preceding chapter, while V_e^T and δ_e^T are of course the total edge deformations.

Edge redundants M_e and H_e can be determined by the application of appropriate boundary conditions at the shell edge. Various support conditions and approaches of evaluating M_e and H_e, which can be applicable to toroidal shells, have be provided by Zingoni (2018) for spherical shells.

For closed toroidal shells with meeting points of shells, the element at the junction of adjacent shell segments must be in equilibrium. That is, the difference between the M_e in the first and second shells will be zero for a particular edge and the difference between the H_e in the first and second shells will be H^m. The parameter H^m is the difference in the horizontal components of the membrane meridional forces at the meeting point of the two shells. That is

$$H^m = \left(N_\phi^m \cos\phi_e\right)_2 - \left(N_\phi^m \cos\phi_e\right)_1$$

This is, of course, zero if there is no slope discontinuity at the meeting point. Therefore, the edge redundants are obtained from the condition of continuity at a particular junction of the two shells:

$$\left(V_e^T\right)_1 = \left(V_e^T\right)_2$$

$$\left(\delta_e^T\right)_1 = \left(\delta_e^T\right)_2$$

That is,

$$\left(V_e^b + V_e^m\right)_1 = \left(V_e^b + V_e^m\right)_2 \tag{5.22a}$$

$$\left(\delta_e^b + \delta_e^m\right)_1 = \left(\delta_e^b + \delta_e^m\right)_2 \tag{5.22b}$$

where the subscripts 1 and 2 represent the first and second adjacent shells at the particular edge under consideration.

5.1.5 Bending-related edge effects

With M_e and H_e now known, the bending-related interior actions follow from expressions (5.17a - d), which after superimposing the effects of M_e and H_e, and eliminating E and D, may be written as

$$N_\phi^b = e^{-\lambda\psi}\cot(\phi_e \mp \psi)\left\{\frac{2\lambda}{r_1}(\sin\lambda\psi)M_e \pm \sqrt{2}\left(\sin(\frac{\pi}{4} - \lambda\psi)\right)H_e\right\} \tag{5.23a}$$

$$N_\theta^b = \frac{r_2\, e^{-\lambda\psi}}{r_1}\left\{\frac{2\lambda^2}{r_1}(\cos\lambda\psi - \sin\lambda\psi)M_e \mp 2\lambda\,(\cos\lambda\psi)H_e\right\} \tag{5.23b}$$

$$M_\phi = e^{-\lambda\psi}\left\{(\cos\lambda\psi + \sin\lambda\psi)M_e \mp \frac{r_1}{\lambda}(\sin\lambda\psi)H_e\right\} \tag{5.23c}$$

$$M_\theta = \nu M_\phi \tag{5.23d}$$

5.2 Stresses due to bending disturbances

The bending stresses in the toroidal shell surfaces may be obtained from the usual relations

$$\sigma_\phi^b = \frac{N_\phi^b}{t} \pm \frac{6M_\phi}{t^2} \tag{5.24a}$$

$$\sigma_\theta^b = \frac{N_\theta^b}{t} \pm \frac{6M_\theta}{t^2} \tag{5.24b}$$

where now, the upper and lower signs $(\pm)$ associated with the M_ϕ and M_θ terms refer to the inner and outer surfaces of the of the outer regions of the toroidal vessel, respectively. The reverse of this is the case for the inner regions of the toroidal shell.

5.3 Total stresses in toroidal shells

The total stresses in the toroidal shell, maximum on the inner and outer fibres of the surfaces of the shell, are obtained by simply superimposing the membrane stresses σ_{ϕ}^{m} and σ_{θ}^{m} (as obtained in Chapter 4) with the bending-related actions from:

$$\sigma_{\phi}^{T} = \sigma_{\phi}^{m} + \sigma_{\phi}^{b} = \frac{N_{\phi}^{m}}{t} + \frac{N_{\phi}^{b}}{t} \pm \frac{6M_{\phi}}{t^{2}} \tag{5.25a}$$

$$\sigma_{\theta}^{T} = \sigma_{\theta}^{m} + \sigma_{\theta}^{b} = \frac{N_{\theta}^{m}}{t} + \frac{N_{\theta}^{b}}{t} \pm \frac{6M_{\theta}}{t^{2}} \tag{5.25b}$$

It will be noted here that, in the regions of the toroidal shells of revolution, where the membrane-hypothesis solution is valid, σ_{ϕ}^{b} and σ_{θ}^{b} will be negligibly small in comparison with the σ_{ϕ}^{m} and σ_{θ}^{m}, respectively.

5.4 Application of the developed approach and validation of results

In this section, the preceding analytical method is used for the analysis of the three novel toroidal configurations that were introduced in Chapter 3: parabolic ogival toroidal vessels, toroidal tanks of semi-circular and semi-elliptic cross-section, and multi-segmented toroidal pressure vessels. The membrane solutions for these vessels have been given in that chapter, but the solutions breakdown at some certain locations within the vessels. These errors are corrected with the present bending-solution approach, which is used to estimate the internal actions at those locations in the shells. In most of the cases considered, the bending and membrane results are superimposed to obtain the total internal actions in the loaded toroidal vessels.

For each of the numerical examples, the commercial finite element program Abaqus is used to validate the results obtained from the proposed analytical formulation, and some important insights generated about vessels are reported. In the numerical modelling of each of the toroidal vessels, a 3-node quadratic axisymmetric shell element (SAX2) was adopted. This element uses a consistent mass matrix and two-point integration of a quadratic interpolation function for the stiffness, and three-point integration of a quadratic interpolation function for the distribution of loads. All integrations are done with the Gauss method in the Abaqus

calculations (Abaqus 2014). For the type of problems in question (axisymmetric geometry and loading conditions), SAX2 is more efficient than a general 3-D element with more degrees of freedom. For each of the cases, an appropriate mesh density was implemented from a preliminary study of mesh convergence. The internal actions of interest in the meridional and hoop directions (S11 and S22 on the bottom and top points in the shells) are plotted against the meridional distance (arc length) from a specified location of the required span within the vessel.

5.4.1 Total stresses in toroidal vessels of parabolic ogival cross-section

5.4.1.1 Numerical example

The novel parabolic ogival toroidal vessel proposed in Section 4.4.3 where the membrane solutions were derived, is revisited here. This time the focus is to apply the membrane solution and approximate bending solution obtained in Section 5.6, to determine completely the numerical stress results in the entire surface of the vessel under the action of uniform internal pressure. The ogival shell is assumed to be fabricated from steel plate of constant thickness $t = 0.05m$ throughout, Young modulus $E = 210\times10^{9}\,N/m^{2}$, and the Poisson ratio υ of the steel is 0.3. Figure 5.3 shows the geometrical parameters of the vessel: $A = 7.5m$, $d = 10.0m$ and $h = 20.0m$. The toroidal vessel is symmetrical about the equatorial plane, and is assumed to be axisymmetrically loaded with uniform pressure $p = 1\times10^{6}\,N/m^{2}$ on the inner surface of the shell. Since the self-weight of the vessel is also neglected, no support conditions are specified.

The analysis of the pressurised vessel is conducted with the developed analytical method and the use of the commercial finite element tool. For ease of comparison, the obtained stress results from each of the two methods are plotted against the coordinate distance s. Note that s is the cumulative distance travelled clockwise to any point on the surface of the toroid from the apex round the curved meridional plane of the local cross-section of the vessel, (see Figure 5.3). This may be obtained numerically from the usual expression for the arc length of a curve

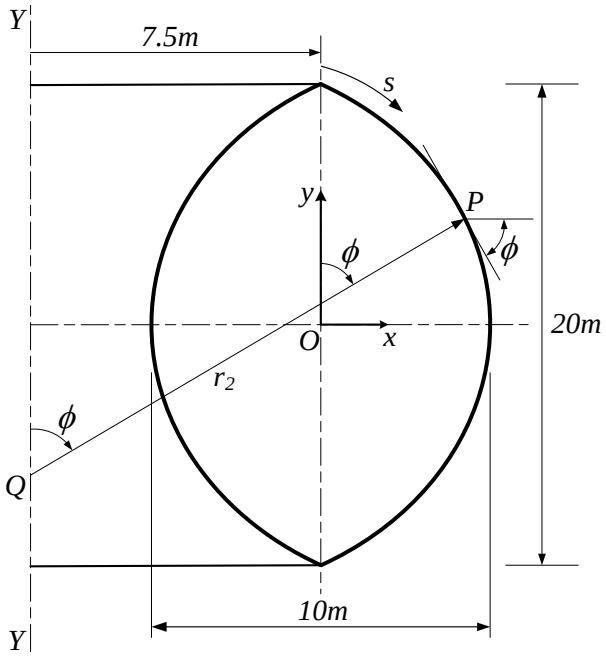

Figure 5.3. Parameters in the right-hand section of the ogival toroid

$$s = \int_{\phi_1}^{\phi_2} \left\{ \sqrt{\left(\frac{dx}{d\phi}\right)^2 + \left(\frac{dy}{d\phi}\right)^2} \right\} d\phi$$

where x and y have been defined in Section 4.4.3 as

$$x = \pm \frac{4d^2 \sin^2\phi - h^2 \cos^2\phi}{8d \sin^2\phi}$$

$$y = \pm \frac{h}{\sqrt{2d}} \sqrt{\frac{d}{2} - x}$$

and at the upper and lower poles of the ogival vessel,

$$\phi_o = \pi - \bar{\phi}_o = \tan^{-1}\left(\frac{h}{2d}\right)$$

In the analytical method, the membrane stress resultant results in the meridional and hoop directions of the parabolic ogival vessel are computed by inputting the given loading and geometrical parameters into the respective expressions (4.37a & b). Similarly, the membrane

deformations V_e^m and δ_e^m at the upper and lower poles of the ogival vessel (ϕ $(=\phi_o)$), where outer and inner segments of the vessel meet are also computed from expressions (4.37c & d). Note that:

at the upper edge of the outer region of the vessel,

$$\phi \ = \phi_o \ = \phi_e \ = \tan^{-1}\left(\frac{h}{2d}\right) = \frac{\pi}{4}$$

$$r_1 = \frac{h^2}{4d\sin^3\phi} = 28.2843m$$

$$r_2 = \frac{A+x}{\sin\phi} = \frac{A}{\sin\phi} + \frac{4d^2\sin^2\phi - h^2\cos^2\phi}{8d\sin^3\phi} = 10.6066m$$

$$\lambda = \left\{3\left(1-\upsilon^2\right)\frac{r_1^4}{r_2^2t^2}\right\}^{1/4} = 49.9244$$

$V_e^m = -1.063\times10^{-3}$; and $\delta_e^m = 7.5761\times10^{-3}m$

at the lower edge of the outer region of the vessel,

$$\phi \ = \bar{\phi}_o \ = \phi_e \ = \pi - \tan^{-1}\left(\frac{h}{2d}\right) = \pi\left(1-\frac{1}{4}\right)$$

$$r_1 = \frac{h^2}{4d\sin^3\phi} = 28.2843m$$

$$r_2 = \frac{A+x}{\sin\phi} = \frac{A}{\sin\phi} + \frac{4d^2\sin^2\phi - h^2\cos^2\phi}{8d\sin^3\phi} = 10.6066m$$

$$\lambda = \left\{3\left(1-\upsilon^2\right)\frac{r_1^4}{r_2^2t^2}\right\}^{1/4} = 49.9244$$

$V_e^m = 1.063\times10^{-3}$; and $\delta_e^m = 7.5761\times10^{-3}m$

at the lower edge of the inner region of the vessel,

$$\phi \;= \phi_o \;= \phi_e \;= \tan^{-1}\left(\frac{h}{2d}\right) = \frac{\pi}{4}$$

$$r_1 = -\frac{h^2}{4d\sin^3\phi} = -28.2843m$$

$$r_2 = \frac{A-x}{\sin\phi} = \frac{A}{\sin\phi} - \frac{4d^2\sin^2\phi - h^2\cos^2\phi}{8d\sin^3\phi} = 10.6066m$$

$$\lambda = \left\{3\left(1-\upsilon^2\right)\frac{r_1^4}{r_2^2 t^2}\right\}^{1/4} = 49.9244$$

$V_e^m = 2.8001\times10^{-3}$; and $\delta_e^m = -7.5761\times10^{-3}m$

and, at the upper edge of the outer region of the vessel,

$$\phi \;= \bar{\phi}_o \;= \phi_e \;= \pi - \tan^{-1}\left(\frac{h}{2d}\right) = \pi\left(1-\frac{1}{4}\right)$$

$$r_1 = -\frac{h^2}{4d\sin^3\phi} = -28.2843m$$

$$r_2 = \frac{A-x}{\sin\phi} = \frac{A}{\sin\phi} - \frac{4d^2\sin^2\phi - h^2\cos^2\phi}{8d\sin^3\phi} = 10.6066m$$

$$\lambda = \left\{3\left(1-\upsilon^2\right)\frac{r_1^4}{r_2^2 t^2}\right\}^{1/4} = 49.9244$$

$V_e^m = -2.8001\times10^{-3}$; and $\delta_e^m = -7.5761\times10^{-3}m$

In which, of course each of the values of r_2 and λ is the same at both the upper and lower edges of the segments. These results can then be used in expressions (5.21) to estimate Edge redundants M_e and H_e in the following way.

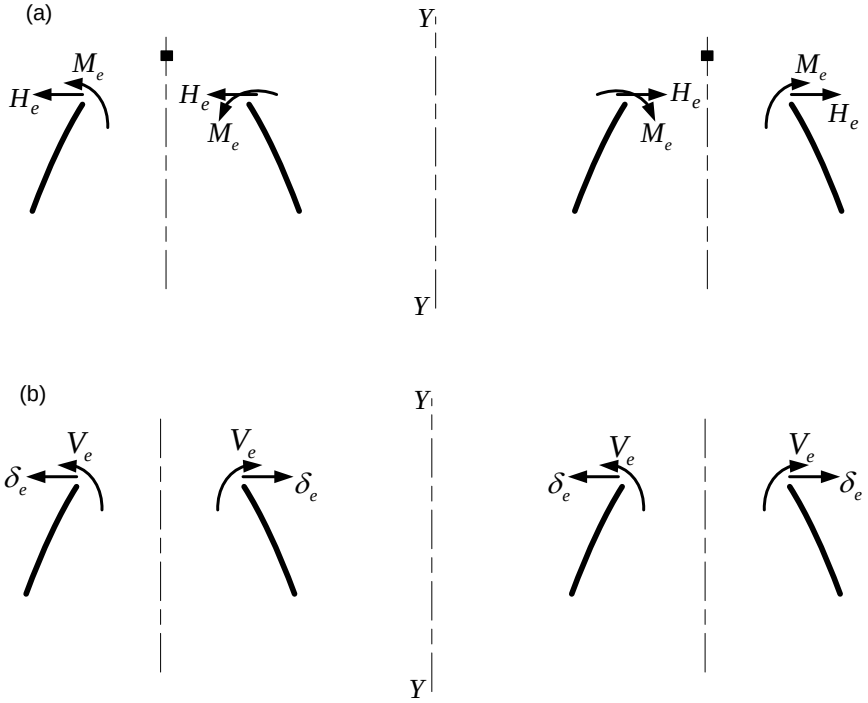

Figure 5.4. Edge actions and deformations at the top edge of the ogival toroid: (a) Horizontal shear force and bending moments; (b) horizontal displacement and meridional rotations

Because the parabolic ogival section in question is symmetrically both about the equatorial plane and the local axis of revolution, and the toroidal vessel is loaded uniformly and axisymmetrically, we focus on one of the edges (knowing that the effects at one edge will be the same at the other edge). Furthermore, for the symmetric nature of the problem, the element at the meeting point of the outer and inner segments of the vessel will not rotation nor displace laterally, acts as if it were fixed (see Figure 5.4). Consequently, the boundary conditions at each of edges correspond to

$$\left(V_e^T\right)_1 = \left(V_e^T\right)_2 = 0$$

$$\left(\delta_e^T\right)_1 = \left(\delta_e^T\right)_2 = 0$$

When these are used in expressions (5.21) with the computed values of the appropriate membrane deformations V_e^m and δ_e^m, the following numerical values are obtained:

$M_e = -5.658\times10^4\, Nm/m$; and $H_e = 1.837\times10^5\, N/m$

for the upper outer edge, and

$M_e = 1.374 \times 10^5 \, Nm/m$; and $H_e = 5.2668 \times 10^5 \, N/m$

for the lower inner edge. With redundants M_e and H_e now known, and subsequently substituted in the bending related effects of expressions (5.23), the total stresses in outermost and innermost fibres of the toroidal vessel are therefore obtained from expressions (5.25) for the entire vessel. These are plotted against $s(m)$ in Figures 5.5a and 5.6a below. The present geometric, material, loading and boundary parameters of the parabolic ogival vessel are idealised in the finite element tool in line with the modelling description given above. The obtained meridional and hoop stress results are shown in Figures 5.5b and 5.6b, respectively.

5.4.1.2 Results and observations on the ogival vessel

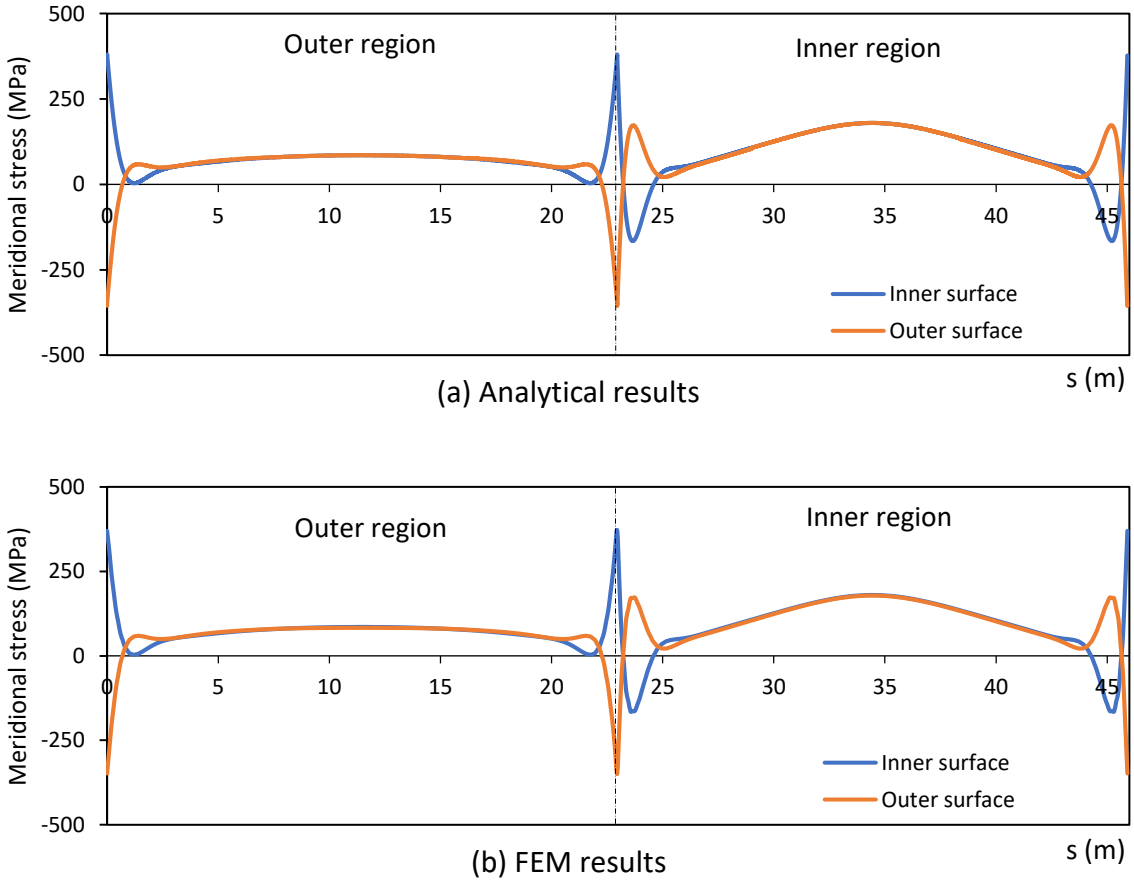

Figure 5.5. Total meridional stresses against arc length s in the pressurised ogival toroidal vessel: (a) analytical results, and (b) FEM results

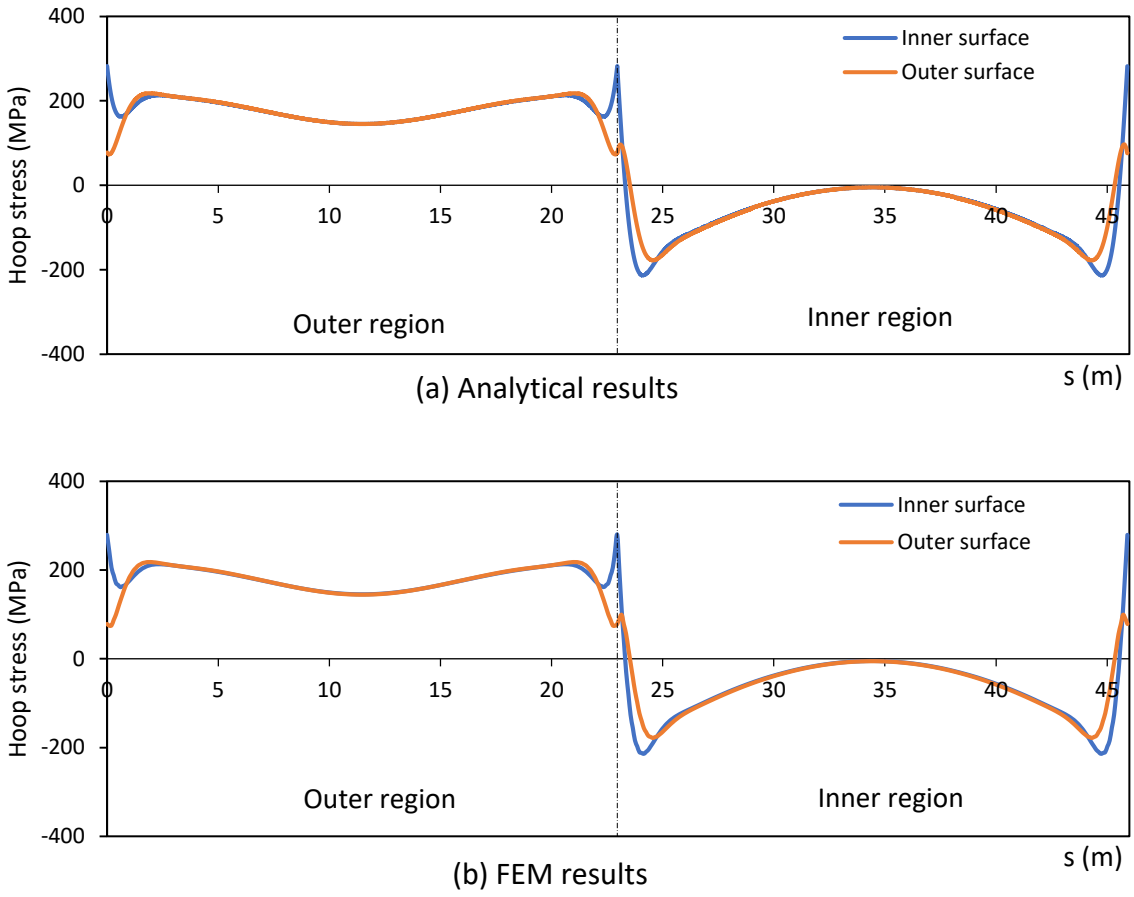

Figure 5.6. Total hoop stresses against arc length s in the pressurised ogival toroidal vessel: (a) analytical results; (b) FEM results.

Note that the results from FEM and analytical method are physically identical, and hence, are not put in the same plots. Each of the FEM-results plots (Figures 5.5b and 5.6b) for the meridional and hoop stresses is respectively placed directly below those from the proposed analytical method. The excellent agreement in the results obtained from the two methods with less than 3% discrepancy throughout the vessel, demonstrates that the proposed analytical approach is practically accurate for the determination of the state of stress and deformation in a pressurized parabolic ogival toroidal shell of revolution. The accuracy of the analytical method for the bending that occurs at the top and bottom zones of the parabolic ogival toroidal shell further demonstrates the validity of the adopted Geckeler approximation for anticlastic and synclastic neighbourhoods. The method was first shown to be a very promising approach for toroidal shells when it was adopted in the study of the bending around the equatorial zones of semi-elliptic toroids and provided excellent results (Zingoni et al., 2015).

In Figures 5.5 and 5.6, the bending-disturbance stresses rise sharply around the narrow zones of the shell junctions; and die out quickly as one moves away from the edges. Hence, the total meridional and hoop stresses in the outer and inner fibre of the vessel are nearly the same in the entire vessel, except in the localised regions of the meeting points of the outer and inner segments of the toroidal vessel. This indicates that the bending disturbances within the shell in zones away from the junctions are negligibly small in comparison with the membrane stresses in these zones. Hence, the membrane results may be conveniently abducted for estimating the state of stress in these interior zones for the ogival toroidal shell.

Although pressurised internally, a part of the vessel (the inner segment) experiences compressive hoop stresses, unlike the conventional toroidal shell of a circular cross session which experiences tensile stresses throughout when internally loaded with uniform pressure, as previously suggested in Chapter 4. Thus, there is a likelihood of local buckling in the inner segment of the ogival vessel. The stability behaviour of the present vessel will be investigated in Chapter 7 of this thesis.

5.4.1.3 Parametric results of the ogival vessel

In the above results, as expected owing to the symmetricity of loading and geometrical configuration of the investigated pressure vessel, the bending disturbances noticed around the top and bottom meeting points of the outer and inner segments of the vessel are symmetrical about the equatorial plane. Hence, the bending stresses obtained from parametric studies into ogival toroidal vessels are only shown for the junction at the apex of the shells in the following. The effect of changes in the opening ratio on the distribution of membrane stress resultants has been examined in Chapter 4 on the basis of membrane hypothesis. Now, the bending stresses that occur within the edge zones are obtained for the various mean toroidal radius A to local width d ratios, various mean toroidal radius A to shell thickness t ratios, and various height h to local width d ratios. This is achieved by first calculating the redundants M_e and H_e at the edges for each of the cases, in the usual way as demonstrated in the above numerical example. A justifiable means of comparison is adopted by plotting the bending results versus percentage distances from the joint at the apex to the joint at the nadir of the toroidal vessel, along the outer region (or the inner region depending on the segment of interest). Also, for the purpose of simplifying the plots, the presented results for the zones of interest are restricted to σ_ϕ^b in the inner surface of the parabolic ogival vessels only.

5.4.1.3.1 Influence of toroidal opening ratios on the edge effects

Here, the changes in the bending stresses that occur around the edge zones of parabolic ogival toroidal vessels are studied by varying the mean toroidal radius A to local width d ratios (A/d). The material, loading and geometric parameters adopted are the same as those in the example above, except that the values of A are varied (while keeping the value of d constant) in accordance with the A/d values as shown in the plots of Figures 5.7, where the bending stresses σ_{ϕ}^{b} in the inner surface of the toroids are given for the outer and inner regions, respectively.

It can be seen in Figures 5.7 that the bending that occurs at the edge zones of the outer and inner regions of the ogival vessels generally increases as A/d increases. Higher bending disturbances are observed in the inner region (with negative Gaussian curvature) of the vessels around the edge zones in comparison with those at the corresponding outer region (with positive Gaussian curvature) of the vessel, even though the bending stress values and of course, the adopted simplified damping parameters λ are the same at the edges.

5.4.1.3.2 Influence of shell thickness on edge effects

The changes in the bending stresses that occur around the edge zones of parabolic ogival toroidal vessels are studied by varying the thickness t of the vessel in relative to the mean toroidal radius A. Also, in this investigation, the material, loading and geometric parameters adopted are the same as those in the numerical example above, except t which assumed values from A/t (= 20, 50, 100, 200, and 500) correspondingly as shown in Figures 5.8, where the bending stresses σ_{ϕ}^{b} in the inner surface of the toroids are given for the outer and inner regions, respectively.

It can be seen in Figures 5.8 that the bending that occurs at the edge zones of the outer and inner regions of the ogival vessels generally increases as A/t increases. This is clearer in the plots of Figures 5.8(b) for the bending stresses around the top-inner edge regions. Just as obtained in the study of the effects of changes in opening ratios above, higher bending disturbances are observed in the inner region (with negative Gaussian curvature) of the vessels around the edge zones in comparison with those at the corresponding outer region (with positive Gaussian curvature) of the vessel, even though the bending stress values and of course,

the adopted simplified damping parameters λ are the same at the edges of each of the present vessels.

5.4.1.3.3 Influence of height to local cross-sectional width ratios on edge effects

Lastly, the changes in the bending stresses that occur around the edge zones of parabolic ogival toroidal vessels are studied by varying the height h of the vessel relative to the local cross-sectional width d. Again, the material, loading and geometric parameters adopted are the same as those in the numerical example above, except that the values of h are varied (while keeping the values of d constant) in accordance with the h/d values as shown in the plots of Figures 5.9, where the bending stresses σ_{ϕ}^{b} in the inner surface of the toroids are given for the outer and inner regions, respectively.

It can also be seen in Figures 5.9 that the bending stresses at the edges of the outer and inner regions of the vessel decrease as h/d increases. A similar occurrence is observed for the bending disturbances in the edge zones of the outer region of the vessels, but the reverse is the case in the edge zones at the inner region of the vessels, where an increase in h/d is seen to cause an increase in bending disturbances in a very gentle manner.

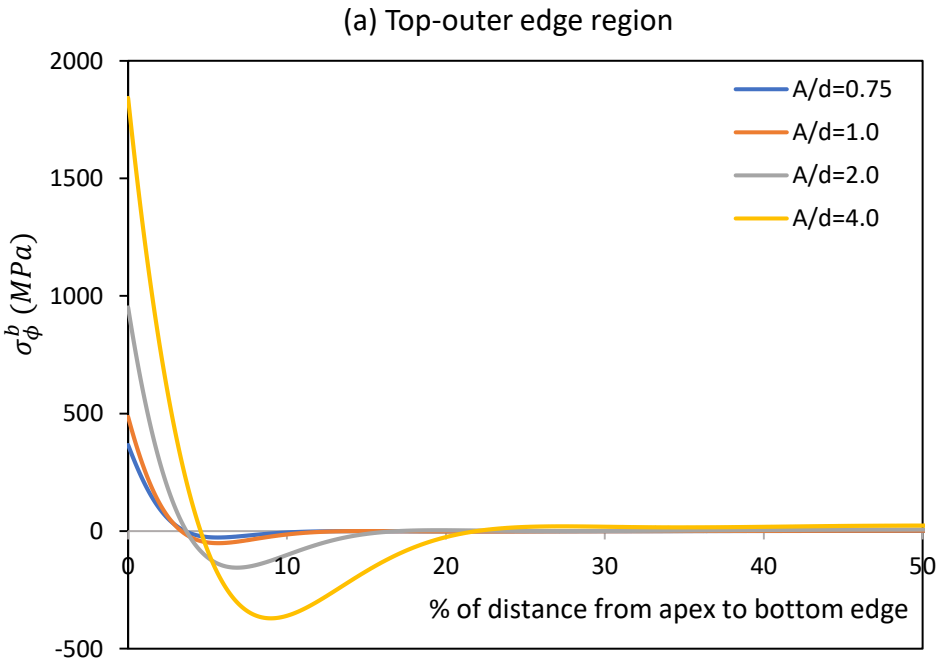

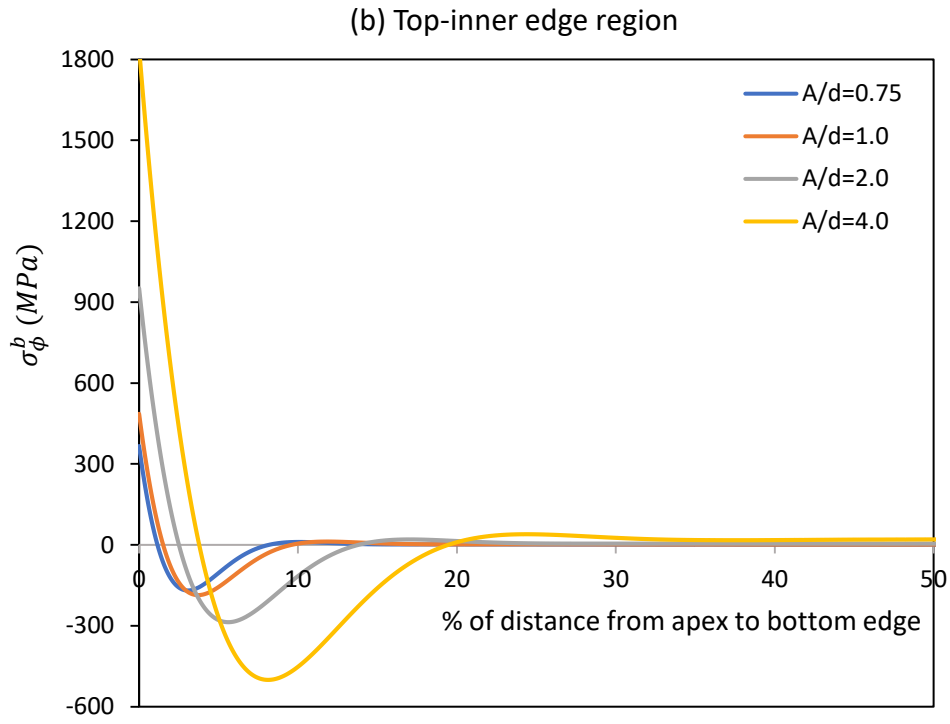

Figure 5.7. Inner fibre bending stresses around the top edge for various opening ratios: (a) inner region; (b) outer region of the ogival vessel.

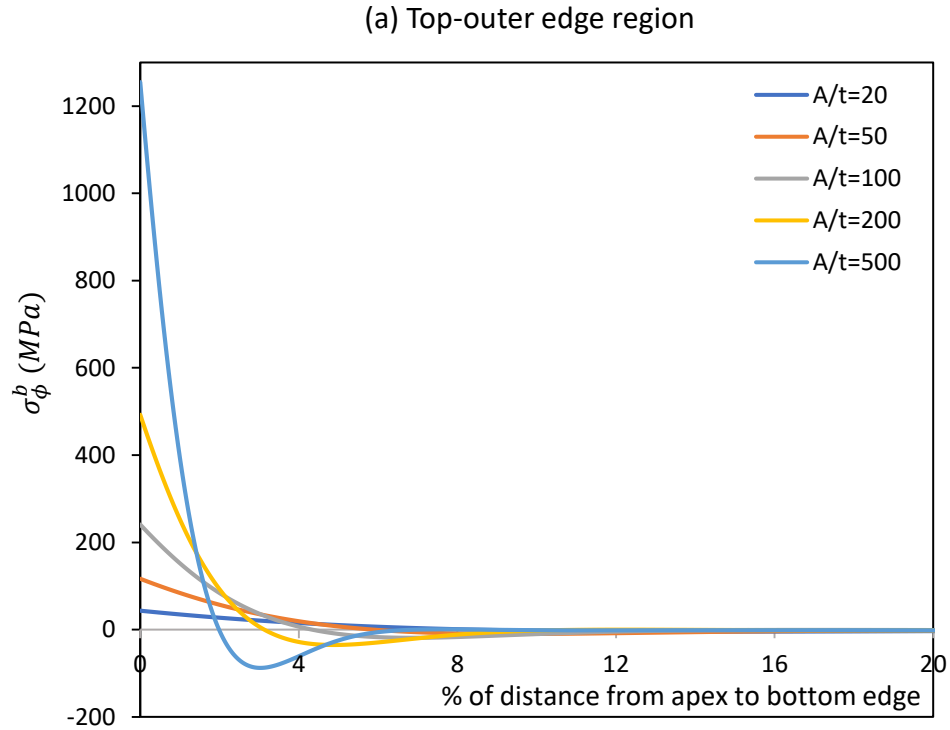

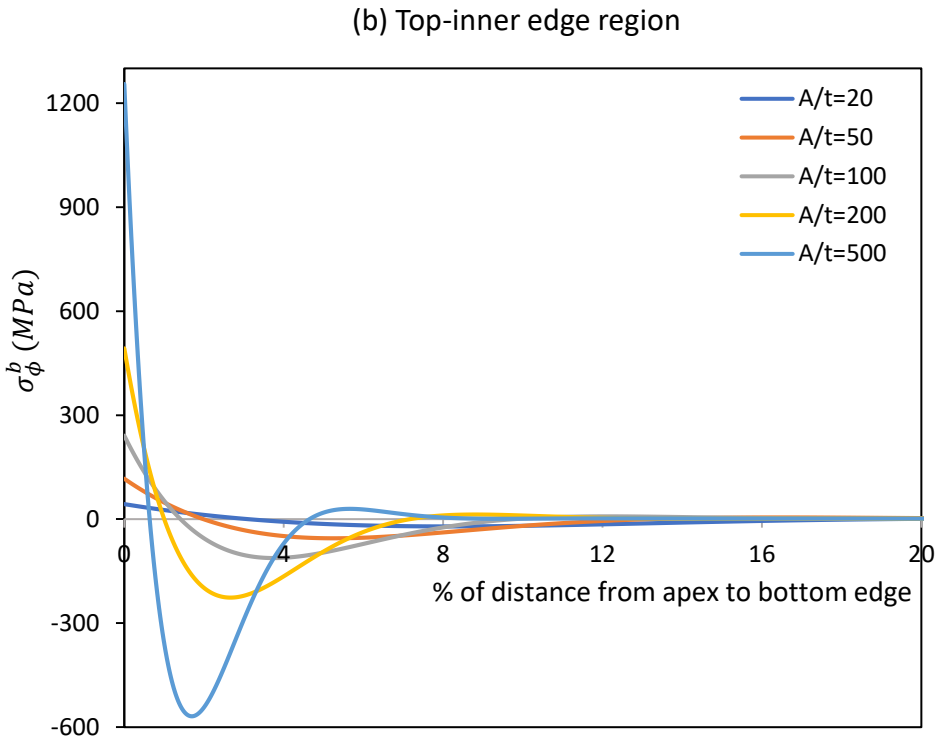

Figure 5.8. Inner fibre bending stresses around the top edge for various shell thickness: (a) inner region; (b) outer region of the ogival vessel

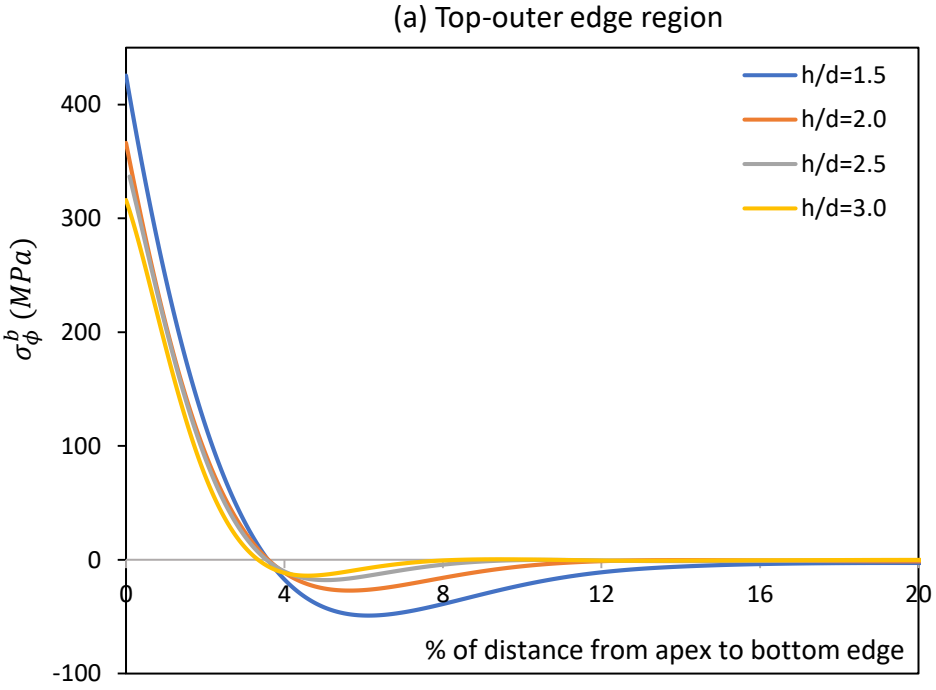

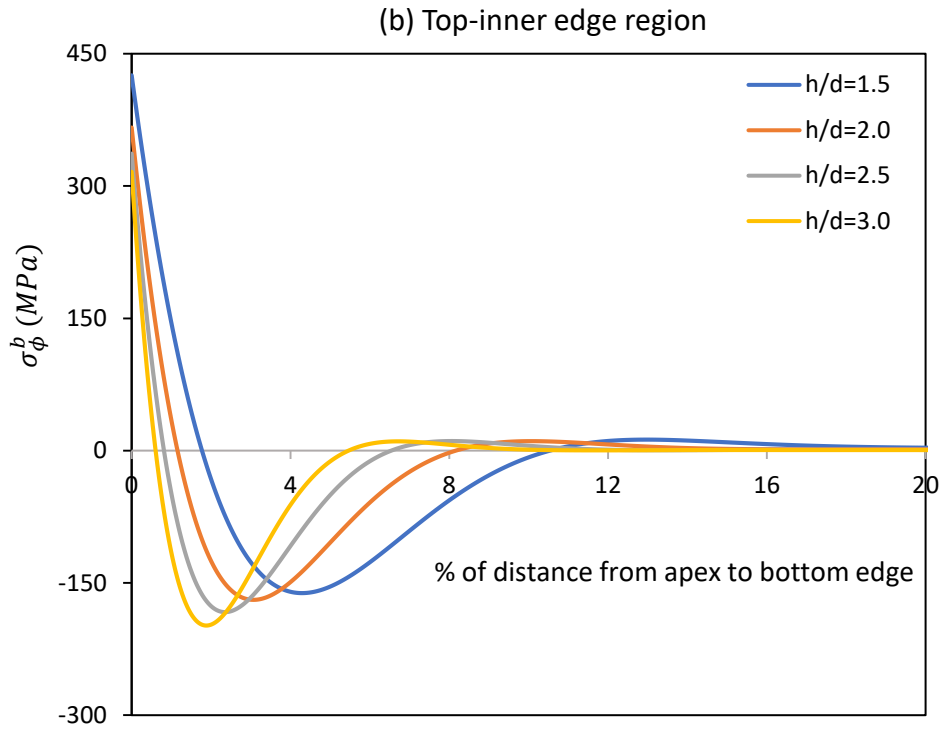

Figure 5.9. Inner fibre bending stresses around the top edge for various local height-to-width ratios: (a) inner region; (b) outer region of the ogival vessel.

Therefore, from the parametric studies, one may conclude that the bending effects at the top and bottom edge zones of a parabolic ogival toroid under uniform pressure is greatly influenced by the toroidal geometric parameters. The bending disturbance stresses increase as each of A/d and A/t increases, but decrease as h/d increases. Although the magnitude of the bending stresses in the meeting point of the outer and inner edges are the same, the bending disturbance stresses observed after that point are generally larger in the inner edge region of the pressurised vessel.

5.4.2 Edge-zone stresses in a complete toroidal tank of circular-elliptic compound cross-section

5.4.2.1 Introduction

In this numerical example, the total stresses in the junction regions of semi-circular and semi-elliptic segments of a toroidal tank are computed using the formulated analytical method. The obtained results are compared with those from the finite element programme. The toroidal tank under investigation has been analysed in Chapter 4 with the membrane theory, which shows

some discontinuities in the values of the hoop stresses at the meeting junctions of the top semi-circular and the bottom semi-elliptic segments of the toroidal tank, owing to the abrupt change in local meridional radius of curvature at the junctions as one moves from one segment to the other, even though the segments are tangentially joined together. Hence, the need to calculate the actual state of stress in the bending disturbance zones of the tank. The geometrical configuration of the vessel is shown in Figure 5.10, where $A = 22m$, $a = 10m$, $b = 20m$, and $t = 0.05m$. The tank is not symmetrical about the equatorial plane of the vessel, but it is assumed to be axisymmetrically supported in the lower region of the elliptic toroidal segment of the vessel, so that the edge effects at the support locations do not significantly interfere with the stress results around the meeting edges of the top and bottom segments of the toroidal tank. It is assumed that the vessel is of uniform thickness throughout, and is filled with water of unit weight $\gamma = 10 \times 10^3 N/m^3$.

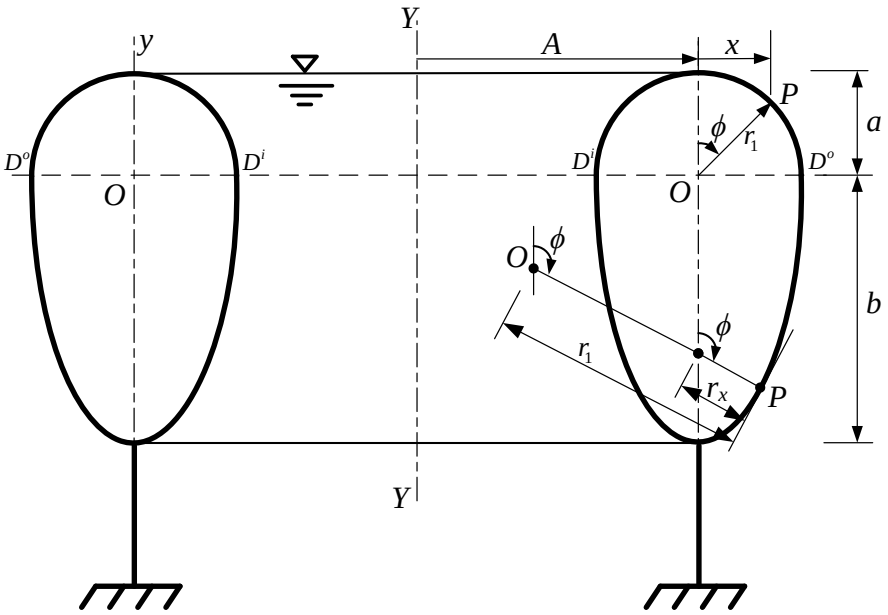

Figure 5.10. Hydrostatically loaded circular-elliptic toroidal tank.

The following material properties of the steel tank is also assumed:

$E = 210 \times 10^9 N/m^2$

$\upsilon = 0.3$

5.4.2.2 The analytical approach and FEM

In the analytical approach, Mathematica 10.0 (Wolfram Research ..., 2014) is employed for the computation of the stresses. The formulated algorithm for ultimately estimating the net stresses at the outer and inner surfaces of a shell of revolution as presented above in this chapter is cast in Mathematica 10.0 for the present problem. The meridional and hoop stresses around the meeting points of the two segments of the toroidal tank, numerically calculated with the tool are plotted against the meridional distance s (measured clockwise around the local cross session from the apex of the tank), are shown in Figures 5.12(a)-5.15(a), where the dotted vertical line denotes the meeting point (junction) of the circular and elliptic segments of the toroidal tank. s is calculated from

$$s = \int_{t_{\phi_1}}^{t_{\phi_2}} \left(\sqrt{a^2 \cos^2 t_\phi + b^2 \sin^2 t_\phi} \right) dt_\phi$$

where the parameter t_ϕ is related to ϕ by

$$t_\phi = \tan^{-1}\left[\frac{b}{a} \tan\phi \right]$$

Note that $b = a$ within the top semi-circular segment of the tank, and the following edge actions and deformation are obtained (see Figure 5.11):

at the outer edge: $V_e^m = -9.7524 \times 10^{-4}$; $\delta_e^m = 7.6231 \times 10^{-3} m$ for the circular side

$V_e^m = -9.7524 \times 10^{-4}$; $\delta_e^m = 9.0832 \times 10^{-3} m$ for the elliptic side

$M_e = 0$; and $H_e = -3.680 \times 10^3 N/m$ are the edge redundant

at the outer edge: $V_e^m = 1.3714 \times 10^{-4}$; $\delta_e^m = -1.1096 \times 10^{-3} m$ for the circular side

$V_e^m = 1.3714 \times 10^{-4}$; $\delta_e^m = -1.3714 \times 10^{-3} m$ for the elliptic side

$M_e = 0$; and $H_e = -2.880 \times 10^3 N/m$ are the edge redundant

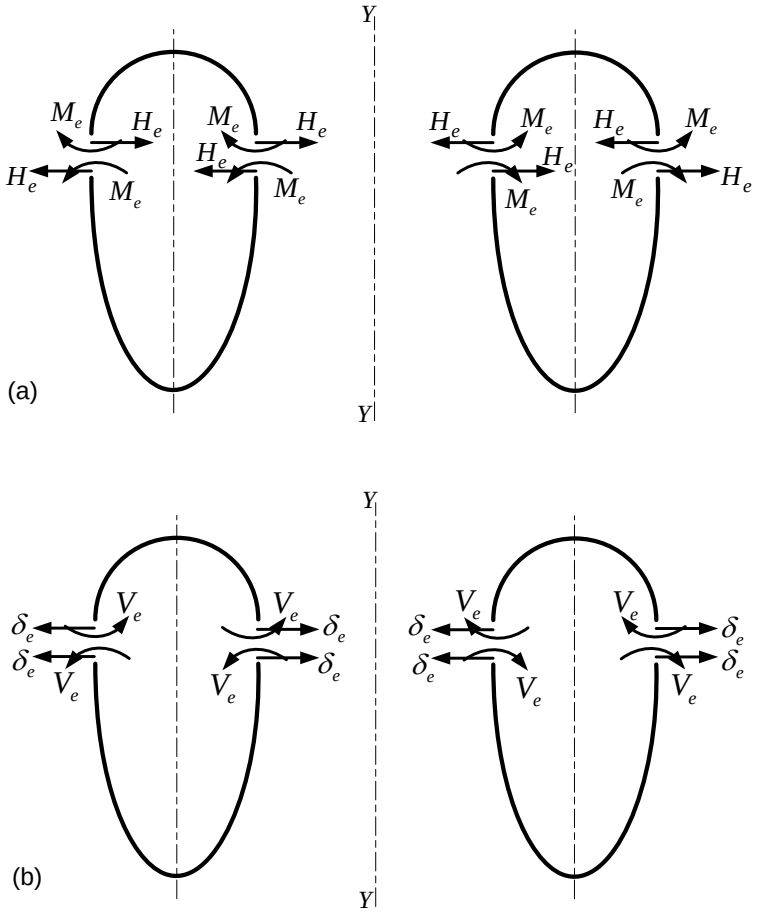

Figure 5.11. Edge actions at the outer and inner regions of the toroid: (a) redundants; and (b) deformations

In the finite element programme, the modelling approach as given above is adopted for the present problem of the circular-elliptic toroidal tank. The model was axisymmetrically supported by restraining the translational movement of the lowest circle of latitude of the bottom semi-elliptic segment of the tank. This was to ensure that the internal actions in the meeting zones of interest in this investigation are negligibly affected by the support effects on the vessel. The FEM results are shown in Figure 5.12(b) for the meridional stresses around the meeting junction at the outer region of the tank, Figure 5.13(b) for the meridional stresses around the meeting junction at the inner region of the tank, Figure 5.14(b) for the hoop stresses around the meeting junction at the outer region of the tank, and Figure 5.15(b) for the hoop stresses around the meeting junction at the inner region of the tank. In each of the figures, the dotted vertical line denotes the meeting point (junction) of the circular and elliptic segments of the toroidal tank.

5.4.2.3 Summary of results

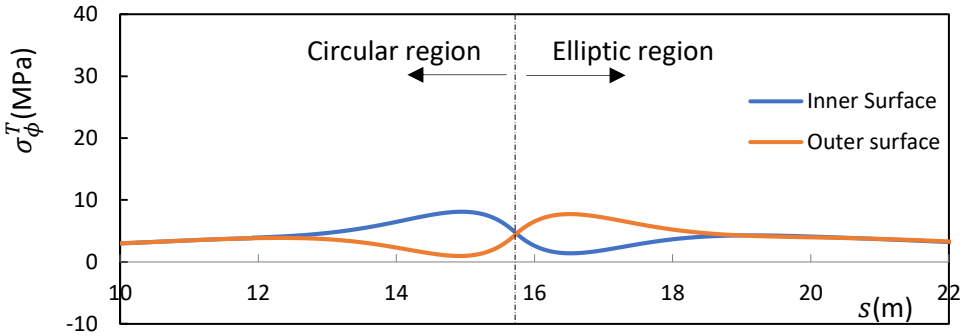

(a) Analytical results

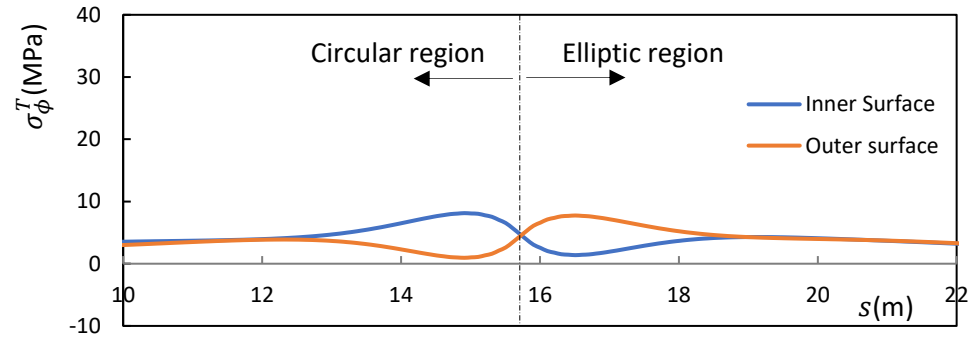

(b) FEM results

Figure 5.12. Meridional stresses at the outer junction versus distance from apex: (a) analytical results; (b) FEM results.

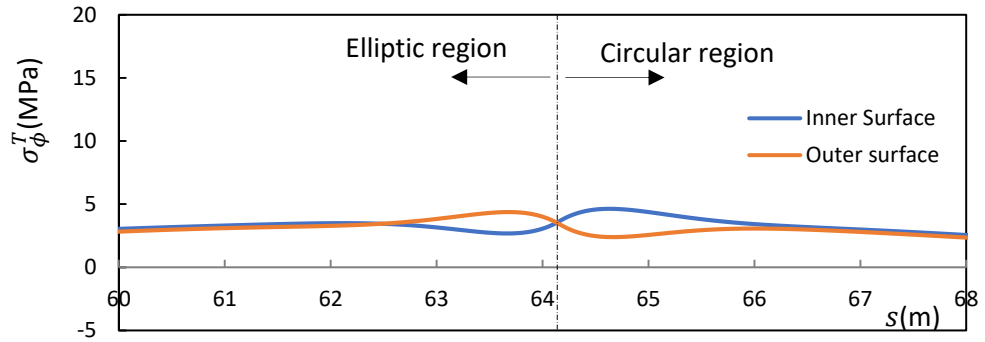

(a) Analytical results

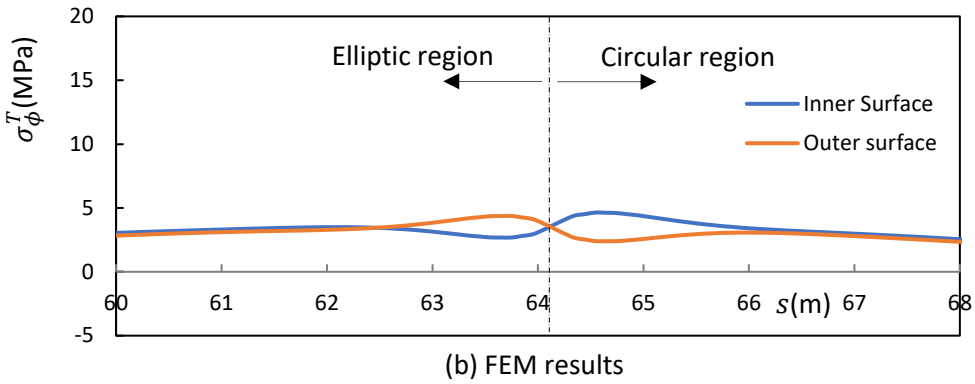

(b) FEM results

Figure 5.13. Meridional stresses at the inner junction versus distance from apex: (a) analytical results; (b) FEM results.

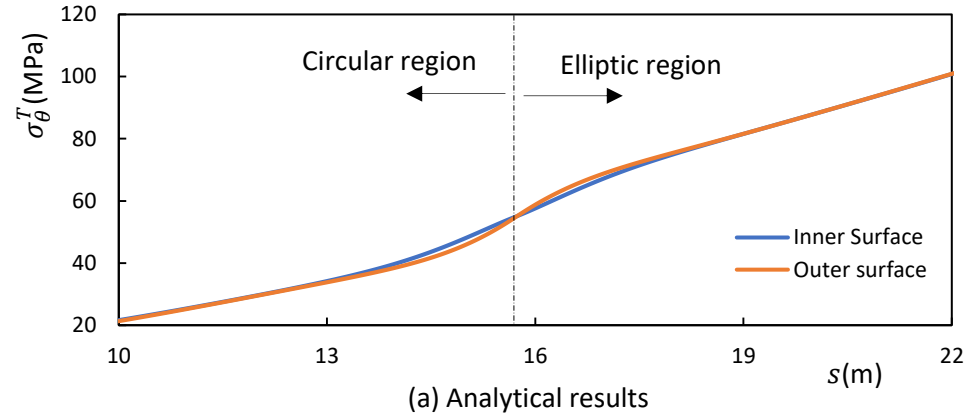

(a) Analytical results

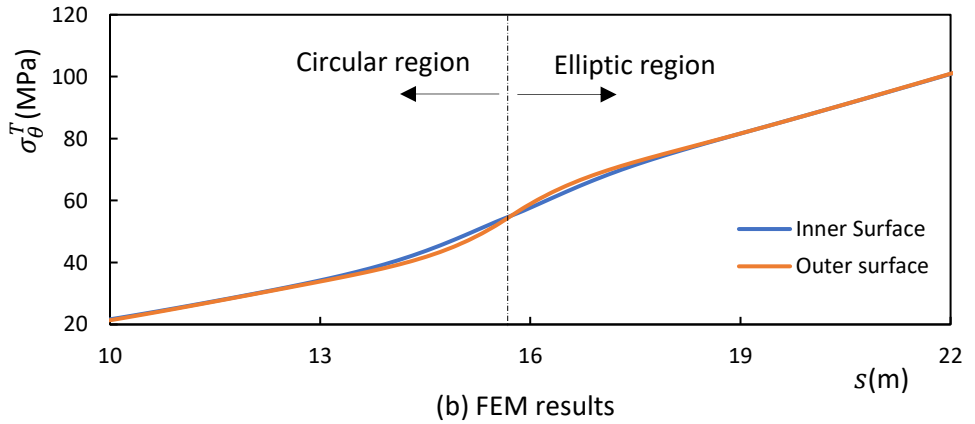

(b) FEM results

Figure 5.14. Hoop stresses at the outer junction versus distance from apex: (a) analytical results; (b) FEM results.

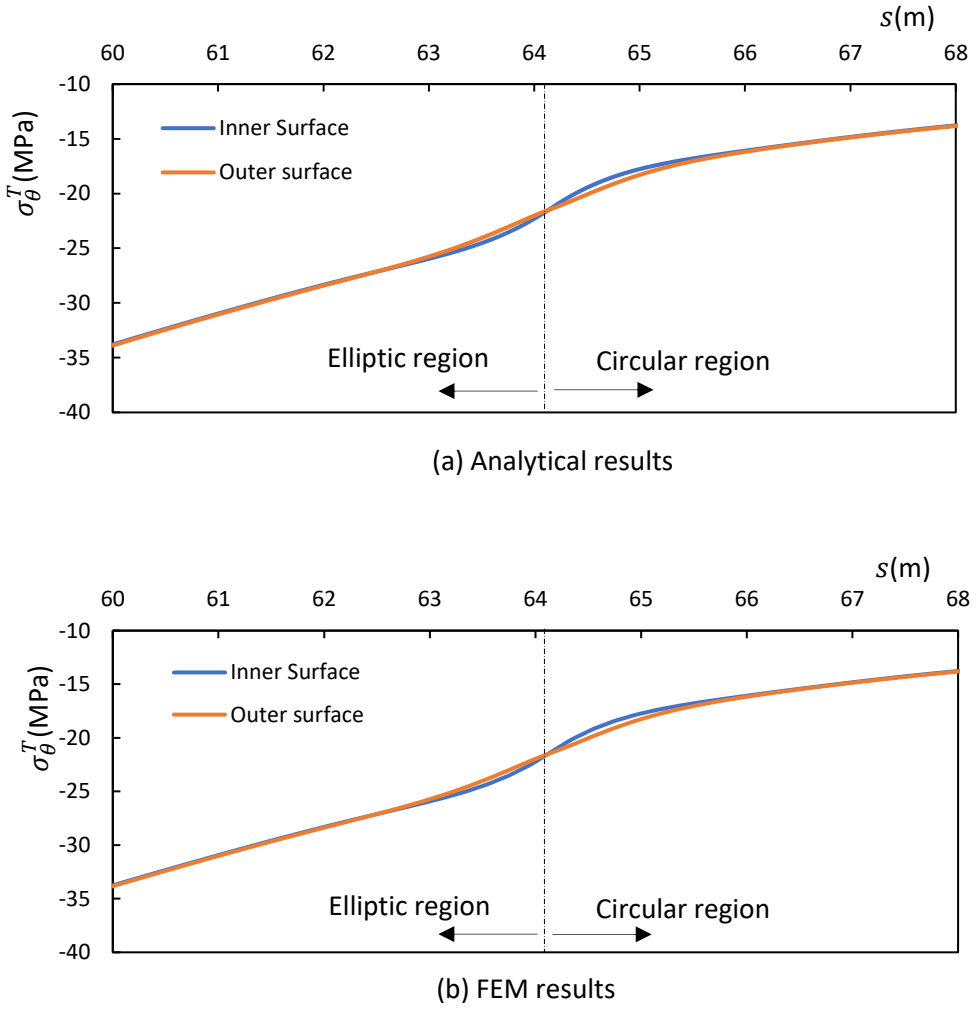

Figure 5.15. Hoop stresses at the inner junction versus distance from apex: (a) analytical results; (b) FEM results.

Again, it can be seen in Figures 5.12 – 5.15 that the agreement between the analytical and FEM results is excellent throughout with a discrepancy of about 3% in both the outer and the inner regions of the joining points of the segments of the toroidal tank. Hence, the each of the meridional and hoop stress results from the formulated analytical method and finite element modelling are not superimposed in the same plot but placed side-by-side as shown. One can, therefore, conclude that the proposed analytical method is very accurate and efficient in the determination of the state of stress around the edges of the toroidal tank.

It is however observed that, for the considered geometric configurations and loading parameter of the present toroidal tank, although there is a significant mismatch in each of the values of membrane hope stresses at the junctions obtained from the membrane-hypothesis results, the

total hoop stresses in the outer and inner fibres around the junctions are nearly the same. Also, due to the larger values of the local radius of curvature r_1 (and hence, λ) at the edges in both the outer and inner sides of the lower semi-elliptic segment, it is noted that the bending disturbances decay more quickly within this segment (even though the hydrostatic loading are higher in these regions of the tank) when compared with their corresponding values in the top semi-circular segment of the tank, where λ are smaller. This is more obvious in the plots for the meridional stresses versus s (Figures 5.12 and 5.13).

5.4.3 Stresses in multi-shell toroidal pressure vessels

5.4.3.1 The numerical example

Consider an extra-large internally pressurised toroidal vessel of four segments with a geometrical configuration that is symmetrical about the equatorial (middle) plane. This numerical example forms part of the work that has been published (Enoma & Zingoni, 2016). Half of the cross-section of the vessel is shown below in Figure 5.16, and the geometrical parameters have been described in Section 4.4.5 of this thesis, where the derivation of the membrane solution applied here was presented.

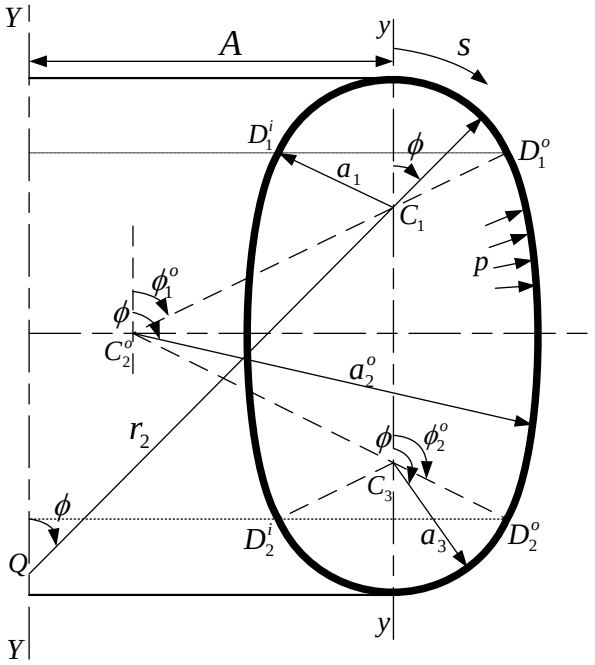

Figure 5.16. The right-half cross-section of the pressurised multi-shells toroid.

The vessel is assumed to be made from a steel plate of Young modulus $E = 200\times10^9 N/m^2$, Poisson ratio $\upsilon = 0.3$ and constant thickness $t = 0.05m$ throughout. The segmented vessel is of $A = 30.0m$, $a_1 = a_3 = 14.04m$, $a_2 = 30.0m$; $\phi_1 = 70^o$ and $\phi_2 = 110^o$ for the outer regions, and $\phi_1 = 110^o$ and $\phi_2 = 70^o$ for the inner regions of the toroid. The toroidal vessel is symmetrical about the equatorial plane and is assumed to be axisymmetrically loaded with uniform pressure $p = 1\times10^6 N/m^2$ on the inner surface of the shell. Since the self-weight of the vessel is also neglected, no support conditions are specified.

5.4.3.2 Solution approach

With these given numerical parameters, firstly, the membrane stress resultants N_ϕ^m and N_θ^m in meridional and hoop directions, respectively, in each of the segments of the inner and outer regions of the pressurized toroidal vessel are determined using appropriate expressions 4.58(a)-(b), 4.61(a)-(b) and 4.63(a)-(b). In a similar way, the membrane results are obtained for the lateral displacements δ_e^m and the meridian rotation about the tangent to the hoop V_e^m at all the edges of each of the segments in the outer and inner regions of the vessel using appropriate expressions 4.58(c)-(d), 4.61(c)-(d) and 4.63(c)-(d). These are used to obtain the equations their respective bending counterparts δ_e^b and V_e^b at each of the edges by invoking the continuity conditions of expressions (5.22). Then, using δ_e^b and V_e^b, the edge redundants M_e and H_e at each of the edges are calculated from expressions (5.21). However, we only present here the numerical values:

$M_e = -7.1515\times10^2 Nm/m$; and $H_e = -1.33\times10^5 N/m$ at the upper outer edge, and

$M_e = 2.20\times10^3 Nm/m$; and $H_e = -1.360\times10^5 N/m$ at the lower inner edge,

This is due to the symmetric nature of the present toroidal geometry and loading. The edge actions and deformations are similar to those in Figure 5.11. The computed edge redundants are used in expressions (5.23) to obtain the edge bending-related actions N_ϕ^b and N_θ^b, M_ϕ and M_θ in the vessel. These are finally superimposed with the membrane-solution effects to get total stresses in the multi-shell toroidal vessel using expressions (5.25).

The variations of the stresses with arc length s over the full cross-sectional profile of the segmented toroidal vessel are shown in Figures 5.17(a) - 5.20(a). As before, the arc length s is the cumulative distance measured clockwise from the apex round the local cross-sectional profile (to the right of the global axis $Y-Y$ of the vessel, for example), up to a point in question. The total arc length of the present vessel is about $110.5m$, but the ranges $8m \le s \le 48m$ and $64m \le s \le 102m$ for the outer and inner regions of the vessel, respectively, are covered by the plots. The restriction is applied because the Geckeler approximation is only valid for non-shallow thin shells of revolution, and cannot account for the bending that occurs in the vicinity of the top and bottom circles of latitude ($\phi = 0,\ \pi$), where the surfaces of the positive and negative meet. The upper outer junction D_1^o, lower outer junction D_2^o, lower inner junction D_2^i, and upper inner junction D_1^i, as well as the meeting segments of the vessel, are indicated in each of the figures.

The commercial finite element tool is used to validate the results obtained from the proposed analytical formulation. In the numerical modelling, the loading, material and geometrical parameters of the current problem are idealised in the programme as described above. The FEM results are shown in Figure 5.17(b) for the total meridional stresses versus arc length s over the outer regions the pressurised vessel, Figure 5.18(b) for the total hoop stresses versus arc length s over the outer regions the pressurised vessel, Figure 5.19(b) for the total meridional stresses versus arc length s over the inner regions the pressurised vessel, and Figure 5.20(b) for the total hoop stresses versus arc length s over the inner regions the pressurised toroidal vessel.

5.4.3.3 Numerical results and discussion

The results from the analytical method and FE modelling are seen to be physically identical. Hence those from the analytical method are placed just above the FEM results for each case. It is interesting to note again that the formulated method which is based on Geckeler's simplifications, is also very valid on the anticlastic side of the present toroidal vessel. The excellent accuracy obtained in this example further demonstrates that the proposed analytical method is an effective tool for estimating stresses in an axisymmetrically loaded toroidal shell of revolution.

As expected, the bending-disturbance stresses at the upper and lower edges of the outer region, as well as those at the inner region of the vessel, are similar because the vessel is symmetrical about the equatorial (middle) plane and is subjected to uniform pressure. These stresses, which are of greater magnitude around the edge zones, die out quickly as one moves away from the edges. To cater for the localized bending-disturbance stresses on either side of the edge, stepwise local thickening of the shell should be adopted in a narrow band around the edges.

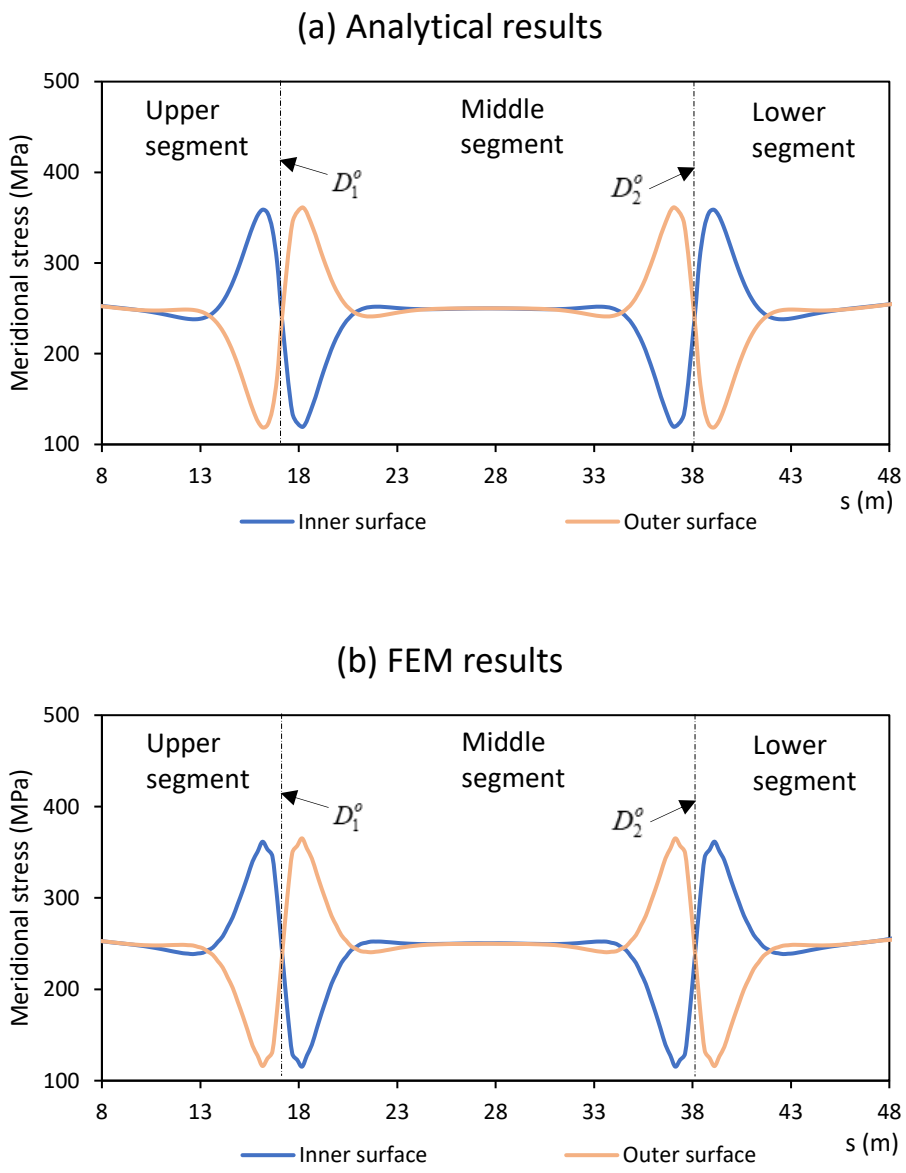

Figure 5.17. The variations of meridional stresses with arc length s over the outer regions of the pressurised toroidal vessel: (a) analytical results; (b) FEM results.

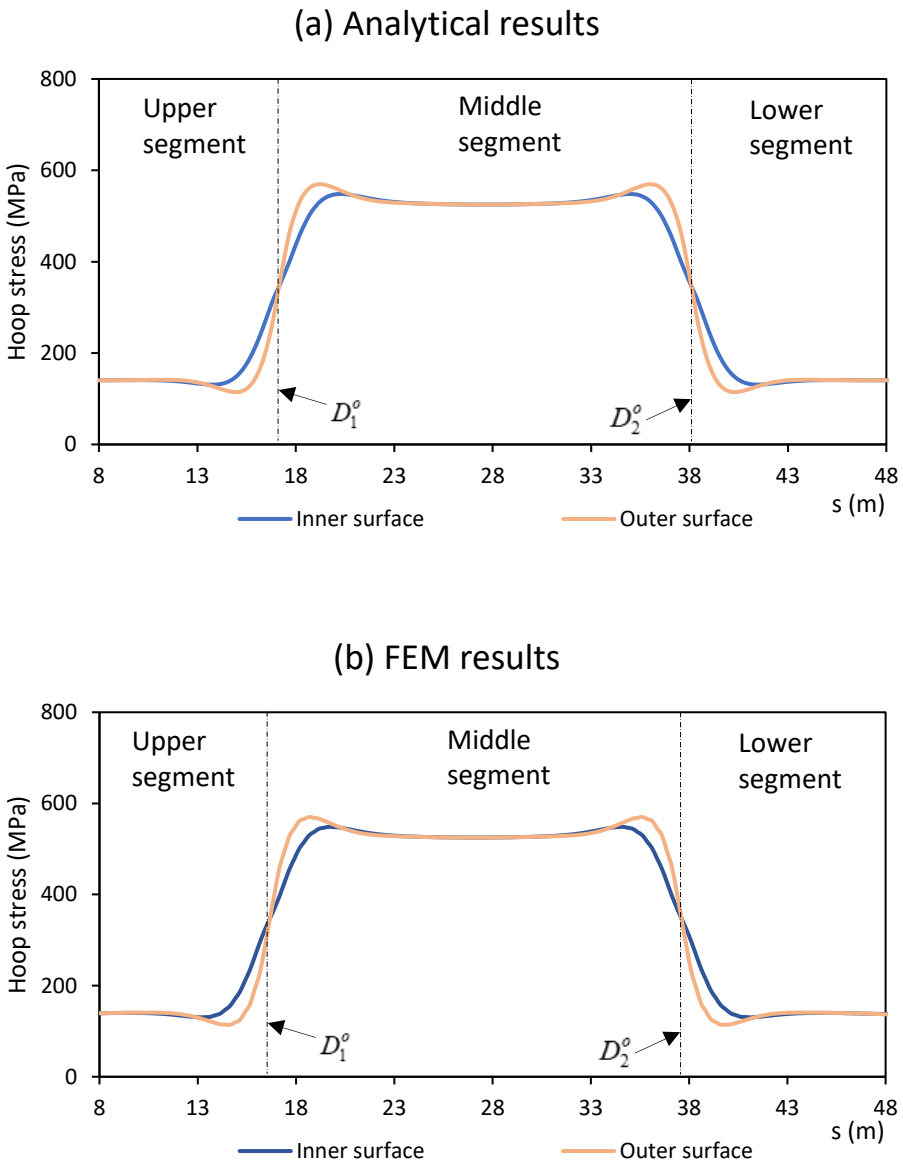

Figure 5.18. The variations of hoop stresses with arc length s over the outer regions of the pressurised toroidal vessel: (a) analytical results; (b) FEM results.

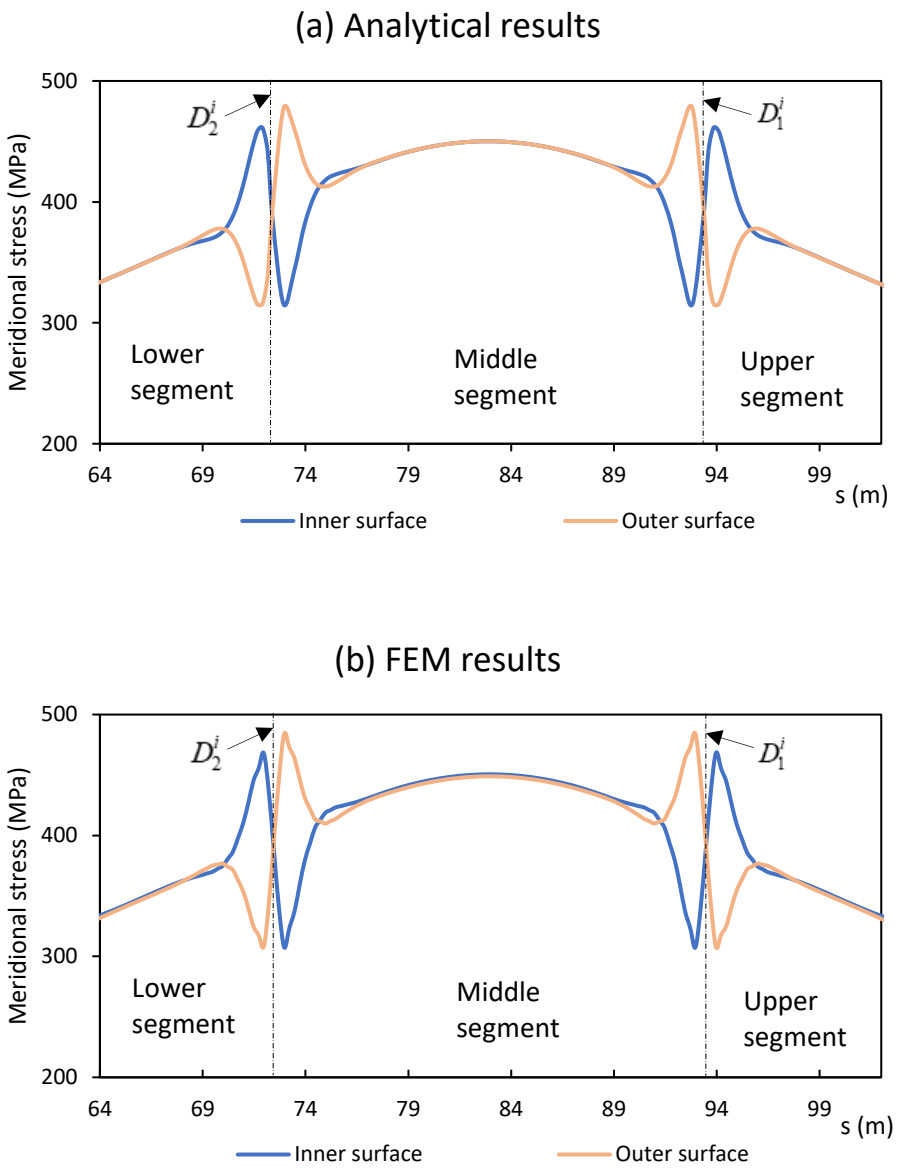

Figure 5.19. The variations of meridional stresses with arc length s over the inner regions of the pressurised toroidal vessel: (a) analytical results; (b) FEM results.

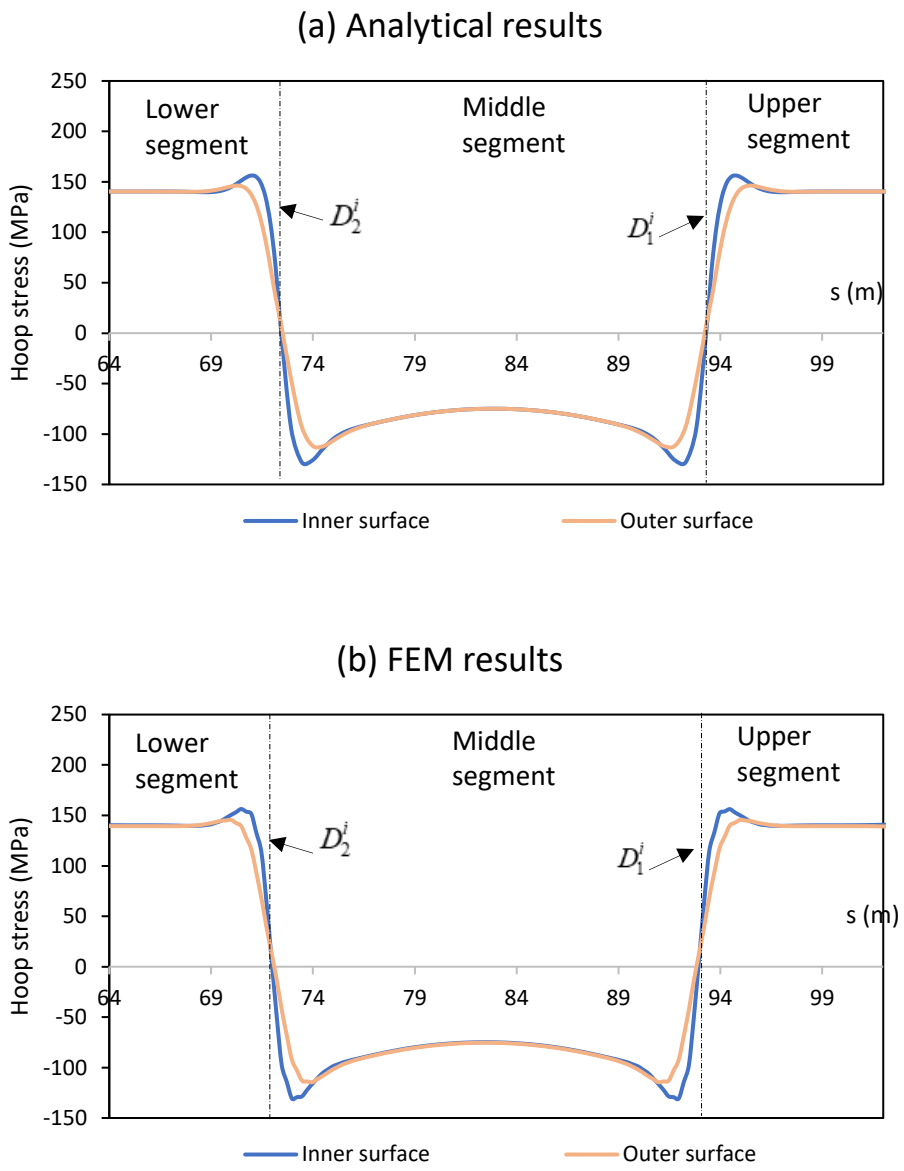

Figure 5.20. The variations of hoop stresses with arc length s over the inner regions of the pressurised toroidal vessel: (a) analytical results; (b) FEM results.

The bending-disturbance stresses seen around the meeting edges at the outer region of the uniformly pressurised multi-shell toroidal vessel are relatively huge in comparison with those noted in egg-shaped sludge digestors (Zingoni, 2001a), even though the cross-sectional profiles are the same. The difference in the bending-disturbance stresses in both cases is most likely due to the differences in the loading conditions. Zingoni considered a problem of hydrostatic pressure loading (varying across the height of the vessel), while the present consideration is centred on a uniformly pressurised case. Also note that the mean toroidal radius term A is

zero for the egg-shaped sludge digestors considered by Zingoni (2001a,b). Vessels of the present type with tangentially meeting segments generally exhibit very low bending-disturbance stresses around the meeting junctions compared to vessels with a discontinuity in the slope of the shell meridian (Zingoni, 2002a).

Also, the FEM results show some bending disturbance stresses around the top and bottom meeting points of the outer and inner regions of the toroidal vessel. The stresses in these zones are not shown in the plots as earlier pointed out since the developed bending solution in this chapter cannot account for the bending that occur in the shallow zones of toroids. It is seen that the bending stresses around the top and bottom meeting points are relatively small in comparison with those that occur around the meeting edges of the segment of the multi-shell vessel. Owing to the smallness of these stresses, the membrane results developed in Chapter 4 could be used to approximate the state of stress around the top and bottom meeting points of the outer and inner regions of the vessel.

Apart from the edge zones, it is observed that the maximum tensile value of meridional stresses at the inner region of the vessel is higher than that at the outer region of the vessel, indicating that the vessel will most likely fail in tension at this inner region. This maximum stress value is seen at the intrados of the vessel. It is also noted that the meridional stresses are entirely in tension throughout the vessel. While considerable pre-stressing will be required in the middle-outer region of the vessel to cater for the high hoop stresses in tension there, the hoop stresses at the middle-inner region of the vessel are compressive. This suggests that stiffeners should be added to, or the thickness t of the shell should be increased in the middle-inner region to avoid local buckling of the vessel. The smaller the size of the vessel, the lesser the buckling problem that will occur.

For very thin shells, local instability may be a problem in the mid-side locations of the inner region of the toroid, where hoop compression prevails. Clearly, the same formulation may also be extended to the analysis of submerged toroidal vessels experiencing external hydrostatic pressure. For this application, buckling of the shell becomes an even more relevant consideration, necessitating further research. Such studies have been carried out in the next two chapters.

5.5 Concluding remarks

A very simple and effective structural-analysis procedure based on Geckeler's approximations has been developed for quantifying bending-discontinuity effects at the non-shallow regions of toroidal shells where the membrane-hypothesis solution given in Chapter 4 fails. When the approximate bending solution is used in conjunction with the particular solution approximated as a membrane solution, a general solution is obtained for the reduced axisymmetric bending-theory equations of toroidal shells of revolution. The formulated method has been applied for the determination of the state of stresses in three new forms of toroidal vessels and the results compared to those obtained from finite-element modelling. Excellent agreement between the analytical and FEM results has been obtained, showing that the presented theoretical formulation is reliable and very accurate for estimating internal stresses in both the synclastic and anticlastic surfaces of toroidal shells, and can be adopted for analysing various toroidal shell forms. Some important insights into each of the vessels have been presented, including those from a parametric study of the parabolic ogival vessel.

.

Chapter 6

Elastic buckling of toroidal shells under axisymmetric loading

6.1 Introduction

This chapter presents the linear stability equations for general toroidal shells of revolution under axisymmetric loading. The equations are formulated on the basis of the classical assumptions of shell theory in which the influence of pre-buckling nonlinearity is neglected (Flügge & Sobel, 1965) and the membrane solution derived in Chapter 4 is used to approximate the pre-buckling state. The stability equations are further simplified and specialised for a multi-shell toroidal vessel buckling problem. These are then solved by employing the well-known Galerkin scheme, to obtain an expression for estimating the critical buckling pressures of middle regions of the vessel. The theoretical buckling solution is validated with a finite-element analysis through numerical examples. Some of the results reported in this chapter have already been published (Enoma & Zingoni, 2017).

6.2 Nonlinear differential equations for toroidal shells

The toroidal shell is assumed to obey Hooke's law. Hence, the only nonlinearity in the governing equilibrium equations for the buckling analysis of the shell can be achieved by considering the influence of rotations of the structural elements on the behaviour of the shell. In the derivation of the governing equations, the terms containing the geometric nonlinearity may easily be introduced directly through the kinematic relations when the equations are derived by the variational (or energy) methods (Brush & Almroth, 1975). However, the summation of forces and moments approach employed in Chapter 3 is adopted here. In this procedure, the nonlinearity is introduced into the governing differential equations by the equilibrium considerations of a toroidal shell element in its deformed (buckled) configuration, as we shall see in the following.

Firstly, for ease of reference, the linear bending equations of toroidal shells presented in Section 3.1.4 are recast here in the form:

$$\left(RN_{\phi}\right)^{\bullet} + r_1 N'_{\phi\theta} - r_1 N_{\theta}\cos\phi - RQ_{\phi} + r_1 R p_{\phi} = 0 \tag{6.1a}$$

$$\left(RN_{\phi\theta}\right)^{\bullet} + r_1 N'_{\theta} + r_1 N_{\phi\theta}\cos\phi - r_1 Q_{\theta}\sin\phi + r_1 R p_{\theta} = 0 \tag{6.1b}$$

$$RN_{\phi} + r_1 N_{\theta}\sin\phi + \left[\frac{1}{r_1}\left\{RM_{\phi}\right\}^{\bullet}\right]^{\bullet} - \left(M_{\theta}\cos\phi\right)^{\bullet} + 2M'^{\bullet}_{\phi\theta}$$

$$+\frac{2r_1}{R}M'_{\phi\theta}\cos\phi + \frac{r_1}{R}M''_{\theta} - r_1 R p_r = 0 \tag{6.1c}$$

These are respectively the equilibrium of forces in each of the directions of the tangent to a meridian, the tangent to a parallel circle of latitude and the normal to the toroidal shell middle surface. Note that in the last expression, the transverse shear force terms Q_{ϕ} and Q_{θ} have been eliminated from the two moment equilibrium equations derived in Chapter 3, recalling that

$$\frac{dR}{d\phi} = r_1\cos\phi$$

All symbols and notations in equations 6.1 are as previously defined.

Now, to take into account the nonlinear interaction between forces and rotations, the equations representing equilibrium of forces in the meridional, hoop and normal directions are derived for a toroidal element in a deformed configuration. The deformed element is shown in Figure 6.1. For the location of the element on the toroidal surface, reference may be made to Figure 3.1(b). The nonlinear terms in the moment equilibrium equations are negligibly small for the thin toroidal shells under present investigation and are, therefore, not considered here. The equilibrium equations for an unbuckled element are different from those of the buckled one in the terms which are nonlinear. Hence, all that is required now are to include the contributions of the nonlinear terms to the equations (6.1) above for an unbuckled toroidal element.

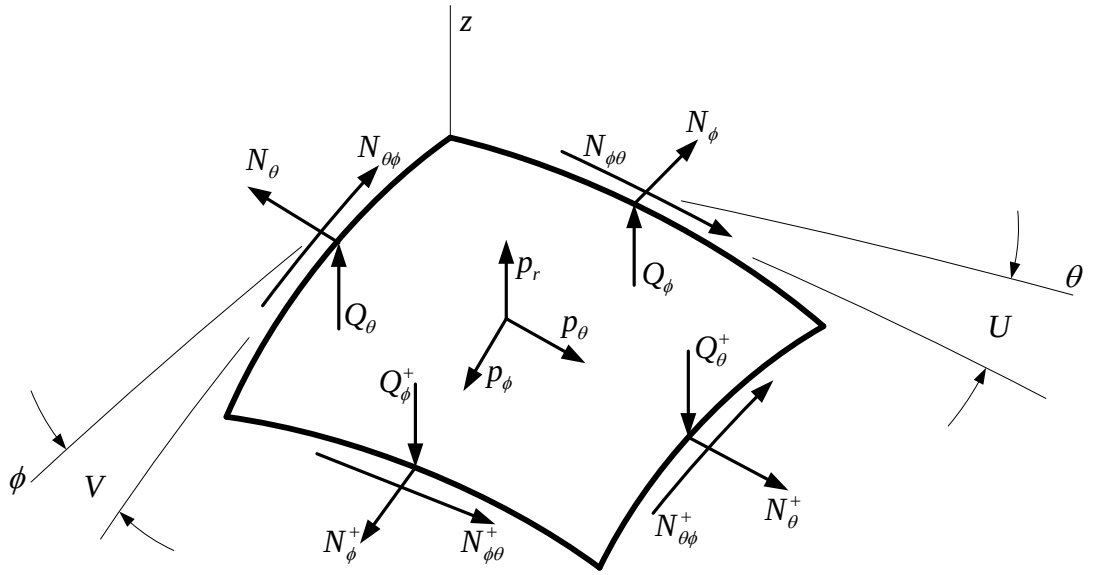

Figure 6.1. Forces on a deformed toroidal shell element

The expressions for V (the angle of rotation of the meridian), U (the angle of rotation of the hoop circle), W_ϕ (the angle of rotation of the tangent to the meridian about the normal) and W_θ (the angle of rotation of the tangent to a parallel circle about the normal) were given in Chapter 3 as

$$V = \frac{v - w^{\bullet}}{r_1}$$

$$U = \frac{u \sin\phi - w'}{R}$$

$$W_\varphi = \frac{u^{\bullet}}{r_1} - \frac{u \cos\phi}{R}$$

$$W_\theta = \frac{v'}{R}$$

where u, v and w denote the displacement components of a point on the shell middle surface in the direction of the tangent to the meridian, in the direction of the tangent to a circle of latitude, in the direction of the normal to the shell middle surface, respectively.

Following the approach of Section 3.1.4, and in consideration of rotations V, U, W_ϕ, W_θ, while, as usual, neglecting quadratic terms representing nonlinear interaction between transverse shearing forces and rotations (since transverse shearing forces are quite small for thin shells (Flügge, 1973; Ventsel & Krauthammer, 2001)), the summation of nonlinear-force terms in the direction of the tangent to a meridian gives, after some simplification,

$$-R\left\{N_\phi V + N_{\phi\theta} U\right\} - \left\{RN_{\phi\theta} W_\theta\right\}^{\bullet} - \left(r_1 N_\theta W_\theta\right)' - r_1 N_{\phi\theta} W_\phi \cos\phi + r_1 R p_r V \tag{6.2a}$$

Similarly, the following is obtained from the summation of nonlinear-force terms in the direction of the tangent to a parallel circle of latitude

$$-r_1 N_{\phi\theta} V \sin\phi - r_1 N_\theta U \sin\phi + \left(r_1 N_{\phi\theta} W_\phi\right)' + \left\{RN_\phi W_\phi\right\}^{\bullet} - r_1 N_\theta W_\theta \cos\phi + r_1 R p_r U \tag{6.2b}$$

And, that from the summation of nonlinear-force terms in the direction normal to the toroidal shell middle surface, follows as

$$\left\{RN_\phi V\right\}^{\bullet} + \left(r_1 N_{\phi\theta} V\right)' + \left\{RN_{\phi\theta} U\right\}^{\bullet} + \left(r_1 N_\theta U\right)' - RN_{\phi\theta} W_\theta + r_1 N_{\phi\theta} W_\phi \sin\phi - r_1 R p_r \left(\varepsilon_\theta + \varepsilon_\phi\right) \tag{6.2c}$$

When these nonlinear terms are added to their corresponding terms in the left-hand sides of expressions (6.1), the following partial differential equations of equilibrium for an element of the deformed toroidal shell are obtained in the meridional, hoop and normal directions, respectively:

$$\left(RN_\phi\right)^{\bullet} + r_1 N'_{\phi\theta} - r_1 N_\theta \cos\phi - RQ_\phi + r_1 R p_\phi + \left[r_1 R p_r V - R\left\{N_\phi V + N_{\phi\theta} U\right\} - \left\{RN_{\phi\theta} W_\theta\right\}^{\bullet} - \left(r_1 N_\theta W_\theta\right)' - r_1 N_{\phi\theta} W_\phi \cos\phi\right] = 0 \tag{6.3a}$$

$$\left(RN_{\phi\theta}\right)^{\bullet} + r_1 N'_\theta + r_1 N_{\phi\theta} \cos\phi - r_1 Q_\theta \sin\phi + r_1 R p_\theta + \left[r_1 R p_r U - r_1 N_{\phi\theta} V \sin\phi - r_1 N_\theta U \sin\phi + \left(r_1 N_{\phi\theta} W_\phi\right)' + \left\{RN_\phi W_\phi\right\}^{\bullet} - r_1 N_\theta W_\theta \cos\phi\right] = 0 \tag{6.3b}$$

$$
\begin{aligned}
&RN_\phi + r_1 N_\theta \sin\phi + \left(\frac{1}{r_1}\left\{RM_\phi\right\}^\bullet\right)^\bullet - \left(M_\theta \cos\phi\right)^\bullet + 2M'^\bullet_{\phi\theta} + \frac{r_1}{R}M''_\theta \\
&\quad + \frac{2r_1}{R}M'_{\phi\theta}\cos\phi_\theta - Rr_1 p_r - \Big[r_1 R p_r\left(\varepsilon_\theta + \varepsilon_\phi\right) - \left\{RN_\phi V\right\}^\bullet - \left(r_1 N_{\phi\theta} V\right)' \\
&\quad - \left(r_1 N_\theta U\right)' + RN_{\phi\theta}W_\theta - \left\{RN_{\phi\theta}U\right\}^\bullet - r_1 N_{\phi\theta}W_\phi \sin\phi\Big] = 0
\end{aligned}
\tag{6.3c}
$$

Expressions (6.3) may be written in toroidal terms as, (since $R = A + x$)

$$
\begin{aligned}
&AN_\phi{}^\bullet + \left(xN_\phi\right)^\bullet + r_1 N'_{\phi\theta} - r_1 N_\theta \cos\phi - \left(A+x\right)Q_\phi + \left(A+x\right)r_1 p_\phi \\
&\quad + \Big[\left(A+x\right)r_1 p_r V - \left(A+x\right)\left\{N_\phi V + N_{\phi\theta}U\right\} - \left\{\left(A+x\right)N_{\phi\theta}W_\theta\right\}^\bullet \\
&\quad - \left(r_1 N_\theta W_\theta\right)' - r_1 N_{\phi\theta}W_\phi \cos\phi\Big] = 0
\end{aligned}
$$

$$
\begin{aligned}
&AN_{\phi\theta}{}^\bullet + \left(xN_{\phi\theta}\right)^\bullet + r_1 N'_\theta + r_1 N_{\phi\theta}\cos\phi - r_1 Q_\theta \sin\phi + \left(A+x\right)r_1 p_\theta \\
&\quad + \Big[\left(A+x\right)r_1 p_r U - r_1 N_{\phi\theta}V\sin\phi - r_1 N_\theta U \sin\phi + \left(r_1 N_{\phi\theta}W_\phi\right)' \\
&\quad + \left\{\left(A+x\right)N_\phi W_\phi\right\}^\bullet - r_1 N_\theta W_\theta \cos\phi\Big] = 0
\end{aligned}
$$

$$
\begin{aligned}
&\left(A+x\right)N_\phi + r_1 N_\theta \sin\phi + \left(\frac{1}{r_1}\left\{\left(A+x\right)M_\phi\right\}^\bullet\right)^\bullet - \left(M_\theta\cos\phi\right)^\bullet + 2M'^\bullet_{\phi\theta} + \frac{r_1}{\left(A+x\right)}M''_\theta \\
&\quad + \frac{2r_1}{\left(A+x\right)}M'_{\phi\theta}\cos\phi_\theta - \left(A+x\right)r_1 p_r - \Big[r_1 p_r\left(A+x\right)\left(\varepsilon_\theta + \varepsilon_\phi\right) \\
&\quad - \left\{\left(A+x\right)N_\phi V\right\}^\bullet - \left(r_1 N_{\phi\theta}V\right)' - \left(r_1 N_\theta U\right)' + \left(A+x\right)N_{\phi\theta}W_\theta \\
&\quad - \left\{\left(A+x\right)N_{\phi\theta}U\right\}^\bullet - r_1 N_{\phi\theta}W_\phi \sin\phi\Big] = 0
\end{aligned}
$$

These represent the nonlinear equilibrium equations specialized for elastic toroidal shells of revolution within the framework of the theory of Flügge & Sobel (1965) for general shells of revolution, which is similar to the commonly adopted nonlinear theory of Sanders (1963) for thin shell analysis, except that the contributions of terms in the rotations around the normal W_ϕ and W_θ are applied separately in the present formulation, whereas in Sanders shell theory, the sum of the rotations is considered together. The terms have been included here for the sake of generality, as it has been shown over the years that they have negligible effects for isotropic thin elastic shells of revolution under axisymmetric loading.

6.3 Linearized stability equations

Here, the linear differential equations for loss of stability of elastic toroidal shells are derived from the nonlinear equilibrium equations (6.3) by the application of the classical adjacent-equilibrium criterion (Flügge, 1973; Brush & Almroth, 1975). In the following, the stability equations with pre-buckling rotation terms are first obtained. These are further reduced to linear equations of stability without pre-buckling rotation terms.

6.3.1 Stability equations with pre-buckling rotations

Following the approach of Brush & Almroth (1975), the unknown terms in the nonlinear equilibrium equations (6.3) are replaced by their respective pre-buckling plus incremental terms given below:

$$N_\phi \to N_{\phi 0} + N_{\phi 1};\; N_\theta \to N_{\theta 0} + N_{\theta 1};\; N_{\phi\theta} \to N_{\phi\theta 0} + N_{\phi\theta 1};\; Q_\phi \to Q_{\phi 0} + Q_{\phi 1};\; Q_\theta \to Q_{\theta 0} + Q_{\theta 1};$$

$$M_\phi \to M_{\phi 0} + M_{\phi 1};\; M_\theta \to M_{\theta 0} + M_{\theta 1};\; M_{\phi\theta} \to M_{\phi\theta 0} + M_{\phi\theta 1};$$

$$V \to V_0 + V_1;\; U \to U_0 + U_1;\; W_\phi \to W_{\phi 0} + W_{\phi 1};\; W_\theta \to W_{\theta 0} + W_{\theta 1};$$

$$\varepsilon_\phi \to \varepsilon_{\phi 0} + \varepsilon_{\phi 1};\; \varepsilon_\theta \to \varepsilon_{\theta 0} + \varepsilon_{\theta 1},$$

where, $(\;)_0$ are the pre-buckling terms, and $(\;)_1$ are the incremental terms that are developed during buckling. No increment is given to the applied loading. When these new terms are introduced into equations (6.3), terms that are linear, quadratic, and cubic in $(\;)_0$ and $(\;)_1$ are obtained. In the new equations, the terms in $(\;)_0$ alone add up to zero due to the equilibrium of the pre-buckling configuration, and the terms that are quadratic and of higher-order in $(\;)_1$ are omitted due to the smallness of the incremental quantities. Hence, the ensuing equations may be written in the form of expression (6.4) below, which are homogeneous and linear in $(\;)_1$ with variable coefficients in $(\;)_0$. This operation can be carried out in a similar way for displacement quantities since equations (6.3) can be expressed in terms of u, v and w using the kinematic and constitutive relations given in Chapter 3.

$$\begin{aligned}&\left(AN_{\phi 1}\right)^{\bullet}+r_1N'_{\phi\theta 1}-r_1N_{\theta 1}\cos\phi-RQ_{\phi 1}+r_1Rp_rV_1\\&\quad-R\left\{N_{\phi 0}V_1+N_{\phi 1}V_0+N_{\phi\theta 0}U_1+N_{\phi\theta 1}U_0\right\}\\&\quad-\left\{R\left(N_{\phi\theta 0}W_{\theta 1}+N_{\phi\theta 1}W_{\theta 0}\right)\right\}^{\bullet}-\left\{r_1\left(N_{\theta 0}W_{\theta 1}+N_{\theta 1}W_{\theta 0}\right)\right\}'\\&\quad-r_1\left(N_{\phi\theta 0}W_{\phi 1}+N_{\phi\theta 1}W_{\phi 0}\right)\cos\phi=0\end{aligned}\tag{6.4a}$$

$$\begin{aligned}&\left(RN_{\phi\theta 1}\right)^{\bullet}+r_1N'_{\theta 1}+r_1N_{\phi\theta 1}\cos\phi-r_1Q_{\theta 1}\sin\phi+r_1Rp_rU_1\\&\quad-r_1\left(N_{\phi\theta 0}V_1+N_{\phi\theta 1}V_0+N_{\theta 0}U_1+N_{\theta 1}U_0\right)\sin\phi+\left\{r_1\left(N_{\phi\theta 0}W_{\phi 1}+N_{\phi\theta 1}W_{\phi 0}\right)\right\}'\\&\quad+\left\{\left(N_{\phi 0}W_{\phi 1}+N_{\phi 1}W_{\phi 0}\right)\right\}^{\bullet}-r_1\left(N_{\theta 0}W_{\theta 1}+N_{\theta 1}W_{\theta 0}\right)\cos\phi=0\end{aligned}\tag{6.4b}$$

$$\begin{aligned}&RN_{\phi 1}+r_1N_{\theta 1}\sin\phi+\left(\frac{1}{r_1}\left\{RM_{\phi 1}\right\}^{\bullet}\right)^{\bullet}-\left(M_{\theta 1}\cos\phi\right)^{\bullet}+2M'^{\bullet}_{\phi\theta 1}\\&\quad+\frac{r_1}{R}M''_{\theta 1}+\frac{2r_1}{R}M'_{\phi\theta 1}\cos\phi_{\theta}-r_1Rp_r\left(\varepsilon_{\theta 1}+\varepsilon_{\phi 1}\right)\\&\quad+\left\{R\left(N_{\phi 0}V_1+N_{\phi 1}V_0\right)\right\}^{\bullet}+\left\{r_1\left(N_{\phi\theta 0}V_1+N_{\phi\theta 1}V_0+N_{\theta 0}U_1+N_{\theta 1}U_0\right)\right\}'\\&\quad-R\left\{N_{\phi\theta 0}W_{\theta 1}+N_{\phi\theta 1}W_{\theta 0}\right\}+\left\{R\left(N_{\phi\theta 0}U_1+N_{\phi\theta 1}U_0\right)\right\}^{\bullet}\\&\quad+r_1\left(N_{\phi\theta 0}W_{\phi 1}+N_{\phi\theta 1}W_{\phi 0}\right)\sin\phi\Big]=0\end{aligned}\tag{6.4c}$$

where the constitutive and kinematic relations presented in Section 3.5 may now take the form:

$$N_{\phi 1}=\frac{Et}{1-\upsilon^2}\left\{\left(\varepsilon_{\phi 1}+V_0V_1\right)+\nu\left(\varepsilon_{\theta 1}+U_0U_1\right)\right\}\tag{6.5a}$$

$$N_{\theta 1}=\frac{Et}{1-\upsilon^2}\left\{\left(\varepsilon_{\theta 1}+U_0U_1\right)+\nu\left(\varepsilon_{\phi 1}+V_0V_1\right)\right\}\tag{6.5b}$$

$$N_{\phi\theta 1}=\frac{Et}{2\left(1+\upsilon\right)}\left(\gamma_{\phi\theta 1}+V_0U_1+U_0V_1\right)\tag{6.5c}$$

$$M_{\phi 1}=-\frac{Et^3}{12\left(1-\upsilon^2\right)}\left\{\frac{1}{r_1}V_1^{\bullet}+\nu\frac{1}{R}\left(U_1'+V_1\cos\phi\right)\right\}\tag{6.5d}$$

$$M_{\theta 1} = -\frac{Et^3}{12\left(1-\upsilon^2\right)}\left\{\frac{1}{R}\left(U_1' + V_1\cos\phi\right) + \frac{\nu}{r_1}V_1^{\bullet}\right\} \tag{6.5e}$$

$$M_{\phi\theta 1} = -\frac{Et^3}{24\left(1+\upsilon\right)}\left\{\frac{1}{r_1}U_1^{\bullet} + \frac{1}{R}\left(V_1' - V\cos\phi\right)\right\} \tag{6.5f}$$

and,

$$V_1 = \frac{v_1 - w_1^{\bullet}}{r_1} \tag{6.6a}$$

$$U_1 = \frac{u_1\sin\phi - w_1'}{R} \tag{6.6b}$$

$$W_{\phi 1} = \frac{u_1^{\bullet}}{r_1} - \frac{u_1\cos\phi}{R} \tag{6.6c}$$

$$W_{\theta 1} = \frac{v_1'}{A+x} \tag{6.6d}$$

$$\varepsilon_{\phi 1} = \frac{1}{r_1}\left(v_1^{\bullet} + w_1\right) \tag{6.6e}$$

$$\varepsilon_{\theta 1} = \frac{1}{R}\left(u_1' + v_1\cos\phi + w_1\sin\phi\right) \tag{6.6f}$$

$$\gamma_{\phi\theta 1} = \frac{1}{r_1}u_1^{\bullet} + \frac{1}{R}\left(v_1' - u_1\cos\phi\right) \tag{6.6g}$$

Expressions (6.4) to (6.6) are the stability equations, which contain pre-buckling rotations, for shells of revolution. Introduction of expressions (6.5) to (6.6) into expressions (6.4) and omitting, in the usual way, the terms in $Q_{\phi 1}$ and $Q_{\theta 1}$ due to their negligible contributions in the first and second equilibration equations (Novozhilov, 1964; Flügge & Sobel, 1965; Calladine, 2007), one gets a set of three equations in u_1, v_1 and w_1 with variable coefficients in $N_{\phi 0}$, $N_{\theta 0}$, $N_{\phi\theta 0}$, U_0, V_0, $W_{\phi 0}$ and $W_{\theta 0}$. The variable coefficients can be determined from the nonlinear equilibrium equations (6.3). The presence of the pre-buckling rotation terms V_0, U_0,

$W_{\phi 0}$ and $W_{\theta 0}$ introduces a substantial complication in the stability equations. This may be eliminated by adopting the classical simplifying assumption of neglecting the influence of pre-buckling rotation terms (Brush & Almroth, 1975), since the toroidal shells under present consideration are thin-shells of revolution under axisymmetric loading. Hence, the pre-buckling nonlinear effects of the rotations are ignored in the following stability equations.

6.3.2 Stability equations without pre-buckling rotations

For the purpose of simplifying the stability problem, the classical assumption that the state of stress is such that rotations are small or confine to a small fraction of the shell surface area so that the influence of pre-buckling nonlinearity can be neglected, is adopted here. Accordingly, and following the approach of Brush & Almroth (1975), the rotations V_0, U_0, $W_{\phi 0}$ and $W_{\theta 0}$ are omitted from the stability expressions (6.4). The ensuing stability equations are of the type presented by Flügge & Sobel (1965) for general shells of revolution, and are as provided below for toroidal geometries:

$$\begin{aligned} &AN_{\phi 1}{}^{\bullet} + \left(xN_{\phi 1}\right)^{\bullet} + r_1 N'_{\phi\theta 1} - r_1 N_{\theta 1}\cos\phi - \left(A+x\right)Q_{\phi 1} + \left(A+x\right)r_1 p_r V_1 \\ &\quad -\left(A+x\right)\left\{N_{\phi 0}V_1 + N_{\phi\theta 0}U_1\right\} - \left\{\left(A+x\right)N_{\phi\theta 0}W_{\theta 1}\right\}^{\bullet} - \left(r_1 N_{\theta 0}W_{\theta 1}\right)' \\ &\quad -r_1 N_{\phi\theta 0}W_{\phi 1}\cos\phi = 0 \end{aligned} \tag{6.7a}$$

$$\begin{aligned} &AN_{\phi\theta 1}{}^{\bullet} + \left(xN_{\phi\theta 1}\right)^{\bullet} + r_1 N'_{\theta 1} + r_1 N_{\phi\theta 1}\cos\phi - r_1 Q_{\theta 1}\sin\phi + \left(A+x\right)r_1 p_r U_1 \\ &\quad -r_1\left(N_{\phi\theta 0}V_1 + N_{\theta 0}U_1\right)\sin\phi + \left(r_1 N_{\phi\theta 0}W_{\phi 1}\right)' + \left\{\left(A+x\right)N_{\phi 0}W_{\phi 1}\right\}^{\bullet} \\ &\quad -r_1 N_{\theta 0}W_{\theta 1}\cos\phi = 0 \end{aligned} \tag{6.7b}$$

$$\begin{aligned} &\left(A+x\right)N_{\phi 1} + r_1 N_{\theta 1}\sin\phi + \left(\frac{1}{r_1}\left\{\left(A+x\right)M_{\phi 1}\right\}^{\bullet}\right)^{\bullet} - \left(M_{\theta 1}\cos\phi\right)^{\bullet} + 2M'^{\bullet}_{\phi\theta 1} \\ &\quad + \frac{r_1}{\left(A+x\right)}M''_{\theta 1} + \frac{2r_1}{\left(A+x\right)}M'_{\phi\theta 1}\cos\phi_\theta - r_1 p_r\left(A+x\right)\left(\varepsilon_{\theta 1} + \varepsilon_{\phi 1}\right) \\ &\quad + \left\{\left(A+x\right)\left(N_{\phi\theta 0}U_1 + N_{\phi 0}V_1\right)\right\}^{\bullet} + \left\{r_1\left(N_{\phi\theta 0}V_1 + N_{\theta 0}U_1\right)\right\}' \\ &\quad -\left(A+x\right)N_{\phi\theta 0}W_{\theta 1} + r_1 N_{\phi\theta 0}W_{\phi 1}\sin\phi = 0 \end{aligned} \tag{6.7c}$$

where, now

$$N_{\phi 1} = \frac{Et}{1-\upsilon^2}\left\{\frac{1}{r_1}\left(v_1^{\bullet} + w_1\right) + \frac{\nu}{A+x}\left(u_1' + v_1\cos\phi + w_1\sin\phi\right)\right\} \tag{6.8a}$$

$$N_{\theta 1} = \frac{Et}{1-\upsilon^2}\left\{\frac{1}{A+x}\left(u_1' + v_1\cos\phi + w_1\sin\phi\right) + \frac{\nu}{r_1}\left(v_1^{\bullet} + w_1\right)\right\} \tag{6.8b}$$

$$N_{\phi\theta 1} = \frac{Et}{2(1+\upsilon)}\left\{\frac{1}{r_1}u_1^{\bullet} + \frac{1}{A+x}\left(v_1' - u_1\cos\phi\right)\right\} \tag{6.8c}$$

$$M_{\phi 1} = D\left[\frac{1}{r_1^2}\left(w_1^{\bullet} - v_1\right)^{\bullet} + \frac{\upsilon}{\left(A+x\right)^2}\left\{\left(w_1' - u_1\sin\phi\right)' + \frac{\left(A+x\right)\cos\phi}{r_1}\left(w_1^{\bullet} - v_1\right)\right\}\right] \tag{6.8d}$$

$$M_{\theta 1} = D\left[\frac{1}{\left(A+x\right)^2}\left\{\left(w_1' - u_1\sin\phi\right)' + \frac{\left(A+x\right)\cos\phi}{r_1}\left(w_1^{\bullet} - v_1\right)\right\} + \frac{\upsilon}{r_1^2}\left(w_1^{\bullet} - v_1\right)^{\bullet}\right] \tag{6.8e}$$

$$M_{\phi\theta 1} = D\frac{1-\upsilon}{2}\left[\frac{1}{r_1}\left(\frac{w_1' - u_1\sin\phi}{A+x}\right)^{\bullet} + \frac{1}{A+x}\left\{\frac{1}{r_1}\left(w_1^{\bullet} - v_1\right)' - \frac{\cos\phi}{A+x}\left(w_1' - u_1\sin\phi\right)\right\}\right] \tag{6.8f}$$

in which, $D = \dfrac{Et^3}{12\left(1-\upsilon^2\right)}$ and $R = A + x$.

Expressions (6.7) and (6.8) lead to a coupled set of three linear homogeneous equations of stability (without pre-buckling rotation terms) for symmetrically loaded thin toroidal shells of revolution. These linearised stability equations provide no information about the initial slope or shape of the secondary equilibrium path but can be used to obtain bifurcation-point loads which represent the loss of stability (Flügge, 1973; Brush & Almroth, 1975). The shearing force terms may be omitted for the reason mentioned before, and the remaining variable coefficients $N_{\phi 0}$, $N_{\theta 0}$ and $N_{\phi\theta 0}$ can be determined from the linear equilibrium equations for toroidal shells obtained in Chapter 3. Note that torsional loading does not apply in the present analysis, and hence, the coefficient $N_{\phi\theta 0}$ may be taken as zero in the equations.

6.4 Buckling solution approach

It was not attempted to solve the linearised stability equations (6.7) and (6.8) for general toroidal shells of revolution, due to the huge complexities involved. Instead, the equations are specialised here for a multi-shell toroidal vessel under external pressure. These equations are then simplified on the account of the Donnell-Mushtari-Vlasov (DMV) thin-shell approximations (Redekop, 2005; Amabili, 2008; Yoo & Lee, 2011), and a buckling solution is obtained for the middle regions of the vessel only, since the membrane analysis-results in Section 4.4.5 suggest that the middle regions of the multi-shell toroidal vessel are most susceptible to buckle first, due to the high compressive stresses experienced there.

6.4.1 Buckling of the multi-shell toroid

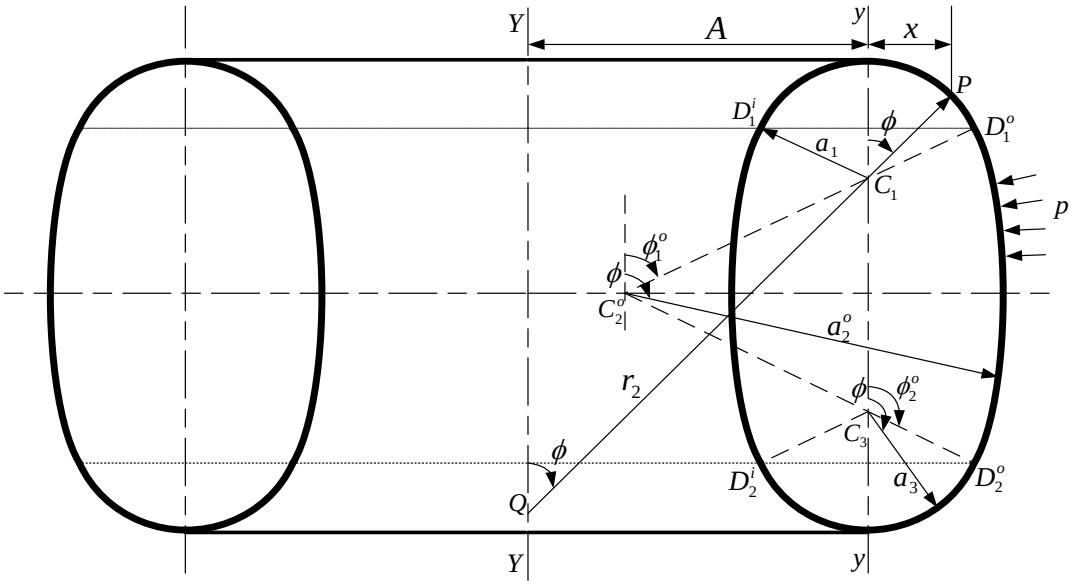

Figure 6.2. The multi-shell toroid.

The externally pressurised multi-shell toroidal vessel is shown in Figure 6.2. The parameters in the figure are as described in Section 4.4.5. The present vessel is assumed to be symmetrical about the equatorial plane. Hence, the magnitudes of the local cross-sectional radii of the upper and lower segments are the same, and that for the inner and outer middle-segments are also the same.

The stability equations for the individual segments of the multi-shell toroidal vessel are obtained from expressions (6.6) - (6.8), in which, the deformation is assumed to be

axisymmetric prior to the loss of stability since the applied load is also axisymmetric, and r_1 and x take their corresponding forms from their equations in Section 4.4.5 for the particular toroidal segment of interest. When the ensuing forms of equations (6.6) and (6.8) are respectively put into (6.7) for each of the toroidal segments, some sets of equations that are rather involved are obtained. However, the complexity of the equations is reduced by focusing on the segments in the middle regions of the vessel, which are expected to locally buckle first, since pressurised segmented toroidal vessels experience the highest compressive stresses around these regions, as indicated above.

6.4.2 Simplifying assumptions

The simplification may be done, by first eliminating from equations (6.7a) and (6.7b), the terms in the rotation components V_1 and U_1, and the terms in the transverse shearing force $Q_{\phi 1}$ and $Q_{\theta 1}$, since the retention of these terms in the two equations is inconsistent with the use of an uncoupled elastic law (Sobel & Flügge, 1967) and their contributions are negligibly small for thin shallow shells (Brush & Almroth, 1975). For a similar reason, the terms in the displacement components u_1, v_1 are also neglected from the last equation of (6.7) after substituting expressions (6.8). Lastly, the terms in the rotation around the normal to the shell middle surface $W_{\phi 1}$ and $W_{\theta 1}$ are are also ignored. These approximations are in accordance with the simplification nature of the Donnell-Mushtari-Vlasov (DMV) thin shell theory (Redekop, 2005; Amabili, 2008; Yoo & Lee, 2011).

Hence, the ensuing stability equations may be reduced to two equations by the introduction of a stress function Φ, which is related to the incremental stress resultants, $N_{\phi 1}$, $N_{\theta 1}$ and $N_{\phi\theta 1}$ as follows (Ventsel & Krauthammer, 2001)*:*

$$N_{\phi 1} = \frac{1}{R^2}\Phi' + \frac{\cos\phi}{r_1 R}\Phi^{\bullet} \tag{6.9a}$$

$$N_{\theta 1} = \frac{1}{r_1^2}\Phi^{\bullet\bullet} \tag{6.9b}$$

$$N_{\phi\theta 1} = \frac{1}{r_1 R}\Phi'^{\bullet} + \frac{\cos\phi}{R^2}\Phi' \tag{6.9c}$$

Now, for only the middle regions of the toroidal vessel, r_1 and R are expressed as (see Section 4.4.5)

$$r_1 = \pm a_2 \tag{6.10a}$$

$$R = A + x = A \pm \left(a_2 \sin\phi - q\right) \tag{6.10b}$$

where

$$q = \left(a_2 - a_1\right)\sin\phi_1 \tag{6.11}$$

and, as before, for the double operations, the upper sign applies to the outer region, while the lower sign applies to the inner region of the segmented toroidal vessel.

6.4.3 Specialized stability equations for the middle regions of the multi-shell toroid

Then, on the basis of the linear elastic DMV theory for thin-walled isotropic shells of revolution (Novozhilov, 1964; Ventsel & Krauthammer, 2001), the stability equations (6.7) and (6.8) in corroboration with (6.9) may be reduced to two in the radial displacement component w and the stress function Φ terms. After some manipulations (Brush & Almroth, 1975; Ventsel & Krauthammer, 2001; Magnucki & Jasion, 2013), and neglecting non-zero terms due to their smallness, these expressions become

$$\begin{aligned} L_1\left(w,\Phi\right) = D\Bigg\{ & \frac{1}{4}w^{\bullet\bullet\bullet\bullet} \pm \frac{2\cos\phi}{{a_2}^3 R}w^{\bullet\bullet\bullet} - \mu_1 w^{\bullet\bullet} + \mu_2 w^{\bullet} + \frac{2}{{a_2}^2 R^2}w''^{\bullet\bullet} \mp \frac{2\cos\phi}{a_2 R^3}w''^{\bullet} + \mu_3 w'' \\ & + \frac{1}{R^4}w'''' \Bigg\} - \frac{\sin\phi}{{a_2}^2 R}\Phi^{\bullet\bullet} - \frac{\cos\phi}{{a_2}^2 R}\Phi^{\bullet} \mp \frac{1}{a_2 R^2}\Phi'' - \frac{N_{\varphi 0}}{{a_2}^2}w^{\bullet\bullet} \\ & - N_{\theta 0}\left(\frac{1}{R^2}w'' \pm \frac{\cos\phi}{a_2 R}w^{\bullet}\right) = 0 \end{aligned} \tag{6.12a}$$

$$L_2\left(w,\Phi\right)=\frac{\sin\phi}{{a_2}^2R}w^{\bullet\bullet}+\frac{\cos\phi}{{a_2}^2R}w^{\bullet}\pm\frac{1}{a_2R^2}w''+Et\left\{\frac{1}{4}\Phi^{\bullet\bullet\bullet\bullet}\pm\frac{2\cos\phi}{{a_2}^3R}\Phi^{\bullet\bullet\bullet}-\mu_1\Phi^{\bullet\bullet}\right.$$
$$\left.+\mu_2\Phi^{\bullet}+\frac{2}{{a_2}^2R^2}\Phi''^{\bullet\bullet}\mp\frac{2\cos\phi}{a_2R^3}\Phi''^{\bullet}+\mu_3\Phi''+\frac{1}{R^4}\Phi''''\right\}=0 \tag{6.12b}$$

In these equations, the subscript 1 with w is omitted, and μ_1, μ_2 and μ_3 are variable coefficients defined as follows:

$$\mu_1=\pm\frac{1}{{a_2}^3R^2}\left(2R\sin\phi\pm a_2\cos^2\phi\right) \tag{6.13a}$$

$$\mu_2=\pm\frac{\cos\phi}{{a_2}^3R^3}\left(-R^2\pm2a_2R\sin\phi+{a_2}^2\cos^2\phi\right) \tag{6.13b}$$

$$\mu_3=\pm\frac{2}{a_2R^4}\left(R\sin\phi\pm2a_2\cos^2\phi\right) \tag{6.13c}$$

The influence of pre-buckling rotations has been neglected, the pre-buckling stress resultants $N_{\phi0}$, $N_{\theta0}$ and $N_{\phi\theta0}$ are assumed to be governed by the membrane analysis. Therefore, for the middle regions of the segmented toroidal shell under external pressure (see Section 4.4.5), we obtain

$$N_{\phi0}=N_{\phi}^{m}=-\frac{1}{\left(A\mp q\ \pm a_2\sin\phi\right)\sin\phi}\left\{\mp\frac{pa_2}{2}\left(2(\mp A+q\ )\sin\phi+a_2\cos^2\phi\right)+k_m\right\} \tag{6.14a}$$

$$N_{\theta0}=N_{\theta}^{m}=-\frac{1}{2a_2}\left\{pa_2^2\left(2+\cot^2\phi\right)\mp\frac{2k_m}{\sin^2\phi}\right\} \tag{6.14b}$$

$$N_{\phi\theta0}=0 \tag{6.14c}$$

where,

$$k_m=\frac{p}{4}\left\{\pm2a_1^2\sin^2\phi_1\ \mp a_2\left(\pm4A\sin\phi_1\ +a_2(-3+\cos2\phi_1\ )\right)\right.$$
$$\left.\mp4a_1(\mp A+a_2\sin\phi_1\ )\sin\phi_1\ \right\}$$

6.4.4 Application of the Galerkin method

For a particular case of a toroidal vessel with only middle segments, which are simply supported around the edges and subjected to uniform external pressure p, the pre-buckling deformation of the vessel may be assumed to be axisymmetric about $Y-Y$. Hence, the critical pressure p_{cr} may be defined as the lowest pressure at which the axisymmetric form loses stability. In line with the solution approach adopted by Magnucki & Jasion (2013) for barrelled shells, the Galerkin scheme is employed here, to approximately solve the stability equations (6.12) for the present toroidal shell problem (Galerkin, 1915; Brush & Almroth, 1975).

Let us start by assuming the following similar form of solutions for the radial displacement component w and the stress function Φ:

$$w = w_{mn} \sin\left[mk\left(\phi-\phi_1\right)\right]\sin n\theta \tag{6.15a}$$

$$\Phi = \Phi_{mn} \sin\left[mk\left(\phi-\phi_1\right)\right]\sin n\theta \tag{6.15b}$$

which are seen to satisfy both the stability equations and the simplified boundary conditions, and where w_{mn} and Φ_{mn} are unknown displacement and stress function coefficients, the integers $m=1,2,3...$, and $n=2,3,4...$ are the longitudinal and circumferential half waves, $\phi_1 \le \phi \le \phi_2$, $0 \le \theta \le 2\pi$, and

$$k = \pm\frac{\pi}{\phi_2-\phi_1} \tag{6.16}$$

Hence, application of the Galerkin method leads to

$$\int_{\phi_1}^{\phi_2}\int_0^{2\pi} L_1\left(w,\Phi\right) a_2 R \sin\left[\bar{m}k\left(\phi-\phi_1\right)\right]\sin\bar{n}\theta d\theta d\phi = 0 \tag{6.17a}$$

$$\int_{\phi_1}^{\phi_2}\int_0^{2\pi} L_2\left(w,\Phi\right) a_2 R \sin\left[\bar{m}k\left(\phi-\phi_1\right)\right]\sin\bar{n}\theta d\theta d\phi = 0 \tag{6.17b}$$

for $\bar{m}=1,2,3...$, and $\bar{n}=1,2,3...$

6.4.5 Critical buckling solution for the middle shells

Now, when expressions (6.12) and (6.15) are substituted into (6.17), the integration with respect to the angular coordinate along the hoop circle θ can be easily carried out and the integral vanishes if $m \neq \bar{m}$ and $n \neq \bar{n}$. The resulting expressions may be cast for the eigenvalues, as

$$p_{cr} = \underset{m,n}{Min}\left[\frac{\Omega - \lambda\Psi}{\mathrm{P}}\left\{\frac{Et^3}{12\left(1-\upsilon^2\right)}\right\}\right] \tag{6.18}$$

here, p_{cr} is the critical buckling pressure, and the terms in the curly bracket is the flexural rigidity of the vessel D, and the functions Ω, Ψ, P and λ depend on the geometric parameters R, a_2, θ and ϕ. These functions are given by

$$\Omega = \int_{\phi_1}^{\phi_2}\int_0^{2\pi} \eta_w a_2 R \sin\left[mk\left(\phi-\phi_1\right)\right]\sin n\theta d\theta d\phi$$

$$\Psi = \int_{\phi_1}^{\phi_2}\int_0^{2\pi} \eta_{k\Phi} a_2 R \sin\left[mk\left(\phi-\phi_1\right)\right]\sin n\theta d\theta d\phi$$

$$\mathrm{P} = \int_{\phi_1}^{\phi_2}\int_0^{2\pi} \eta_p a_2 R \sin\left[mk\left(\phi-\phi_1\right)\right]\sin n\theta d\theta d\phi$$

$$\lambda = -Et\frac{\lambda_{kw}}{\lambda_\Phi}$$

where;

$$\lambda_{kw} = \int_{\phi_1}^{\phi_2}\int_0^{2\pi} \eta_{kw} a_2 R \sin\left[mk\left(\phi-\phi_1\right)\right]\sin n\theta d\theta d\phi$$

$$\lambda_\Phi = \int_{\phi_1}^{\phi_2}\int_0^{2\pi} \eta_\Phi a_2 R \sin\left[mk\left(\phi-\phi_1\right)\right]\sin n\theta d\theta d\phi$$

and,

$$\eta_w = \frac{1}{w_{mn}}\left(\frac{1}{4}w^{\bullet\bullet\bullet\bullet} \pm \frac{2\cos\phi}{a_2{}^3R}w^{\bullet\bullet\bullet} - \mu_1 w^{\bullet\bullet} + \mu_2 w^{\bullet} + \frac{2}{a_2{}^2R^2}w''^{\bullet\bullet} \mp \frac{2\cos\phi}{a_2R^3}w''^{\bullet} + \mu_3 w'' + \frac{1}{R^4}w''''\right)$$

$$\eta_{k\Phi} = \frac{1}{\Phi_{mn}}\left(\frac{\sin\phi}{a_2{}^2R}\Phi^{\bullet\bullet} + \frac{\cos\phi}{a_2{}^2R}\Phi^{\bullet} \pm \frac{1}{a_2R^2}\Phi''\right)$$

$$\eta_p = \pm\frac{1}{pw_{mn}}\left\{\frac{N_\phi^m}{a_2{}^2}w^{\bullet\bullet} + N_\theta^m\left(\frac{1}{R^2}w'' \pm \frac{\cos\phi}{a_2R}w^{\bullet}\right)\right\}$$

$$\eta_{kw} = \frac{1}{w_{mn}}\left(\frac{\sin\phi}{a_2{}^2R}w^{\bullet\bullet} + \frac{\cos\phi}{a_2{}^2R}w^{\bullet} \pm \frac{1}{a_2R^2}w''\right)$$

$$\eta_\Phi = \frac{1}{\Phi_{mn}}\left(\frac{1}{4}\Phi^{\bullet\bullet\bullet\bullet} \pm \frac{2\cos\phi}{a_2{}^3R}\Phi^{\bullet\bullet\bullet} - \mu_1\Phi^{\bullet\bullet} + \mu_2\Phi^{\bullet} + \frac{2}{a_2{}^2R^2}\Phi''^{\bullet\bullet} \mp \frac{2\cos\phi}{a_2R^3}\Phi''^{\bullet} + \mu_3\Phi'' + \frac{1}{R^4}\Phi''''\right)$$

The expression (6.18), for the eigenvalues, can be solved for different values of m and n, but only one critical value of pressure will be obtained for any fixed value of the number of half waves m. For the vessel in question, the smallest eigenvalues usually occur for $m=1$ in equation (6.18).

6.4.6 Validation and discussion of results

The above analytical procedure for obtaining the eigenvalues of a pressurised and simply supported multi-shell toroid was coded in Mathematica 10. 0 (Wolfram Research Inc., 2014) and has been used to generate the following results, which are compared with their counterparts from the ADINA finite element code (Anon, 2012). In the finite element modelling of the linearised buckling analysis, a 9-nodes per shell element which is available in ADINA 9.0.3 and an appropriate mesh density were implemented from a preliminary study of mesh convergence. The edges of the segments in the inner and outer region of the model (without the top and bottom segments) are, of course, restrained translationally in the radial and circumferential directions.

Although the eigenvalue expression (6.18) can be used for higher eigenmodes, only the first buckling pressures for $m=1$ are reported here. It was observed that the first buckling occurred at the outer segment of all the cases investigated. This is expected, given the high pre-buckling values of the hoop stress in that region of the vessel. A typical first eigenmode for this type of vessels under external pressure is shown in Figure 6.3. For this very case shown, the following parameters were used: Young modulus $E=200\times10^{9}N/m^{2}$, Poisson's ratio $\upsilon=0.3$, constant wall thickness t, $a_1/t=20$, $a_2/A=4.67$, $a_1=a_3=7.99m$, $\phi_1=80^{o}$ and $\phi_2=100^{o}$ for the outer region; and $\phi_1=100^{o}$ and $\phi_2=80^{o}$ for the inner region of the toroid. Note that the vessel lost its stability through static bifurcation at $p_{cr}=4.42MPa$ with a mode shape of one longitudinal and eleven circumferential half-waves.

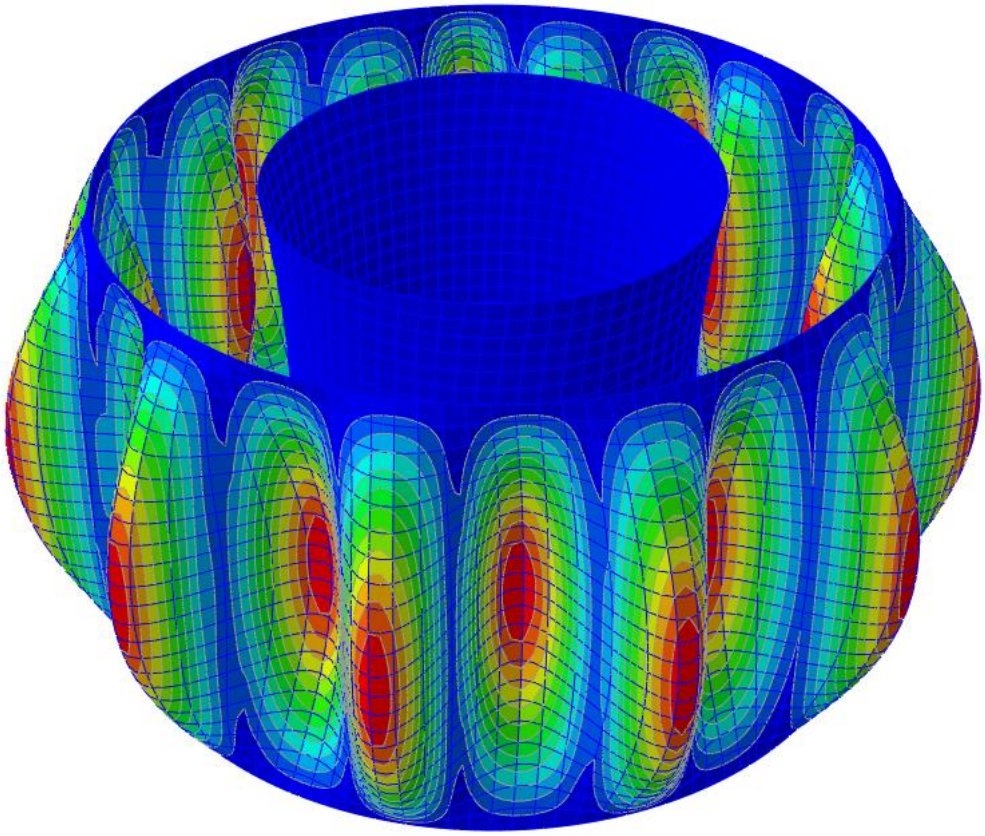

Figure 6.3. A typical first eigenmode of the externally pressurised multi-shell toroid, $m=1$, $n=11$

The critical pressure at which a vessel of the type in question loses its stability is very much a function of its A/a_2 ratio. This can be seen in Figure 6.5, which shows the plots of the first

critical pressures p_{cr} versus the ratio of the toroidal mean radius A to local radius of the segment a_2 obtained from the analytical method and finite element analysis. The material and geometric parameters of the multi-shell vessels considered here are the same as those given above, except for $a_1/t = 160$ and different values of A/a_2 as shown in the figure. The tighter the toroidal vessel (lower value of A/a_2), the stiffer it becomes, and hence the higher the buckling pressure. On the other hand, for increasing values of A/a_2, the weaker toroidal curvature effects, and hence the critical buckling pressures reduces.

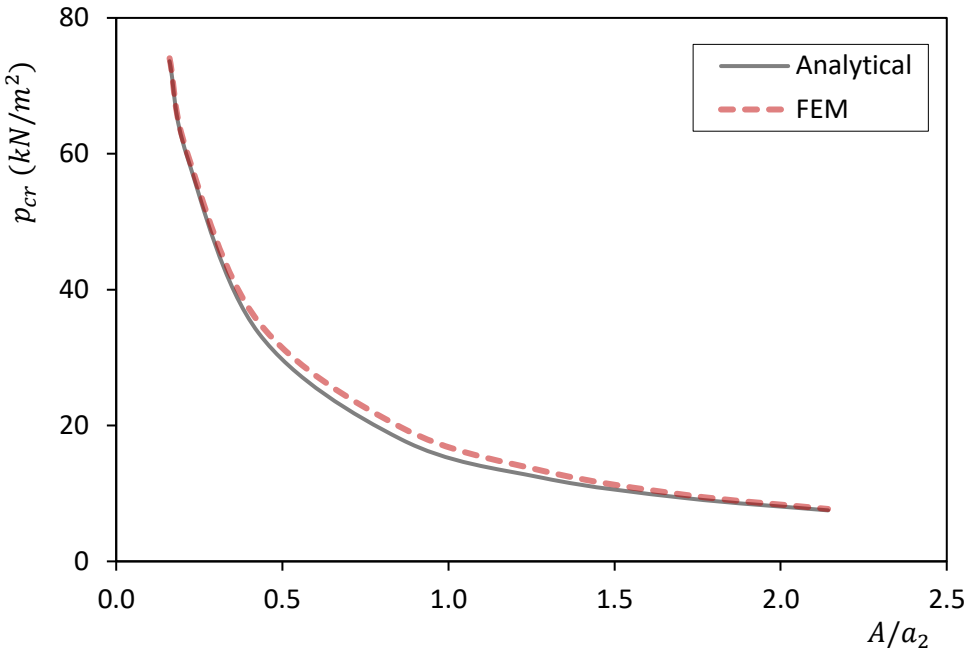

Figure 6.4. Bifurcation buckling pressures versus A/a_2

The agreement between analytical and FEM results is seen to be excellent in Figure 6.4, with accuracy within 7% throughout. However, this is subject to the shallowness of the toroidal vessel as encapsulated in the adopted approximation theory of the Donnell-Mushtari-Vlasov for thin shells of revolution. To demonstrate the limit of accuracy of the proposed critical buckling expression, we conducted a comparative analysis of critical buckling pressures of multi-shell toroids of various rise ratios λ_r using the analytical method (ANA) and the finite element method (FEM). Six different cases of constant $A = 30m$ with other geometric parameters given in Table 6.1, and with the same material properties as given before, were studied. For a toroid, which is symmetrical about the equatorial plane, the rise ratio λ_r is

defined as the ratio of the vertical distance of the edge from the equatorial plane and the lateral distance between the edge of the particular shell and the point its touches the equatorial plane. That is,

$$\lambda_r = \frac{\sin\left(\pi/2 - \phi_1\right)}{1 - \sin\phi_1} \tag{6.19}$$

It is seen in the table that, as the toroidal rise ratio λ_r increases, the percentage difference between the formulated method and the finite element method reduces, or the accuracy of the analytical procedure increases. The only negative percentage differential value in the Table implies that the bifurcation pressure obtained with the analytical method is greater than that from the FEM for that particular case. Depending on the required accuracy for practical application, this table clearly shows the strength and weakness of the developed algorithm. Hence, for a rise ratio less than 4 (i.e. $\lambda_r < 4.0$), the eigenvalue expression (6.18) will give critical buckling pressure values of a pressurised multi-segmented toroidal vessel that may be practically unacceptable.

Table 6.1. Comparison of analytical and numerical results

Case	a_1 (m)	a_2 (m)	ϕ_1 (deg)	λ_r	$p_{cr}\left(kN/m^2\right)$		Diff. (%)
					ANA	FEM	
1	12.90	30.39	37.60	2	397.1	218.4	-45.0
2	8.92	51.66	61.93	4	171.5	206.3	20.3
3	8.32	74.99	70.08	6	111.7	117.9	5.5
4	8.12	98.76	75.75	8	84.2	87.1	3.4
5	7.93	195.29	82.85	16	43.5	44.0	1.2
6	7.89	389.33	86.42	32	24.5	24.8	1.1

Recall that only eigenvalues for $m = 1$ are discussed here. The number of circumferential half-waves n against the toroidal rise ratio λ_r was also plotted for each of the 6 cases from the analytical method and the numerical method, see Figure 6.5. Like the observations in the Table above, and as already established, there is much discrepancy between the n values obtained from ANA and FEM for toroidal rise ratio less than 4. Identical results are seen for cases 4 and 5, with $n = 33$ and 24, in that order. For cases 3 and 6, the analytical method returned $n = 39$ and 18, while FEM gave $n = 38$ and 19, which are nearly the same. The agreement is very

close for each of cases 3 to 6, showing that the theoretical formulation developed is very accurate for $\lambda_r > 4.0$.

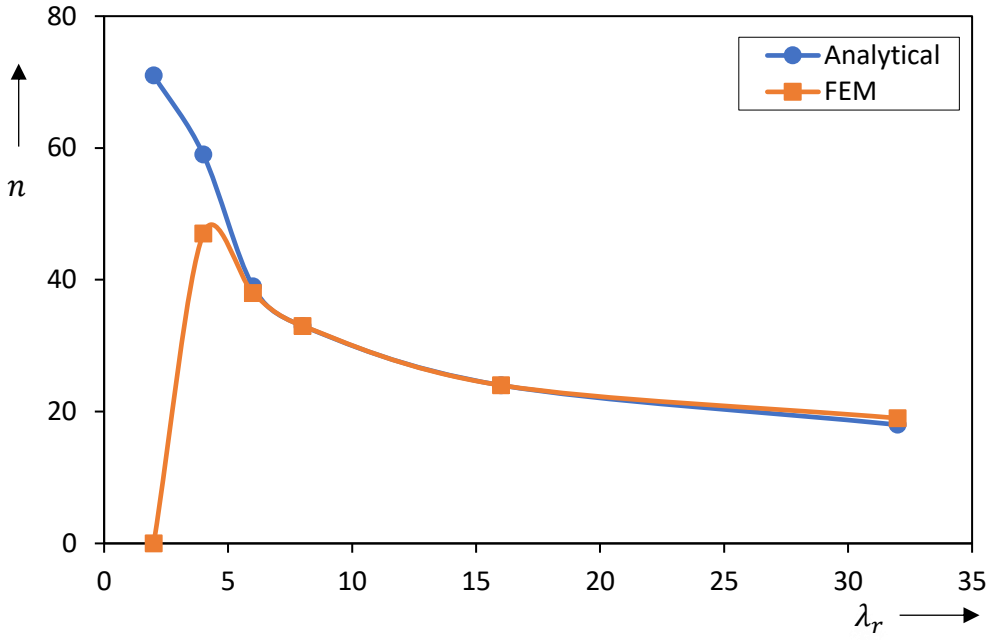

Figure 6.5. Comparison of analytical and numerical results for n versus λ_r

Looking at the critical pressure values in relative to the value of λ_r in the Table, one will notice that, as the toroidal rise ratio λ_r increases (that is, as the toroidal segment local radius tends to infinity), the first critical pressure load p_{cr} reduces and tends toward that for a cylindrical shell. On the other hand, as λ_r decreases, p_{cr} increases. This makes sense since a decrease in the rise ratio results in a decrease in the toroidal segment local radius a_2 and if other dimensions (like the thickness of the shell) remain constant or are not too changing, then the vessel will become stiffer, and the critical buckling pressures will increase. Next, an investigation is carried out on the effect of shell thickness t on the critical buckling pressures of the vessel.

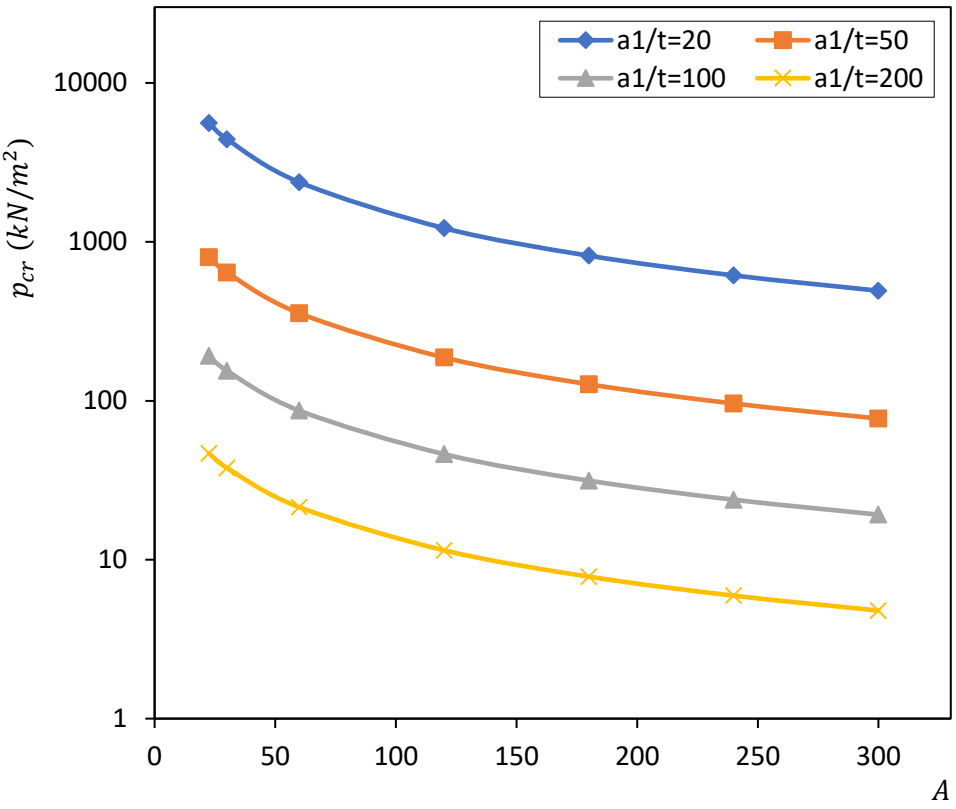

Figure 6.6. Effects of shell thickness on bifurcation pressures for various A

Figure 6.6 shows the plot of the critical buckling pressures versus A obtained from pressurised toroids with different values of a_1/t. The material and geometric parameters are the same as those in the analyses above, but with different values of a_1/t and A as shown. For any of the plots, it is observed that as A increases, the toroid as well as the critical buckling strength reduces and tends toward that of a long cylindrical shell. As expected, the critical buckling pressures are also seen to reduce generally as a_1/t increases (the shell becomes thinner). This is obvious in the expression (6.18) for eigenvalues and further buttresses the later part of the last paragraph.

6.5 Concluding remarks

Linear stability analysis of elastic toroidal shells is discussed in this chapter, based on the non-linear shell theory. The governing equations of stability of general toroidal shells of revolution are presented and specialised for multi-shell toroids under external pressure loading. The approximations of the Donnell-Mushtari-Vlasov theory are applied to simplify the derived

stability equations while adopting the classical assumption of employing membrane-theory solution to approximate the pre-buckling state of the problem. On application of the Galerkin scheme, the resulting stability equations are solved to obtain an approximate solution for the eigenvalues of the segments in the middle location of the toroidal vessel. The critical buckling formula obtained permits the ease of studying the influence of geometric parameters on critical failure loads and mode shapes of the present toroidal vessels.

Numerical examples conducted with the proposed analytical approach indicate that toroidal opening ratio and thickness ratio affect the critical buckling pressures of multi-shell toroidal vessels under uniform external pressure. The results show excellent agreement with those obtained from the finite element code, especially for multi-shell toroids with rise ratio $\lambda_r > 4.0$. The discrepancies observed for $\lambda_r < 4.0$ are mainly due to the shallowness assumptions of the adopted approximation theory of the D-M-V for thin-shells of revolution. Also, the present work has been limited to eigenvalue analysis of shells without imperfections and having simple boundary conditions. The proposed analytical model for estimating the buckling of multi-shell toroids under uniform external pressure can also be modified for different load cases and support conditions by simply adopting the appropriate forms of displacement and stress functions. Non-linear effects on buckling response, post-bifurcation behaviour and geometries imperfection sensitivity investigations are included in the numerical studies presented in the next chapter.

Chapter 7

Numerical studies on the buckling of selected toroidal vessels under uniform external pressure

7.1 Introduction

The preceding chapter presented the stability of loaded toroidal shells by focussing on the linear-based eigenvalue buckling analysis. This is extended in this chapter, to include the nonlinear response and post-buckling behaviour of circular-elliptic toroidal assemblies, parabolic ogival toroids, and complete multi-shell toroidal vessels, using mainly the Abaqus FE code. An attempt is also made to address the effects of geometric parameters and initial imperfection on the failure load of each of the selected toroidal vessels. It will be shown that perfect toroidal vessels can have stable post-buckling behaviour and may, therefore, be able to resist further load beyond the estimated elastic bifurcation load and that the buckling behaviour of each of the vessels with initial eigenmode-type imperfections is dependent on certain geometrical parameters of the treated toroidal vessels under external pressure.

7.2 Buckling of uniformly pressurised circular-elliptic toroidal assemblies

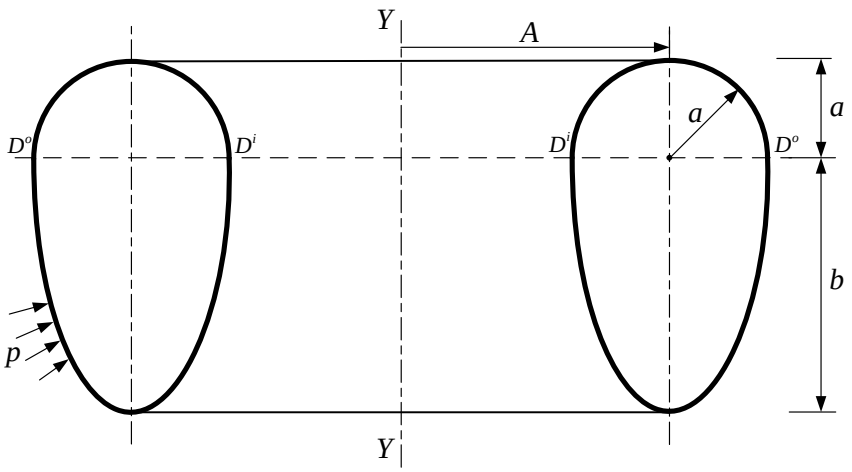

Figure 7.1. The pressurised circular-elliptic toroidal vessel

The buckling of toroidal shells with circular-elliptic cross-section is discussed in this section. Figure 7.1 shows the sketch of the vessel with the loading and geometrical parameters, which were described in Section 4.4. The vessel consists of a top semi-circular toroidal segment that is joined tangentially to a bottom semi-elliptical segment at their equatorial circles of latitude (at D^o in the outer region and D^i in the inner region of the vessel). Consequently, the total height of the vessel is $a+b$, where a is the local radius and the local (horizontal) semi-axis of the semi-circular and semi-elliptic toroidal segments, respectively, and b is the local (vertical) semi-axis of the semi-elliptic segment. The toroidal mean radius of the vessel is denoted by A and the entire external surface of the vessel is subjected to a uniform pressure, which is denoted by a patch pressure load p in the figure.

7.2.1 Finite element modelling of the circular-elliptic toroids

The FE model of the circular-elliptic toroidal vessel specimens were done in Abaqus/CAE using both the three-node quadratic axisymmetric thin shell element (SAX2) and four-node doubly curved thin shell element (S4R) for the eigenvalue analysis. The element-type that gives the smallest eigenvalues was adopted in the modified Riks algorithm (Crisfield, 1981), which is implemented in Abaqus for nonlinear static equilibrium solutions of unstable problems. The Riks algorithm has been employed here to investigate the nonlinear load-deflection behaviour of toroids, since it can detect and go beyond limit points. It is an incremental approach in which loads and/or displacemeant are varied during the path-dependent solution process. In the modified Riks algorithm, the loading is set to vary with a single scaler parameter and the response is assumed to be very smooth by limiting the increment size to avoid sudden bifurcations, so that a single equilibrium path is achieved. For static cases in Abaqus, the increment size is limited by moving a given distance (determined by the standard, convergence rate-dependent, automatic incrementation algorithm) along the tangent line to the current solution point and then searching for equilibrium in the plane that passes through the point thus obtained and that is orthogonal to the same tangent line (Abaqus 2014).

The toroidal shell material is modelled in Abaqus FE tool as elastic steel with Young modulus $E = 210\times10^9 N/m^2$, and Poisson's ratio $\upsilon = 0.3$.

7.2.1.1 Boundary conditions for the SAX2 and S4R models

Buckling results including eigenvalues and mode shapes of loaded toroidal vessels are dependent on the boundary and support conditions employed for the analysis. Different combinations of continuous boundary conditions applied at either the inner-most circle of latitude or outer-most cycle of latitude or both (i.e. at the inner and outer junctions) of the vessels were considered in a preliminary study on the effect of boundary conditions on the buckling strength of the vessel. It was observed that the buckling pressure of over restrained vessels could be as much as four times larger than the minimum buckling pressure and that the minimum buckling pressure could be obtained from more than one combination of boundary configurations.

The adopted boundary conditions leading to the lowest eigenvalues in this chapter are presented in Table 7.1 for the axisymmetric models (SAX2) and the full models (S4R). As shown in the table, the nodes at the inner meeting circle of latitude are restrained translationally in the axial (meridional), and normal directions in the SAX2 models and all the nodes at the inner meeting circle of latitude are fully restrained translationally in the S4R models.

Table 7.1. Boundary conditions at the inner-most circle of latitude

SAX2 models			S4R models					
u_r	u_z	Φ_{rz}	u_x	u_y	u_z	Φ_x	Φ_y	Φ_z
0	0	$\neq 0$	0	0	0	$\neq 0$	$\neq 0$	$\neq 0$

7.2.1.2 Mesh densities

In the usual way, a preliminary mesh convergence study was conduction for each of the element types to establish the suitable mesh densities to be adopted. The following mesh densities were found to be appropriate for the toroidal models: an approximate global seeds size of 0.25 with a maximum deviation factor of 0.1 for the axisymmetric models (SAX2); and quad-dominated local seeds of approximate size 0.25 with a maximum deviation factor of 0.1 for the full models (S4R).

7.2.2 Numerical results

Eigenvalue analysis was conducted on an externally pressurised circular-elliptical toroidal vessel with $b/a = 4.0$, $A/a = 2.0$, $a/t = 200$, and elastic properties, $E = 210 \times 10^9 N/m^2$ and $\upsilon = 0.3$ using both the SAX2 and S4R algorithms. The mesh densities and boundary conditions at the inner-most circle of latitude applied for each of the models are as discussed above. The buckling plots of the first eigenmodes obtained from the two models are shown in Figures 7.2. The axisymmetric buckling mode from the SAX2 model is shown in a deformation scale of +4 in Figures 7.2(a), while the asymmetric bifurcation buckling mode (characterised by $n = 27$ circumferential waves) from the S4R model is shown in a deformation scale of +2 in Figures 7.2(b).

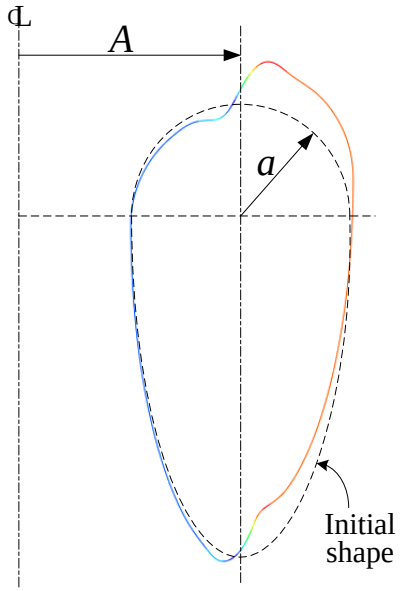

Figure 7.2 (a). SAX2 first axisymmetric buckling mode for a toroid with $b/a = 3.0$, $A/a = 2.0$, $a/t = 200$

Figure 7.2 (b). S4R first buckling mode for a toroid with $b/a = 3.0$, $A/a = 2.0$, $a/t = 200$, $n = 27$

The magnitude of each of the first buckling pressures obtained from the two approaches is given in Table 7.2. It is noticed that, for this particular example, the first eigenvalue obtained from the axisymmetric model (SAX2) is over three times larger than that from the full model (S4R). This is an indication that the lowest buckling mode of the pressurised vessel is asymmetrical about the global axis $Y-Y$ of the vessel, as seen in Figure 7.1 (b). Hence, the critical buckling pressure of interest is $p_{cr} = 0.160MPa$, (the first eigenvalue obtained from the S4R model for this case), as shown in the table.

Table 7.2. Comparison of buckling pressures from SAX2 and S4R shell models

b/a	A/a	a/t	$p(MPa)$		
			SAX2	S4R	p_{cr}
3.0	2.0	200	0.252	0.160	0.160

The critical buckling pressure was then used in the nonlinear static Riks analysis of the pressurised vessel. The program was set to terminate after 400 increments, and 0.4, 10^{-6} and 0.4 initial, minimum and maximum arc length increments. A typical load-deflection curve obtained for the toroidal vessel with $b/a = 3.0$, $A/a = 2.0$, $a/t = 200$ is shown in Figure 7.3, where the variation in the external pressure to critical buckling pressure ratio (p/p_{cr}) is

plotted against the vertical displacement of the lowest circle of latitude (nadir) per shell thickness $(\Delta y / t)$.

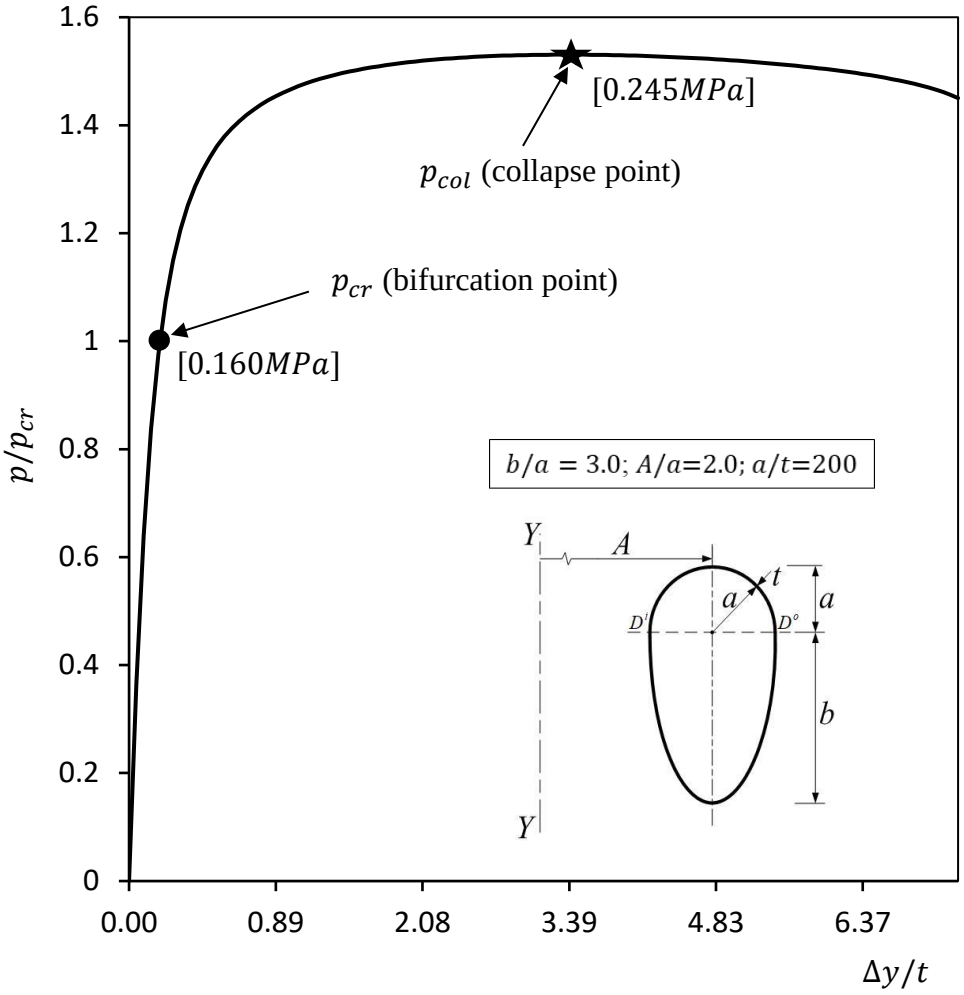

Figure 7.3. The plot of external pressure versus nadir deflection for a toroid with $b/a = 3.0$, $A/a = 2.0$, $a/t = 200$

As expected, for a thin elastic shell of the type under present investigation, the load-deflection curve in Figure 7.3 is almost linear in the pre-buckling equilibrium path from 0 to around bifurcation point. After this point, it is seen that the post-bifurcation state is stable as the pressurised vessel continued to carry more loads in a generally nonlinear manner until nonlinear buckling 'snap-through' occurred at the collapse point. This fundamental equilibrium path corresponds to the axisymmetric mode of deformation of the toroidal vessel, and rapidly growing non-axisymmetric deformations characterise the initial failure of this particular vessel.

One would notice that the collapse pressure 0.245MPa obtained from the nonlinear Riks analysis with the S4R shell model is less than the lowest (bifurcation) buckling pressure 0.252MPa obtained from eigenvalue analysis with the SAX2 shell model (see Table 7.2). This suggests that critical buckling result from SAX2 model may not always be the minimum buckling pressure for all geometrical parameters of the present vessel, and hence only results from S4R shell model is adopted in the study of the vessel.

As indicated earlier, the initial failure of the externally pressurised circular-elliptic toroid is generally characterised by rapid growing non-axisymmetric deformations (bifurcation). These asymmetry deformations spring up as bubbles within the semi-elliptic segment near the outer junction of the toroidal assembly. The buckling mode is like alternating loops going in and out around the circumference of the vessel, as shown in the buckling plot in Figure 7.3.

As seen in Figure 7.3, the bifurcation buckling is initiated in the zone with the least stiffness mainly as a result of relatively large values of the principal radius of curvature r_1 spaning through a wide spectrum of the meridional profile on the positive Gaussian side of the vessel where the failure started. The span of the meridional spectrum with large values of r_1 is a function of b/a ratio, since

$$r_1 = \pm \frac{a^2 b^2}{\left(a^2 \sin^2 \phi + b^2 \cos^2 \phi\right)^{3/2}}$$

as given in Section 4.4.4. In the meridional span under discussion, ϕ is around π and for $b/a >> 1$, the angle ϕ changes very slowly as one moves away from the equator of the semi-elliptical segment. This results in a wider meridional span with large values of r_1. The value of b/a from which the present toroidal vessel starts to fail in a non-symmetric mode by bifurcation buckling is established in Section 7.2.4 where results obtained from a parametric study on the toroidal vessel are reported. It will also be shown that toroidal vessels with a smaller b/a buckle symmetrically with $n = 0$.

7.2.3 Comparison of results

For $b/a = 1$, the circular-elliptic toroidal vessel coincides with a circular toroidal shell, which has established results from numerical and experimental studies in the literature. Some of these

results are used here to validate the present idealisation employed in the Abaqus finite element software for the buckling study of circular-elliptic toroidal vessels. For circular toroids $(b = a)$, SAX2 shell element as described earlier can be used to obtain the required critical buckling pressures, but S4R shell elements have been adopted in this section due to the reasons stated above. The mesh density and boundary conditions are the same as presented in Section 7.2.1, and the vessels are subjected to uniform external pressure. For ease of comparison, linear eigenvalue analyses were conducted on a set of circular toroids with geometrical parameters adopted from (Galletly & Błachut, 1995) where the buckling pressures were calculated using the French finite element program, INCA. The critical buckling results obtained from the present FEM approach are compared with those from the studies by Sobel & Flügge (Sobel & Flügge, 1967), Wang & Zhang (Wang & Zhang, 1991), and Galletly & Błachut (Galletly & Błachut, 1995) in Table 7.3. It could be seen that the obtained numerical results in the last column are almost identical to the results obtained from the French finite element program, INCA by Galletly & Błachut, and also compare very well with the results from the studies by Sobel & Flügge, Wang & Zhang.

Table 7.3. Comparison of critical buckling pressures for perfect circular toroidal shells under uniform external pressure.

a/t	A/a	p_{cr} (MPa)			
		Sobel & Flügge, 1967	Wang & Zhang, 1991	Galletly & Błachut, 1995	Abaqus (S4R) Present study
100	2.0	0.563	0.563	0.545	0.545
100	8.0	0.239	0.222	0.221	0.221
500	2.0	0.0126	0.0128	0.0125	0.0125
500	8.0	0.0052	0.005	0.005	0.00499

It is also observed that the critical buckling pressures computed using the long-standing algebraic expression (7.1) below, proposed by Jordan, 1973 for an externally pressurised circular toroidal shell, are in accordance with the results in the last column of Table 7.3. With the achieved excellence agreement between the results obtained from this study and the those from the literature, one can conclude that the adopted idealisation in the Abaqus finite element program for the buckling analysis of circular-elliptic toroidal vessels under external pressure in this section is very accurate.

$$p_{cr} = 0.185E\left(\frac{t}{a}\right)^{7/3}\left(\frac{a}{A}\right)^{2/3} \tag{7.1}$$

7.2.4 Parametric results

A wide range of geometric parameters of the circular-elliptical toroidal vessel was systematically considered and studied in this section to investigate the influence of the toroidal cross-sectional height to width ratio, opening ratio, and thickness ratio on the bifurcation and collapse behaviour of the toroidal assemblies.

7.2.4.1 Effects of the toroidal cross-sectional heigh-to-width ratios

Using the Abaqus finite element code, eigenvalue buckling and nonlinear Riks static analyses were conducted on circular-elliptical toroidal vessels under uniform external pressure with S4R shell models, in a similar procedure as in Section 7.2.2. This time, the boundary conditions, elastic material properties and geometric parameters are the same as above, except that various ratios of the local (vertical) semi-axis of the semi-elliptical segment b to the local radius of the semi-circular segment (or the local (horizontal) semi-axis of the semi-elliptical toroidal segment) a were investigated. The b/a ratios are 0.5, 0.75, 1, 2, 3, and 4 as shown with the other geometric parameters and corresponding failure values in Table 7.4, where the numbers in brackets denote the number of circumferential waves developed at the bifurcation.

Table 7.4. Bifurcation pressure, p_{bif} and collapse pressure, p_{col} for externally pressurised toroidal vessels with various b/a.

b/a	A/a	a/t	$p(MPa)$		
			p_{bif}	p_{col}	p_{cr}
0.5	2.0	200	-	0.0601	0.0601
0.75	2.0	200	-	0.0843	0.0843
1.0	2.0	200	0.1068(0)	0.4383	0.1068
2.0	2.0	200	-	0.1848	0.1848
3.0	2.0	200	0.1603(27)	0.2434	0.1603
4.0	2.0	200	0.0918(22)	0.1931	0.0918

In Table 7.4, it is noticed that for some values of b/a ratios, the pressurised vessels did not fail by asymmetric bifurcation. Interestingly, within this range of values of b/a, a vessel with $b/a = 1$ (which is, of course, a complete circular toroidal vessel) is found to bifurcate with

$n = 0$ circumferential waves. This externally pressurised vessel is seen to have a very stable post-buckling state as the final collapse pressure p_{col} of the vessel is over four times higher than the bifurcation buckling pressures of $0.1068MPa$. This is the highest collapse pressure to bifurcation pressure ratio obtained for the various b/a studied.

In the last column of Table 7.4, one would note that as b/a increases from 0.5, the critical pressure p_{cr} increases steadily until the highest value is attained before reducing steadily. The increase in the values of p_{cr} as b/a increases is seen among the relatively short vessels with characteristic first failure modes that are not asymmetric. For the taller vessels, the values of p_{cr} decrease as b/a increases. The critical failure mode for these tall vessels is asymmetric about the principal axis of revolution of the vessels.

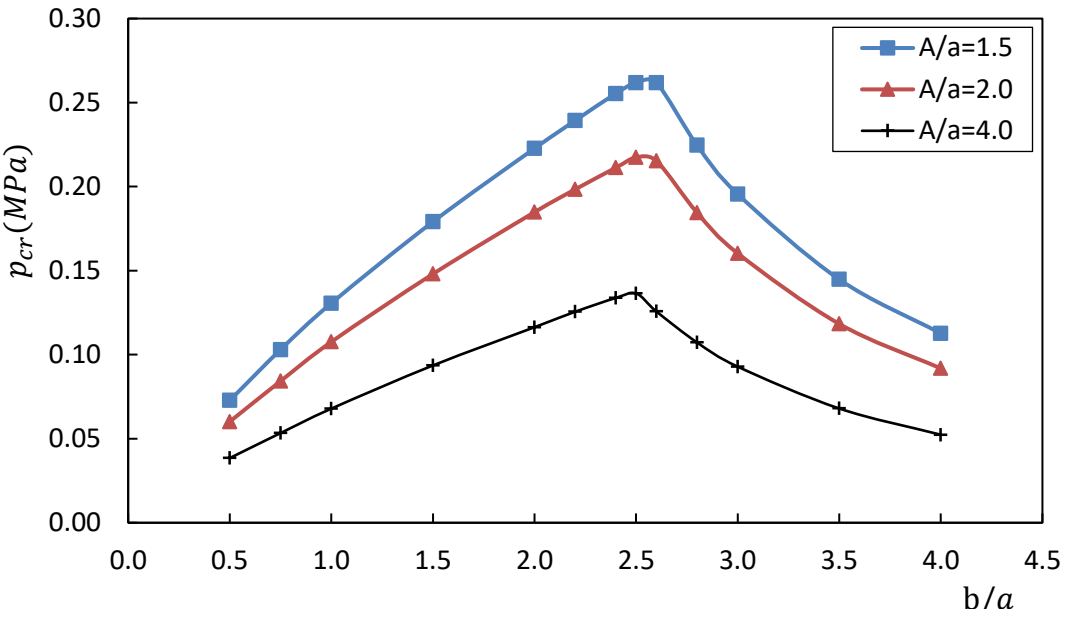

Figure 7.4. Critical buckling pressure versus b/a ratio for different toroidal opening ratios A/a

To get a clearer picture of the vessels to be called 'short' or 'tall' vessels, changes in b/a were investigated with different values of the toroidal opening ratios A/a. The values of A/a considered are relatively for compact $(A/a = 1.5)$, medium $(A/a = 2.0)$ and large diameter $(A/a = 4.0)$ geometries of the circular-elliptic toroidal vessel, while the b/a value was varied from 0.5 to 4.0, and the thickness ratio a/t, support conditions applied only to the inner-most

equator and material properties remained the same as before. The critical buckling pressures for the various b/a ratios are shown in Figure 7.4.

For the different values of A/a, results in Figure 7.4 show that the critical buckling pressure of the vessels increases steadily until a peak value is reached before reducing as b/a increases from 0, as seen before in Table 7.4. Hence, as far as first buckling pressure is concern, Figure 7.4 indicates that toroidal vessels of the type under present investigation are stronger (with peak critical buckling values) if the value of b/a is around 2.5 for $a/t = 200$. However, as mentioned earlier, the highest collapse pressure of all b/a ratios studied was obtained for circular toroids $(b/a = 1.0)$.

It is also observed that there are distinctly different critical buckling modes corresponding to the toroidal vessels on both sides of the peak pressure value in Figure 7.4. For $a/t = 200$, the critical buckling modes for toroidal geometries with b/a up to 2.5 are axisymmetrical about the global axis of revolution of the toroids with zero circumferential wave number $(n = 0)$, while those after $b/a = 2.5$ are not symmetrical about the global axis of revolution of the toroids with corresponding circumferential wave number that is always greater than zero $(n > 0)$. This transition from buckling mode with $n = 0$ to that of $n > 0$ is seen not be a function of A/a. Typical examples of these distinctive buckling modes and their corresponding sectional views are depicted in Figure 7.5 for each of the indicated circular-elliptic toroidal geometries.

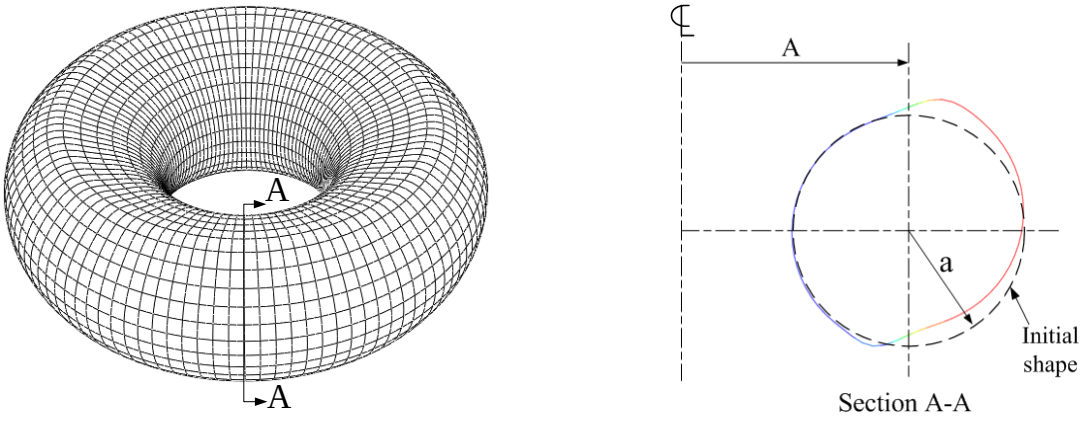

Figure 7.5(a). View of axisymmetric bifurcation buckling mode for a short toroid with $b/a = 1$, $A/a = 2$, $a/t = 200$, $n = 0$, $p_{cr} = 0.108MPa$

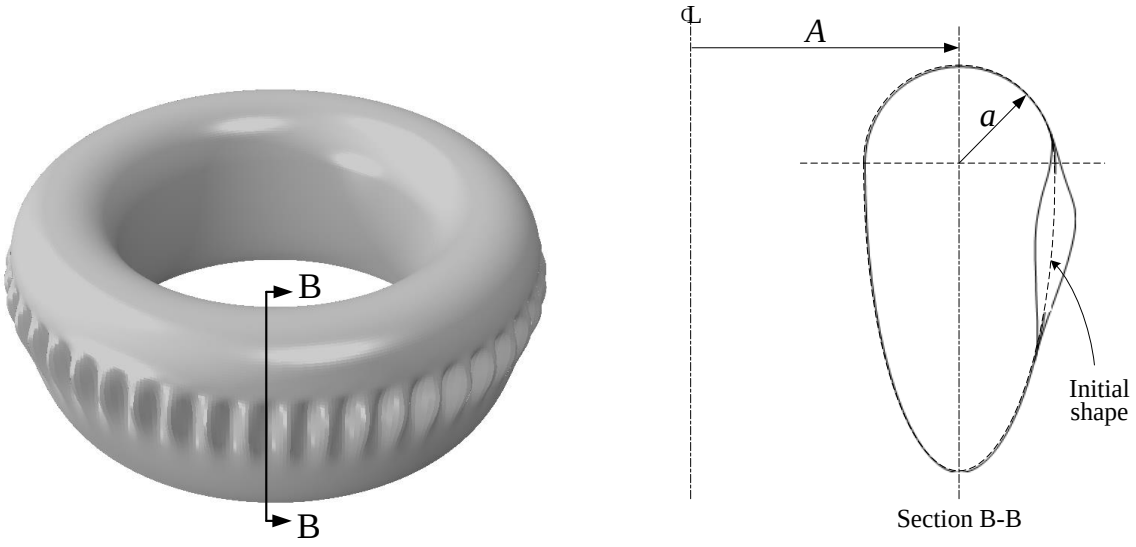

Figure 7.5(b). View of asymmetric bifurcation buckling mode for a tall toroid with $b/a = 3.0$, $A/a = 4$, $a/t = 200$, $n = 45$, $p_{cr} = 0.093MPa$

7.2.4.2 Effects of the toroidal opening ratios

The effects of change in toroidal opening ratios on buckling pressures could be seen in Figure 7.4, where results of critical buckling pressures calculated for different values of A/a are shown. It is observed that the failure pressure of a circular-elliptic toroidal vessel greatly depends on the compactness of the vessel. For the three A/a values, i.e. 1.5, 2, and 4 studied, the critical pressure values of the vessels generally reduce in that order. It shows that higher failure pressures are associated with 'compact' vessels when compared to corresponding vessels with larger opening A/a ratios.

The rate at which the buckling pressure changes with A/a was investigated for various circular-elliptic toroidal geometries. Constant values of $b/a = 2$ and $a/t = 200$ were adopted, and the toroidal opening A/a ratio was varied from 1.25 to 16. The vessels were modelled in Abaqus with S4R shell elements by adopting the mesh densities, boundary constraints, and elastic material properties of the previous examples. Eigenvalue and nonlinear static analyses were conducted on perfect toroidal vessels using a similar approach of the type discussed in Section 7.2.2, and the critical pressure values for the different toroidal opening ratios were recorded and plotted in Figure 7.6. The plot shows that critical pressure value of the pressurised vessels reduces rapidly as the opening ratio A/a increases to 4 approximately, and then steadily until A/a reaches around 9, after which the critical pressure value then reduces

slowly, so that the behaviour of the vessel will be identical to that of a long cylindrical shell, as $A/a \to \infty$.

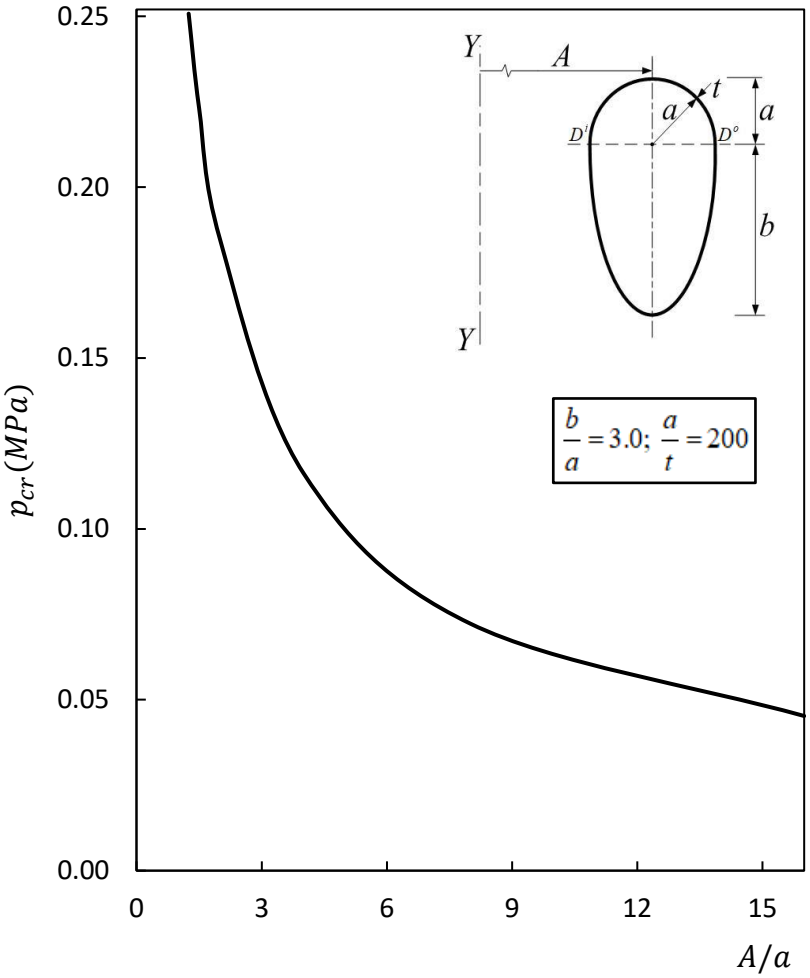

Figure 7.6. Critical buckling against A/a for toroids with $b/a=2$, $a/t=200$

7.2.4.3 Effects of wall thickness ratios

The influence of changes in wall thickness on the buckling strength of circular-elliptic toroidal assemblies was investigated with S4R shell models. The eigenvalue and nonlinear Riks analyses in Abaqus were employed in the study. Consistent with the material properties and support conditions as adopted above, toroids with $b/a=1$, $A/a=2$ and various thickness ratios were first considered. The load-deflection curves obtained for externally pressurised vessels with values of a/t ranging from 50 to 500 are shown in Figure 7.7. As before, the reference point for the deflection values was assumed to be the nadir of the vessels.

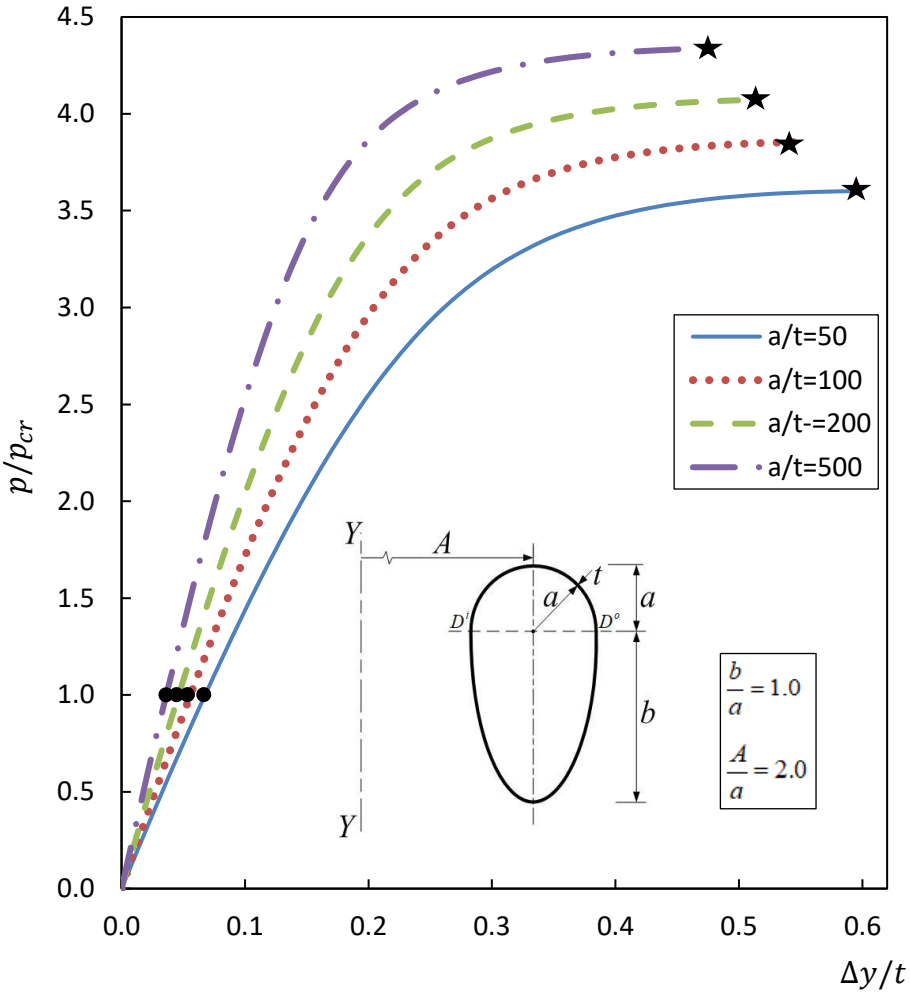

Figure 7.7. Plot of external pressures against nadir deflection for circular-elliptic toroids with different a/t values.

Table 7.5. Bifurcation and collapse pressures of externally pressurised circular-elliptical toroids with different a/t values.

b/a	A/a	a/t	$p_{bif}\,(MPa)$	$p_{col}\,(MPa)$
1.0	2.0	50	2.7996	10.0810
1.0	2.0	100	0.5470	2.1084
1.0	2.0	200	0.1076	0.4383
1.0	2.0	500	0.0127	0.0549

The position of the bifurcation pressure p_{bif} and the axisymmetric collapse pressure p_{col} are indicated in Figure 7.7. The magnitudes of these pressure loads are given in Table 7.5. As expected, it is seen that both bifurcation and axisymmetric collapse pressures of the toroidal

vessel reduce as the thickness ratio a/t increases. That is, as the wall thickness t increases, the failure pressure of the vessel increases.

The rate at which the buckling pressure changes with a/t was also investigated for various circular-elliptic toroidal geometries with three different values of b/a and a single value of $A/a = 2.0$. The toroidal thickness ratio a/t was varied from 50 to 500. The idealisation employed in the modelling of the perfect vessels, including the support conditions and material properties are the same as above. Eigenvalue and nonlinear static analyses were used for the calculation of pressure values in Abaqus, and the critical pressure values for the different values of b/a obtained are plotted against the toroidal thickness ratio a/t in Figure 7.8. The plot shows that critical pressure values of the pressurised vessels reduces spontaneously as a/t increases to 140 approximately, and then reduces slowly afterwards.

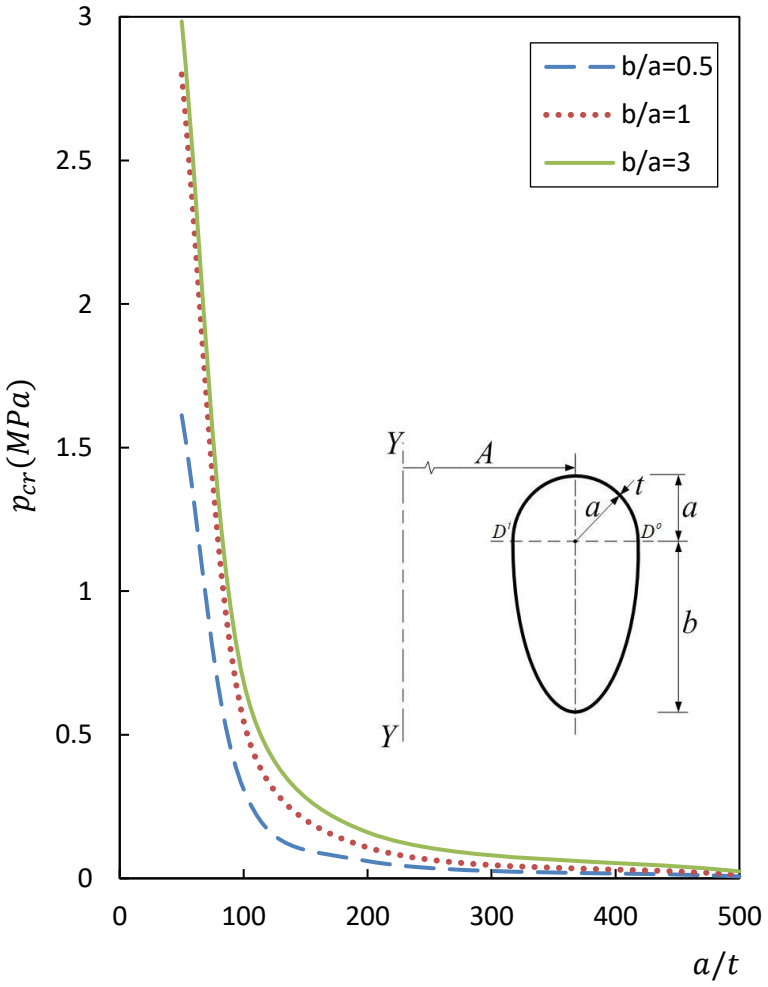

Figure 7.8. Plot of external pressures versus thickness ratios a/t for toroids with different b/a values.

7.2.5 Effects of initial geometric imperfections in circular-elliptic toroidal vessels

The possibility of buckling load reduction due to initial geometric imperfections (i.e., deviations from perfect geometry) in the form of associated eigenshapes of toroidal vessels with circular-elliptic cross-sections is examined in this sub-section. Only $a/t = 200$ toroids with $b/a = 0.5$ and 3.0 were considered for the short and tall toroids respectively, as described above. The usual support conditions applied at the inner-most circle of latitude and appropriate mesh densities were adopted for the models of the four-node doubly curved thin shell elements (S4R).

Firstly, a linear eigenvalue buckling analysis was conducted to obtain the required number of eigenmodes. The modes are characterised by either local or global circumferential and longitudinal wave numbers. By varying the imperfection amplitude (scaling factor) of the each of the modes, the selected modes are superimposed individually on the perfect toroidal shell model. This is then analysed by the modified Riks algorithm in Abaqus to obtain the failure load of the toroid. The buckling pressure results obtained for various toroids with $b/a = 0.5$ and 3.0 are presented in the following. These are shown for a range of modulated imperfection amplitude to the average wall thickness ratio, Δ/t, between 0.0 to 1.0.

7.2.5.1 Imperfection in toroids with b/a=3.0

A toroid with $b/a = 3.0$ is an example of tall circular-elliptic assemblies which usually fail by asymmetric bifurcation with $n > 0$. Each of the first ten modes obtained from the linear buckling analysis of an externally pressurised toroid with $b/a = 3.0$, $A/a = 2.0$ and $a/t = 200$ is found to have a single longitudinal wave. The eigenmodes are very closely spaced. This suggests that these may interact and lead to a lower buckling strength of the imperfect toroid. Also, odd and even mode numbers are seen be of the same eigenmodes that are only different in terms of phase due to the axis-symmetry of the present toroidal geometry, and some of the modes were found to have the same n number. Hence, the first, third and seventh eigenmodes with distinctive shapes were selected to perform checks on the sensitivity of the buckling load to eigenshape deviations from the perfect geometry. The bottom view of each of the three modes is shown in Figure 7.9, and a cross-sectional view can be seen in Figure 7.5(b), for example. The first, third and seventh eigenshapes are characterised by 27, 28, 29 circumferential waves, respectively. The deformations of the three modes are seen to be affine

to the upper zone of the semi-elliptical segment near the junction of the circular-elliptic shells of the toroidal vessel.

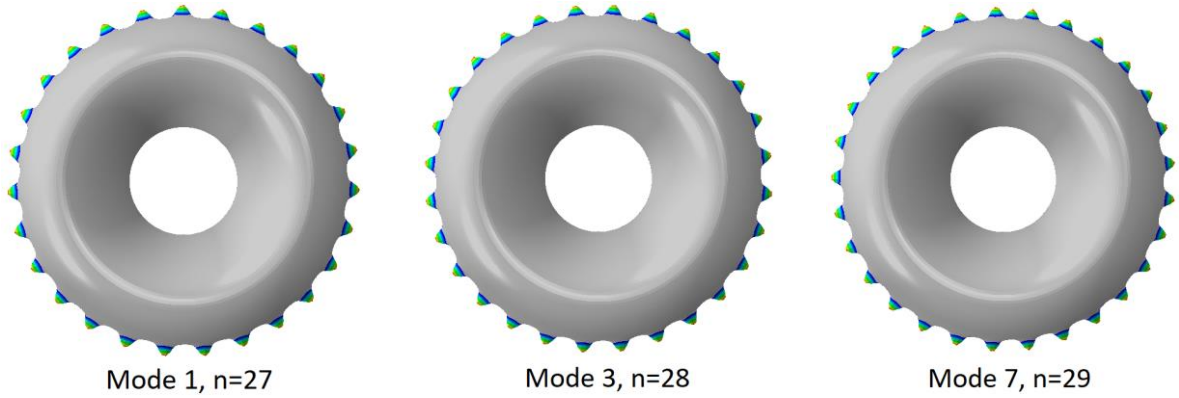

Figure 7.9. Bottom views of eigenmodes of a *tall* circular-elliptic toroid with $b/a = 3.0$, $A/a = 2.0$, $a/t = 200$

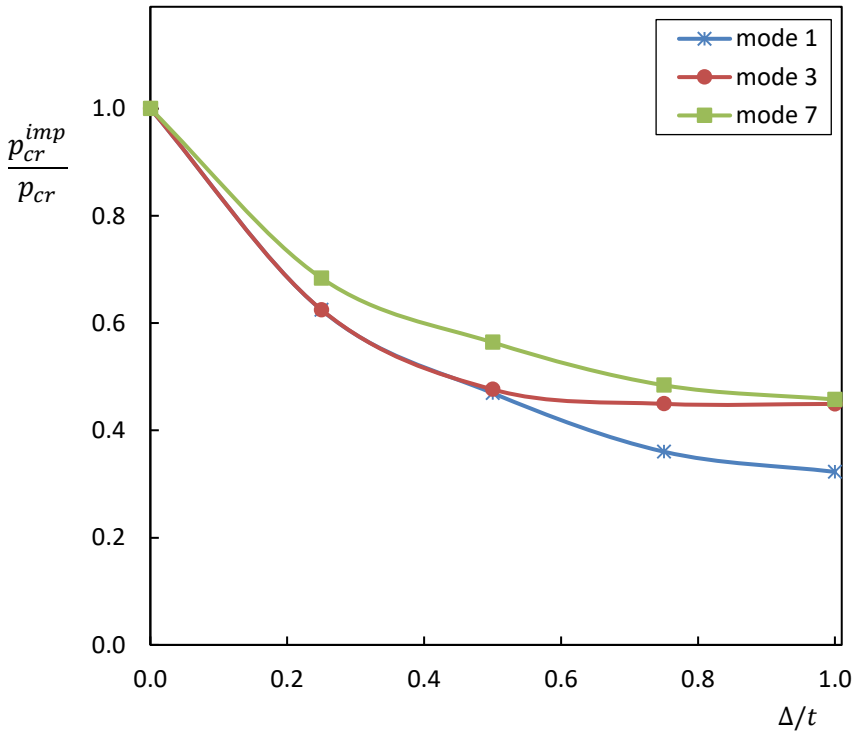

Figure 7.10. Effect of imperfection amplitude of various eigenmodes on the buckling pressures of toroids with $b/a = 3.0$, $A/a = 2.0$, $a/t = 200$

Different scaling factors of the shape deviation of each of the three eigenmodes were separately superimposed on perfect circular-elliptic toroidal vessels to assess the imperfection sensitivity

of the toroids. The effect of imperfection amplitude Δ on the collapse pressure of the toroidal vessel, using the Riks method, is shown in Figure 7.10 based on each of the buckling modes 1, 3 and 7. The figure shows the ratio of critical buckling pressures of imperfect toroids to that of corresponding perfect toroids (p_{cr}^{imp} / p_{cr}) against modulated imperfection amplitude to average wall thickness ratio, (Δ / t). The results indicate that the toroid with $b/a = 3.0$, $A/a = 2.0$ and $a/t = 200$ is sensitive to initial eigenmode type geometric imperfections within the modulated amplitude range of $0 \le \Delta / t \le 1.0$.

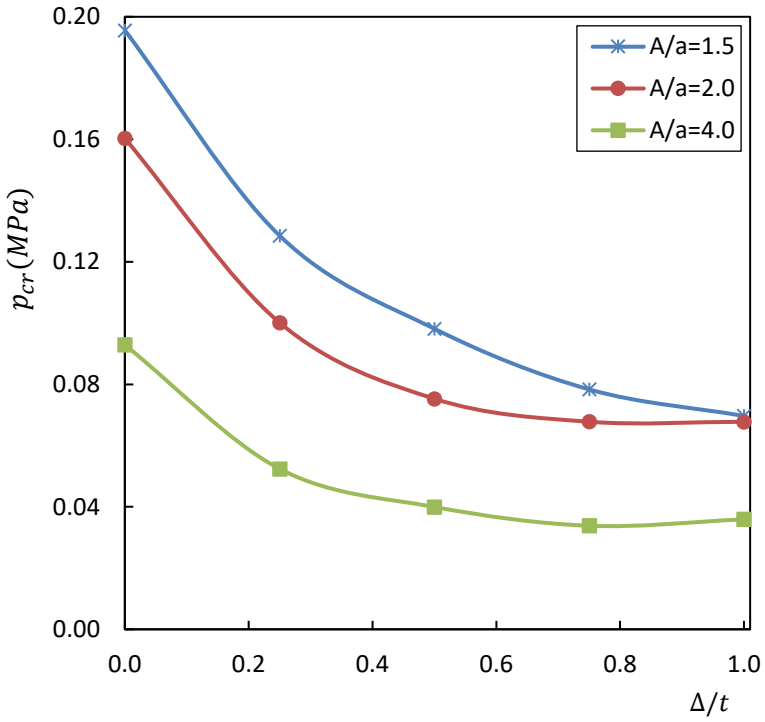

Figure 7.11. Sensitivity of critical buckling load to various amplitudes of first eigenmode imperfection in toroids with $b/a = 3.0$, $a/t = 200$ and different A/a ratios

Next, the imperfection sensitivity of toroids with three different values of A/a and a single value of each of $b/a = 3.0$ and $a/t = 200$ were investigated by superimposing various amplitude of imperfection of only the first eigenmode. On account of 'lower bound' concept of the lowest practically achievable buckling load, the first mode shape was easily chosen from the cases studied above since it leads to the largest imperfection reduction of buckling strength of the toroidal shells. Typical buckling results for each of the toroids with A/a = 1.5, 2.0 and 4.0 are plotted against various degrees of the imperfection of mode 1. These are shown in Figure 7.11. Again, this shows that toroidal shells of this type are sensitive to a single

eigenmode imperfection with a modulated amplitude of $0 \le \Delta / t \le 1.0$. One can conclude that the buckling pressures of *tall* circular-elliptic toroidal vessels with $a/t = 200$, which usually fail asymmetrically with $n > 0$, are greatly reduced by the presence of initial geometric-type imperfections with scaling factor Δ of up to the thickness of the toroidal vessels.

7.2.5.2 Imperfection in toroids with b/a=0.5

Here, the imperfection sensitivity of a $a/t = 200$ toroid with $b/a = 0.5$, which is an example of *short* circular-elliptic toroidal assemblies and usually fails with $n = 0$ is considered. An eigenvalue analysis was first conducted on the vessel with $A/a = 2$. The ensuing first, third and sixth eigenmodes with distinctive shapes were selected to perform checks on the sensitivity of the buckling load to eigenshape deviations from the perfect geometry. The bottom view of each of the three modes is shown in Figure 7.12. The first eigenmode of the vessel is characterised by $n = 0$ (this is similar to that of the circular toroid of Figure 7.5(a)). The third mode is characterised by 2 longitudinal waves and 4 circumferential waves, while the sixth mode is also characterised by 2 longitudinal waves but 5 circumferential waves. The deformation in modes 2 and 5 are seen to be affine to the semi-elliptical segment of the toroidal vessel.

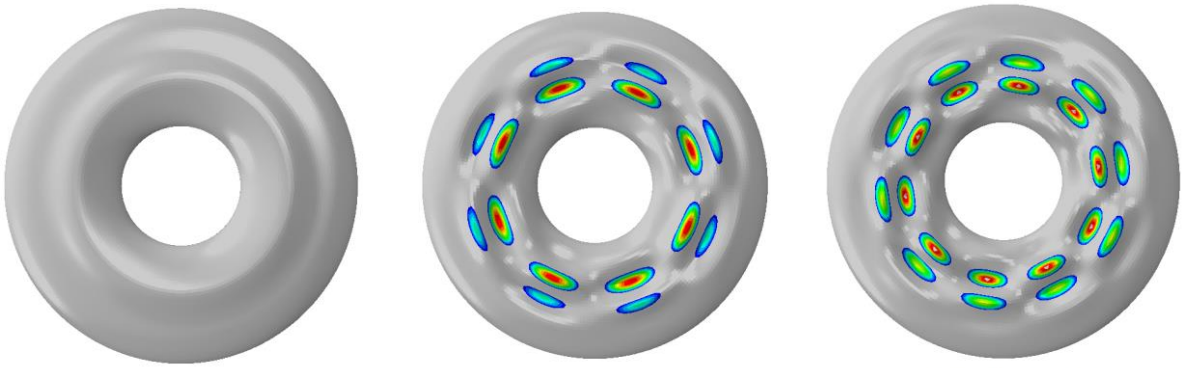

Figure 7.12. Bottom view of eigenmode of a *short* circular-elliptic toroid with $b/a = 0.5$, $A/a = 2.0$, $a/t = 200$

As in the case for $b/a = 3.0$, different scaling factors of the shape deviation of each of the three eigenmodes were separately superimposed on perfect circular-elliptic toroidal vessels to assess the imperfection sensitivity of the toroids. The effect of imperfection amplitude, Δ, on the collapse pressure of the toroidal vessel, using Riks method, is shown in Figure 7.13 based

on each of the buckling modes 1, 3 and 6. The figure shows the ratio of critical buckling pressures of imperfect toroids to that of perfect toroids (p_{cr}^{imp} / p_{cr}) against modulated imperfection amplitude to average wall thickness ratio, (Δ / t). The results indicate that the toroid with $b/a = 0.5$, $A/a = 2.0$ and $a/t = 200$ appears not be sensitive to initial eigenmode-type geometric imperfections within the modulated amplitude in the range $0 \le \Delta / t \le 1.0$.

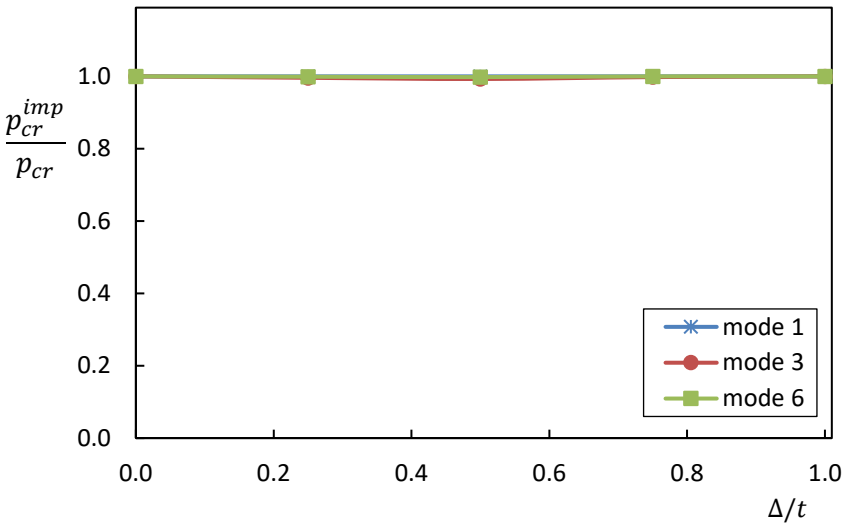

Figure 7.13. Effect of imperfection amplitude of various eigenmodes on the buckling pressures of toroids with $b/a = 0.5$, $A/a = 2.0$, $a/t = 200$

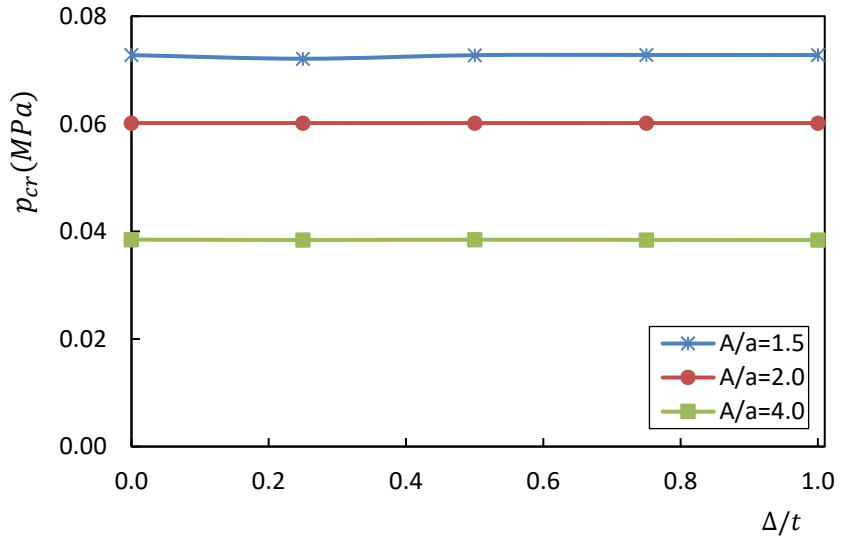

Figure 7.14. Sensitivity of critical buckling load to various amplitudes of first eigenmode imperfection in toroids with $b/a = 0.5$, $a/t = 200$ and different A/a ratios

The imperfection sensitivity of toroids with three different values A/a and a single value of each of $b/a = 0.5$ and $a/t = 200$ were also investigated by superimposing various amplitudes of imperfection of only the first eigenmode. Typical buckling results for each of the toroids with A/a = 1.5, 2.0 and 4.0 are plotted against various degrees of the imperfection of mode 1, are shown in Figure 7.14. This, again, shows that toroidal shells of this type are not sensitive to a single eigenmode imperfection with a modulated amplitude of $0 \le \Delta/t \le 1.0$.

One may infer from the figure, that the buckling pressures of *short* circular-elliptic toroidal vessels, which usually fail axisymmetrically with $n = 0$, are negligibly affected by the presence of initial geometric imperfections with scaling factor Δ of up to the thickness of the toroidal vessels. This is not the case for most structural shell elements. Blachut and his team (Błachut & Jaiswal, 1998, 2000) have shown that the critical loads of circular toroids (which of course, fall within the range of toroids under discussion), are not too sensitive to eigenshape imperfections. A quick look on the spacing of the eigenmodes of some of these short toroids, further buttresses that they are likely not affected by initial imperfections of eigenmode types, as there is a very wide difference between the first buckling mode and the other modes (which appear to be close to each other though). Other imperfection types and larger scaling factors of eigenshape imperfections, including the superimposition of more than one eigenmode may have interesting effects on the buckling pressures of these compressed vessels. Further studies in the regards may be required.

7.2.6 Summary on the buckling behaviour of circular-elliptic toroidal vessels

From the buckling study of the circular-elliptic toroidal vessel under uniform external pressure loading, it can be concluded that the vessel generally has a stable post-buckling behaviour and may, therefore, be able to resist further load beyond the elastic bifurcation loads. The buckling shape or weakest zone where the buckling normally starts from is a function of b/a. For $b/a >> 1$, the buckling initiates non-axisymmetrically in the elliptic segment near the meeting edges of the vessels before nonlinear buckling 'snap-through' occurs at a larger collapse pressure load, while toroidal vessels with smaller b/a buckle symmetrically with $n = 0$. For $b/a = 1$, the circular-elliptic toroidal vessel coincides with a circular toroid. Buckling results of pressurised circular toroidal shells in the literature were used to validate the accuracy of the adopted approach. Of all the different b/a studied, circular toroids are found to have the highest collapse pressure to bifurcation pressure ratio of up to 4. It is also observed that, as

b/a increases, the critical pressure p_{cr} increases steadily until the highest value is attained before reducing steadily. The increase in the values of p_{cr} as b/a increases is seen among the relatively short vessels with characteristic first failure modes that are not asymmetric. For the taller vessels, the values of p_{cr} decrease as b/a increases. The critical failure mode for these tall vessels is asymmetric about the principal axis of revolution of the circular-elliptic vessels. For toroids with $a/t = 200$, the critical buckling modes for toroidal geometries with b/a up to 2.5 are axisymmetric about the global axis of revolution of the toroids with zero circumferential wave number $(n = 0)$, while those after $b/a = 2.5$ are not symmetrical about the global axis of revolution of the toroids with corresponding circumferential wave number that is always greater than zero $(n > 0)$. This transition from buckling mode with $n = 0$ to that of $n > 0$ is seen not be a function of A/a.

It was also shown that higher failure pressures are associated with 'compact' vessels when compared to corresponding vessels with larger opening A/a ratios and failure loads of the toroids generally reduce as the thickness ratio a/t increases.

For the tall circular-elliptic toroidal assemblies, the various pressurised vessels were found to have closely spaced eigenmodes, and the different opening ratios A/a investigated within a modulated imperfection amplitude range of $0 \le \Delta/t \le 1.0$ were generally imperfection sensitive, with up to 70% reduction in failure load recorded in some cases. On the other hand, for the tall circular-elliptic toroidal assemblies, the parametric study on the sensitivity of the toroid under uniform external pressure generally shows that the buckling strength of a perfect tall circular-elliptic toroid is not substantially affected by the presence of eigenmode-type initial imperfections.

7.3 Buckling of externally pressurised parabolic-ogival toroidal vessels

The procedure adopted in Section 7.2 is closely followed here to study the buckling behaviour of perfect and imperfect parabolic-ogival toroidal vessels under uniform external pressure loading. The geometrical and loading parameters of the present toroidal vessel were described in Section 4.4.3. The vessel consists of two parabolic-toroidal segments - one in the outer region and the other in the inner region - meeting at the top and bottom edges, so that the cross-section of the toroidal vessel is like a parabolic-ogival, as shown in the in Figure 7.15. All terms in the figure are as described in Section 4.4.3.

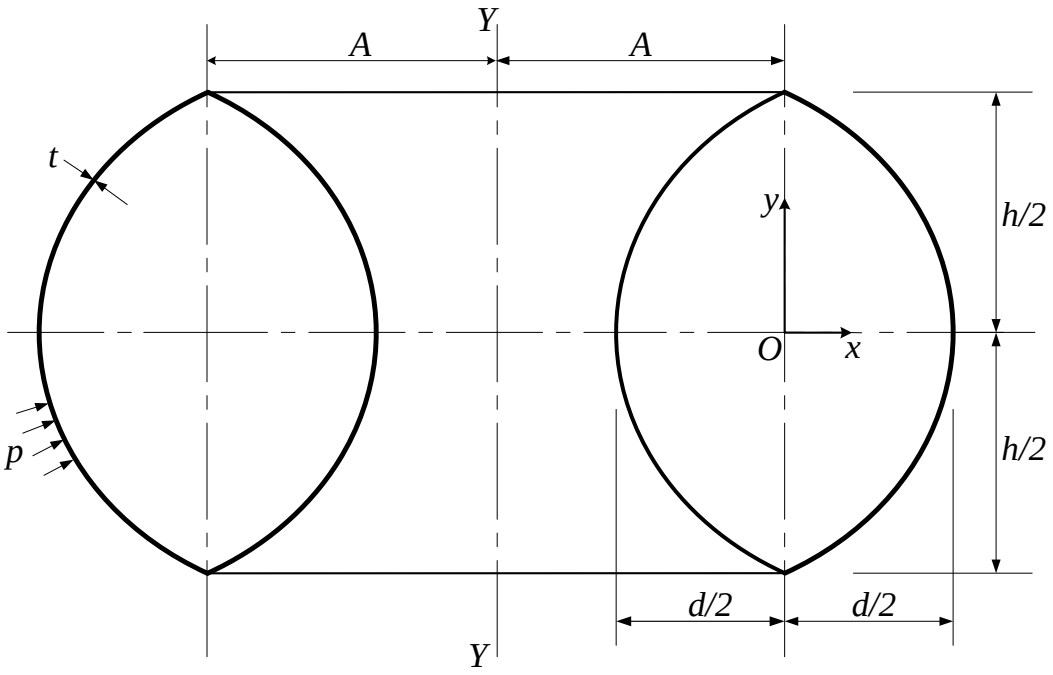

Figure 7.15. Parabolic-ogival toroid under external pressure

7.3.1 FE calculation of parabolic-ogival toroids

The accuracy of the idealisation employed in the modelling of circular-elliptic toroids in Abaqus finite element code was demonstrated by comparing the results obtained for pressurised circular toroids with those in the open literature in Section 7.2.3. The approach has been adopted here for the buckling pressure and equilibrium path calculations of parabolic-ogival toroidal vessels under the action of uniform external static pressure. As in Section 7.2.1, the parabolic-ogival toroids were modelled with both the three-node quadratic axisymmetric thin shell element (SAX2) and four-node doubly curved thin shell element (S4R) for the eigenvalue analysis. Then, the shell model that gives the smallest eigenvalues was employed in the modified Riks algorithm in Abaqus for the non-linear static analysis. The material was modelled as elastic steel with Young modulus, $E = 210 \times 10^9 N/m^2$, and Poisson's ratio $\upsilon = 0.3$. The boundary conditions employed are also similar to those of circular-elliptic toroids above, in which, the nodes at the inner-most circle of latitude (the inner equator of the vessels) are restrained translationally in the axial (meridional) and normal directions for SAX2 models and all the nodes at the inner-most circle of latitude in the inner region of the vessels are fully restrained translationally for S4R models, see Table 7.1 for example. The following mesh densities were implemented from a preliminary mesh convergence study on each of the element types: an approximate global seeds size of 0.5 with a maximum deviation factor of 0.1 for the

axisymmetric models (SAX2) and quad-dominated local seeds of approximate size 0.5 with a maximum deviation factor of 0.1 for the full models (S4R).

7.3.2 Numerical results for ogival toroids

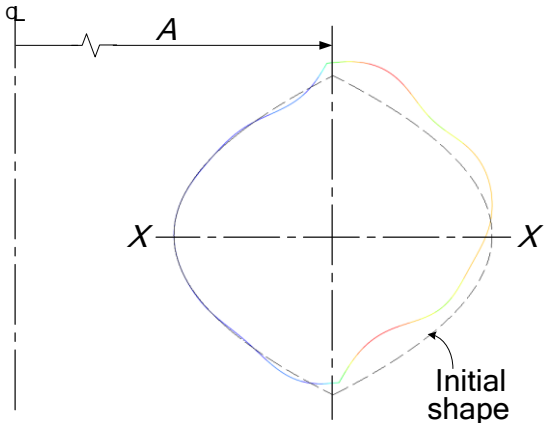

Figure 7.16 (a). SAX2 first axisymmetric buckling mode for an ogival toroidal vessel with $h/d=1.0$, $A/a=1.5$, $a/t=200$

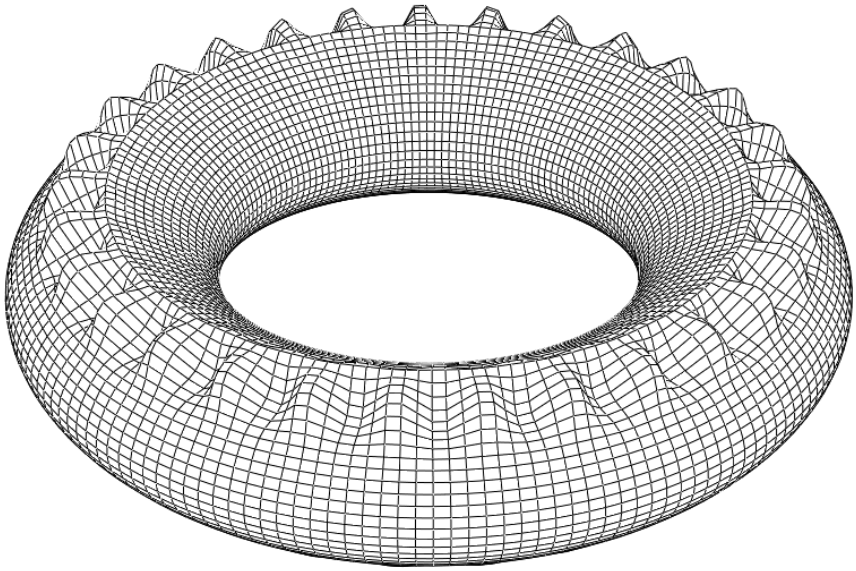

Figure 7.16 (b). S4R first buckling mode for an ogival toroidal vessel with $h/d=1.0$, $A/a=1.5$, $a/t=200$, $n=29$

Linear eigenvalue analyses were conducted on a uniformly pressurised parabolic-ogival toroidal vessel with $h/d=1.0$, $A/a=1.5$, $a/t=200$, and elastic properties, $E=210\times10^9 N/m^2$ and $\upsilon=0.3$ using both the SAX2 and S4R algorithms in Abaqus commercial finite element code. The mesh densities and the boundary conditions at the inner-

most circle of latitude applied for each of the models are as discussed above. Different buckling mode shapes corresponding to the first positive eigenvalues are obtained from both models. These are shown in Figures 7.16. The first buckling shape of the axisymmetric SAX2 model is anti-symmetrical about the equatorial plane $X-X$, is shown in Figures 7.16(a) in a deformation scale of +1, while that of the full S4R model is asymmetric about the axis of revolution with $n=29$ circumferential waves, but symmetrical about the equatorial plane of the toroid, as shown in Figures 7.16(b) in a deformation scale of +1.

The critical buckling results obtained from the SAX2 and S4R models are shown in Table 7.6. The first eigenvalue obtained from the axisymmetric models (SAX2) is over two times larger than the first eigenvalue obtained from the full models (S4R). This indicates that the SAX2 shell element may not be appropriate for calculating critical buckling pressure of the present vessel. Consequently, the S4R shell element is henceforth adopted in the study of pressurised parabolic ogival toroidal vessels. Therefore, for the present example, the critical buckling mode, as seen in Figure 7.16 (b), is asymmetrical about the global axis $Y-Y$ of the vessel and the critical buckling pressure of interest is $p_{cr}=1.053MPa$, as shown in the table.

Table 7.6. Comparison of buckling loads from SAX2 and S4R shell models

h/d	A/d	d/t	$p(MPa)$		
			SAX2	S4R	p_{cr}
1.0	1.5	200	2.716	1.053	1.053

This critical buckling pressure calculated from the linear eigenvalue analysis with the S4R shell model was used in a nonlinear Riks static analysis of the perfect pressurised vessel. The program was set to terminate after 200 increments, and 0.02, 10^{-6} and 0.4 initial, minimum and maximum arc length increments. A typical load-deflection curve obtained for the toroidal vessel with $h/d=1.0$, $A/a=1.5$, $a/t=200$ is shown in Figure 7.17, where the variation in the external pressure per critical buckling pressure (p/p_{cr}) is plotted against the vertical displacement of the lowest circle of latitude (nadir) per shell thickness $(\Delta y/t)$. The fundamental equilibrium path shows that the post-bifurcation state of the pressurised parabolic ogival toroid is stable until a collapse load of $2.351MPa$ is reached. This load is seen to be smaller than the bifurcation load $2.716MPa$ obtained from SAX2 shell model of the linear eigenvalue analysis. This, again shows that the SAX2 shell model is not suitable for the present study.

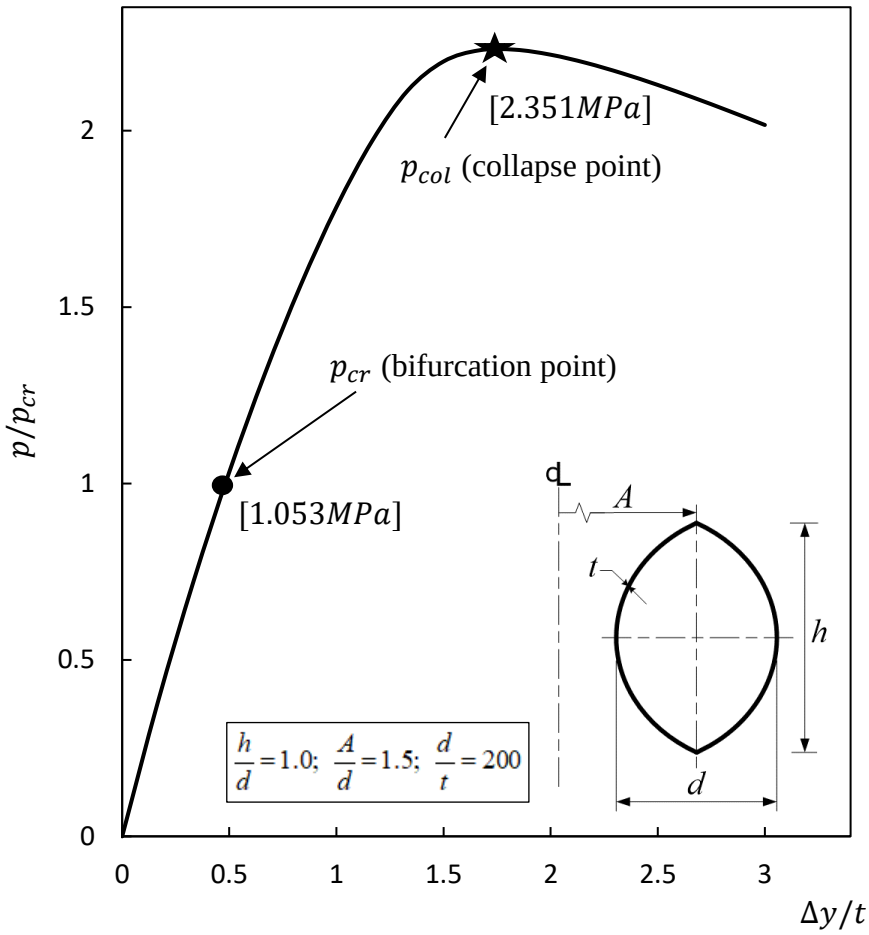

Figure 7.17. Plot of external pressure versus nadir deflection for an ogival toroid with $h/d=1.0$, $A/a=1.5$, $a/t=200$

The fundamental path of the loaded ogival toroid shown in Figure 7.17 suggests that the initial failure is characterised by rapidly growing non-axisymmetric deformations since bifurcation load is reached before the vessel experienced axisymmetric buckling (snap-through) at the collapse load. The asymmetric bubbles start springing up near the edges of the outer segment of the toroidal vessel, as shown in the buckling plot of Figure 7.16 (b). This local bifurcation buckling is not only caused by the effects of junction-edge-discontinuities at the meeting edges of the positive and negative Gaussian surfaces (outer and inner segments) of the toroid, which was discussed in Chapter 5. The weakness in the zones due to large values of the principal radius of curvature r_1 there may also be responsible for the local buckling. Recall that r_1 is largest in these zones for the outer parabolic ogival toroid, (see Section 4.4.3):

$$r_1 = \frac{h^2}{4d\sin^3\phi}$$

and, at the upper and lower poles (top and nadir) of the toroid $(\phi = \phi_o)$,

$$\phi_o = \pi - \bar{\phi}_o = \tan^{-1}\left(\frac{h}{2d}\right)$$

7.3.3 Parametric results and discussions

Systematic parametric studies were carried out to investigate: (i) the influence of toroidal cross-sectional height to width ratio, (ii) the influence of toroidal opening ratio, and (iii) the influence of wall thickness ratio on the buckling behaviour of parabolic-ogival toroidal assemblies. The results obtained from each of these investigations for the various toroidal geometries considered are presented in the following.

Table 7.7. Bifurcation pressure p_{bif} and collapse pressure p_{col} for externally pressurised ogival toroids with various h/d.

h/d	A/d	d/t	$p\,(MPa)$	
			p_{bif}	p_{col}
0.5	1.0	200	0.7749(18)	0.8547
0.75	1.0	200	1.1092(22)	2.1817
1.0	1.0	200	1.3315(22)	3.6388
2.0	1.0	200	1.3297(21)	5.0380
3.0	1.0	200	0.9174(18)	2.5574
4.0	1.0	200	0.5885(16)	0.5930

7.3.3.1 Influence of the toroidal cross-sectional heigh-to-width ratios

In the usual way, eigenvalue buckling and nonlinear Riks static analyses were conducted on various parabolic ogival toroidal vessels under uniform external pressure using the S4R shell models. The boundary conditions and elastic material properties adopted are also the same as above. The bifurcation buckling pressures and collapse loads were obtained for various pressurised ogival vessels with geometries characterised by $A/d = 1.0$, $d/t = 200$ and different local diameter to height ratio, h/d (=0.5, 0.75, 1, 2, 3 and 4). The results are given in Table 7.7, where the numbers in brackets denote the number of circumferential waves

developed at the bifurcation. All the vessels failed by asymmetric bifurcation with varying number of circumferential waves and their primary equilibrium paths show that they have stable post-bifurcation states before the axisymmetric collapse. The highest value of collapse load is seen to be associated with the $h/d = 2.0$ ogival toroid.

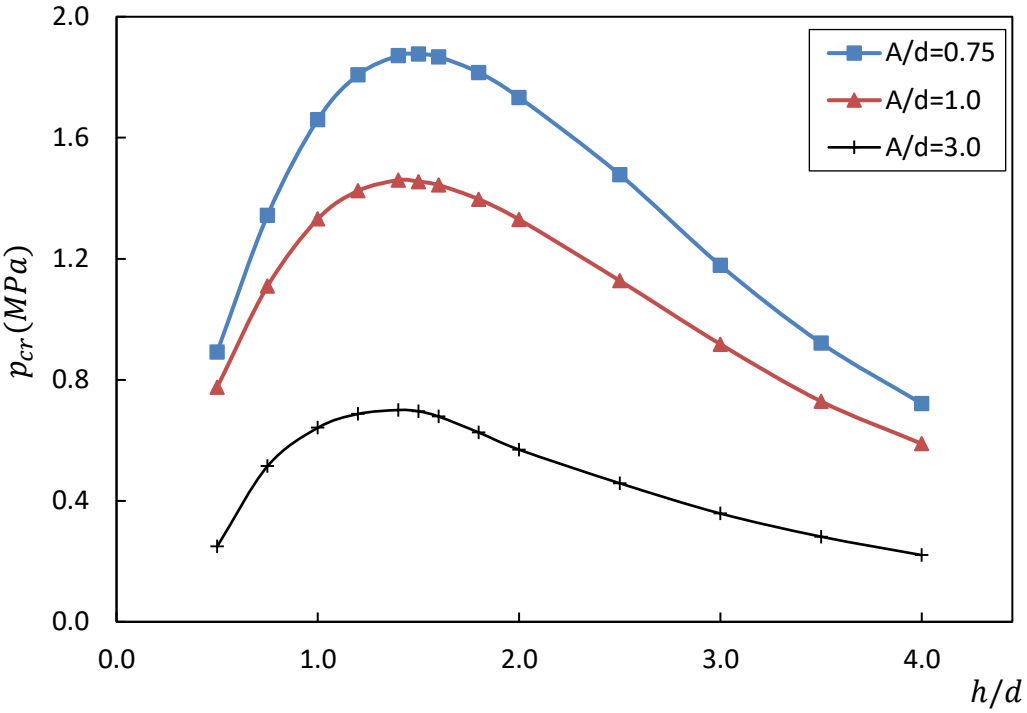

Figure 7.18. Critical buckling pressure versus h/d ratio for various toroidal opening ratios A/d

It can also be seen in the table that as h/d increases from 0.5, the critical bifurcation pressure value of the externally pressurised toroids increases steadily to a peak value at some h/d. A reduction in p_{cr} is then observed afterwards. A similar trend is noticed in the percentage difference between each of the values of the bifurcation pressure and collapse load as h/d changes. The trend in critical buckling pressure against h/d is also noticed for different values of the toroidal opening ratios A/d, as shown in Figure 7.18. The values of A/d considered are relatively for compact $(A/d = 0.75)$, medium $(A/d = 1.0)$ and large diameter $(A/d = 3.0)$ geometries of parabolic ogival toroidal vessels, while a modest range of $0.5 \le h/d \le 4.0$ is adopted for each of the toroidal opening ratios A/d. The thickness ratio $d/t = 200$, support conditions applied only to the inner equator and material properties remained the same as before. The calculated critical buckling pressures plotted against h/d for each of the various A/d ratios are shown in Figure 7.18. Note that the highest value of critical

buckling load is seen to be generally associated with the $h/d=1.5$ parabolic-ogival toroidal vessels.

7.3.3.2 Influence of the toroidal opening ratios

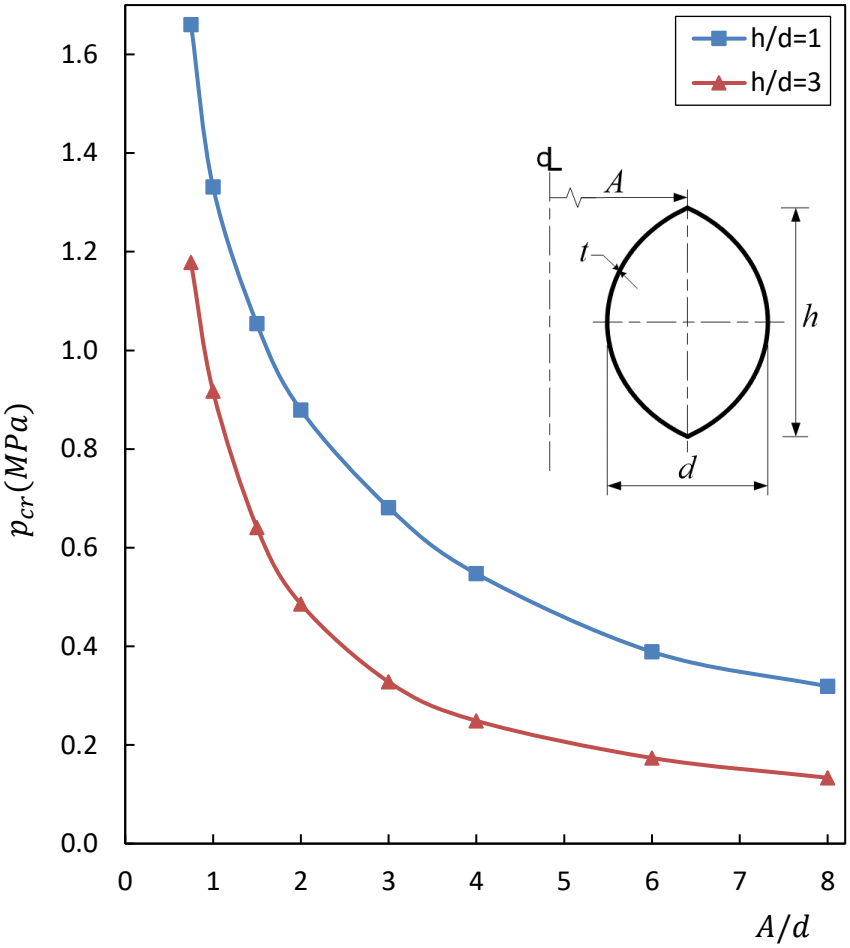

Figure 7.19. Critical buckling against A/d for various toroids with $d/t=200$

The critical buckling pressure of parabolic ogival shells changes with the compactness (opening ratio) of the vessels. This can be seen in Figure 7.18, where results of critical buckling pressures obtained for different values of A/d are shown. For the three A/d values, i.e. 1.5, 2, and 4 studied, the critical failure pressure of the vessels is seen to generally reduces as the opening ratio increases. This shows that higher failure pressures are associated with 'compact' vessels when compared to corresponding vessels with larger opening A/d ratios. The rate at which the buckling pressure changes with A/d was also investigated for various perfect ogival toroidal geometries with a single value $d/t=200$. The toroidal opening A/d ratio was varied from 0.75 to 8.0 for two different h/d values, i.e. 1.0 and 3.0. The vessels were

modelled in Abaqus with S4R shell elements for eigenvalue and nonlinear static analyses by adopting the usual mesh densities, boundary constraints, and elastic material properties of the previous examples. The critical pressure values versus opening ratio for the various toroidal vessels under external pressure obtained are shown in Figure 7.19.

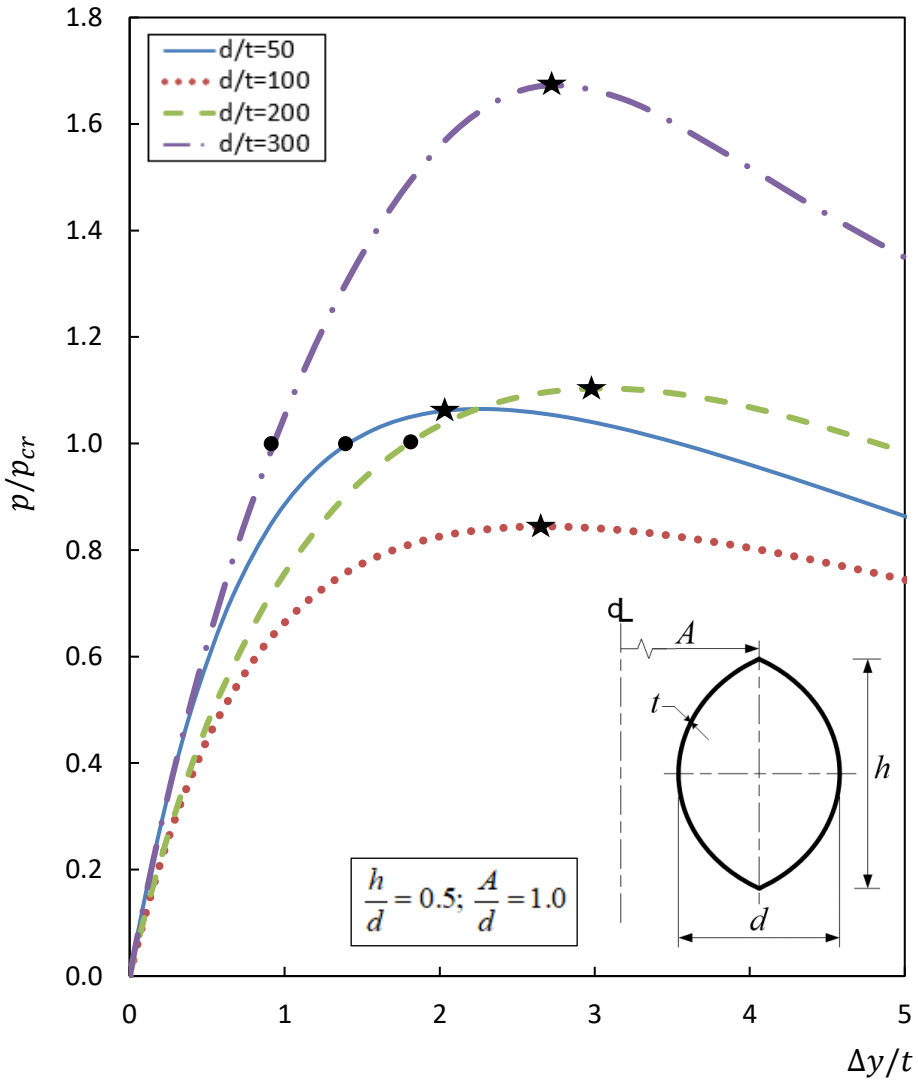

Figure 7.20. Plot of external pressures against nadir deflection of parabolic ogival toroids with different d/t values.

7.3.3.3 Influence of wall thickness ratios

Here, the influence of d/t on the critical buckling pressure of externally pressurised parabolic ogival shells was investigated by adopting the same modelling approach as previous sections and varying d/t from 50 to 300. The local cross-sectional height to width ratio h/d and the toroidal opening ratio A/d employed for each of the toroidal vessels are 0.5 and 1.0,

respectively. The load-deflection curves obtained from the nonlinear Riks analyses in Abaqus after conducting a linear eigenvalue analysis for each of the vessels are given in Figure 7.20. The primary equilibrium path of the ogival vessel with $d/t = 100$ indicates that the vessel reaches axisymmetric collapse load without bifurcating like the other ogival toroids studied here.

The position of the bifurcation pressure, p_{bif} and the axisymmetric collapse pressure, p_{col} and are indicated in Figure 7.20 with their usual signs. The magnitudes of these pressure loads are given in Table 7.8. As expected, it is seen that axisymmetric collapse pressure of the toroidal vessel reduces as the thickness ratio d/t increases. That is, as the wall thickness t increases, the failure pressure of the vessel increases.

Table 7.8. Bifurcation and collapse pressures of externally pressurised ogival toroids with different d/t values.

h/d	A/d	d/t	$p_{bif}\,(MPa)$	$p_{col}\,(MPa)$
0.5	1.0	50	11.645(0)	12.3990
0.5	1.0	100	-	2.7495
0.5	1.0	200	0.7749(18)	0.8547
0.5	1.0	300	0.2735(22)	0.4572

The rate at which the buckling pressure changes with d/t was also investigated for various parabolic-ogival toroidal with three different values of h/d and a single value of $A/d = 1.0$. The toroidal thickness ratio d/t was varied from 50 to 500. All the toroids were assumed to be perfect and supported in the usual manner. Eigenvalue and nonlinear static analyses were used for the calculation of pressure values in Abaqus, and the critical pressure values for the different values of h/d obtained are plotted the toroidal thickness ratio d/t in Figure 7.21. The plot shows that the critical pressure values of the pressurised vessels reduces spontaneously as d/t increases to 140 approximately, and then slowly afterwards, just as in the case of circular-elliptic toroidal assemblies.

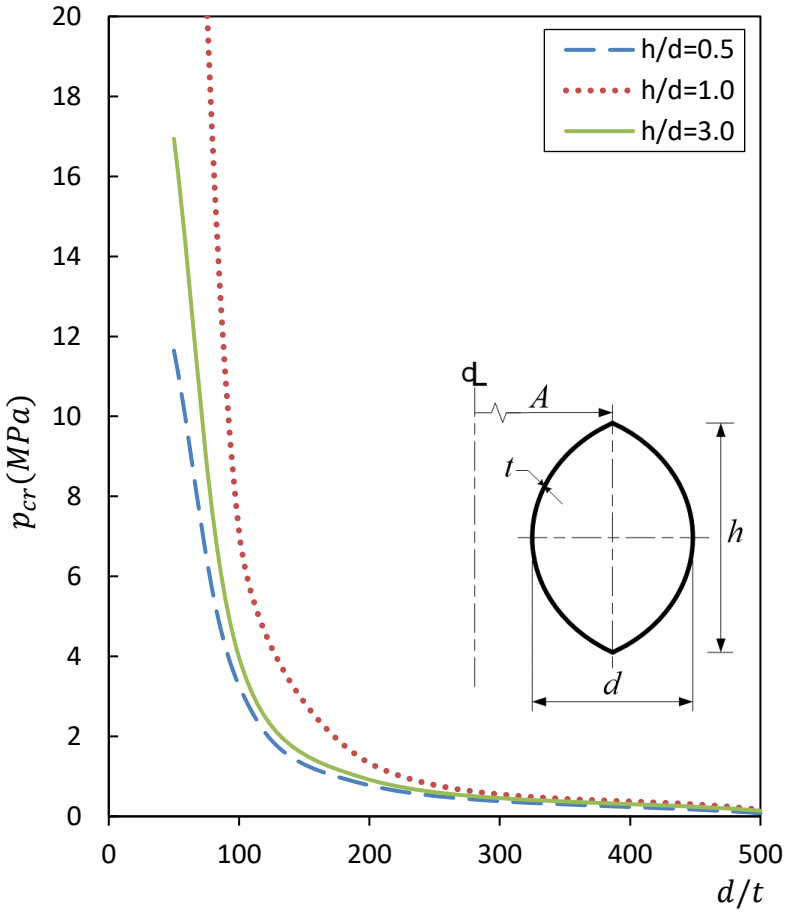

Figure 7.21. Plot of external pressures versus thickness ratio d/t for ogival toroids with $A/d=1.0$ and different h/d values.

7.3.4 Initial geometric imperfections sensitivity of ogival toroids

Geometric imperfections in structural elements can take several forms. Here, as adopted for circular-elliptic toroidal assemblies above, only the effects of initial geometric imperfections in the form of associated eigenshapes on the failure loads of externally pressurised toroidal vessels with parabolic ogival cross-section is examined. It has been established that the failure pressure of some toroidal vessels with certain geometrical parameters are not substantially affected by the presence of eigenmode imperfections, unlike most thin-walled structures. For the present parabolic ogival toroids, attention is focussed on a single h/d ratio. The aim is mainly to show if there is the possibility of buckling load reduction in this class of toroidal vessels with eigenmode-type imperfections. $h/d=1.5$ ogival toroids, modelled with four-node doubly curved thin shell elements (S4R) with appropriate mesh densities and the usual boundary constraints applied at the inner-most circles of latitude, were employed in the study.

A series of eigenvalue buckling analyses were conducted to obtain the required number eigenshapes. The selected modes with various imperfection amplitudes (scaling factor) are then superimposed individually on the perfect toroidal shell model in the modified Riks algorithm to obtain the failure pressures of the toroids.

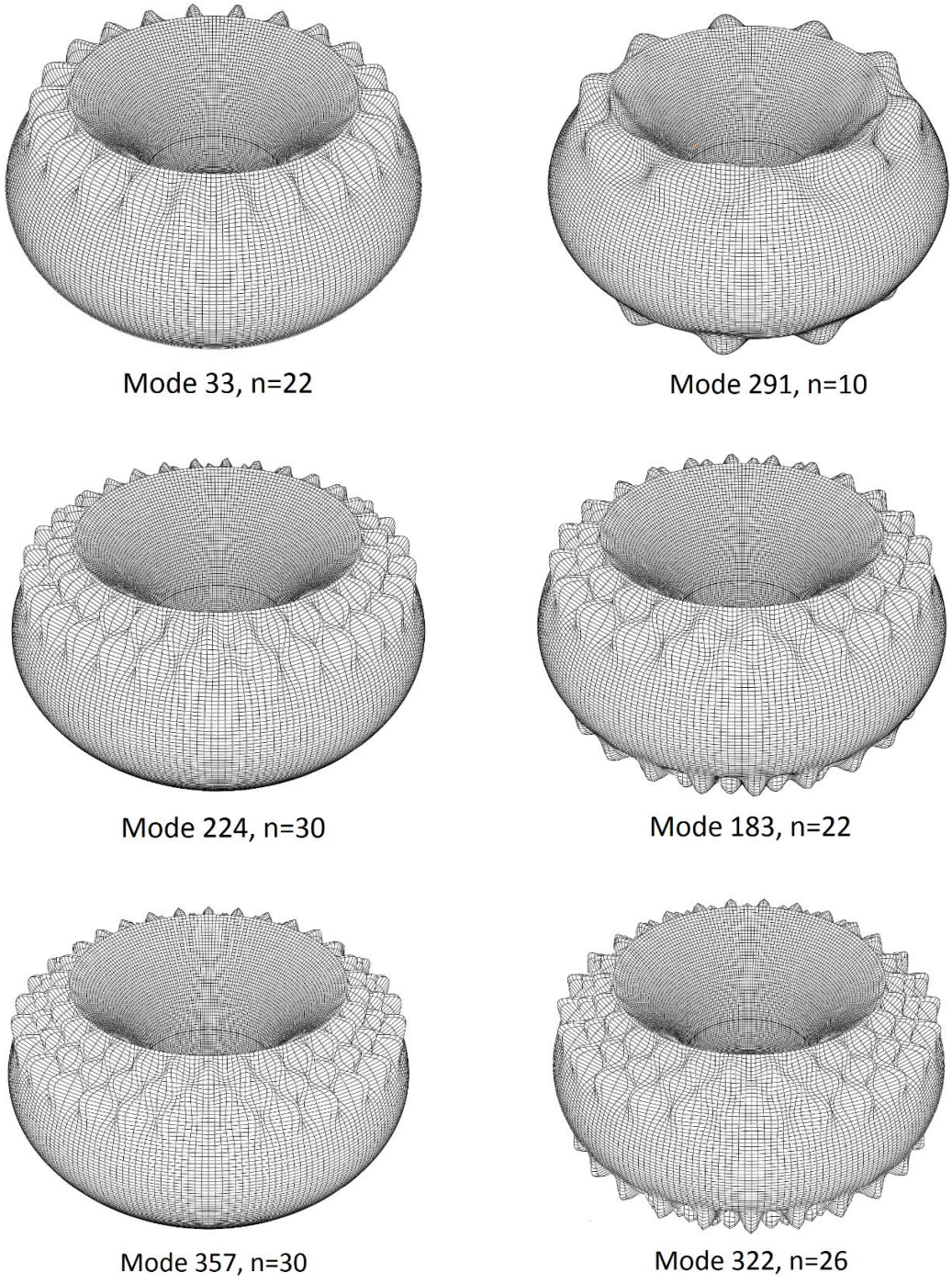

Figure 7.22. Selected eigenmodes for the imperfection sensitivity study of ogival toroid with $h/d = 1.5$, $A/d = 1.0$, $d/t = 200$

Closely spaced eigenmodes were obtained from the linear eigenvalue analysis of an ogival toroid with $h/d=1.5$, $A/d=1.0$ and $d/t=200$. This initially suggested that the buckling pressure of the vessel will likely be affected by the presence of eigenmode imperfections. Figures 7.22 shows distinctive asymmetric eigenmodes with positive eigenvalues that were selected to perform checks on the sensitivity of the buckling load to eigenshape deviations from the perfect geometry. Each of the modeshapes has different circumferential and longitudinal wave numbers at the upper and lower regions of the outer segment of the ogival vessels, as shown.

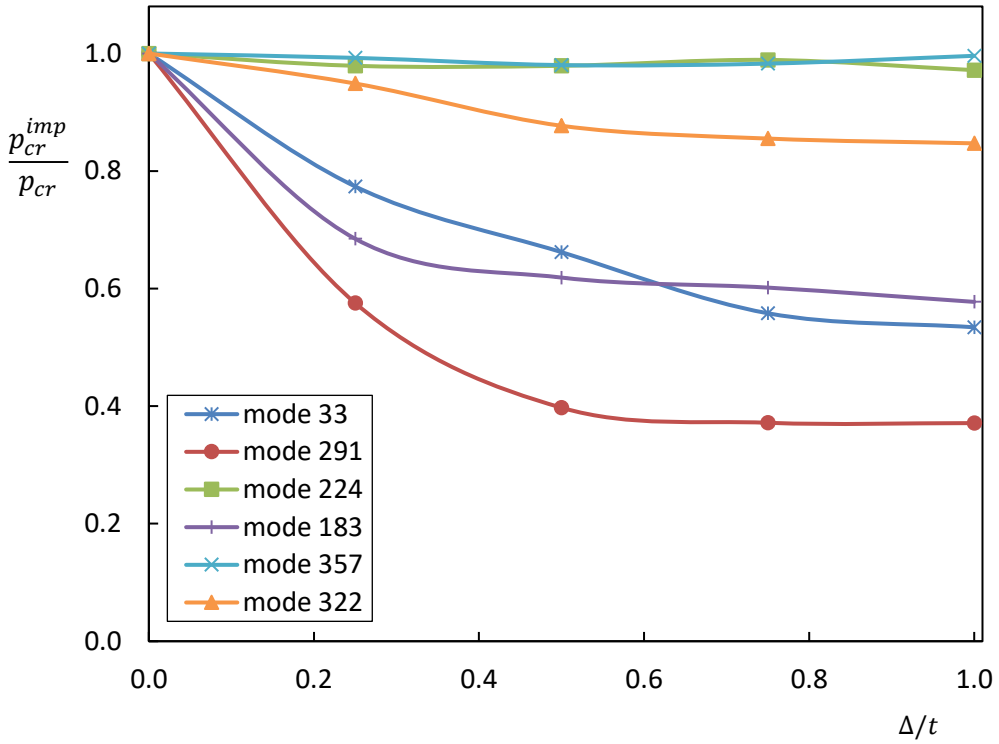

Figure 7.23. Effect of imperfection amplitude of various eigenmodes on the buckling pressure of ogival toroids with $h/d=1.5$, $A/d=1.0$, $d/t=200$

Different scaling factors of the shape deviation of each of these six eigenmodes were separately superimposed on perfect ogival toroidal vessels to assess the imperfection sensitivity of the toroids. The effect of imperfection amplitude Δ on the buckling pressure of the toroidal vessel, is shown in Figure 7.23, based on each of the selected buckling modes. The figure shows the ratio of critical buckling pressures of imperfect toroids to that of perfect toroids (p_{cr}^{imp}/p_{cr})

against modulated imperfection amplitude to average wall thickness ratio, (Δ/t). The results indicate that the toroid with $h/d=1.5$, $A/d=1.0$ and $d/t=200$ is generally sensitive to eigenmode-type initial geometric imperfections within the modulated amplitude in the range $0\le\Delta/t\le1.0$. The effect is seen to be negligible for eigenmodes 224 and 357.

Parabolic ogival toroidal geometries of opening ratios $A/d=0.75$ and 2.0 were also studied in addition to that of $A/d=1.0$ above, while $h/d=1.5$ and $d/t=200$ were kept constant. This was to see if $h/d=1.5$ ogival toroids with other A/d ratios are sensitive to initial geometric imperfections. A similar approach as described above was adopted in the study, but only the first buckling mode with positive eigenvalue was used as the imperfection shape. Different scaling factors of each of the first modes were separately superimposed with the corresponding perfect toroidal geometries. Typical buckling results for each of the toroids with A/d = 0.75, 1.0 and 2.0 are plotted against various degrees of the imperfection of the first mode are shown in Figure 7.24. This shows that ogival toroidal shells with various opening ratios are sensitive to a single eigenmode imperfection with the modulated amplitude of $0\le\Delta/t\le1.0$. The results suggest that the buckling pressures of ogival toroidal vessels can be substantially reduced by the presence of eigenmode-type initial imperfections with scaling factor Δ of up to the thickness of the toroidal vessels.

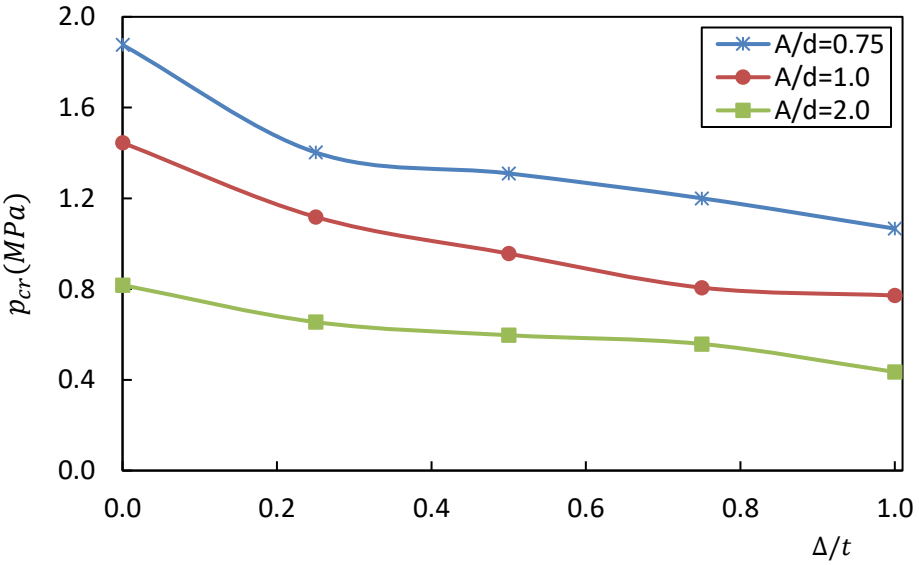

Figure 7.24. Sensitivity of critical buckling load to various amplitudes of first eigenmode imperfection in ogival toroids with $h/d=1.5$, $d/t=200$ and different A/d ratios

Similarly, the sensitivity of buckling pressure to the initial geometric imperfections was computed for externally pressurised ogival toroidal shells with two different thickness ratios $d/t=100$ and 500. $h/d=1.5$ and $A/d=1.0$ were kept constant for the two toroidal geometries. Imperfections were assumed to have an affinity with the corresponding first eigenmode. Shape deviations were taken as modulated eigenmodes, and then they were superimposed on the perfect toroidal geometry. The load-bearing capacity was calculated numerically for imperfections amplitude of $0\le\Delta/t\le1.0$. The results are shown in Figure 7.25. This indicates that buckling pressures of ogival toroidal shells with different thickness ratios are sensitive to eigenmode imperfections.

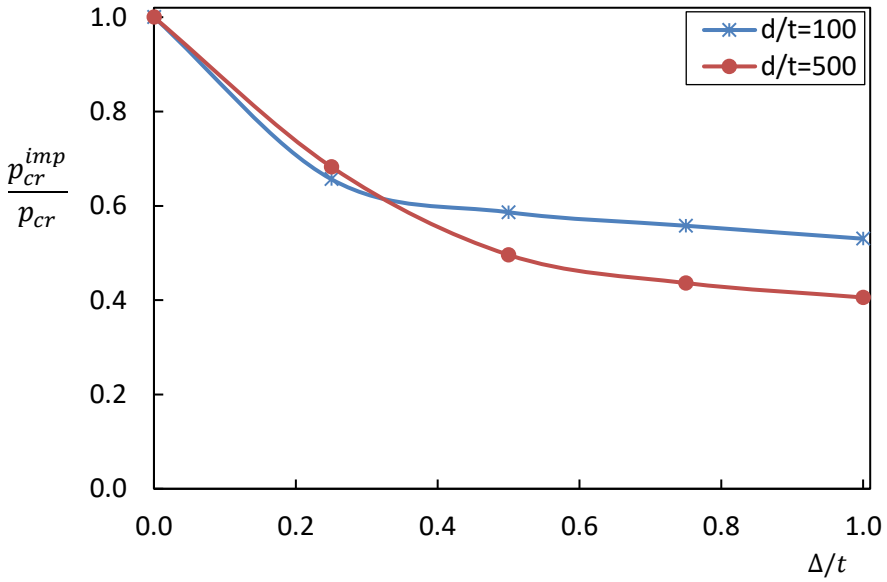

Figure 7.25. Effect of imperfection amplitude of the first eigenmode on the buckling pressure of ogival toroids with $h/d=1.5$, $A/d=1.0$ and different d/t ratios

7.3.5 Summary on the buckling behaviour of parabolic ogival toroids

It can generally be concluded that buckling initiates asymmetrically in the weakest zones near the edges of the outer segment of a parabolic ogival vessel under uniform external pressure before axisymmetric buckling (snap-through) occurs at a higher load. This suggests that the vessel has a stable post-bifurcation response and the shell thickness around the weak zones can be systematically enhanced so that the vessel could be stiffer. It was noted that, for the geometrical and loading cases studied, both axisymmetric collapse pressure and critical failure pressure of parabolic ogival toroidal vessel reduces as the thickness ratio and opening ratio

increase, respectively, indicating how the scale of the structure will affect its design. Also, the highest value of the critical buckling load was found to be associated with parabolic ogival toroidal vessels with $h/d = 1.5$.

The parametric study on the sensitivity of failure loads due to the presence of initial imperfections in the form of eigenmodes in a parabolic ogival toroid under uniform external pressure generally reveals that the buckling strength of a perfect parabolic ogival toroid greatly reduces if the shell contains initial imperfections. The various pressurised vessels were found to have closely spaced eigenmodes, and the different thickness ratios d/t and opening ratios A/d investigated within a modulated imperfection amplitude range of $0 \le \Delta/t \le 1.0$ were generally imperfection sensitive, with up to 64% reduction in failure load in some cases.

7.4 Buckling of complete multi-shell toroidal vessels under uniform pressure

This section examines the buckling behaviour of externally pressurised complete multi-shell toroidal vessels. An approximate critical buckling formula was obtained for the vessel without the top and bottom segments in Chapter 6. This formula is shown here to be reasonably accurate for the estimation of the lowest buckling pressure of complete multi-shell toroidal vessels which include the top and bottom toroidal segments, depending on the value of the rise ratio λ_r of the middle segments of the complete toroidal vessel. The modified Riks method in Abaqus FE code is employed to study the response of the externally pressurised multi-shell toroids including the post-buckling state, which is not available in the eigenvalue analysis results. The section ends with the imperfection sensitivity study of the vessel by only considering the eigenmode-type imperfections. In line with the other sections of this chapter, Abaqus FE is the main tool used here, although ADINA FE was employed in Chapter 6 to validate the analytical buckling solution of the present toroidal shell form. Within the framework of this these, similar results are obtained from both FE tools, especially for linear analysis.

The multi-shell toroid consists of two outer and inner toroidal segments that are tangentially connected at the upper edges (junctions D_1^o and D_1^i) to the edges of a top toroidal segment, and at the lower edges (junctions D_2^o and D_2^i) to the edges of a bottom toroidal segment, as described in Chapter 4, see also Figure 7.26. The uniform pressure loading acts on the entire

external surface of the vessel, but this is denoted by a patch pressure loading p in the figure. The shell-wall thickness t is assumed to be constant throughout the vessel, and other terms in the figure, are as previously defined. The rise ratio λ_r of the middle segments was given as

$$\lambda_r = \frac{\sin\left(\pi/2 - \phi_1\right)}{1 - \sin\phi_1}$$

for toroids, which are symmetrical about the equatorial plane. The pressurised vessel is assumed to be made of elastic steel with Young modulus $E = 200\times10^9\, N/m^2$ and Poisson's ratio $\upsilon = 0.3$.

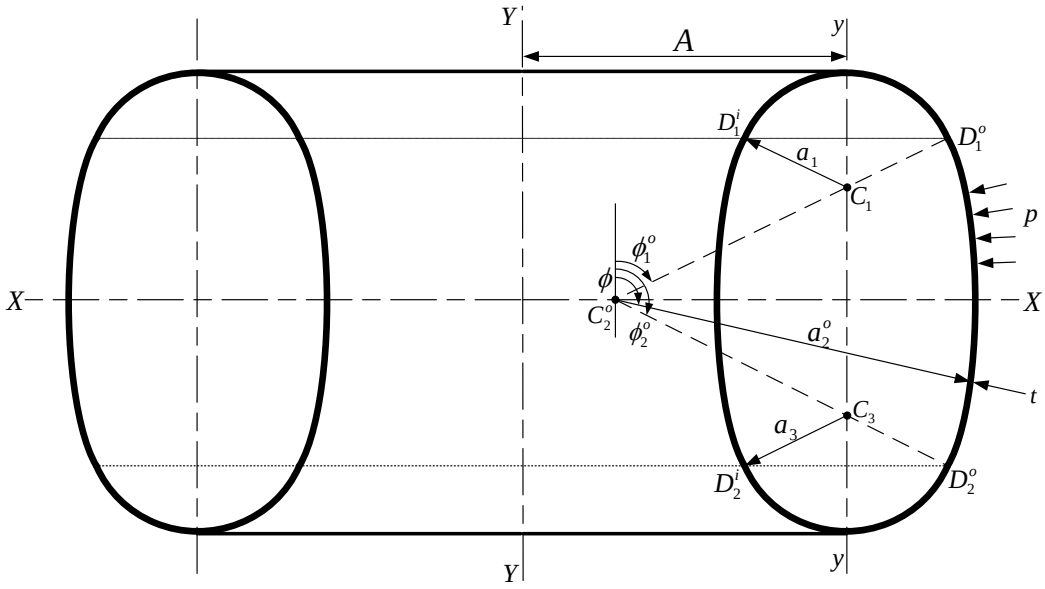

Figure 7.26. Sketch of a pressurised multi-shell toroid

7.4.1 Numerical modelling of multi-shell toroids

The present toroidal vessel under consideration is symmetrical about both the axis of revolution $Y-Y$ and the equatorial plane $X-X$, and is subjected to a uniform axisymmetric pressure loading. However, preliminary studies show that the first buckling mode of some geometrical parameters of the vessel does not buckle axisymmetrically. Hence, the three-node quadratic axisymmetric thin shell element (SAX2) is not used here. Rather, four-node doubly curved thin shell element (S4R) is employed throughout for the modelling of the pressurised multi-shell toroidal vessels, in the linear eigenvalue analysis and the nonlinear Riks static analysis within the framework of Abaqus code. The S4R element mesh of quad-dominated local seeds of

approximate size 0.75 with a maximum deviation factor of 0.1 was adopted for the study, and the toroidal material was modelled as elastic steel with the properties given above.

To replicate the boundary conditions adopted in the formulation of the critical buckling formula in Section 6.4.5, no rotational/displacement constraints are specified in the Abaqus eigenvalue analyses here, since the vessels under discussion are geometrically symmetric and are also loaded axisymmetrically. However, boundary conditions are required in the Abaqus nonlinear Riks static analyses, so a set of configurations leading to the lowest buckling load as employed in Sections 7.2 and 7.3 above, was adopted here for the nonlinear analyses. That is $u_x = 0$, $u_y = 0$, $u_z = 0$, $\Phi_x \neq 0$, $\Phi_y \neq 0$ and $\Phi_z \neq 0$, where all the nodes at the inner equator of the vessels are fully restrained translationally for the S4R models. It turns out that the critical buckling values obtained with this boundary condition and without constraints are the same.

7.4.2 FE Calculations and comparison of results

Externally pressurised complete multi-shell toroids with constant $a = 30m$ and $a_1 / t = 160$ and other geometrical parameters are shown in Table 7.9 were modelled in Abaqus FE using S4R shell elements and boundary conditions as described above. The toroidal parameters are the same as those treated in Chapter 6, for pressurised multi-shell toroids without the top and bottom segments, for ease of comparison. Where appropriate, linear eigenvalue and nonlinear collapse (Riks) analyses were used to predict the magnitude of the critical buckling pressures of the loaded complete toroids. The obtained results from the FEM analyses are given in Table 7.9 with those obtained in Chapter 6 for the toroids without the top and bottom segments, using the proposed critical buckling formula (see Section 6.4.5):

$$p_{cr} = \underset{m,n}{Min}\left[\frac{\Omega - \lambda\Psi}{\mathrm{P}}\left\{\frac{Et^3}{12\left(1-\upsilon^2\right)}\right\}\right]$$

Similar to Table 6.1 of Section 6.4.6 where critical buckling results for toroids without top and bottom segments obtained using FEM and analytical formula were compared, Table 7.9 shows that, even for the complete vessels, the buckling predictions from both methods compare excellently well for toroids with $\lambda_r > 4.0$, despite the approximations adopted in the derivation of the critical buckling formula. Hence, the proposed formula can simply be used for the estimation of critical buckling results for toroidal geometries with $\lambda_r > 4.0$. Although the

adopted finite element modelling approach has been validated in Section 7.2.3, one can also mention at this juncture that the buckling formula has provided an alternative means of validating the FEM employed in this chapter.

Table 7.9. Comparison of analytical and S4R shell Abaqus models buckling pressures

λ_r	$a_2(m)$	$\phi_1(^o)$	$a_1(m)$	$p_{cr}(MPa)$		Diff. (|%|)
				ANA	FEM	
2	30.39	37.60	12.90	0.3971	0.1572	60.4
4	51.66	61.93	8.92	0.1715	0.1233	28.1
6	74.99	70.08	8.32	0.1117	0.1179	5.6
8	98.76	75.75	8.12	0.0842	0.0869	3.2
16	195.29	82.85	7.93	0.0435	0.0428	1.6
32	389.33	86.42	7.89	0.0245	0.0242	1.2

Vessels with $\lambda_r < 4.0$ are found to be generally stiffer than those with $\lambda_r > 4.0$. This mainly due to the value of the radius of curvature r_1 in the weak segment, which is typically the middle segments of the vessel.

Two toroidal geometries - one from from $\lambda_r < 4.0$ and another from $\lambda_r > 4.0$ - were analysed with nonlinear Riks method to study the response of the toroids under stepwise pressure loading. In particular, toroids with $\lambda_r = 2.0$ and 6.0 were studied. The critical buckling pressures obtained from the eigenvalue analyses (see mode-shape in Figures 7.29 and 7.30) were used in the nonlinear Riks static analysis of the pressurised vessels. Each of the programs was set to terminate after 300 increments, and 0.4, 10^{-6} and 0.4 initial, minimum and maximum arc length increments. The variation in the external pressure to critical buckling pressure ratio (p / p_{cr}) is plotted against the vertical displacement of the lowest circle of latitude (nadir) per shell thickness $(\Delta y / t)$ for each of the toroidal vessels are shown in Figure 7.27 with their geometrical parameters. The points of bifurcation and collapse are indicated in the figures with their respective values. Like the other pressurised vessels that have been studied in this chapter, the primary equilibrium path for the present complete multi-shell toroidal vessel under uniform external pressure shows that vessel has a stable post-bifurcation state before axisymmetric collapse occurred. A larger percentage difference between the bifurcation load and collapse load is observed for toroid with $\lambda_r = 2.0$ compared to that for toroid with $\lambda_r = 6.0$.

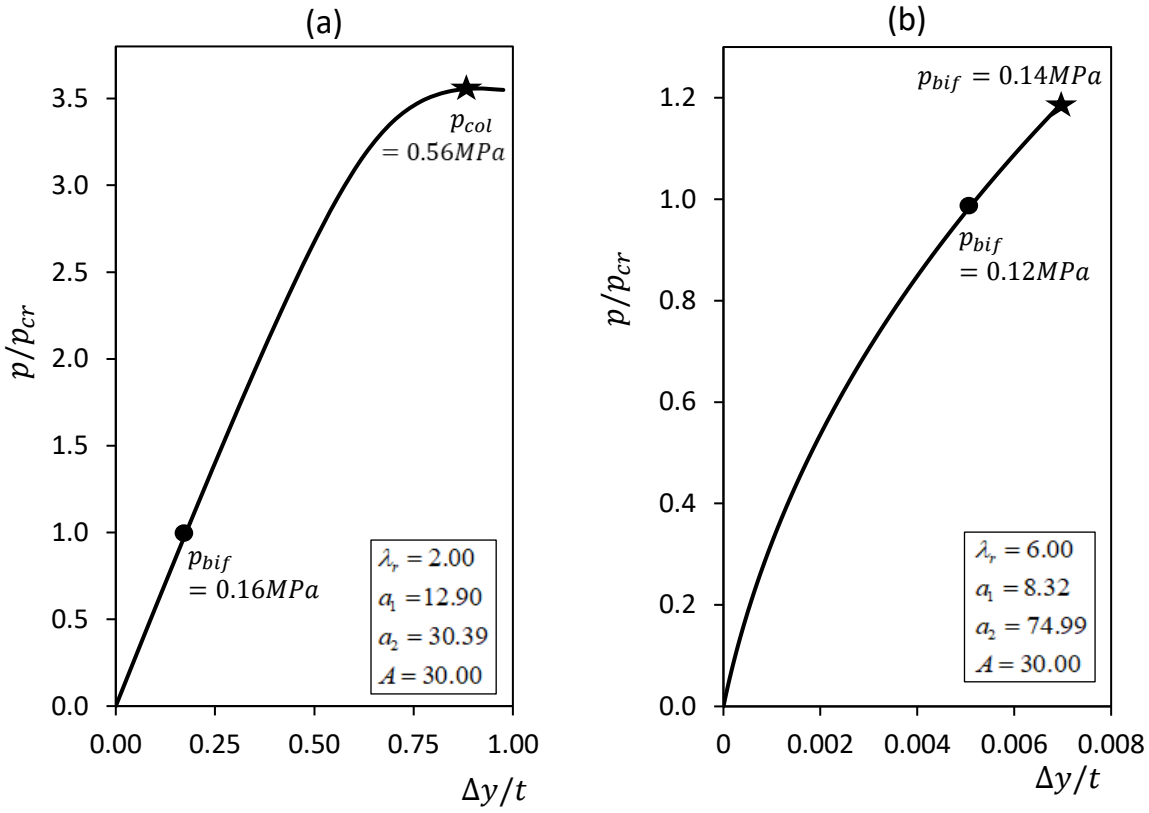

Figure 7.27. Plot of external pressure versus nadir deflection for complete multi-shell toroids with: (a) $\lambda_r = 2.0$, (b) $\lambda_r = 6.0$

7.4.3 Variations in toroidal mean radius and thickness ratios for toroids with rise ratio of 2

Buckling pressures are also affected by the toroidal mean radius, and the wall thickness ratio of complete multi-shell toroidal vessels with $\lambda_r < 4.0$, as in the case of geometric parameters with $\lambda_r > 4.0$ that were studied in Section 6.4.6 with the analytical buckling formula. Here, a series of numerical calculations were carried out on toroidal vessels with $\lambda_r = 2.0$ and different values of A using the modelling idealisation and the boundary conditions described in Section 7.4.1 above. Single values of $a_1 = 12.90m$, $a_2 = 30.39m$ and thickness ratio $a_1 / t = 160$ were adopted for all the toroids. The critical buckling results obtained are plotted against the toroidal mean radius in Figure 7.28(a). A further parametric study was conduction on the $\lambda_r = 2.0$ multi-shell for different a_1 / t ratios. The numerical results are shown in Figure 7.28(b), where two values of toroidal mean radius, i.e. $A = 30.0m$ and $60.0m$ were considered.

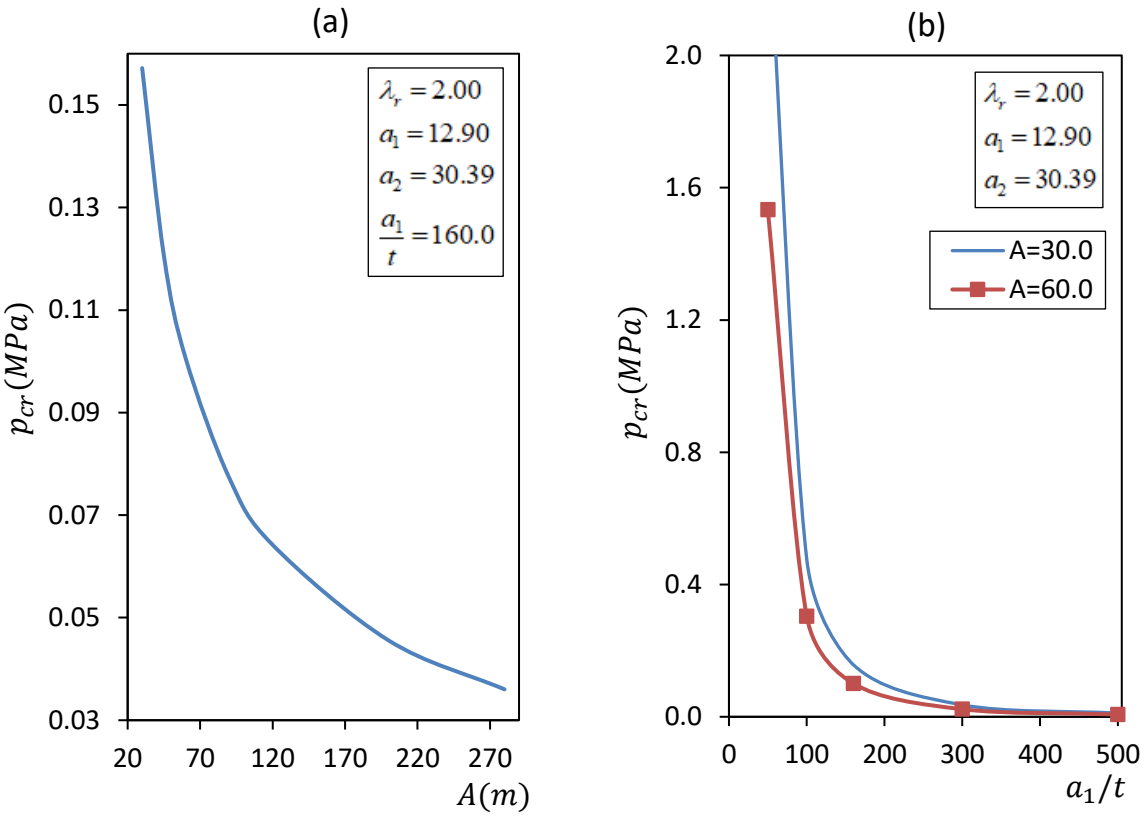

Figure 7.28. Critical buckling pressures versus (a) toroidal mean radius, and (b) thickness ratio of complete multi-shell toroidal vessels

7.4.4 Multi-shell toroids with eigenmode-type imperfections

The initial imperfection sensitivity of the present vessel was studied. The focus was made on the toroid with $\lambda_r = 2.0$ for an example of complete multi-shell toroidal vessels with $\lambda_r < 4.0$, and the toroid with $\lambda_r = 6.0$ for an example of toroidal vessels with $\lambda_r > 4.0$. The critical bucking pressures and other geometrical parameters can be found in Table 7.9. The approach in Section 7.2.5 is adopted here in the investigation of the possibility of failure load reduction due to the presence of eigenmode-type imperfections in toroids with $\lambda_r = 2.0$ and 6.0. In the approach, linear eigenvalue buckling analyses are first carried out to obtain the required number of eigenshapes. A selection of the modes to be used as the imperfection shapes is made based on the number of circumferential and longitudinal waves. Various imperfection amplitude (scaling factor) in the range of $0 \le \Delta / t \le 1.0$ for each of the selected modes are superimposed individually on the perfect toroidal shell models using the modified Riks algorithm in Abaqus, and the failure pressure loads of the toroids are computed.

The distinctive eigenmodes selected from the linear buckling analysis results for the multi-shell toroids with $\lambda_r = 2.0$ and 6.0 are given in Figure 7.29 and 7.30, respectively, with their mode numbers and corresponding circumferential wavenumbers.

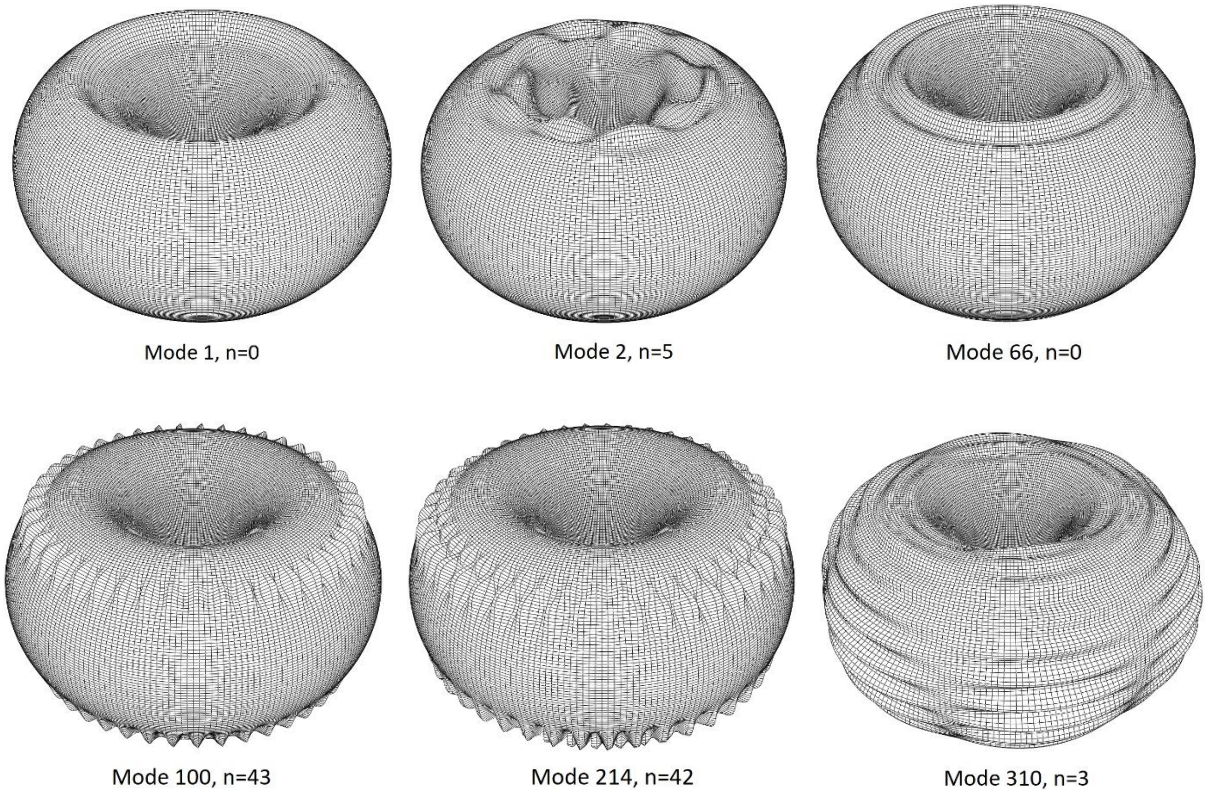

Figure 7.29. Selected eigenmodes for the imperfection sensitivity study of multi-shell toroids with $\lambda_r = 2.0$

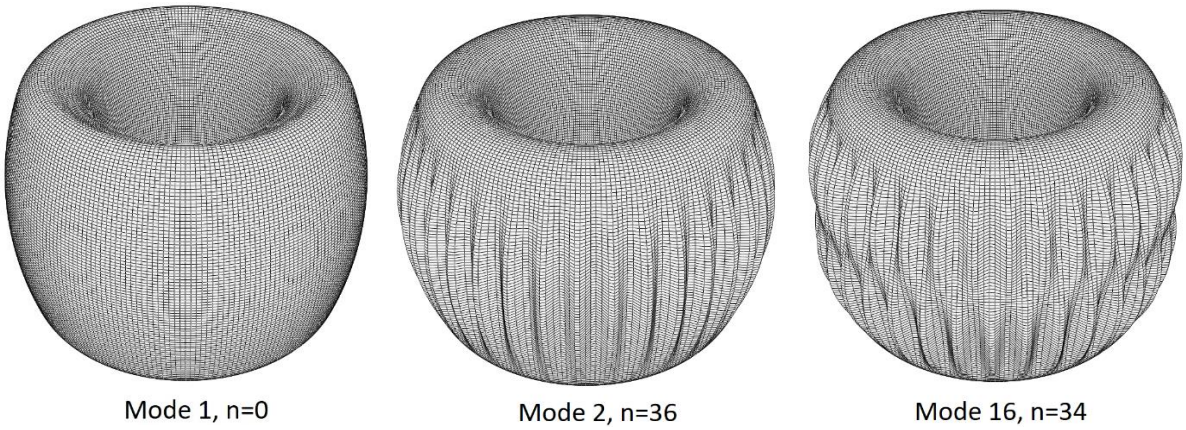

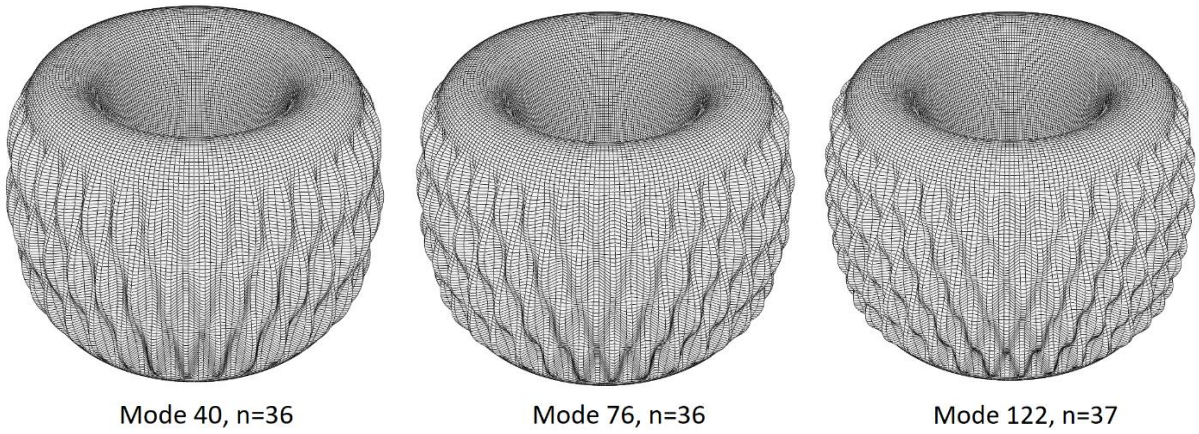

Figure 7.30. Selected eigenmodes for the imperfection sensitivity study of multi-shell toroids with $\lambda_r = 6.0$

When these selected modes are scaled based on $0 \le \Delta / t \le 1.0$ and separately superimposed on their corresponding $\lambda_r = 2.0$ and 6.0 perfect toroids in the nonlinear Riks analyses, the following buckling results in Figure 7.31 are obtained for each of the modes and their respective vessels. The figure shows the ratio of critical buckling pressures of imperfect toroids to that of perfect toroids (p_{cr}^{imp} / p_{cr}) against modulated imperfection amplitude to average wall thickness ratio (Δ / t). It can be seen in Figure 7.31(a), the effect of eigenmodes imperfection amplitude Δ on the critical buckling pressure of the toroidal vessel with $\lambda_r = 2.0$ is negligible. However, in Figure 7.31(a), the toroidal vessel with $\lambda_r = 6.0$ is seen to be sensitive to eigenmode-type imperfections. However, mode 1 did not result in any substantial effect on the buckling response of the vessel with $\lambda_r = 6.0$.

Various multi-shell toroids with different values of toroidal mean radius as indicated in Figure 7.32 were analysed. A single mode was used for each of the toroids: mode 1 for the $\lambda_r = 2.0$ toroids and mode 40 for the $\lambda_r = 6.0$ toroids. Note that the buckling response trends for each of the geometries considered are respectively similar to that of $\lambda_r = 2.0$ and $\lambda_r = 6.0$ multi-shell toroids described above.

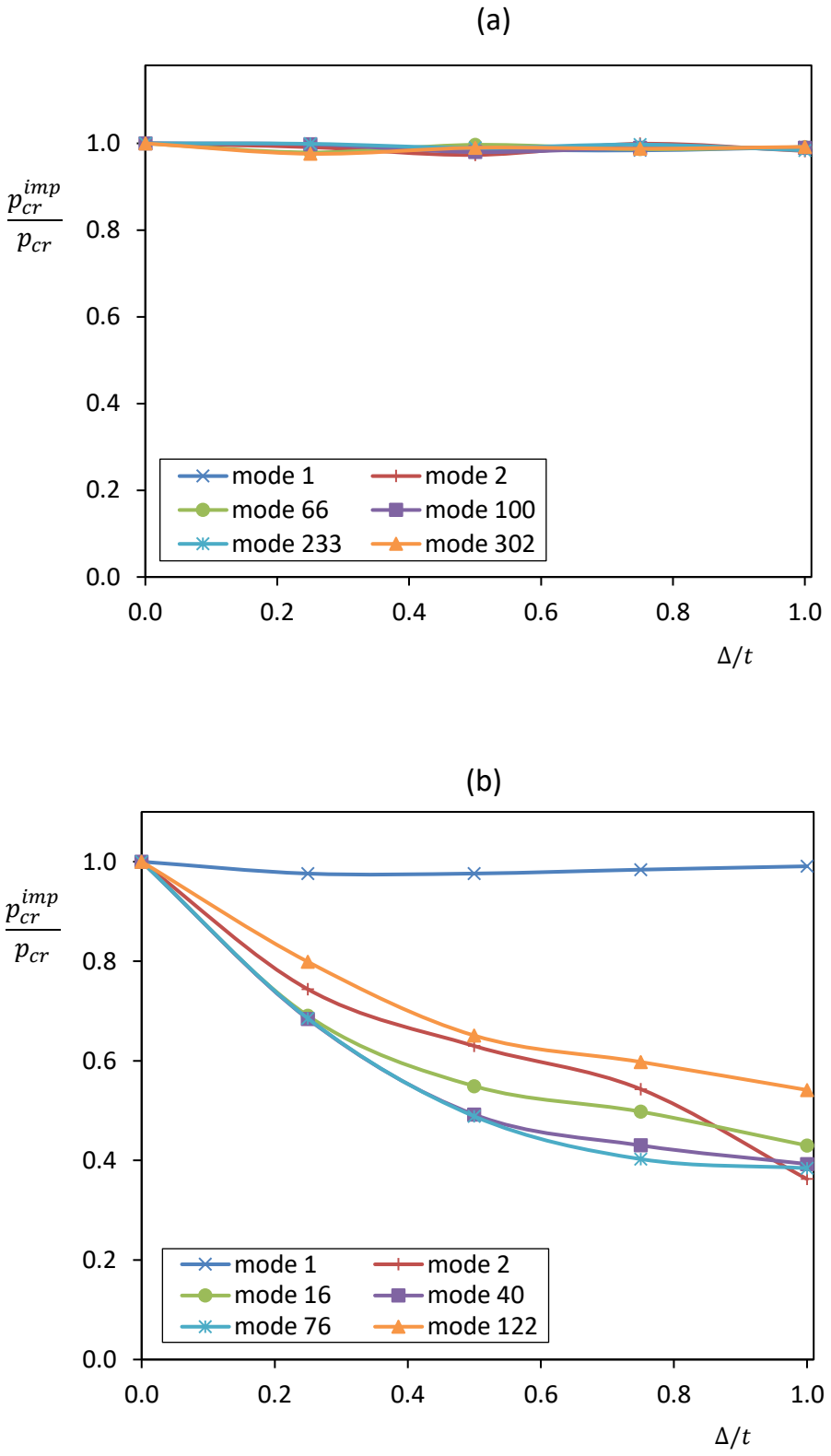

Figure 7.31. Effect of imperfection amplitude of different eigenmodes on the buckling pressure of complete multi-shell toroids with (a) $\lambda_r = 2.0$, (b) $\lambda_r = 6.0$

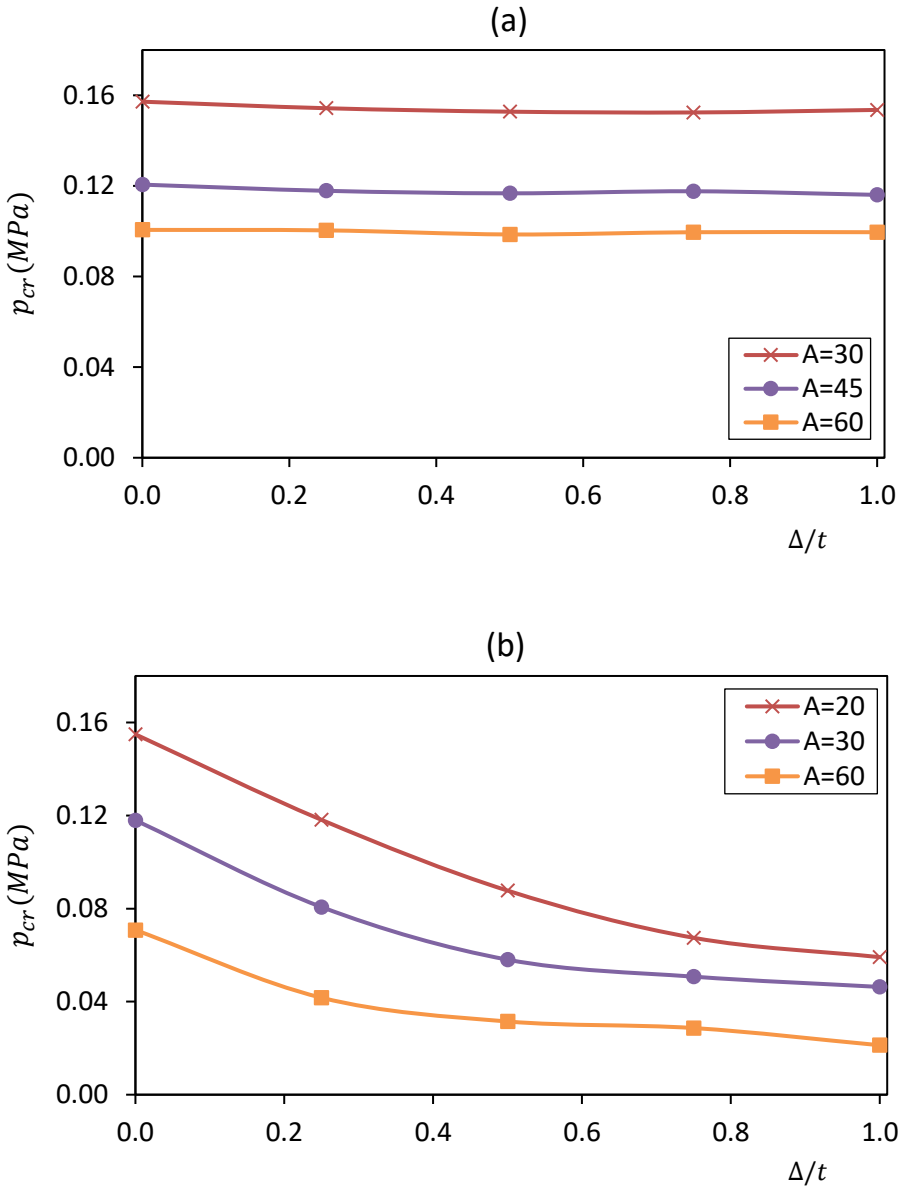

Figure 7.32. Sensitivity of critical buckling load to eigenmode-imperfection amplitudes for various toroidal mean radii of complete multi-shell toroids with (a) $\lambda_r = 2.0$, (b) $\lambda_r = 6.0$

Similarly, the sensitivity of buckling pressure to the initial geometric imperfections was computed for externally pressurised toroidal shells with different thickness ratios d/t as shown in Figure 7.33 for toroid with $\lambda_r = 2.0$ and 6.0.

Imperfections were assumed to have an affinity with the corresponding first eigenmode for the $\lambda_r = 2.0$ toroids and fortieth eigenmode for the $\lambda_r = 6.0$ toroids. Shape deviations were taken as modulated eigenmodes for both cases, as before. The load-bearing capacity was calculated

numerically for imperfections amplitude of $0 \le \Delta / t \le 1.0$. The results in Figure 7.25 indicate the usual trends for each of the multi-shell toroidal types.

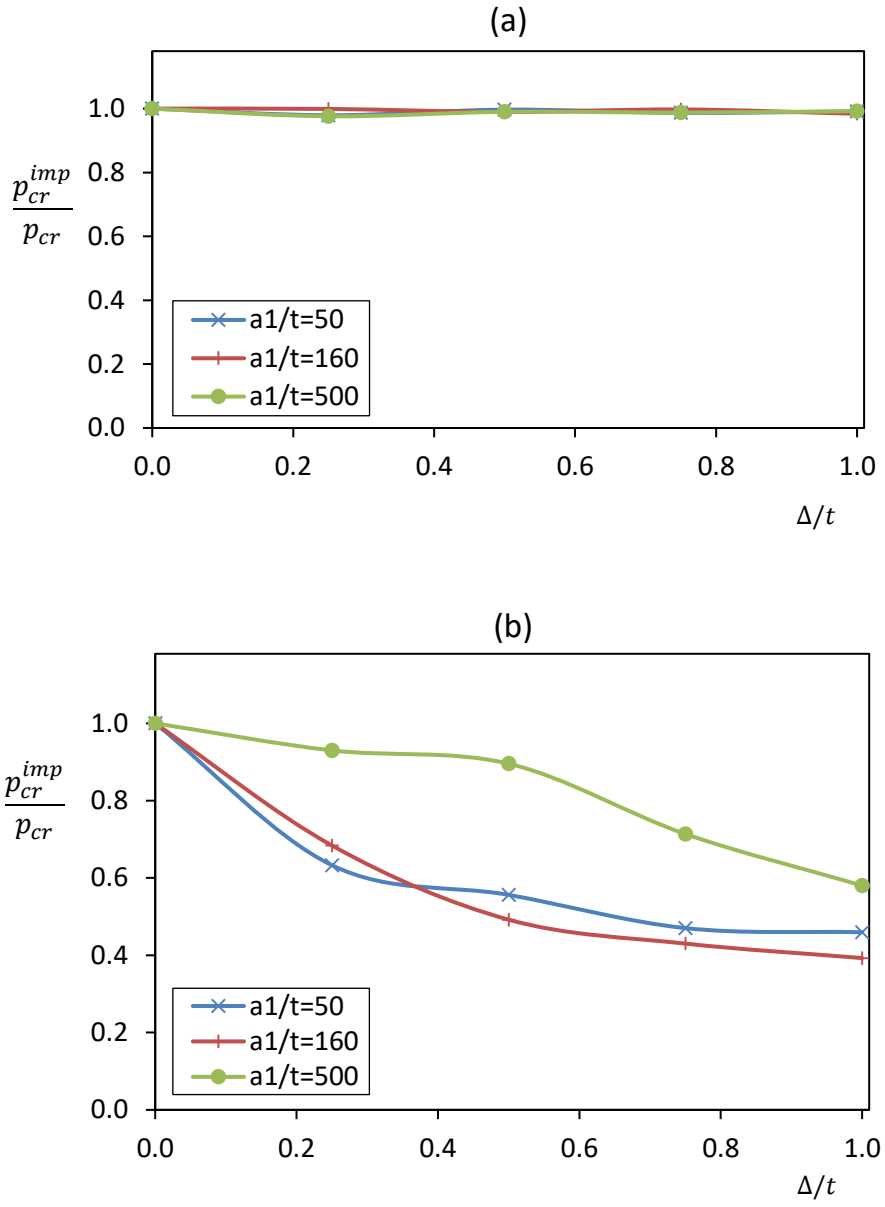

Figure 7.33. Effect of eigenmode-imperfection amplitudes on the buckling pressure for various complete multi-shell toroids with different thickness ratios: (a) $\lambda_r = 2.0$, (b) $\lambda_r = 6.0$

7.4.5 Summary on the buckling behaviour of multi-shell toroids

Several insights can be drawn from the investigation of the buckling of multi-shell toroidal vessels in this Section 7.4. The behaviour of vessels with $\lambda_r > 4.0$ is found to be generally distinct from those with $\lambda_r < 4.0$. For toroids with $\lambda_r > 4.0$, the analytical buckling solution

developed in Chapter 6 gives reasonably accurate critical buckling pressure and mode, while this is not the case for $\lambda_r < 4.0$. Vessels with $\lambda_r < 4.0$ are found to be generally stiffer than those with $\lambda_r > 4.0$, and a larger percentage difference between the bifurcation load and collapse load is largely observed for toroid with $\lambda_r < 4.0$ compared to that for toroid with $\lambda_r > 4.0$. However, both classes of vessels are seen to have stable post-bifurcation behaviour, and each of their critical buckling pressure reduces as the mean toroidal radius (or thickness ratio)) reduces.

The parametric study on the sensitivity of multi-shell toroid under uniform external pressure generally shows that the buckling strength of a multi-shell toroid is not substantially affected by the presence of eigenmode-type initial imperfections for toroids with $\lambda_r < 4.0$. This is not the same for toroids with $\lambda_r > 4.0$, where the various pressurised vessels were found to have closely spaced eigenmodes, and the different thickness ratios and opening ratios investigated within a modulated imperfection amplitude range of $0 \le \Delta / t \le 1.0$ were generally imperfection sensitive, with up to 60% reduction in failure pressure load in some cases.

7.5 Concluding remarks

This chapter presents numerical results on the elastic buckling behaviour and collapse strength of three novel toroidal vessels under uniform external pressure. The vessels are of the form of:

(a) circular-elliptic toroidal assemblies;
(b) Parabolic-ogival toroids; and
(c) Multi-shell (segmented circular) toroidal vessels.

The cross-sectional parameters leading to the ultimate buckling strength for each of the pressurised vessels were identified, after validating the adopted numerical method through the well-known case of circular toroidal vessels in the literature and the analytical approach proposed in Chapter 6. For the circular-elliptic toroidal assemblies investigated, highest failure pressure is found to be associated with $b/a = 2.5$ toroids of $a/t = 200$, and the buckling shape or weakest zone (where the buckling normally start from) is a function of b/a . For $b/a >> 1$, the buckling initiates asymmetrically with $n > 0$ in the elliptic segment near the meeting edges of the vessels, while toroids with smaller b/a buckle symmetrically with $n = 0$. For the parabolic ogival toroidal vessels investigated, the highest value of critical buckling load was

found to be associated with $h/d = 1.5$ toroids of thickness ratio $d/t = 200$, and the weakest zones are generally near the edges of the outer segment, where asymmetry deformations spring up as bubbles. For the multi-shell toroidal vessels investigated, distinctive behaviour is noted for shells with $\lambda_r > 4.0$ and $\lambda_r < 4.0$. Vessels with $\lambda_r < 4.0$ are found to be generally stiffer than those with $\lambda_r > 4.0$ and the analytical buckling solution developed in Chapter 6 can be used effectively to determine the critical buckling pressures and modes for toroids with $\lambda_r > 4.0$, but the accuracy is not good for multi-shell toroids with $\lambda_r < 4.0$.

It has been found that perfect toroidal vessels under external pressure loading can generally have stable post-buckling behaviour and may, therefore, be able to resist further load beyond the elastic bifurcation loads. Also, higher failure pressures are associated with 'compact' toroidal vessels when compared to corresponding vessels with larger opening ratios and failure loads of the toroids generally reduce as the thickness ratio increases. This is an indication of how the scale of the structure will affect its design.

The buckling sensitivity to eigenmode-type initial geometric imperfections in each of the three vessels appeared to be different for a modulated imperfection amplitude range of $0 \le \Delta/t \le 1.0$ Parabolic-ogival toroids are observed to be generally sensitive to initial imperfections with up to 64% reduction of buckling strength recorded for some geometries. However, for circular-elliptic toroids, the failure loads of the vessels with $b/a < 2.5$ are not significantly affected by initial imperfections, while those of the vessels with $b/a > 2.5$ are sensitive to initial imperfections with up to 70% reduction in buckling strength recorded in certain geometries. Similarly, for multi-shell toroidal vessels, the buckling response of the vessels with $\lambda_r < 4.0$ are not significantly affected by initial imperfections, while those of the vessels with $\lambda_r > 4.0$ are sensitive to initial imperfections.

Chapter 8

General conclusions

8.1 Introduction

In this chapter, an end is brought to this report, and some salient conclusions are drawn from the preceding chapters with a brief overview of the study and some recommendations for future research work.

8.2 Summary of research and contributions

The main objective of this study was to propose simplified models that could help stakeholders within the field of containment shells of revolution to adequately analyse the response of loaded elastic toroidal shells of any cross-section, with the aim of increasing the applicability of the toroidal shell form. The thesis also sought to generate new knowledge and provide the following sub-objectives that would facilitate the design and development of new toroidal shell forms that are fit for purpose, through the investigation of toroids using classical shell theory in conjunction with an appropriate solution and numerical modelling approaches:

- To develop closed-form solutions for the complete determination of the state of stress and deformation within toroidal vessels of interest;
- To develop simple rules for predicting the buckling characteristics of toroidal vessels under relevant loading conditions;
- Specifically, to investigate and understand the key structural features of each of the following toroidal shell forms under uniform and hydrostatic pressure:
    i. Circular toroids
    ii. Elliptic toroids
    iii. Circular-elliptic toroids
    iv. Parabolic ogival toroids
    v. Multi-shell toroids

The above objectives have been met in this thesis, and the conclusions and contributions of the study are discussed in the following subsections.

8.2.1 State of stress in toroidal shells under axisymmetric loading

The governing equations of general toroidal shells of revolution were presented in Chapter 3, and based on the approximations of membrane hypothesis, general solution algorithm specialised for the determination of membrane stress resultants in meridional and hoop directions of axisymmetrically loaded toroidal shells of arbitrary cross-section was formulated in Chapter 4. The membrane solution algorithm was employed in the derivation of membrane stress results and deformations of various toroidal shell forms: circular toroidal shells, elliptic toroids, parabolic-ogival toroids, circular-elliptic toroidal assemblies, and multi-shells toroidal vessels under uniform pressure loading. Membrane results were also presented for each of these toroids when loaded hydrostatically. It was demonstrated that toroidal shells of the same cross-section respond differently under the action of uniform pressure and linearly varying (hydrostatic) pressure.

Some of the membrane results were also presented in non-dimensional forms to permit the ease of estimating the response of the loaded shells. These were also used to conduct parametric investigations that span over the most practical range of the toroidal shells. Some insightful behaviour of each of the shell forms were identified, and a set of design recommendations has been proposed for each of the toroidal shells, including the positioning of supports.

Owing to the simplifying assumption of neglecting bending effects in the membrane theory of shells, membrane stress results (which provide good estimates of the state of stress in the regions of the shells that are away from edges and discontinuities) are invalid in the regions of the shells that are close to support locations, discontinuities in surface loading, meeting points of shell segments, turning points, and some other axisymmetric lines of distortions. To estimate the bending-disturbance actions in these zones of toroidal shells, a very simple and effective structural-analysis procedure based on the Geckeler's approximations for the non-shallow regions was proposed in Chapter 5.

The complete state of stress in axisymmetrically loaded toroidal shells can therefore, be estimated by superimposing the approximate bending-disturbance solution (which account for the generally localised edge effects and act as the homogeneous solution of the governing

differential equations of toroidal shells of revolution) with the particular solution (approximated as membrane solution presented in Chapter 4). With this approach, the toroidal shell problem, which is hitherto very complex and difficult to obtain an analytical solution, is solved easily and accurately. This simplified solution approach was used to evaluate the state of stress in (i) a pressurised parabolic-ogival toroidal vessel, (ii) the edge zones of a circular-elliptic toroidal storage tank, and (iii) a multi-shells toroidal shell under uniform external pressure loading. A parametric investigation into the effects of toroidal opening ratio, shell thickness ratio, and cross-sectional height to width ratio on the bending-disturbance stresses within the junction zones of a pressurised parabolic-ogival toroidal vessel was also conducted. Important features of the toroids were highlighted.

8.2.2 Buckling of loaded toroidal shells

In Chapter 6, the stability equations for general toroidal shells of revolution were presented. The equations can be specialized for any toroidal shell form. However, the governing stability equations were simplified for only multi-shell toroids under uniform external pressure loading, by employing the approximations of the Donnell-Mushtari-Vlasov shell theory and the classical assumption of adopting membrane-theory solution (of the type given in Chapter 4) to predict the pre-buckling state of the problem. On application of the Galerkin's scheme, the resulting stability equations were approximately solved for the segments in the middle regions of the toroidal vessel. This leads to an expression for estimating the critical buckling pressures of pressurised isotropic multi-shell toroids. Numerical results from the proposed method were compared with those from a finite element method solution. The critical buckling formula permits the ease of investigating the influence of geometric parameters of the toroidal vessels on critical failure loads and mode shapes. The proposed analytical model for estimating the buckling of multi-shells toroids under uniform external pressure can also be modified for different load cases and support conditions by simply adopting the appropriate forms of displacement and stress functions.

Apart from the eigenvalue analysis, numerical calculations were carried out on the multi-shell toroidal vessel under uniform external pressure to study the non-linear effects on buckling response, post-bifurcation behaviour and geometric imperfection sensitivity of the toroid in Chapter 7. These studies were also conducted for pressurised parabolic ogival toroidal vessels and circular-elliptic toroidal assemblies. A parametric study on the pressurised vessels was

conducted, and the cross-sectional parameters that lead to the ultimate buckling strength for each of the vessels were identified, after validating the adopted numerical method through the well-known case of circular toroidal vessels in the literature and the analytical approach proposed in Chapter 6 for externally pressurised multi-shells toroidal vessels.

It has been shown that perfect toroidal vessels under external pressure loading can generally have stable post-buckling behaviour and may, therefore, be able to resist further load beyond the elastic bifurcation loads. The buckling sensitivity to eigenmode-type initial geometric imperfections in pressurised parabolic-ogival toroidal vessels, semi-circular and semi-elliptical toroidal assemblies and multi-shells toroidal vessels appeared to be different for $0 \le \Delta / t \le 1.0$ modulated amplitude. The parabolic-ogival toroids were observed to be generally sensitive to initial imperfections with up to 64% reduction of buckling strength recorded for some geometries. However, for the semi-circular and semi-elliptic toroids, the failure loads of the vessels with $b/a < 2.5$ are not significantly affected by initial imperfections, while those of the vessels with $b/a > 2.5$ are sensitive to initial imperfections with up to 70% reduction in buckling strength recorded in certain geometries. Similarly, for multi-shells toroidal vessels, the buckling response of the vessels with $\lambda_r < 4.0$ are not significantly affected by initial imperfections, while those of the vessels with $\lambda_r > 4.0$ are sensitive to eigenmode-type initial imperfections.

8.3 Recommendations for future research

The analytical algorithms presented in this thesis for strength and buckling analysis of toroidal shells of revolution can be extended to explore the behaviour of different cross-sectional shapes of toroidal shells under various loading conditions. The solution approach can also be adopted for the study of other structural components in the form of a shell of revolution, by applying appropriate modifications to the solution algorithms. For example, the analytical buckling solution proposed in this thesis can be modified and utilised to gain a fundamental understanding of the buckling phenomena of a specific toroidal shell problem. An investigation of this type will be a useful contribution to the field of containment shells. Furthermore, the developed analytical solutions have permitted the ease of conducting parametric studies on each of the toroidal cross-sections considered. The scope of this parametric investigation can

be extended by focusing on a single cross-section and also applying non-uniform shell thickness, for example.

In the estimation of the state of stress within the bending-disturbance zones of loaded toroidal shells of revolution, the current study adopted a particularly convenient approach in the linear elastic analysis of shells of revolution, in which the membrane solution is used to approximate the particular integral of the general bending-theory equations of the shells and the axisymmetric bending-disturbance (edge actions) is used to approximate the homogeneous solution. The edge actions are obtained on account of Geckeler's approximations which have been demonstrated to be applicable for the bending disturbances that occur in regions of the shell that are not too shallow. The description of 'shallowness' has been given by Zingoni (1997). Hence, the general bending solution given in the thesis may not accurately describe the localised state of stress in the shallow regions of the shells. These are the vicinities of the turning points where the positive and negative Gaussian surfaces meet in a circular or elliptical toroid, for example. Various approximation methods have been presented in the literature for specific cases (Sutcliffe, 1971; Sun, 2010a; Levyakov, 2013), it may be worthwhile to obtain a closed-form solution that can fully describe the general state of stress in these regions of toroidal shells.

For the buckling solution of pressurised multi-shells toroidal vessels, this study adopted the DMV-type simplifications to reduce the stability problem and the obtained analytical formulae. This solution is found to be accurate for toroids with rise ratio $\lambda_r > 4.0$, but not reasonably accurate for $\lambda_r < 4.0$ toroids. It will be good if an analytical buckling solution (that can allow an easy way to study the influence of dimensions) is formulated for pressurised multi-shells toroidal vessels with rise ratio $\lambda_r < 4.0$. In addition, full analytical buckling solution model could also be developed in the future for parabolic-ogival toroidal vessels, circular-elliptic toroidal assemblies and other novel toroidal shell forms.

The buckling behaviour of the commonest toroidal shells (i.e. circular toroids) under external pressure is not too sensitive to initial geometric shape deviations in the elastic toroids. So, it was necessary to investigate if the buckling response of each of the three novel toroidal shells studied in this thesis is imperfection sensitive. In the study, only initial eigenmode-type imperfections within the modulated amplitude range of $0 \le \Delta / t \le 1.0$ were considered for each of the vessels. This initial imperfection-type may not always be the worst case. Other shape

imperfections and larger scaling factors of eigenmode imperfections, including the superimposition of more than a single eigenmode may have interesting effects on the buckling response of these shells.

Finally, the three toroidal shells were studied based on elastic material properties. A more realistic material modelling with appropriate plasticity properties may be carried out. Similarly, because of concerns about weight and harsh environment, the investigation of these shells with composite material properties is suggested. Also, the increase of the buckling strength of such toroids can be achieved by stiffening them. It would be advisable for a study to be conducted on the behaviour of the toroidal shells when stiffened with different stiffener arrangements (i.e. stringer, ring reinforcement).

References

Abaqus. 2014. Theory and user's guide version 6.14. Providence: Dassault Systèmes.

ADINA Tech Briefs: Dynamic behavior of a nuclear reactor steel containment. n.d. Available: http://www.adina.com/newsgH104.shtml [2016, October 11].

Almroth, B.O., Sobel, L.H. & Hunter, A.R. 1969. An experimental investigation of the buckling of toroidal shells. *AIAA*. 7(11):2185–2186.

Amabili, M. 2008. *Nonlinear vibrations and stability of shells and plates*. New York: Cambridge University Press.

Anon. 2012. *ADINA Theory and Modeling Guide, Volume I : ADINA Solids & Structures*. Watertown: ADINA R & D, Inc.

Argyris, J.H. 1960. *Energy theorems and structural analysis*. V. 26. Springer US. DOI: 10.1007/978-1-4899-5850-1.

Baker, E.H., Cappelli, A.P., Kovalevsky, L., Rish, F.L. & Verette, R.M. 1968. *Shell analysis manual*. Washington DC: North American Aviation, Inc.

Balderes, T. & Armenakas, A.E. 1973. Free vibrations of ring-stiffened toroidal shells. *American Institute of Aeronautics and Astronautics Journal*. 11:1637–1644.

Bathe, K.-J. 1996. *Finite element procedures*. New Jersey: Prentice Hall.

Bickell, M.B. & Ruiz, C. 1967. *Pressure vessel design and analysis*. London: Macmillan and Company Limited.

Blaauwendraad, J. & Hoefakker, J.H. 2014. *Structural shell analysis*. V. 200. London: Springer. DOI: 10.1007/978-94-007-6701-0.

Błachut, J. 2004. Buckling and first ply failure of composite toroidal pressure hull. *Computers & Structures*. 82(23–26):1981–1992. DOI: 10.1016/j.compstruc.2003.07.009.

Błachut, J. & Jaiswal, O.R. 1998a. Buckling of imperfect ellipsoids and closed toroids subjected to external pressure. *ASME PVP*. 368:121–128.

Błachut, J. & Jaiswal, O.R. 1998b. Buckling under external pressure of closed toroids with circular and elliptical cross sections. In *Advances in civil and structural engineering computing for practice*. B.H.. Topping, Ed. Edinburgh: Civil- Comp Press. 323–334.

Błachut, J. & Jaiswal, O.R. 1999. Instabilities in torispheres and toroids under suddenly applied external pressure. *International Journal of Impact Engineering*. 22(5):511–530. DOI: 10.1016/S0734-743X(98)00067-0.

Błachut, J. & Jaiswal, O.R. 2000. On buckling of toroidal shells under external pressure. *Computers & Structures*. 77:233–251.

Bogomol'nyl, V.M. & Zhidyaev, N.A. 1992. Optimization of the geometric parameter of elbows. *Chemical and Petroleum Engineering*. 28(7):418–420.

Brush, D.O. & Almroth, B.O. 1975. *Buckling of bars, plates, and shells*. New York: McGraw-Hill.

Buchanan, G.R. & Liu, Y.J. 2005. An analysis of the free vibration of thick-walled isotropic toroidal shells. *International Journal of Mechanical Sciences*. 47(2):277–292. DOI: 10.1016/j.ijmecsci.2004.12.004.

Calladine, C.R. 2007. *Theory of shell structures*. Cambridge: Cambridge University Press.

Campos, E.J.D., França, C.A.S., Nonnato, L. V, Neto, F. V, Barreira, L. & Cole, R. 2013. Atlas-B: The development and mooring of a Brazilian prototype of the Atlas buoy. *2013 Oceans - San Diego*. 1–4. DOI: 10.23919/OCEANS.2013.6741373.

Chapelle, D. & Bathe, K.-J. 2011. *The finite element analysis of shells - fundamentals*. Berlin: Springer-Verlag.

Chernyshenko, I.S. & Maksimyuk, V.A. 2000. On the stress-strain state of toroidal shells of elliptical cross section formed from nonlinear elastic orthotropic materials. *International Applied Mechanics*. 36(1):90–97.

Chien, W.Z. 1979. *Selected papers in applied math and mechanics*. Jiangsu Sciences and Technology. Jiangsu, China.

Clark, R.A. 1950. On the theory of thin elastic toroidal shells. *Journal of Mathematics and Physics*. 29:146–178.

Clough, R.W. 1990. Original formulation of the finite element method. *Finite Elements in Analysis and Design*. 7:89–101.

Colbourne, J.R. & Flügge, W. 1967. The membrane theory of the toroidal shell - a singular perturbation problem. *International Journal of Non-Linear Mechanics*. 2:39–53. DOI: 10.1016/0020-7462(67)90017-0.

Combescure, A. & Galletly, G.. 1999. Plastic buckling of complete toroidal shells of elliptical cross-section subjected to internal pressure. *Thin-Walled Structures*. 34(2):135–146. DOI: 10.1016/S0263-8231(99)00006-3.

Crisfield, M.A. 1981. A fast incremental/iterative solution procedure that handles "snap-through". *Computers & Structures*. 13(1–3):55–62. DOI: 10.1016/0045-7949(81)90108-5.

Cristian, P. & Marcel, S. 2010. Stress analysis of toroidal shell. *Incas Bulletin*. 2(4):215–224. DOI: 10.13111/2066-8201.2010.2.4.27.

Dahl, N.C. 1953. Toroidal-shell expansion joints. *ASME J. Appl. Mech*. 20:4876–503.

Dean, W.R. 1939. The distortion of a curved tube due to internal pressure. *Philosophical Magazine*. 28(189):452–464.

Enoma, N. & Zingoni, A. 2016a. On the feasibility of the parabolic ogival cross-section for liquid-filled toroidal vessels. In *Insights and Innovations in Structural Engineering, Mechanics and Computation. Proceedings of the Sixth International Conference on Structural Engineering, Mechanics and Computation (SEMC 2016), 5-7 September 2016, Cape Town, South Africa*. A. Zingoni, Ed. Cape Town: Taylor & Francis Group. 793–798.

Enoma, N. & Zingoni, A. 2016b. Behaviour of submerged circular toroidal vessels. In *The 8th International Conference on Steel and Aluminium Structures (ICSAS 2016), 7-9 December 2016, Hong Kong, China*. B. Young & Y. Cai, Eds. Hong Kong: The University of Hong Kong. Paper No. 75.

Enoma, N. & Zingoni, A. 2016c. Stresses in multi-shell toroidal pressure vessels. In *Insights and Innovations in Structural Engineering, Mechanics and Computation. Proceedings of the Sixth International Conference on Structural Engineering, Mechanics and Computation (SEMC 2016), 5-7 September 2016, Cape Town, South Africa*. A. Zingoni, Ed. London: Taylor & Francis Group. 799–805.

Enoma, N. & Zingoni, A. 2017. Analytical formulation and numerical modelling for multi-shell toroidal pressure vessels. *Computers & Structures* (in press). DOI: 10.1016/j.compstruc.2017.07.013.

Enoma, N., Egware, H.O., Itoje, H.J. & Unueroh, U.G. 2015. Membrane solutions for circular toroidal shells under internal hydrostatic pressure. *Journal of Multidisciplinary Engineering Science and*

Technology. 2(10):2895–2900.

Fedosov, Y.A. 1969. Experimental study of toroidal shell stability. *Izvestiya VUZ, Aviatsionnaya Tekhnika*. 12(3):154–157 (English translation).

Fedosov, Y.A. 1971. Stability of a toroidal shell subject to external pressure. *Izvestiya VUZ, Aviatsionnaya Tekhnika*. 14(3):108–112 (English translation).

Fedosov, Y.A. 1977. Theoretical and experimental study of the stability of toroidal shells with external pressure. *Izvestiya VUZ, Aviatsionnaya Tekhnika*. 20(4):98–102 (English translation).

Fishlowitz, E.G. 1970. *Investigation of elastic stability of circular toroidal shells under uniform external pressure*. Naval Ship Research and Development Center. Report 3338.

Flügge, W. 1973. *Stresses in shells*. Berlin: Springer-Verlag. DOI: 10.1115/1.3641763.

Flügge, W. & Sobel, L.H. 1965. Stability of shells of revolution: general theory and application to the torus. Stanford University. DOI: 10.1007/978-3-642-20617-7.

Foroughi, H., Moen, C.D., Myers, A., Tootkaboni, M., Vieira, L. & Schafer, B.W. 2014. Analysis and design of thin metallic shell structural members – current practice and future research needs. In *Proceedings of the Annual Stability Conference*. Toronto: Structural Stability Research Council.

Fowler, C.P., Orifici, A.C. & Wang, C.H. 2016. A review of toroidal composite pressure vessel optimisation and damage tolerant design for high pressure gaseous fuel storage. *International Journal of Hydrogen Energy*. 41:22067–22089. DOI: 10.1016/j.ijhydene.2016.10.039.

Galerkin, B.G. 1915. Rods and plates: Series in some problems of elastic equilibrium of rods and plates. *Vestnik Ingenerov Tech. (USSR)*. 1(19):897–908.

Galletly, G.D. 1998. Elastic buckling of complete toroidal shells of elliptical cross-section subjected to uniform internal pressure. *Thin-Walled Structures*. 30(1–4):23–34. DOI: 10.1016/S0263-8231(97)00030-X.

Galletly, G.D. & Błachut, J. 1995. Stability of complete circular and non-circular toroidal shells. *Proceedings of the Institution of Mechanical Engineers: Journal of Mechanical Engineering Science*. 209:245–255.

Gavelya, S.P. & Kononenko, N.I. 1974. Calculation studies of the dynamics characteristics of spherical and toroidal shells. *Journal of Applied Mechanics and Technical Physics*. 15(2):251–254.

Gibson, J.E. 1965. *Linear elastic theory of thin shells*. London: Pergamon Press.

Goldberg, J.E., Bogdanoff, J.L. & Marcus, L. 1960. On the calculation of the axisymmetric modes and frequencies of conical shells. *Journal of the Acoustical Society of America*. 32:738–742.

Govender, N. 2017. A parametric investigation into the membrane stresses of hydrostatically loaded circular and elliptic toroidal shells. University of Cape Town. Available: https://open. uct.ac.za/ handle/11427/25284 [2018, July 16].

Van der Heijden, A.M.. Ed. 2009. *W. T. Koiter's elastic stability of solids and structures*. Cambridge: Cambridge University Press.

Hutchinson, J.W. 1967. Initial post-buckling behavior toroidal shell segments. *International Journal of Solids and Structures*. 3:97–115.

Jasion, P. & Magnucki, K. 2012. Elastic buckling of horizontal barrelled shells filled with liquid - numerical analysis. *Thin-Walled Structures*. 52:117–125. DOI: 10.1016/j.tws.2011.12.014.

Jha, A.K., Inma, D.J. & Plaut, R.H. 2002. Free vibration analysis of an inflated toroidal shell. *Journal of Vibration and Acoustics*. 124:387–396.

Jiang, W. & Redekop, D. 2002. Polar axisymmetric vibration of a hollow toroid using the differential quadrature method. *Journal of Sound and Vibration*. 251:761–765. DOI: 10.1006/jsvi.2001.3865.

Jordan, P.F. 1962. Stresses and deformations of the thin-walled pressurized torus. *The Aerospace Sciences*. 29:213–225.

Jordan, P.F. 1965. *Analytical and experimental investigation of pressurized toroidal shells*. NASA Contractor Report CR-261.

Jordan, P.F. 1973. Buckling of toroidal shells under hydrostatic pressure. *AIAA*. 11(10):1439–1441.

Khazaeinejad, P., Najafizadeh, M.M., Wang, X.H. & Tanbakukuei Kashani, M. 2010. FEM buckling analysis of functional graded toroidal shells. In *Proceedings of the second Asian Conference on Mechanics of Functional Materials and Structures*. Nanjing, China. 247–250.

Koiter, W.T. 1964. On the stability of torus-shaped shells by O. Machnig. *Applied Mechanics Reviews*. 17(786).

Kosawada, T., Suzuki, K. & Takahashi, S. 1985. Free vibrations of toroidal shells. *Bulletin of JSME*. 28(243):2041–2047.

Kosawada, T., Suzuki, K. & Takahashi, S. 1986. Free vibrations of thick toroidal shells. *Bulletin of JSME*. 29(255):3036–3042.

Kosheleva, T.I. 1967. Stability of a toroidal shell. *Soviet Applied Mechanics*. 3(1):31–34. DOI: 10.1016/0891-3919(58)90124-4.

Kraus, H. 1967. *Thin elastic shells*. New York: John Wiley & Sons, Inc.

Kutsenko, G. V. 1967. Axisymmetric deformation of a thick-walled toroidal shell. *Soviet Applied Mechanics*. 3(1):27–30.

Levyakov, S.V. 2013. Evaluation of Reissner's equations of finite pure bending of curved elastic tubes. *Journal of Applied Mechanics*. 81(4). DOI: 10.1115/1.4025414.

Li, X. & Steigmann, D.J. 1995. Finite deformation of a pressurized toroidal membrane. *International Journal of Non-Linear Mechanics*. 30(4):583–595. DOI: 10.1115/1.3625832.

Liepins, A.A. 1965. Free vibrations of prestressed toroidal membrane. *American Institute of Aeronautics and Astronautics Journal*. 3:1924–1933.

Magnucki, K. & Jasion, P. 2013. Analytical description of pre-buckling and buckling states of barrelled shells under radial pressure. *Ocean Engineering*. 58:217–223. DOI: 10.1016/j.oceaneng.2012.11.004.

McGill, D.J. & Lenzen, K.H. 1967. Circumferential axisymmetric free oscillations of thick hollowed tori. *International Journal of Solids Structures*. 3:771–780.

Ming-de, D. 1985. New solutions of Novozhilov's equation of toroidal shells. *Applied Mathematics and Mechanics*. 6(5):417–430.

Murthy, M. & Kiusalaas, J. 1966. Toroidal-type shells free of bending under uniform normal pressure. *Journal of The Franklin Institute*. 282(4):232–241.

Navaratna, D.R., Pian, T.H.H. & Witmer, E.A. 1968. Stability analysis of shells of revolution by the finite element method. *AIAA*. 6:355–361.

Novozhilov, V. V. 1951. *The theory of thin shells*. The Netherlands: Wolters-Noordhoff Publishing.

Novozhilov, V. V. 1970. *Thin elastic shells*. P.G. Lowe, Ed. Groningen: Wolters-Noordhoff.

Panagiotopoulos, G.D. 1985. Stress and stability analysis of toroidal shells. *International Journal of Pressure Vessels and Piping*. 20(2):87–100. DOI: 10.1016/0308-0161(85)90070-5.

Pomares, R.J. & Durlofsky, H.P. 1988. Collapse analysis of toroidal shell. *ASME PVP*. 199:23–33.

Redekop, D. 2005. Buckling analysis of an orthotropic thin shell of revolution using differential quadrature. *International Journal of Pressure Vessels and Piping*. 82(8):618–624. DOI: 10.1016/j.ijpvp.2005.02.003.

Redekop, D., Xu, B. & Zhang, Y.M. 1999. Stability of a toroidal fluid-containing shell. *International Journal of Pressure Vessels and Piping*. 76:575–581.

Reissner, E. 1963. On stresses and deformations in toroidal shells of circular cross section which are acted upon by uniform normal pressure. *Quarterly of Applied Mathematics*. 21(3):177–187.

Ruojing, Z. 1999. A novel solution of toroidal shells under axisymmetric loading. *Applied Mathematics and Mechanics*. 20(5):519–526.

Sander, J.L. & Liepins, A.A. 1963. Toroidal membrane under internal pressure. *AIAA*. 1(9):2105–2110.

Sanders, J.L. 1963. Nonlinear theories for thin shells. *Quarterly of Applied Mathematics*. 21(1):21–36.

De Silva, C.N. 1964. The effect of transverse shear deformation on the bending of elliptic toroidal shells. *Journal of the Society for Industrial and Applied Mathematics*. 12(2):465–476. DOI: 10.1177/002199836900300316.

Singer, J., Arbocz, J. & Weller, T. 2002. *Buckling experiments: Experimental methods in buckling of thin-walled structures: Shells, built-up structures, composites and additional topics – Volume 2*.

Sobel, L.H. & Flügge, W. 1967. Stability of toroidal shells under uniform external pressure. *AIAA*. 5(3):425–431.

Steele, C.R. 1965. Toroidal pressure vessels. *J. Spacecraft and Rockets*. 2:937–943.

Sun, B. 2010a. Closed-form solution of axisymmetric slender elastic toroidal shells. *Journal of Engineering Mechanics*. 136:1281–1288. DOI: 10.1061/(ASCE)EM.1943-7889.0000175.

Sun, B. 2010b. Deformation, vibration, buckling of continuum nanotorus. *Journal of Nanomaterials*. 2010:1–6. DOI: 10.1155/2010/480628.

Sutcliffe, W.J. 1971. Stress analysis of toroidal shell of elliptical cross-section. *Int. J. Mech. Sci*. 13:951–958.

Teng, J.G. & Rotter, J.M. Eds. 2004. *Buckling of thin metal shells*. London: Spon Press.

Teng, J.G. 1996. Buckling of thin shells: recent advances and trends. *Applied Mechanics Reviews*. 49(4):263.

The tower of the pressure - Tarnów. n.d. Available: http://wiezecisnien.eu/malopolskie/ tarnow_ wodociag/ [2015, May 07].

Timoshenko, S. & Woinowsky-Krieger, S. 1959. *Theory of plates and shells*. New York: McGraw-Hill.

Tizzi, S. 2015. A free vibration analysis of toroidal composite shells in free space. *Journal of Sound and Vibration*. 337:116–134.

Ugural, A.C. 1981. *Stresses in plates and shells*. New York: McGraw-Hill.

Universal Industrial Gases, Inc. Project Showcase: Underground coal gasification (UCG) oxygen and nitrogen production site in Alabama, USA - Relocate and Upgrade. n.d. Available: http://www. uigi.com/hunt_refinery.html [2015, April 10].

Velickovic, V. 2007. Stress and strain states in the material of the stressed toroidal container for liquefied petroleum gas. *Scientific Technical Review*. LVII(3):94–105.

Ventsel, E. & Krauthammer, T. 2001. *Thin plates and shells: theory, analysis, and applications*. New York: Marcel Dekker, Inc.

Vu, V.T. 2010. Minimum weight design for toroidal pressure vessels using differential evolution and particle swarm optimization. *Structural and Multidisciplinary Optimization*. 42(3):351–369. DOI: 10.1007/s00158-010-0494-x.

Vu, V.T. 2013. Optimum shape of constant stress toroidal shells. *Journal of Pressure Vessel Technology*. 135(024501):1–4. DOI: 10.1115/1.4007043.

Vu, V.T. & Błachut, J. 2009. Plastic instability pressure of toroidal shells. *Journal of Pressure Vessel Technology*. 131(051203):1–10. DOI: 10.1115/1.3148824.

Wang, A. & Zhang, W. 1991. Asymptotic solution for buckling of toroidal shells. *International Journal of Pressure Vessels and Piping*. 45(1):61–72. DOI: 10.1016/0308-0161(91)90044-3.

Wang, X.H. & Redekop, D. 2005. Natural frequencies and mode shapes of an orthotropic thin shell of revolution. *Thin-Walled Structures*. 43:735–750. DOI: 10.1016/j.tws.2004.12.001.

Wang, X.H. & Redekop, D. 2011. Natural frequencies analysis of moderately-thick and thick toroidal shells. *Procedia Engineering*. 14:636–640. DOI: 10.1016/j.proeng.2011.07.080.

Wang, X.H., Xu, B. & Redekop, D. 2006. FEM free vibration and buckling analysis of stiffened toroidal shells. *Thin-Walled Structures*. 44:2–9. DOI: 10.1016/j.tws.2005.11.002.

Wolfram Research Inc. 2014. Mathematica version 10.0. Illinois: Wolfram Research, Inc. Available: http://support.wolfram.com/kb/472.

Xu, B. & Redekop, D. 2006. Natural frequencies of an orthotropic thin toroidal shell of elliptical cross-section. *Journal of Sound and Vibration*. 293:440–448. DOI: 10.1016/j.jsv.2005.09.020.

Yamada, G., Kobayashi, Y., Ohta, Y. & Yokota, S. 1989. Free vibration of a toroidal shell with elliptical cross-section. *Journal of Sound and Vibration*. 135(3):411–425.

Yoo, C.H. & Lee, S.C. 2011. *Stability of structures: principles and applications*. Amsterdam: Elsevier. DOI: 10.1016/B978-0-12-385122-2.10001-6.

Zhan, H.J. & Redekop, D. 2008. Vibration, buckling and collapse of ovaloid toroidal tanks. *Thin-Walled Structures*. 46:380–389. DOI: 10.1016/j.tws.2007.09.005.

Zhan, H.J. & Redekop, D. 2009. Static and dynamic loading of an ovaloid toroidal tank. *Thin-Walled Structures*. 47:760–767. DOI: 10.1016/j.tws.2008.12.006.

Zhang, W. 1949. Toroidal shells. *Science Report of National Tsing Hua University.* Serial A:259–349.

Zhenhui, W., Hongbin, Z. & Zhupei, S. 1986. Approximated-asymptotic solution of the complex variable equation of toroidal shells under axial symmetric loads. *ACTA Mechanica Sinica*. 2(l):58–65.

Zhou, D., Au, F.K.T., Lo, S.H. & Cheung, Y.K. 2002. Three-dimensional vibration analysis of a torus with circular cross section. *Journal of the Acoustical Society of America*. 112:2831–2839.

Zhu, J. & Redekop, D. 1995. Band loading of a thick-walled toroidal shell. *International Journal of Pressure Vessels and Piping*. 61:99–109.

Zienkiewicz, O.C., Taylor, R.L. & Fox, D.D. 2014. *The finite element method for solid & structural mechanics*. 7th ed. Oxford: Elsevier Ltd.

Zingoni, A. 1991. Bending-disturbance considerations in the axisymmetric response on non-shallow spherical shell structures. University of London.

Zingoni, A. 1997. *Shell structures in civil and mechanical engineering*. London: Thomas Telford Publishing.

Zingoni, A. 2001a. Stresses and deformations in egg-shaped sludge digestors: membrane effects. *Engineering Structures*. 23:1365–1372. DOI: 10.1016/S0141-0296(01)00056-6.

Zingoni, A. 2001b. Stresses and deformations in egg-shaped sludge digestors: discontinuity effects. *Engineering Structures*. 23(11):1373–1382. DOI: 10.1016/S0141-0296(01)00056-6.

Zingoni, A. 2002a. Parametric stress distribution in shell-of-revolution sludge digesters of parabolic ogival form. *Thin-Walled Structures*. 40:691–702. DOI: 10.1016/S0263-8231(02)00020-4.

Zingoni, A. 2002b. Discontinuity effects at cone-cone axisymmetric shell junctions. *Thin-Walled Structures*. 40(10):877–891. DOI: 10.1016/S0263-8231(02)00022-8.

Zingoni, A. 2004. On analytical solutions for liquid-filled non-shallow conical shell assemblies. *Journal of the South African Institution of Civil Engineering*. 46(3):10–15.

Zingoni, A. 2005. Shell forms for egg-shaped concrete sludge digesters: A comparative study on structural efficiency. *Structural Engineering and Mechanics*. 19(3):321–336. DOI: 10.12989/sem.2005.19.3.321.

Zingoni, A. 2009. Simplification of the derivation of influence coefficients for symmetric frusta of shells of revolution. *Thin-Walled Structures*. 47(8–9):912–918. DOI: 10.1016/j.tws.2009.02.005.

Zingoni, A. 2015a. Liquid-containment shells of revolution: a review of recent studies on strength , stability and dynamics. *Thin-Walled Structures*. 87:102–114.

Zingoni, A. 2015b. *Vibration analysis and structural dynamics for civil engineers*. London: CRC Press.

Zingoni, A. 2018. *Shell structures in Civil and Mechanical engineering: Theory and Analysis (Second Edition)*. London: ICE Publishing. DOI: 10.1680/ssicame.36369.

Zingoni, A. & Pavlović, M.N. 1990. Computation of bending disturbances in axisymmetrically loaded spherical shells: a study of the accuracy of Geckeler's approximation. *Engineering Computations*. 7(2):125–143. DOI: 10.1108/eb023800.

Zingoni, A. & Pavlović, M.N. 1991a. Effect of support conditions in liquid-filled spherical vessels. Part 2. Inclined supports. *Proceedings of the Institution of Civil Engineers*. 91(2):347–363. DOI: 10.1680/iicep.1991.14999.

Zingoni, A. & Pavlović, M.N. 1991b. Effect of support conditions in liquid-filled spherical vessels. Part 1. Limiting ring-beam stiffnesses. *Proceedings of the Institution of Civil Engineers*. 91(2):323–346. DOI: 10.1680/iicep.1991.14998.

Zingoni, A. & Pavlović, M.N. 1992. On edge-disturbance interaction and decoupling errors in thin-walled nonshallow spherical-shell frusta. *Thin-Walled Structures*. 13(5):375–386. DOI: 10.1016/0263-8231(92)90019-S.

Zingoni, A. & Pavlović, M.N. 1993a. Discontinuity phenomena around the supports of stepwise-thickened spherical steel tanks. Part 1: Theoretical considerations and parametric results. *International Journal of Pressure Vessels and Piping*. 53(3):405–435. DOI: 10.1016/0308-0161(93)90071-Z.

Zingoni, A. & Pavlović, M.N. 1993b. Discontinuity phenomena around the supports of stepwise-thickened spherical steel tanks. Part 2: Numerical examples and design recommendations. *International Journal of Pressure Vessels and Piping*. 53(3):437–456. DOI: 10.1016/0308-0161(93)90072-2.

Zingoni, A. & Pavlović, M.N. 1993c. A note on the accuracy of the Geckeler approximation. *Engineering Computations: International Journal for Computer-Aided Engineering and Software*. 10(4):369–379. DOI: 10.1108/eb023914.

Zingoni, A., Enoma, N. & Govender, N. 2015. Equatorial bending of an elliptic toroidal shell. *Thin-Walled Structures*. 96:286–294. DOI: 10.1016/j.tws.2015.08.017.

Zingoni, A., Mokhothu, B. & Enoma, N. 2015. A theoretical formulation for the stress analysis of multi-segmented spherical shells for high-volume liquid containment. *Engineering Structures*. 87:21–31. DOI: 10.1016/j.engstruct.2015.01.002.

Zu, L., Koussios, S. & Beukers, A. 2010. Optimal cross sections of filament-wound toroidal hydrogen storage vessels based on continuum lamination theory. *International Journal of Hydrogen Energy*. 35:10419–10429. DOI: 10.1016/j.ijhydene.2010.07.142.